

Roubi Hamid Ahmad Abuobeid

The effect of Minor Triterpenic
Components of Virgin Olive Oil on
the Gene Expression Profiles in
the Livers of Several Animal
Models

Director/es

De La Osada García, Jesús
Martínez Beamonte, Roberto

<http://zaguan.unizar.es/collection/Tesis>



Universidad de Zaragoza
Servicio de Publicaciones

ISSN 2254-7606

Tesis Doctoral

THE EFFECT OF MINOR TRITERPENIC
COMPONENTS OF VIRGIN OLIVE OIL ON THE
GENE EXPRESSION PROFILES IN THE LIVERS OF
SEVERAL ANIMAL MODELS

Autor

Roubi Hamid Ahmad Abuobeid

Director/es

De La Osada García, Jesús
Martínez Beamonte, Roberto

UNIVERSIDAD DE ZARAGOZA
Escuela de Doctorado

Programa de Doctorado en Bioquímica y Biología Molecular

2024



Universidad
Zaragoza

**The effect of Minor Triterpenic
Components of Virgin Olive Oil on the
Gene Expression Profiles in the Livers of
Several Animal Models**

Author

Roubi Hamid Ahmad Abuobeid

Directores

Prof. Dr. Jesús Osada García

Dr. Roberto Martínez Beamonte

**Department of Biochemistry and Molecular and
Cellular Biology**

University of Zaragoza

December 2023

Los doctores Roberto Martínez Beamonte y Jesús de la Osada García, profesores del Departamento de Bioquímica y Biología Molecular y Celular de la Universidad de Zaragoza.

INFORMAN: que Dña. **Roubi Hamid Ahmad Abuobeid** ha realizado bajo nuestra dirección el trabajo que presenta como memoria de doctorado con el título: “The effect of Minor Triterpenic Components of Virgin Olive Oil on the Gene Expression Profiles in the Livers of Several Animal Models”.

Este trabajo se ha llevado a cabo durante los años 2018 al 2023 en este departamento.

Zaragoza, 15 de diciembre de 2023

Fdo. Roberto Martínez Beamonte

Fdo: Jesús de la Osada García

El presente trabajo ha sido financiado por la red CIBER de Fisiopatología de la Obesidad y Nutrición (CB06/03/1012), como iniciativa FEDER-ISCIII, la Agencia Estatal de Investigación (SAF2016-75441-R), el Ministerio de Ciencia e Innovación-Fondo Europeo de Desarrollo Regional (PID2019-104915RB-I00 y PID2022--104915RB-I00), y el Gobierno de Aragón, grupo de Referencia B16_20R y B16_23R.

ACKNOWLEDGEMENTS

I would like to express my deepest gratitude to all of those who have contributed to the completion of this thesis.

I am immensely and sincerely grateful to Prof. Dr. Jesús Osada García for his excellent and valuable advice, tremendous guidance and mentorship, constructive feedback, generous and constant assistance, unwavering support and encouragement, and invaluable insights throughout my research process. I am very grateful to him for his outstanding supervision, for sharing his wealth of expertise, knowledge and resources with me, and for his patience, all of which helped me to overcome all the challenges and difficulties I faced in my research and to successfully complete my thesis. It is a great privilege for me to work under the guidance and supervision of Prof. Jesus. I could not ask for anything more 😊. At the same time, he took care of every member of his team and made us feel at home. I am overwhelmed with gratitude for your support Professor 😊.

I would like to express my sincere gratitude to Dr Roberto Martínez Beamonte for his mentorship, valuable advice, wealth of expertise and constructive feedback; he has provided me with tremendous support, constant assistance and encouragement to overcome the challenges I have faced in my research and to successfully complete the thesis. Dr Roberto's guidance and advice have been invaluable in my work. At the same time, he was always there for me whenever I needed help with anything. I really appreciate it all Doctor 😊.

I would like to acknowledge the contribution of Dr. M^a Ángeles Navarro Ferrando and express my sincere gratitude for providing me with all the valuable expertise, wealth advice, support and encouragement I needed at all times 😊. I owe a great debt of gratitude to Prof. Dr. M^a Jesus Rodriguez-Yoldi and Prof. Dr. Carmen Arnal for the wealth of expertise, constructive feedback and constant support and assistance I needed to successfully complete my manuscripts and thesis 😊. I would like to express my deepest gratitude and appreciation to the faculty members and friends for Cristina Barranquero, Santiago Morales Andres, Dr. Luis Herrera-Marcos, Dr. Javier Sánchez Marco, Seyed Hesamoddin Bidooki, Tania Herrero-Contiente and Raylen Escobar, they have been so generous and supportive to me, they helped me in every aspect of my work, even when they were so busy. They shared their valuable expertise, constant guidance, support and encouragement 😊. Cris and Seyed 😊, you really provided me with endless support and happiness and made every day so beautiful and let me feel at home 😊. Sofía Blasco Haro. Sofi 😊. I don't know how to thank you enough. You have always been there for me in every way, every day. You have given me endless support and encouragement. You helped me with countless papers for university, residency, etc. You took me to the hospital many times and comforted me when I came to your office crying. You helped me cope when my sister passed away. You are my sister and my best friend. When i was not in our lab, everyone knew I was in your office 😊. The department lost its soul when you left. B.M You have supported me in everything. No word is enough to thank you. Much appreciated my friend 😊. I also owe a huge debt of gratitude to Prof. Dr. Julio Montoya, Prof Dr. Eduardo Ruiz Pesini, Adriana Casao, Rosaura Pérez-Pé, Ana Vela Sebastián, Sonia Emperador, Irene Jiménez, Ester Lopéz, Carmen Hernández, Mouna Habbane, Melissa Carvajal, Vicky Peña for their assistance, support and encouragement. They were always there for me and made me feel welcome and comfortable from day one 😊. They gave me access to their instruments and equipment with all the necessary training anytime 😊.

To all of you: I will never forget how you supported me when I lost my sister. In fact, you stood by me through the hardest days I have ever faced. It means a lot to me. More than you can know.



I send my efforts, manuscripts and thesis to the soul of my sister Abeer Abuobeid, who passed away two years ago after a hard month of severe illness. This pain actually killed everything alive in me and almost stopped me from going on, but her words, her support, she is actually the one who always protected me 1000000% when the world was against me and she helped me to go on, and this protection didn't stop when she passed away. I don't understand why she left so early. She always wanted to see me graduate, I really wish her to do so from heaven. All my efforts and every word written and every scientific benefit of this thesis is from me to your blessed soul sister. I know you will receive my gift and you will be happy and proud. My trust in God makes me so sure of this sister.



To my parents, Hamid Abuobeid and Zahra Busaileh, you are more than parents and supporters to me in every way. In every possible scenario, you have provided me with assistance, advise and inspiration. You have stood by my side and encouraged me with your strong motivation. You paid all my expenses to study and live in Spain all these years, which I know was not easy at all, but you never complained and never made me feel pressured. You always helped me to overcome any difficulties and never let me see the pain during those hard years we went through. This is my thesis and I want to share it with you as a gift and to thank you from all my heart 😊. My uncles and aunt Mohammed Busaileh, Aida, Mohammed, Mahmoud and my sisters Suhad and Rula Abuobeid. They have all always supported me and given me all the positive energy and advice to carry on and to do very well through their encouragement and they been a great source of inspiration for me. Their words are always in my mind and have helped me a lot in my PhD journey. I appreciate all their efforts 😊.

Abbreviations

ABBREVIATIONS

A₂₆₀/A₂₈₀	Ratio de absorbances at 260 and at 280 nm
ABCA1	ATP-binding cassette A1
ACS	American Chemical Society
ADP	Adenosine diphosphate
AML12	Alpha mouse liver cell line 12
AMPK	Adenosine monophosphate activated protein kinase
Apo	Apolipoprotein
AS	Alternative splicing
A3SS	Alternative 3' splicing site
A5SS	Alternative 5' splicing site
ATCC	American Type Culture Collection
ATGL	Adipose triglyceride lipase
ATP	Adenosine triphosphate
AUC	Area under the ROC curve
BLAST	Basic local alignment search tool
BMR	Basal metabolic rate
bp	Base pair
CAGE	Cap analysis of gene expression
cDNA	Complementary DNA
CE	Capillary electrophoresis
CETP	Cholesteryl ester transfer protein
Chol	Cholesterol
ChREBP	Carbohydrate regulatory element binding protein
CI	Chemical ionization
COX2	Cyclooxygenase 2
CPC	Cuffcompare
CRP	C-reactive protein
CT	Cycle threshold
CTP	Phosphocholine cytidyltransferase- α

Abbreviations

CVD	Cardiovascular disease
DAG	Diacylglycerol
DEG	Differentially expressed genes
DEPC	Diethylpyrocarbonate
DHCR7	7-dehydrocholesterol reductase
DHCR24	24-dehydrocholesterol reductase
DMAPP	Dimethylallyl diphosphate
DMEM	Dulbecco's modified eagle's minimum essential medium
DMSO	Dimethyl sulfoxide
DNA	Deoxyribonucleic acid
DNase	Deoxyribonuclease
DNB	DNA nanoball
DNL	<i>De novo</i> lipogenesis
dNTPs	Deoxynucleotide triphosphates
dsDNA	Double-stranded DNA
DSG	Differentially spliced gene
ECM	Extracellular matrix
EDTA	Ethylenediaminetetraacetic acid
ER	Endoplasmic reticulum
ES	Embryonic stem
EST	Expressed sequence tag
EtBr	Ethidium bromide
EVOO	Extra virgin olive oil
FA	Fatty acid
FDR	False discovery rate
FIT2	Fat storage-inducing transmembrane 2
FLIP	Fatty liver inhibition of progression
FPP	Farnesyl pyrophosphate
× g	Times gravity
Gb	Gigabyte
GC-MS	Gas chromatography-mass spectrometry

Abbreviations

GEO	Gene Expression Omnibus
GITC	Guanidine isothiocyanate
GO	Gene ontology
gRNA	guide RNA
GTP	Guanosine triphosphate
H₂O₂	Hydrogen peroxide
H&E	Hematoxylin and eosin
HEPG2	Human hepatoma cell line
HCC	Hepatocellular carcinoma
HDL	High-density lipoprotein
HFD	High-fat diet
HISAT2	Hierarchical indexing for spliced alignment of transcripts
HMG-CoA	3-hydroxy-3-methylglutaryl coenzyme A
HMGR	HMG-CoA reductase
HPC	Hepatic progenitor cell
HPLC	High-performance liquid chromatography
HRP	Horseradish peroxidase
HSC	Hepatic stellate cell
HSL	Hormone-sensitive lipase
HSPG	Heparan sulphate proteoglycan
IDL	Intermediate-density lipoprotein
IL	Interleukin
INDEL	Insertion-deletion
IPP	Isopentenyl diphosphate
IR	Insulin resistance
JNK	c-Jun n-terminal kinase
kDa	Kilodalton
KEGG	Kyoto encyclopedia of genes and genomes
KO	Knock-out
K-R	Kandutsch-Russell
LD	Lipid droplet

Abbreviations

LDL	Low-density lipoprotein
LDLR	LDL receptor
lncRNA	Long non-coding RNA
LP	Lipoprotein
LRP	LDL receptor-related protein
LSS	Lanosterol synthase
MAG	Monoacylglycerol
MAGL	Monoacylglycerol lipase
MCD	Methionine-choline-deficient
MD	Mediterranean diet
MetS	Metabolic syndrome
MIQE	Minimum information for publication of quantitative real-time PCR experiments
miRNA	microRNA
MLX	Max-like factor X
MPSS	Massively parallel signature sequencing
mRNA	messenger RNA
MS	Mass spectrometry
MUFA	Monounsaturated fatty acid
MVA	Mevalonate
MXE	Mutually exclusive exon
NA	Not applicable
NADPH	Nicotinamide adenine dinucleotide phosphate hydrogen
NAFLD	Non-alcoholic fatty liver disease
NASH	Non-alcoholic steatohepatitis
NCBI	National Center for Biotechnology Information
ncRNA	non-protein-coding RNA
NEFA	Non-esterified fatty acid
NF-κB	Nuclear factor kappa B
NGS	Next-generation sequencing
NMR	Nuclear magnetic resonance

Abbreviations

OD	Optical density
PBS	Phosphate buffered saline
PC	Phosphatidylcholine
PCR	Polymerase chain reaction
PGE₂	Prostaglandin E ₂
piRNA	piwi-interacting RNA
PL	Phospholipid
PLGA	Polylactic-co-glycolic acid
PLIN3	Perilipin3
Pol I	DNA polymerase I
Poly-A	Polyadenylated
Poly-T	Poly-thymine
PPARα	Peroxisomal proliferator-activated receptor alpha
PPIB	Peptidylprolyl isomerase B
PUFA	Polyunsaturated fatty acids
P value	Probability value
R	Correlation coefficient
RCR	Rolling circle replication
RER	Rough endoplasmic reticulum
RI	Retained intron
RIN	RNA integrity number
RNA	Ribonucleic acid
RNases	Ribonucleases
RNase H	Ribonuclease H
RNA-seq	RNA sequencing
ROC	Receiver operating characteristic
ROS	Reactive oxygen species
Rpm	Revolutions per minute
rRNA	ribosomal RNA
RT	Reverse transcription
RTK	Receptor tyrosine kinase

Abbreviations

RT-qPCR	Reverse transcription quantitative real-time PCR
SAF	Steatosis Activity Fibrosis
SAGE	Serial analysis of gene expression
SD	Standard deviation
SE	Skipped exon
SER	Smooth endoplasmic reticulum
SFA	Saturated fatty acid
SIM	Selective ion monitoring
siRNA	small interfering RNA
SL₂R	Signal log ₂ ratio
SLC2A	Solute carrier family 2-member
SNP	Single nucleotide polymorphism
snRNA	Small nuclear RNA
snoRNA	Small nucleolar RNA
SQLE	Squalene epoxidase
SQS	Squalene synthase
SREBP-1	Sterol regulatory element binding protein-1
ssDNA	Single-stranded DNA
TAG	Triacylglycerol
TBE	Tris-borate-EDTA
TBME	Tertiary butyl methyl ether
TBP	TATA-box binding protein
TCA	Tricarboxylic acid
TEI	Total energy intake
TG	Triglyceride
TGF	Transforming growth factor
TLR9	Toll-like receptor 9
T_m	Melting temperature
TNF	Tumor necrosis factor
TRL	TG-rich lipoproteins
tRNA	Transfer RNA

Abbreviations

TSIM	N-trimethylsilylimidazole
UBA52	Ubiquitin A-52
UPLC	Ultra-performance liquid chromatography
UV	Ultraviolet
VIS	Visible
VLDL	Very low-density lipoprotein
VOO	Virgin olive oil
Vs	Versus
ω6/ω3	Omega-6/omega-3

Table of Contents

Table of Contents

ABBREVIATIONS.....	1
I. ABSTRACT.....	10
I. RESUMEN.....	11
II. INTRODUCTION.....	14
The Biology of Liver Cells.....	14
The Metabolic Functions of Hepatocytes	15
Metabolism of Proteins	15
Bile Secretion.....	15
Blood Detoxification	16
Carbohydrate and Lipid Homeostasis.....	16
Lipids Synthesis.....	18
Lipid Droplets.....	21
LDs Formation.....	21
LD Functions	23
Non-Alcoholic Fatty Liver Disease	24
The Pathogenesis of Non-Alcoholic Fatty Liver Disease.....	25
Progression of Non-Alcoholic Fatty Liver Disease	27
The Mediterranean Diet	30
Extra Virgin Olive Oil.....	32
Essential Minor Bioactive Compounds	35
Animal Models	40
<i>Mus musculus</i> (NCBI: txid39442).....	40
<i>Oryctolagus cuniculus</i> (NCBI: txid9986).....	43
<i>Sus scrofa</i> (NCBI: txid9823).....	44
Cell Culture	44
Analytical Procedures.....	46
Histological Analysis.....	46
Functional Analysis.....	47
III. OBJECTIVES	54
III. OBJETIVOS	55
IV. MATERIALS AND METHODS.....	56
i. Biological Samples.....	56
1. <i>In Vivo</i> Experiments.....	56
2. <i>In Vitro</i> Assays	63
ii. Gene Expression Experiments	69
1. Good Laboratory Practices for RNA Extraction and Handling	69
2. Total RNA Extraction.....	69
3. RNA Quantification.....	72
4. Gel Electrophoresis	72
5. Removal of DNA Contamination.....	73
6. RNA Sequencing.....	74
7. Reverse Transcription.....	77
8. Good Laboratory Practices for PCR Work	77

Table of Contents

9.	Primer Design and Optimization	78
10.	Real-Time Quantitative PCR.....	78
iii.	Histological Examination of the Liver.....	80
1.	Preparation of liver tissue blocks.....	80
2.	Deparaffinization of Liver Tissue Sections.....	81
3.	Hematoxylin and Eosin Staining.....	82
4.	LD Area	83
5.	NASH Activity Index and SAF Score	83
6.	Masson's Trichrome Stain	84
iv.	Enzyme-Based Hepatic Lipid Assays	85
1.	Lipids Extraction.....	85
2.	Cholesterol Quantification	85
3.	Triglyceride Quantification.....	86
4.	Unesterified and Esterified Fractions of Cholesterol	87
v.	Analyses of Metabolites.....	88
1.	Squalene.....	88
2.	Sterols	90
vi.	Quality Control and Statistics.....	92
V.	RESULTS	102
i.	Dietary Erythrodiol Modifies Hepatic Transcriptome in Mice in a Sex and Dose-Dependent Way.....	102
ii.	Squalene through its Post-Squalene Metabolites is a Modulator of Hepatic Transcriptome in Rabbits.	133
iii.	Differentially Expressed Genes in Response to a Squalene-Supplemented Diet Are Accurate Discriminants of Porcine Non-Alcoholic Steatohepatitis 158	
VI.	DISCUSSION	191
i.	Dietary Erythrodiol Modifies Hepatic Transcriptome in Mice in a Sex and Dose-Dependent Way.....	191
ii.	Squalene through its Post-Squalene Metabolites is a Modulator of Hepatic Transcriptome in Rabbits.	197
iii.	Differentially Expressed Genes in Response to a Squalene-Supplemented Diet Are Accurate Discriminants of Porcine Non-Alcoholic Steatohepatitis 202	
VII.	CONCLUSIONS	208
VII.	CONCLUSIONES.....	210
VIII.	REFERENCES	212

I. ABSTRACT

Minor bioactive triterpene compounds of extra virgin olive oil, including the dialcohol, erythrodiol, and hydrocarbon, squalene, have shown significant biological effects in animal studies. For further characterization of changes through the hepatic transcriptome, both compounds have been studied in different animal models using RNA sequencing.

Long term administration of 10 mg/kg erythrodiol in a purified Western diet to *Apoe*-deficient mice significantly upregulated 68 and down-regulated 124 hepatic genes at the level of 2-fold change. These genes belonged to detoxification processes, protein metabolism and nucleic acid related metabolites. Confirmation by reverse transcription and quantitative real-time PCR showed significant changes by erythrodiol. When some of them were analyzed in female *Apoe*-deficient mice, no change was observed. Likewise, no significant variation was observed in *Apoe*-deficient mice receiving doses ranging from 0.5 to 5 mg/kg erythrodiol. These results provide evidence that erythrodiol has a selective role in regulating hepatic gene expression, depending on sex and dose.

The effect of squalene was assessed in two groups of male New Zealand rabbits fed either a diet supplemented with 1% sunflower oil or the same diet supplemented with 0.5% squalene for 4 weeks. The gene ontology of the altered hepatic transcriptome was classified into: protein and sterol transport, lipid metabolism, lipogenesis, anti-inflammatory and anti-neoplastic actions. Confirmation by reverse transcription quantitative real-time PCR showed that rabbits receiving squalene showed a marked hepatic expression of *PNPLA3*, *GCK*, *TFCP2L1*, *ASCL1*, *ACSS2*, *OST4*, *FAM91A1*, *MYH6*, *LRRC39*, *LOC108176846*, *GLT1D1* and *TREH*. Squalene also accumulated in the livers so did its post-squalene metabolites of cholesterol biosynthesis, including lanosterol, dihydrolanosterol, lathosterol, zymostenol and desmosterol. The effect of lanosterol, dihydrolanosterol, zymostenol and desmosterol, tested in the mouse liver 12 cell line (AML12), reproduced the same expression pattern of the rabbit liver for *Acss2*, *Fam91a1* and *Pnpla3*. Taken together, the results suggest that squalene and its metabolites are key

molecules for the hepatic transcriptional changes required to protect the liver dysfunction.

The effect of squalene on the hepatic transcriptome was also tested in two groups of male Large White x Landrace pigs developing non-alcoholic steatohepatitis by feeding with a steatotic diet high in fat/cholesterol/fructose and low in methionine and choline, or the same diet supplemented with 0.5% squalene for a month. In pigs receiving the squalene-containing diet, *PPP1R1B*, *OASL*, *PPP4R4*, *NEURL3*, *TMEM45B*, *AFP*, *ENPEP*, *LOC110256649*, *LOC100526118*, *SPRY3*, *SQLE* and *CHL1* were significantly modulated. These pigs also had lower hepatic triglycerides and lipid droplet areas and higher cellular ballooning. Strong correlations were identified between these parameters and the modified transcripts. Moreover, the expression of *PPP1R1B*, *TMEM45B*, *AFP* and *ENPEP* followed the same pattern *in vitro* using human hepatoma (HEPG2) and mouse liver 12 (AML12) cell lines incubated with squalene, indicating a direct effect of squalene on these expressions. Overall, these data indicate that squalene is able to modulate gene expression changes that may influence the progression of non-alcoholic steatohepatitis.

I. RESUMEN

Los compuestos minoritarios triterpénicos bioactivos del aceite de oliva virgen extra, incluidos el dialcohol, eritrodiol, y el hidrocarburo escualeno, han mostrado efectos biológicos significativos en estudios con animales. Para una mejor caracterización de los cambios a nivel del transcriptoma hepático, ambos compuestos se han estudiado en diferentes modelos animales mediante secuenciación de ARN.

La administración a largo plazo de 10 mg/kg de eritrodiol en una dieta occidental purificada a ratones carentes de *ApoE* aumentó significativamente 68 genes y redujo 124 genes hepáticos con un nivel de cambio de 2 veces. Estos genes pertenecían a procesos de desintoxicación, metabolismo de proteínas y metabolitos relacionados con ácidos nucleicos. La confirmación mediante transcripción inversa y PCR cuantitativa en tiempo real mostró cambios significativos por eritrodiol. Cuando se analizaron algunos de ellos en ratones hembra deficientes en *ApoE*, no se observó ningún cambio. Asimismo, no se observaron variaciones significativas en ratones deficientes en *ApoE* que recibieron dosis que oscilaban entre 0,5 y 5 mg/kg de eritrodiol. Estos resultados demuestran que el

eritrodiol desempeña un papel selectivo en la regulación de la expresión génica hepática, en función del sexo y de la dosis.

El efecto del escualeno se evaluó en dos grupos de conejos machos de Nueva Zelanda alimentados durante 4 semanas con una dieta suplementada con un 1% de aceite de girasol o con la misma dieta suplementada con un 0,5% de escualeno. La ontología génica del transcriptoma hepático alterado se clasificó en: transporte de proteínas y esteroides, metabolismo lipídico, lipogénesis, acciones antiinflamatorias y antineoplásicas. La confirmación mediante transcripción inversa y PCR cuantitativa en tiempo real mostró que los conejos que recibían escualeno presentaban una marcada expresión hepática de *PNPLA3*, *GCK*, *TFCP2L1*, *ASCL1*, *ACSS2*, *OST4*, *FAM91A1*, *MYH6*, *LRRC39*, *LOC108176846*, *GLT1D1* y *TREH*. El escualeno también se acumuló en los hígados, al igual que sus metabolitos de la cascada biosintética del colesterol, incluidos el lanosterol, el dihidrolanosterol, el lathosterol, el zymostenol y el desmosterol. El efecto del lanosterol, el dihidrolanosterol, el zimostenol y el desmosterol, probado en la línea celular 12 de hígado de ratón (AML12), reprodujo el mismo patrón de expresión del hígado de conejo para *Acss2*, *Fam91a1* y *Pnpla3*. En conjunto, los resultados sugieren que el escualeno y sus metabolitos son moléculas clave para los cambios transcripcionales hepáticos necesarios para proteger la disfunción hepática.

El efecto del escualeno sobre el transcriptoma hepático también se comprobó en dos grupos de cerdos machos Large White x Landrace que desarrollaban esteatohepatitis no alcohólica al ser alimentados con una dieta esteatósica rica en grasa/colesterol/fructosa y pobre en metionina y colina, o con la misma dieta suplementada con un 0,5% de escualeno durante un mes. En los cerdos que recibieron la dieta con escualeno, *PPP1R1B*, *OASL*, *PPP4R4*, *NEURL3*, *TMEM45B*, *AFP*, *ENPEP*, *LOC110256649*, *LOC100526118*, *SPRY3*, *SQLE* y *CHL1* se modularon significativamente. Estos cerdos también presentaban menores áreas de triglicéridos y gotas lipídicas hepáticas y un mayor *ballooning* celular. Se identificaron fuertes correlaciones entre estos parámetros y los transcritos modificados. Además, la expresión de *PPP1R1B*, *TMEM45B*, *AFP* y *ENPEP* siguió el mismo patrón *in vitro* utilizando líneas celulares de hepatoma humano (HEPG2) y de hígado de ratón 12 (AML12) incubadas con escualeno, lo que indica un efecto directo del escualeno sobre estas expresiones. En conjunto, estos datos indican que

Abstract

el escualeno es capaz de modular los cambios de expresión génica que pueden influir en la progresión de la esteatohepatitis no alcohólica.

II. INTRODUCTION

The Biology of Liver Cells

The liver is the largest solid organ in the body and the second largest organ-after the skin (1, 2), accounting for approximately 2% of an adult's body mass and 1.5-2.5% of lean body mass (3, 4). More than 12% of blood volume is in the liver (5). The liver has a double simultaneous blood supply, with about 25% coming directly from the aorta via the hepatic artery, while the remaining 75% is nutrient-rich and comes from various organs in the gastrointestinal system via the portal vein (3, 6). The functional unit of the liver is the lobule (Figure 1). Each lobule is made up of hexagons and central veins located in the center of the lobule, while the portal triad including the portal vein, bile duct and hepatic artery are located at the border of the liver lobule (2, 3). Within the lobule, the primary cell types are parenchymal hepatocytes, bile duct cells and nonparenchymal cells (2, 7). The non-parenchymal cells comprise 40% of the cell population, of which approximately 40% are sinusoidal cells, 30% are Kupffer cells, 10-25% are hepatic stellate cells (HSCs) and the remaining 5% are other cells (8, 9). Sinusoidal cells are endothelial cells involved in endocytosis, blood clearance, filtration and transport of nutrients from the bloodstream, secretion of cytokines and interferons, and adhesion for leukocytes (10-12), Kupffer cells are phagocytic macrophages (4, 12) and HSCs are fibroblasts involved in lipid and vitamin storage, extracellular matrix (ECM) turnover and fibrogenesis (11, 13, 14). 30-50% of total liver lymphocytes are natural killer cells (15) with a primary role in the immune response (16). Bile duct cells play a key role in the production and secretion of bile and the excretion of circulating xenobiotics, as well as a crucial role in forming a barrier to the diffusion of toxins from the bile into the interstitial tissue of the liver (17). Hepatocytes are epithelial cells that make up about 60% of the total cell population (18) and 80% of the cytoplasmic mass of the liver (19). Multifunctional hepatocytes are the major site of protein synthesis, bile formation, detoxification and metabolic conversion for a variety of physiological functions including carbohydrate, lipid and lipoprotein (LP) homeostasis (5, 7, 20).

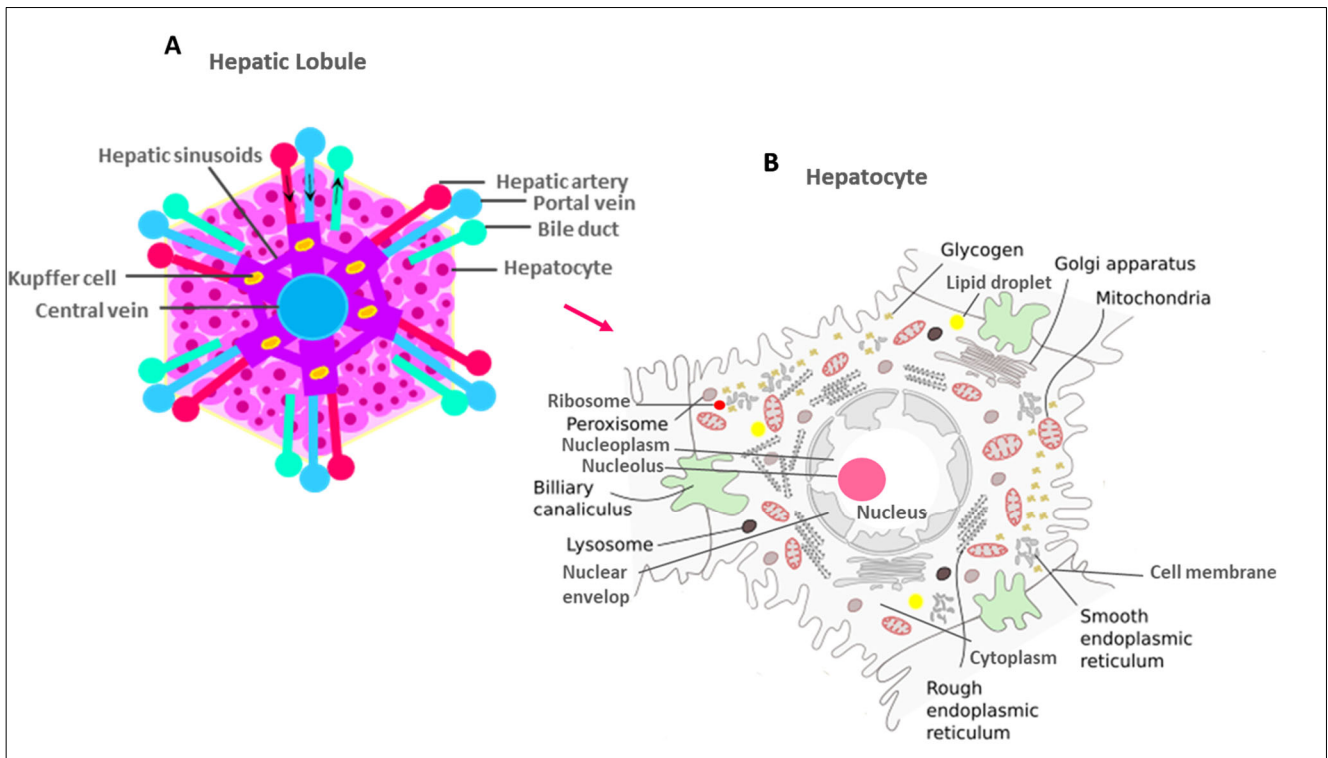


Figure 1. Biological structure of hepatic lobules (A) and hepatocytes (B). Adapted from (21).

The Metabolic Functions of Hepatocytes

Metabolism of Proteins

The high hepatic content of ribosome-containing rough endoplasmic reticulum (RER) reflects an important function of these cells in protein metabolism (22). Hepatocytes orchestrate protein metabolism using amino acids derived from dietary and muscle proteins as building blocks, as well as producing new amino acids by transamination of amino acids to α -keto acids via transaminase, except for the deamination of glutamate, which ends up as ammonia via glutamate dehydrogenase, while the remaining amino acids containing carbon and hydrogen atoms are used in the hydrolysis of glucose and lipid molecules to produce energy. Due to the toxicity of ammonia, it is converted to urea via the ornithine cycle (4) (Figure 2).

Bile Secretion

Hepatocytes secrete bile containing acids, bilirubin, water, electrolytes, phospholipids and cholesterol (Chol). Bile secretion helps to excrete endogenous

Introduction

substances such as bilirubin, steroid hormones and calcium, as well as exogenous substances such as drug metabolites. Some are reabsorbed from the small intestine into the bloodstream to be excreted by the kidneys (4).

Blood Detoxification

Hepatocytes are organized into plates separated by sinusoids. This structure is key to directing the excretion of detoxification products from the hepatocytes into the bile and blood circulation. In addition, the extensive meshwork of the endoplasmic reticulum (ER) contains large amounts of detoxification enzymes, in addition to the cytosol (22). Hepatocytes detoxify endotoxins and exotoxins. Lipophilic toxins are metabolized in phase I by oxidative and reductive reactions by cytochrome P450 enzymes embedded in the ER membranes. Many of the phase I products become substrates for phase II enzymes that catalyze conjugation reactions. Overall, endogenous cofactors are used to produce water-soluble waste products that are excreted in bile, urine or sweat (22-24).

Carbohydrate and Lipid Homeostasis

Characteristic of hepatocytes include round nuclei and numerous mitochondria, suggesting that these cells play a crucial role in energy metabolism (22). In the fed state, excess glucose entering the bloodstream via the portal vein is sequestered in the cytosol by glycogenesis via glycogen synthase to form glycogen (4, 25, 26). This process is stimulated by insulin released from pancreatic cells (4).

In the fasting state, glucose is released by the breakdown of glycogen by glycogenolysis via glycogen phosphorylase stimulated by glucagon released from pancreas cells, and by gluconeogenesis, where glucose is synthesized from pyruvate derived from lactate as an anaerobic product, and from glycerol released from lipolysis (27), as well as from amino acids entering gluconeogenesis via the tricarboxylic acid (TCA) cycle (4, 25, 28). Gluconeogenesis is stimulated by glucagon, growth hormone, epinephrine, and cortisol (25, 29).

Glucose is metabolized by cytosolic glycolysis to pyruvate, which is oxidized to adenosine triphosphate (ATP) via the TCA cycle and mitochondrial oxidative phosphorylation. Prolonged fasting promotes lipolysis of triglycerides (TGs) in

Introduction

adipocyte lipid droplets (LDs) to glycerol and fatty acids (FAs) by adipocyte lipases (4, 25).

Short and medium-chain non-esterified fatty acids (NEFAs) enter into the hepatocyte cytosol, via protein-mediated FA translocases or FA-binding proteins. NEFAs are then converted to fatty acyl coenzyme A (CoA) molecules by acyl-CoA synthetase. Fatty acyl-CoA is transported across the outer mitochondrial membrane by carnitine palmitoyltransferase I to form fatty acyl-carnitine, which is then transported across the inner membrane into the mitochondrial matrix by carnitine acyl translocase to be converted back to fatty acyl-CoA by carnitine palmitoyltransferase II, which is now ready for oxidation. In β -oxidation, fatty acyl-CoA molecules are broken down by the removal of two carbons to form acetyl-CoA, which then enters the TCA cycle to produce ATP (Figure 2). In addition to hepatocytes, β -oxidation also occurs in adipocytes and muscle cells (30).

When excessive acetyl CoA is produced by FA oxidation and the TCA cycle is overloaded, acetyl CoA is diverted to ketone bodies, including acetoacetate, 3-hydroxybutyrate and acetone, which serve as a fuel source when glucose levels are too low during prolonged starvation. This process takes place in the mitochondria of hepatocytes (31, 32).

Introduction

As for the glycerol molecules, they undergo gluconeogenesis to produce glucose or they are involved in glycolysis to produce ATP (4, 25, 30).

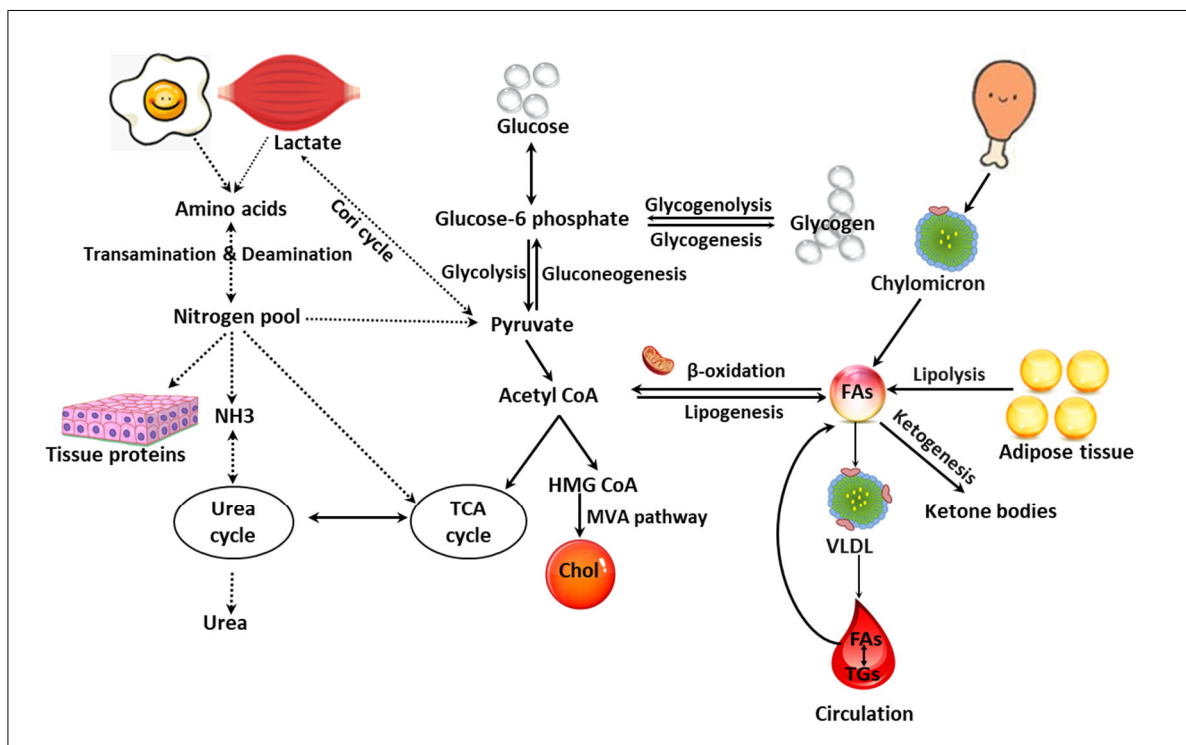


Figure 2. Metabolic functions of hepatocytes.

Lipids Synthesis

Lipids are heterogeneous hydrophobic or amphipathic molecules (33) that serve as building blocks for cell membranes, energy storage, cellular signaling and hormone precursors. The maintenance of lipid homeostasis requires the coordination of lipid uptake, distribution, storage and utilization in cells and organs (33).

- o **Fatty acids (FAs):** Long hydrocarbon chains with a carboxyl group. The carbon chain is linked by double bonds, as in unsaturated FAs, or by single bonds, as in saturated FAs. Hepatic FAs are derived from the diet (15-30%) or are released from adipocytes during fasting and transported to the liver or via de novo lipogenesis (DNL) in the cytoplasm of hepatocytes (almost 30% during feeding) by the addition of two-carbon units to acetyl-CoA derived from carbohydrate glycolysis (34). Long-chain FAs are then incorporated into triacylglycerols (TAG), phospholipids and cholesterol esters and then secreted into the

circulation as very low-density lipoprotein (VLDL) particles, oxidized in mitochondria or stored in membrane structures and LDs (34).

- **Triglycerides (TGs) (triacylglycerol, (TAGs)):** TGs are synthesized in the ER of hepatocytes by esterification of three FAs to a glycerol molecule. These lipids act as transporters of FAs and as a source of ATP (34). 60-80% of hepatic TG is derived from circulating NEFA, while around 25% is derived from increased DNL. When catabolized to FAs and glycerol, both products serve as substrates for ATP production and metabolic pathways (34).
- **Phospholipids (PLs):** PLs contain a phosphate group and two hydrophobic tails derived from two FAs esterified by a glycerol molecule. These lipids are synthesized at high levels in the ER of hepatocytes via a complex and multi-branched process initiated by the condensation of two molecules of acyl-CoA with glycerol to form phosphatidic acid, the precursor of all phospholipids. PLs maintain the permeability barrier of membranes and serve as a support matrix for membrane-associated proteins and as a surface for many catalytic processes in addition to signal transduction (34).
- **Cholesterol (Chol):** a sterol alcohol. Approximately 70% of its content is obtained by endogenous synthesis, mainly in the cytoplasm and smooth ER (SER) of hepatocytes and in the intestine, while the rest is obtained from the diet (35-37). Lipid synthesis starts with acetyl-CoA (37, 38) Hepatic Chol is packaged with LPs and made available to the rest of the body. The rest is excreted in the bile as Chol or after conversion to bile acids (4). Chol forms the backbone of steroid hormones and vitamin D analogues. It also stabilizes cellular plasma membranes and regulates membrane fluidity and permeability for gene transcription (39).
- **Lipoproteins (LPs):** LPs are complexes of lipids and apolipoproteins (34, 40) that are synthesized in the cytoplasm of hepatocytes and enterocytes (5). LPs function to transport lipids in the circulation. The major lipids transported by LPs are Chol, TGs and phospholipids. The structure of LPs

Introduction

includes a nucleus and a cortex. The nucleus contains esterified Chol and TGs, whereas the cortex contains phospholipids, non-esterified Chol and apolipoproteins (34, 40):

- Chylomicrons are the largest and least dense LPs with a density of less than 1,000 g/ml and are highly enriched in TGs. They contain several apolipoproteins, including APOB-48, APOA1, APOC2, APOC3 and APOE. These LPs originate in the intestine and transport TGs to adipocytes and muscle cells.
- Very low-density lipoproteins (VLDLs) are large LPs with a density of less than 1,006 g/ml, highly enriched in TGs, with an apolipoprotein composition similar to that of chylomicrons, but lacking APOA1 and expressing APOB100 instead of APOB-48. VLDL transports TGs from the liver to adipocytes and muscle cells. VLDL metabolism produces low-density lipoprotein (LDL) and intermediate-density lipoprotein (IDL).
- Intermediate-density lipoproteins (IDLs) are a smaller group of lipoproteins with a density of less than 1.019 g/ml and greater than 1.006 g/ml and an apolipoprotein composition similar to VLDL, but smaller in size, with fewer TGs and containing APOE. Half of IDLs are captured by hepatic receptors that recognize APOE, while the rest are further processed to become LDLs.
- Low-density lipoproteins (LDLs) have a density of less than 1.063 g/ml and greater than 1.019 g/ml. They contain APOB100 and cholesteryl esters as their major lipid component, and function to transport Chol to peripheral tissues and hepatocytes.
- High-density lipoproteins (HDLs) have a density of less than 1.21 g/ml and greater than 1.063 g/ml. The LP contains APOA-I and Chol esters, and functions to transport Chol from peripheral tissues to hepatocytes where it is secreted into the bile as free Chol or bile salts via reverse Chol transport (40, 41).

Lipid Droplets

In the 1890s, LDs were defined as fat droplets inside cells (42). In 1991, these droplets were defined as organelles containing proteins involved in lipid and LDs homeostasis (42). LDs are now known as lipid-rich cytoplasmic organelles (43, 44) consisting of a hydrophobic core of neutral hydrophobic lipids, predominantly TAG and sterol esters, surrounded by a polar PL monolayer (33, 45) that acts as a surfactant between the hydrophobic core and the hydrophilic aqueous plasma or cytosol. Embedded within this monolayer are heterogeneous sets of proteins and enzymes responsible for neutral lipid metabolic reactions, membrane trafficking and protein degradation (33, 45-47). Proteins access the LD surface by relocalization from the ER bilayer or from the cytosol (42).

LDs Formation

LDs are formed by lipogenesis from the ER by means of acyltransferases (45, 48, 49) in three steps (Figure 3):

- **Lens formation:** Neutral lipids aggregate due to thermal fluctuations and electrostatic interactions with integral membrane proteins or lipids (66). Once the accumulated lipids reach a critical concentration, cytoplasmic distension of the outer leaflet of the ER bilayer occurs, followed by the formation of an oil lens (50, 51). No enzyme is directly linked to lens formation (44), but perilipin3 (PLIN3) binds and stabilizes nascent lenses (51).
- **Drop formation:** the oil lens grows and deforms the ER bilayer membrane until it reaches a critical size that triggers budding of mature LDs into the cytoplasm (51, 52) via a dewetting pathway. The nascent droplet may remain attached to the ER or be completely shed (51). This step is promoted by fat storage-inducing transmembrane 2 (FIT2) (44, 51) and it is dependent on the level of TGs in the ER bilayer, with the LD lens being formed when the level of TGs is between 5-10 mol% (46). Seipin is required for the correct budding of LDs (44) and facilitates their initial growth (51).
- **Fusion processes:** initially, almost all cell types form small droplets with a diameter of 300-800 nm, called initial LDs (iLDs) (53). Later during LD formation, some iLDs are transformed into larger ones, called expanding

Introduction

LDs, with a diameter greater than 1 μm (54). LDs in hepatocytes and adipocytes can be up to tens of μm in diameter and are therefore known as giant or supersized LDs (42). These droplets are formed by fusion processes including ripening, where neutral lipids from one LD diffuse into a larger LD (47, 55, 56) or by rapid fusion of LDs in a process called coalescence (56), although this process is rare due to the presence of phosphatidylcholine (PC) on the surface of LDs, which acts to reduce surface tension and stabilize LDs against coalescence (44, 57). Among the enzymes required for the fusion process, CTP: phosphocholine cytidyltransferase- α maintains phospholipid homeostasis, while the coat protein, COPI, facilitates the fusion of LDs (44).

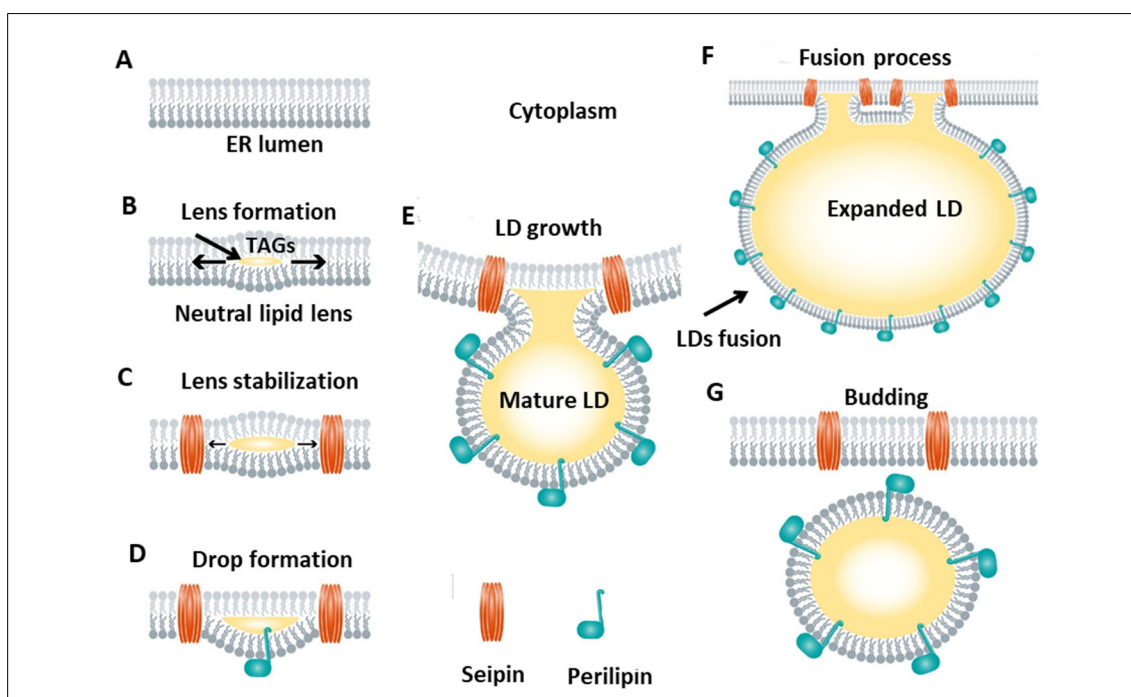


Figure 3. The process of LD formation. Figure was adapted from (50).

LDs Breakdown

- **Lipolysis:** LDs are broken down by lipolysis mediated by cytosolic neutral lipases (58), which removes one FA at a time from the glycerol backbone of the TAG stored in the LDs (Figure 4). First, TAG is hydrolyzed to diacylglycerol (DAG) and NEFA by adipose triglyceride lipase (ATGL), which is the rate-limiting enzyme of lipolysis. The DAG is then hydrolyzed to monoacylglycerol (MAG)

Introduction

and NEFA by hormone-sensitive lipase (HSL). The MAG is finally hydrolyzed to glycerol and NEFA by monoacylglycerol lipase (MAGL) (59, 60).

- Lipophagy: LDs are degraded by bulk microlipophagy, in which lysosomes directly engulf LDs, or by selective autophagy (45, 61, 62), in which a specialized autophagic membrane called phagophores is formed around LDs, called autophagosomes, which selectively target LDs for degradation in lysosomes (63) (Figure 4). Subsequent transfer of lysosomes to the autophagosome results in lipid degradation by acid lipases (42, 45, 58).

The morphology of LDs influences their degradation pattern; lipolysis targets large LDs, whereas autophagy targets small LDs with a diameter of less than 1 μm (64). Furthermore, reduced autophagy leads to the accumulation of small LDs (64).

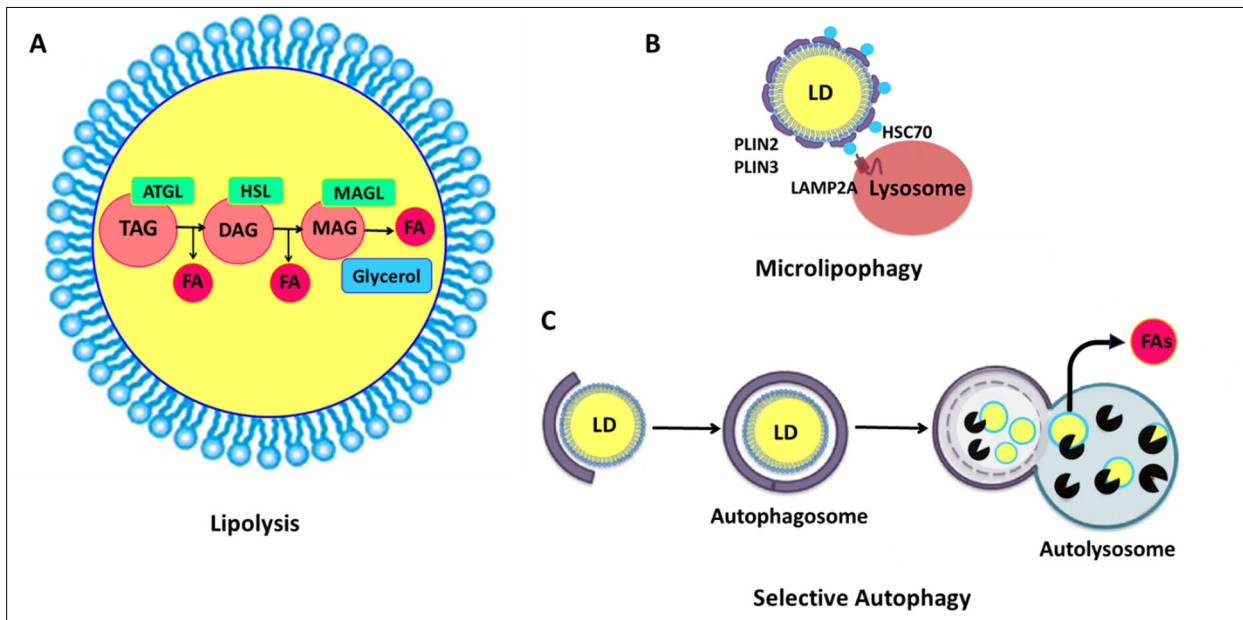


Figure 4. LDs Breakdown. LDs lipolysis (A), Microlipophagy (B), Selective Autophagy (C). B & C were adapted from (60).

LD Functions

Metabolic Homeostasis and Stress Management: LDs store neutral lipids essential for energy metabolism (65) and can adapt their size, abundance, lipid composition and organelle interactions according to metabolic changes (33). Degradation of TGs by lipolysis or autophagy provides essential FAs for membrane synthesis (46) and for energy production (45). Meanwhile, TG biosynthesis and aggregation in LDs prevents excessive lipid accumulation and

protects against hepatotoxic FAs (51) and ER stress (65). During hypoxia, ischemia or stress, and in response to aberrant FAs oxidation or accumulation, hepatic FAs move from the cytoplasm to the LDs to provide as little energy as possible to reduce consumption, which then limits oxidative stress (55, 65-67). During fasting, LDs undergo lipid catabolism via lipolysis and lipophagy to provide FAs for β -oxidation (68, 69). In the fed state, LDs catabolism prevents lipid accumulation (42). LDs also reduce the damage caused by reactive oxygen species (ROS) by scavenging 4-hydroxynonenal, a product of lipid oxidation that causes protein damage, from the cell membrane (70).

- Cellular detoxification of endogenous or exogenous lipid-soluble compounds (65).
- Accumulation of intercellular signaling precursors, such as steroid hormones and FA signals (65).
- In LDs, cyclooxygenase (COX)-2 promotes the synthesis of prostaglandin E₂ (PGE₂), which acts as an immunosuppressive factor against T-cells. High LD levels are associated with high PGE₂ synthesis (70).
- Synthesis of phospholipid monolayers through the accumulation of monoalk(en)yl diacylglycerol as an ether phospholipid precursor (65).
- HSCs LDs store 70-80% of vitamin A (retinol), while smaller amounts are stored in hepatocyte LDs (65).

Non-Alcoholic Fatty Liver Disease

The terminology of metabolic syndrome (MetS) encompasses several correlated metabolic alterations implying hepatic inflammation, insulin resistance, overproduction and secretion of VLDL, reduced clearance of TG-rich lipoproteins (TRLs), hypertriglyceridemia, increased NEFAs and dyslipidemia (71). Non-alcoholic fatty liver disease (NAFLD) is the most chronic liver disease (72) characterized by steatosis, in the absence of alcohol consumption or the use of steatogenic drugs (73) and is determined by estimating the proportion of hepatocytes containing LDs (74). Steatosis is characterized by the accumulation of significant amounts of neutral lipids, typically TAG and Chol esters in more than 5% of hepatocytes (45, 75). Pathologically, steatosis is classified as microvesicular steatosis, in which small LDs accumulate while cellular

architecture is preserved. This contrasts with macrovesicular steatosis, in which larger droplets displace the cell nucleus (76).

The global prevalence of NAFLD is currently estimated to be 24% (77). About 90% of NAFLD patients have more than one aspect of MetS, while about 33% have three or more aspects (78). Two primary components of MetS including glucose and TGs are overproduced in NAFLD and both share a similar background of low-grade chronic inflammation (78). Due to the close association of NAFLD with MetS, the increasing tendency of MetS is expected to cause an increasing tendency in NAFLD incidence (79, 80). Consequently, in 2020, a consensus of twenty-two countries redefined NAFLD as metabolically associated fatty liver disease (81).

The Pathogenesis of Non-Alcoholic Fatty Liver Disease

Insulin Resistance

Insulin normally inhibits the production of VLDL. Once impaired, with unchanged VLDL clearance, this results in hypertriglyceridemia and low HDL levels (82, 83). Chronic hyperinsulinemia also stimulates hepatic DNL (84) and NEFA uptake from plasma and adipocytes and a dysregulation of intracellular lipid partitioning in which oxidation of NEFAs is impaired and their esterification is enhanced (85, 86). The excess NEFAs mediate the hepatic inflammatory response and increased insulin resistance, hepatic glucose and VLDL production, and lipolysis of adipocyte TG stores (78, 87).

Alteration of Lipid Homeostasis

- Hepatic TG accumulation is caused by an imbalance in FA delivery to hepatocytes, lipid synthesis, TG oxidation and transport from hepatocytes in the form of VLDL (31, 33, 88). Both VLDL secretion and β -oxidation are increased in the early stages of NAFLD to compensate for the high influx of FAs into the hepatocytes. If the influx is sustained, lipotoxicity will result (30)
- Formation of very large LDs in hepatocytes is the hallmark of NAFLD and is primarily caused by LD-localized triglyceride synthesis (54) by flux of dietary, hepatocyte and adipocyte FAs (42) exceeding their lipid storage capacity (85, 89), in conjunction with LD biogenesis or growth, or due to

Introduction

decreased LD catabolism by reduced FA oxidation or by decreased mobilization of TGs or impaired TG or VLDL secretion, defective lipolysis or lipophagy, or fusion (42).

- Catabolism of TGs and other esterified neutral lipids from LDs generates metabolites that alter cell homeostasis, leading to organelle dysfunction, cell injury, dysfunction and ultimately death (46).
- Excessive lipolysis and lipophagy lead to lipid overload and cell damage by increasing NEFAs and altering signaling pathways involved in oxidative metabolism and membrane homeostasis (90, 91).
- During ER stress, cytosolic Ca^{2+} accumulation inhibits LD lipophagy by down-regulating autophagosomal fusion, resulting in ubiquitinated proteins and LD accumulation, which increases ER stress and ROS production (92, 93), leading to hepatic inflammation and NAFLD progression (46).

Oxidative Stress

The hepatocyte contains between 500-4000 mitochondria, occupying 18% of the cell volume (94). Mitochondria are essential for ATP production, β -oxidation, ROS production (95-97) (superoxide anion radicals and hydrogen peroxide) (98), inflammasome activation and apoptotic response (99).

In general, oxidative stress is caused by an imbalance between ROS production and the scavenging capacity of the antioxidant defense system (100). This pathway is triggered by increased production of pro-oxidant products, dysfunction of the antioxidant system (100), and lipid accumulation in hepatocytes, which affects metabolic organelles, leading to lipotoxicity, lipid peroxidation, chronic ER stress, and mitochondrial impairment (101). The latter also induces ROS production (102). High levels of ROS cause oxidative modifications to nucleic acids, lipids and proteins involved in lipid metabolism, insulin signaling and inflammation. The accumulation of these damaged macromolecules is a major factor leading to the inflammation and fibrogenesis involved in the progression of NAFLD (103-105).

Progression of Non-Alcoholic Fatty Liver Disease

Depending on pathogenesis, NAFLD can be primary or secondary. Primary NAFLD is associated with abnormalities in carbohydrate and lipid metabolism (78, 83, 106, 107). In secondary NAFLD, the liver becomes an ectopic site of lipid storage for reasons other than MetS, including chronic use of steatogenic drugs, viral infections, endocrine disorders, parenteral nutrition, inherited conditions or surgery (107-110). As highlighted by the "two-hit hypothesis", NAFLD includes a broad histological spectrum of liver damage ranging from simple macrovesicular steatosis to non-alcoholic steatohepatitis (NASH), advanced fibrosis, cirrhosis (83) and malignancy (111) (Figure 5). The "first hit" is lipid load and IR as risk factors for steatosis. The "second hit" is induced by oxidative stress, mitochondrial dysfunction, lipid peroxidation, pro-inflammatory cytokines and adipokines causing hepatocyte injury, inflammation and fibrosis (78, 83).

Non-alcoholic steatohepatitis (NASH)

Approximately 20-30% of NAFLD patients progress to irreversible NASH (112). NASH is a severe and chronic mixed hepatic inflammation and cellular infiltration and ballooning degeneration of hepatocytes, with or without fibrosis (77), ultimately leading to cirrhosis, end-stage liver failure and hepatocellular carcinoma (HCC) (112). Ballooning hepatocytes that characterize NASH are apoptotic, swollen and enlarged cells with dilated ER and clear, flocculent, non-vacuolar, ballooning cytoplasm (113-116), substantial accumulation of LDs, cytoskeletal damage with Mallory-Denk bodies and parenchymal lesions (46).

Prolonged lipid overload leads to adipocyte insulin resistance (IR) and systemic inflammation. Together with ectopic lipid accumulation, this leads to IR in the liver and muscle. IR causes an imbalance in glucose and lipid homeostasis. As a result, more NEFAs are released from adipocytes into the circulation (60% of total lipids). At the same time, dietary carbohydrates are converted to NEFA by DNL (40% of total lipids). NEFA overload overwhelms the mitochondria, leading to mitochondrial uncoupling and ROS production. The prolonged and uncontrolled stimulation of ROS production leads to a pro-inflammatory response in addition to apoptosis and thus to NASH. Kupffer cells

Introduction

take up large amounts of NEFA, triggering an inflammatory response that activates the immune system via Kupffer cells for phagocytosis and inflammatory cells, including infiltrating macrophages, T lymphocytes, neutrophils and dendritic cells (DCs), culminating in the secretion of cytokines such as interleukins (IL-6 and IL-10) and tumor necrosis factor (TNF)- α have been implicated in the progression of NASH (73).

Fibrosis

Approximately 25-33% of NAFLD patients (117) and 30-50% of steatohepatitis patients develop fibrosis. Fibrosis is an abnormal proliferation of connective tissue in the liver (118). Chronic inflammation in NASH activates hepatocyte death and apoptosis, which triggers signals including nucleic acids, intracellular proteins and ATP molecules, thereby activating hepatic progenitor cells (HPCs). At the same time, apoptotic bodies are phagocytosed by HSCs and Kupffer cells, inducing a pro-fibrogenic response. Nucleic acids from apoptotic hepatocytes activate the immune response via Toll-like receptor (TLR)-9 on HSCs and collagen production. Immune cell infiltration activates the trans differentiation of HSCs into collagen-producing myofibroblasts, leading to the production and accumulation of ECM, followed by fibrous scar formation (73, 119). Advanced fibrosis is associated with a high risk of liver-related mortality, vascular disease and non-hepatic malignancies (120, 121).

Cirrhosis

Approximately 5-15% of NAFLD patients progress to cirrhosis (46) and 9-25% of NASH patients develop cirrhosis within 10-20 years (122). Cirrhosis is characterized by the transformation of normal architecture into nodules of regenerating hepatocytes with reduced blood supply. Long-term fibrogenesis leads to encapsulation of injured hepatocytes by a collagenous scar that separates hepatocytes from the central vein, creating islands of hepatocytes. In addition to vascular changes, including loss of sinusoidal fenestrae and appearance of basal membrane. These changes increase the intravascular resistance within the portal system and decrease hepatic perfusion. Overall, this leads to a loss of liver function (73).

Hepatocellular Carcinoma (HCC)

HCC is the fifth most common cancer and the third leading cause of cancer-related deaths worldwide (123, 124). In NAFLD, around 2-5% progress to HCC (46), while cirrhosis remains a major risk factor for the development of 13% of HCCs (125, 126). Hepatocarcinogenesis involves chronic inflammation, p53 inactivation, oxidative stress and telomere shortening, which cause genomic instability and activate various oncogenic signaling pathways (127). The process mediating the interaction between NAFLD and HCC is not fully understood, but essentially lies in the second hit, allowing progression from steatosis to cirrhosis (128, 129). The deposition of ECM in fibrosis modulates multiple signaling pathways by binding directly to specific receptors or by forming complexes with ligands that enhance their activity and promote binding to their receptors (130), ultimately stimulating the growth and survival of transformed cells (131). In addition, elevated leptin levels (132) lead to angiogenesis and vascular invasiveness (133).

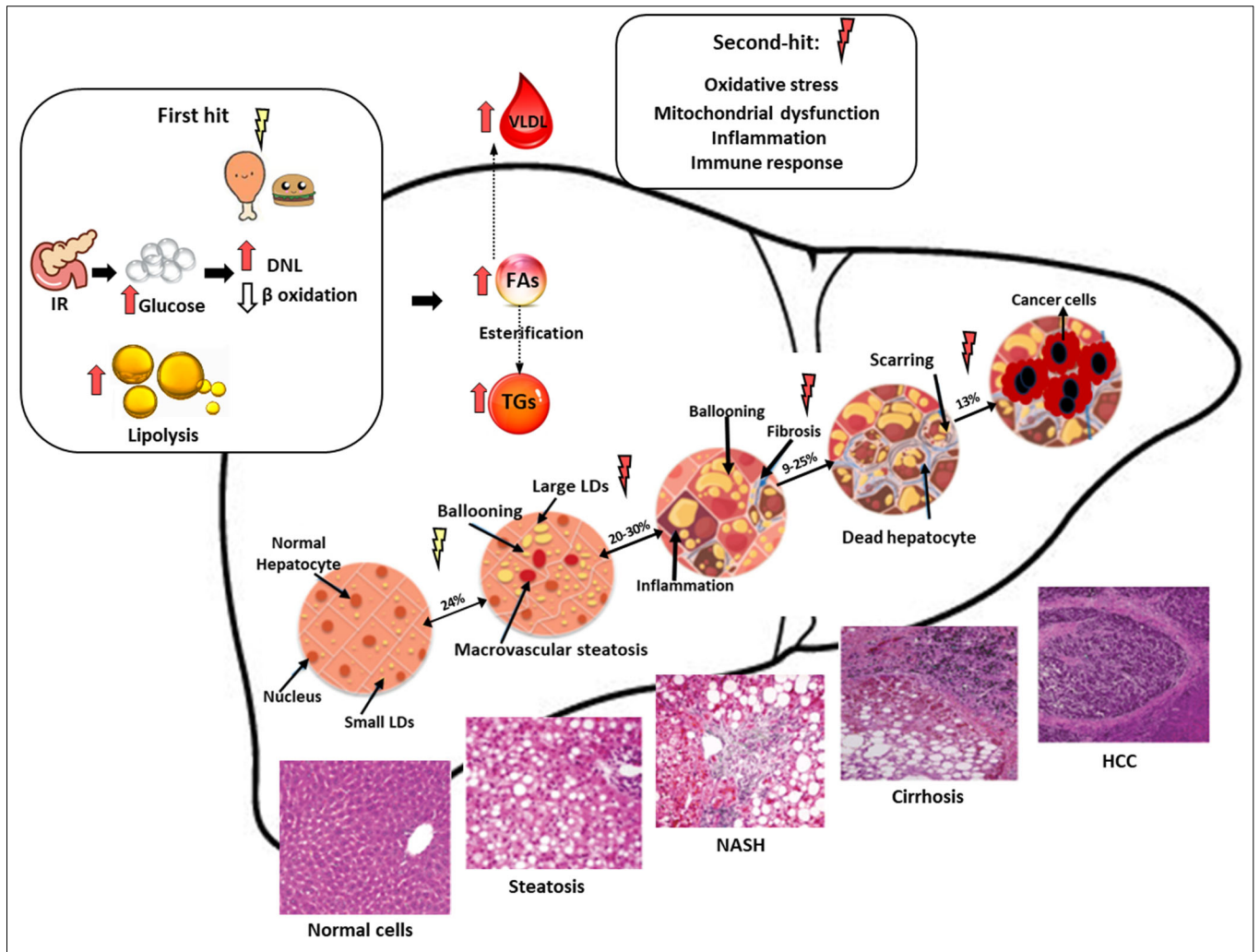


Figure 5. Progression of NAFLD from Steatosis to HCC. Adapted from (102, 134-136).

The Mediterranean Diet

The Mediterranean diet (MD) is a dietary model that originated in the early civilizations around the Mediterranean Sea. The MD is a plant-based diet, rich in olive oil, especially virgin and extra virgin olive oil, as the main source of lipids, together with nuts, and fiber, mainly from vegetables, whole grains, legumes and fruits, with a high intake of fish and seafood, and limited red meat, processed meat, dairy products, sweets and wine (137-141) (Figure 6).

Introduction

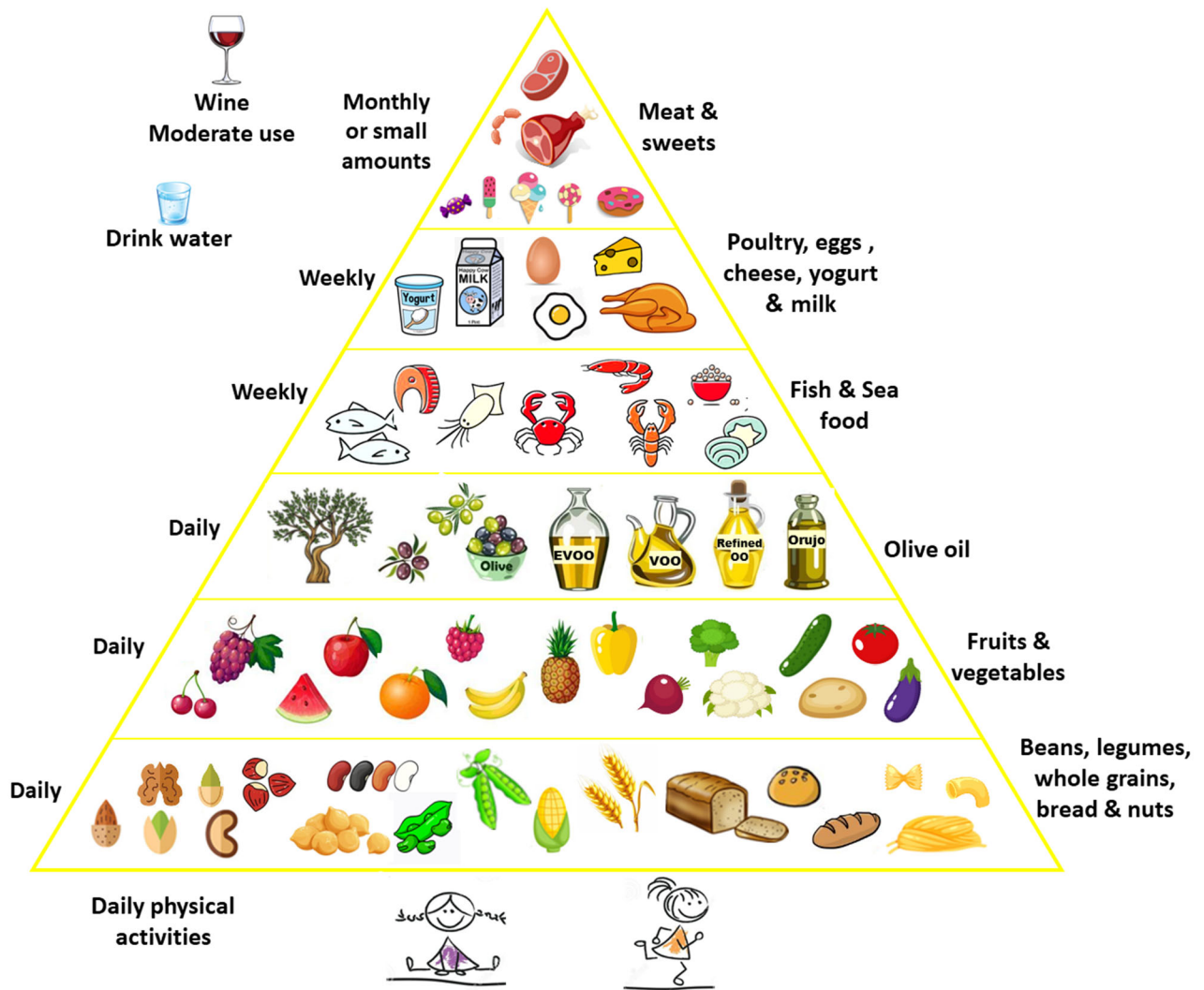


Figure 6. The Mediterranean Diet Pyramid.

The diet has attracted the attention of researchers by demonstrating widespread health benefits, starting with Ancel Keys' seven-country study in Finland, Greece, Italy, Japan, the Netherlands, the United States and Yugoslavia in the 1960s. This study showed a significant reduction in the risk of cardiovascular disease in people living in Greece and in certain parts of Italy and Yugoslavia compared with other populations in response to dietary patterns (141-144).

Since then, numerous studies have demonstrated the health-promoting effects of MD on a wide range of chronic metabolic disorders, including type 2 diabetes (145-147), hypertension (148), obesity (145), NAFLD (149), and cancer (150, 151), thereby increasing longevity (139). These effects are attributed to the anti-inflammatory, antioxidant and lipid-lowering properties of the dietary components (140, 152-154). The main characteristics of MD are a high lipid content of 36-40% of total energy intake (TEI),

Introduction

consisting of a high proportion (19-25%) of monounsaturated fatty acids (MUFA) to a low proportion (7-10%) of saturated fatty acids (SFA), and a balanced proportion (3-6%) of polyunsaturated fatty acids (PUFA) with an adequate ratio of omega-3 to omega-6 fatty acids. Carbohydrates and proteins, which make up 35-40% and 15-20% of the TEI respectively, and a high fiber content (137, 155), together with a low intake of water, nitrogen and carbon (139). The low intake of saturated fats reduces plasma total Chol, LDL and TG (140).

The high MUFA content and balanced omega-6/omega-3 (ω_6/ω_3) PUFA ratio are based on a high intake of vegetables, legumes, nuts, olive oil and fish instead of red meat (140). EVOO is the main source of MUFA and fish is the main source of ω -3 PUFA (155). MUFA intake inhibits metabolic risk factors by reducing lipid accumulation, including the proportion of lipids in NAFLD (156), and by reducing postprandial adiponectin expression, thereby reducing hepatic glucose production (140). PUFA regulate key transcription factors in hepatic carbohydrate and lipid metabolism via activation of hepatic peroxisome proliferator-activated alpha (PPAR α), which is involved in FA oxidation, and inhibition of sterol regulatory element binding protein-1 (SREBP-1) and carbohydrate regulatory element binding protein (ChREBP)/Max-like factor X (MLX), thereby suppressing glycolysis and DNL. As such, PUFA promote a shift in metabolism towards the oxidation of FAs and away from the synthesis and storage of FAs (140). PUFA also activate an anti-inflammatory response by suppressing TNFs and IL-6 (140). This is in contrast to ω -6 PUFA, which have pro-inflammatory functions by regulating the production of inflammatory cytokines (140). Vitamins and phenolic compounds found in whole grains, vegetables and fresh fruit, olive oil, nuts and red wine have anti-inflammatory and antioxidant effects (140). Water-soluble fiber, mainly from vegetables, whole grains and legumes, increases the rate of bile excretion and reduces serum total and LDL Chol (140).

Extra Virgin Olive Oil

The olive tree (*Olea europaea* L.) is a small tree that was first cultivated in Asian countries 6000 years ago. Later it spread to all continents, but Mediterranean countries remained the main olive producers, led by Spain, Italy and Greece, which produce about 70% of the world's olives (144). Extra virgin olive oil (EVOO) is extracted mechanically

by washing, decantation, centrifugation and filtration under thermal conditions that do not modify the oil's composition. EVOO content varies according to the genotypic characteristics of the plant, olive variety, ripeness of fruit, time of harvest, environmental factors, agricultural factors, and the conditions of extraction and storage. EVOO, as pure fruit juice, is considered the highest quality oil, with acidity ≤ 0.8 g per 100 g (141, 144). The health properties of EVOO are derived from its unique composition; as lipid profile and bioactive compounds (144).

Olive pomace oil also named Orujo olive oil (acidity ≤ 1 g per 100 g (144)), is a blend of refined oil from olive residues (pomace oil) and virgin olive oil obtained by centrifugation process (157, 158). The oil is a good dietary source of triterpenic compounds and has anti-inflammatory (158) and lipid-lowering effects (159).

Main Components of EVOO (the Saponifiable Fraction)

TAGs make up a high percentage of the saponifiable fraction of EVOO. FA make up 97-99% of lipids and 65.2-80.8% are MUFA (144), particularly oleic acid, which makes up 49-83% of total FA (160) and is correlated with EVOO acidity. Low acidity ensures a high-quality oil produced from healthy fruit under ideal conditions (141, 144). PUFAs make up about 14% of the oil composition (144). The PUFA content is mainly linoleic acid (18:2 ω -6) (6.6-14.8% total FA) and α -linolenic acid (18:3 ω -3) (0.46-0.69% total FA) (144, 160). About half of the total TAG in EVOO is oleic-oleic-oleic, in addition to palmitic-oleic-oleic, oleic-oleic-linoleic, palmitic-oleic-linoleic and stearic-oleic-oleic. DAGs and MAGs are present in concentrations of 1-2.8% and 0.25% respectively (144).

Minor Bioactive Compounds (the Unsaponifiable Fraction)

The minor components of EVOO account for 1-3% of its composition (144). These include hydrocarbons, phytosterols, triterpenes, phenolic compounds and tocopherols, among others (141, 144).

With regard to hydrocarbons, squalene accounts for more than 90% of hydrocarbons and is the most abundant compound in the unsaponifiable matter, ranging from 200 to 7500 mg/kg of oil, while β -carotene pigment accounts for 0.15-0.67 mg/kg of oil (144).

Introduction

The total phytosterol content of EVOO varies between 1000 and 2000 mg/kg. β -Sitosterol is the main sterol fraction with values between 75-90%, while Δ^5 -Avenasterol is between 5-20% (144).

Triterpenes represent a primary fraction and are divided into dialcohols and triterpenic acids (141). The most important dialcohols are erythrodiol and uvaol (141, 144). Both make up 0.9-2.8% of the total sterol fraction (144). Triterpenic acids include oleanolic (17-344 mg/kg) and maslinic (19-250 mg/kg), with traces of ursolic acid, compared to higher levels in olive pomace oil (141, 160)

Phenols are hydrophilic compounds present in the range of 50-1000 mg/kg of oil and include hydroxytyrosol, oleuropein and tyrosol. Phenols impart aroma and flavor to EVOO (144). In pomace oil, this fraction is lost through chemical processes (161).

Tocopherols (vitamin E) are methylated phenols. α -tocopherol accounts for more than 90% of tocopherols (156), ranging from 191.5 to 292.7 mg/kg compared to 10 mg/kg, 20 mg/kg of β -tocopherol and γ -tocopherol (144).

Biological Features of EVOO

EVOO reduces risk factors for MetS, including type 2 diabetes and NAFLD, by suppressing lipogenic, ROS and pro-inflammatory genes and by reducing levels of IL-6, TNF- α and C-reactive protein (CRP) (144). A dose of 20 g/d may reduce the degree of fatty liver (156). EVOO also has atheroprotective properties. A dose of 10-50 ml/day reduces diastolic blood pressure by up to 0.73 mm Hg. In addition to antimicrobial, anti-tumor and anti-cancer properties. Oil consumption is inversely associated with any pattern of carcinogenesis (34% lower risk with EVOO consumption) (144).

For MUFAs, oleic acid promotes pancreatic cell secretion and bile secretion in hepatocytes (160). It also improves blood pressure, carbohydrate, lipid and LP metabolism, and has anticoagulant, anti-inflammatory and antioxidant effects (160).

Among PUFAs, linoleic acid and linolenic acid are crucial elements in cell structure (160). Linoleic acid reduces LDL (144) but is metabolized to arachidonic acid, which has proinflammatory, prothrombotic and pro-aggregatory properties. On the other hand, α -linolenic acid is metabolized to eicosapentaenoic acid and docosahexaenoic acid and both metabolites modulate hepatic lipid composition, increase anti-inflammatory mediators and decrease IR (156). Therefore, the ω 6/ ω 3 PUFA ratio protects against

Introduction

autoimmune and inflammatory diseases (144), together with β -oxidation, tipping the balance towards DNL (156). In addition, oleanolic acid, maslinic acid and dialcohols have anti-inflammatory, anti-diabetic, hypolipidemic, hepatoprotective, anticancer, antiviral, antimicrobial and antifungal properties (141, 160).

β -Sitosterols are effective in reducing total and LDL Chol levels, and stimulating apoptosis of cancer cells (160).

Tocopherols are important natural lipophilic antioxidants (162, 163). These compounds modify the expression of homeostatic genes involved in the prevention of lipid peroxidation (160) and protect against inflammatory and oxidative processes (144, 160), including degenerative diseases and cancer (160), in addition to antimicrobial and antitumor effects.

Phenolic compounds reduce Chol, LDL, HDL, lipopolysaccharides and pro-inflammatory factors such as CRP and IL-6 (144), in addition to strong antioxidant and free radical scavenging activity (141). Phenolics and tocopherols are responsible for olive oil's oxidative stability (164). Carotenoid pigments are precursors of vitamin A and have antioxidant and anti-cancer properties (160).

Essential Minor Bioactive Compounds

Squalene

Squalene (2,6,10,15,19,23-hexamethyl-6,6,10,14,18,20-tetracosahexane, $C_{30}H_{50}$) (Figure 7), is a polyunsaturated linear terpenoid with six double bonds (165-168) and a molecular mass of 410.3913 (166, 169). The double bonds allow squalene to exist in various conformations, including symmetrical, stretched and coiled forms (170), in addition to the sterol form, which allows it to be accommodated in membranes (165).

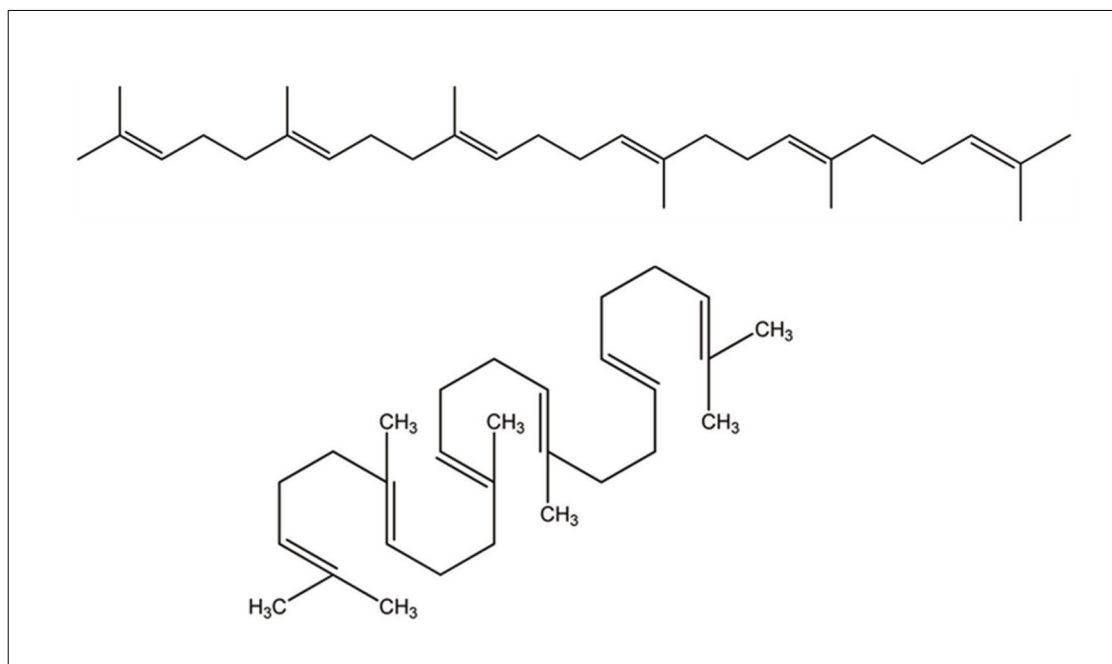


Figure 7. Squalene chemical structure. Adapted from (171).

Squalene was discovered in 1916 by the Japanese scientist Mitsumaru Tsujimoto, who described the compound as highly unsaturated and named it after the genus of shark from which it was extracted (*Squallus* spp, *Centrophorus squamosus*) (172, 173).

Squalene is highly abundant in shark liver oil, where it constitutes almost 40-70% of the oil weight (174), but the intense fishing for this isoprenoid and the presence of organic pollutants, including organochlorine pesticides, polycyclic hydrocarbons, dioxins and heavy metals, have provided compelling motivation to search for alternative sources of squalene, particularly from the plant kingdom (165, 168, 175). Among the plant sources, detectable amounts of squalene are found in wheat germ and rice bran oils (0.1-0.7% of oil content) (176), as well as in palm oil, soybean oil (9.9 mg/100 g), grape seed oil (14.1 mg/100 g), peanut (27.4 mg/100 g), maize, amaranth (5942 mg/100 g) and olive oil (564 mg/100 g) (165, 177).

In EVOO, squalene is present at a concentration of 1.5 to 10.1 g per kg, depending on the variety, agronomic issues such as region, climate, crop, harvesting method and olive processing (166). Where consumption of EVOO is high, such as in Mediterranean countries, intake of squalene is increased to 200-400 mg/day (178).

In humans, squalene is secreted by the sebaceous glands and makes up 10-15% of the lipids at a concentration of 300-500 $\mu\text{g/g}$. The triterpenoid is also present in the liver

Introduction

and small intestine, but at much lower levels than in the skin (less than 75 $\mu\text{g/g}$) (172, 173, 179). The squalene content represents a balance between dietary intake and endogenous synthesis in the intestine and hepatocytes (180). Approximately 60-85% of dietary squalene is absorbed and distributed to the different tissues (181, 182). Exogenous and intestinal squalene is transported into the bloodstream by chylomicrons, followed by hepatic uptake for conversion to sterols and bile acids (182), or is re-secreted (183) together with hepatic-synthesized squalene into VLDL and LDL for distribution to various tissues (180). Endogenous squalene is synthesized via de novo mevalonate (MVA pathway) (184) in which acetyl-CoA is converted to 3-hydroxy-3-methylglutaryl coenzyme A (HMG-CoA) and then reduced to MVA by HMG-CoA reductase (HMGR), followed by phosphorylation and decarboxylation of MVA to isopentenyl diphosphate (IPP) and dimethylallyl diphosphate (DMAPP), accompanied by subsequent condensation with another IPP to form farnesyl pyrophosphate (FPP) (185-187). Squalene synthase (SQS) then combines two FPP molecules to form squalene (188-190).

The terpenoid is a structural and regulatory component of eukaryotic cell membranes and plays a key role as an intermediate in sterol metabolism (160, 165, 168), in which the cyclization of squalene via squalene epoxidase (SQLE) and lanosterol synthase (LSS) leads to lanosterol (191), followed by the enzymatic conversion of lanosterol to Chol via the parallel Bloch and Kandutsch-Russell (K-R) pathways (191) (Figure 8). The Bloch pathway consists of a subsequent side-chain of unsaturated intermediates ending in desmosterol, which is then reduced to Chol via 24-dehydrocholesterol reductase (DHCR24) (192), whereas the K-R pathway involves the reduction of the Δ^{24} bond of lanosterol and the conversion of dihydrolanosterol to Chol via 7-dehydrocholesterol reductase (DHCR7) using the same enzymes as in the Bloch pathway (193).

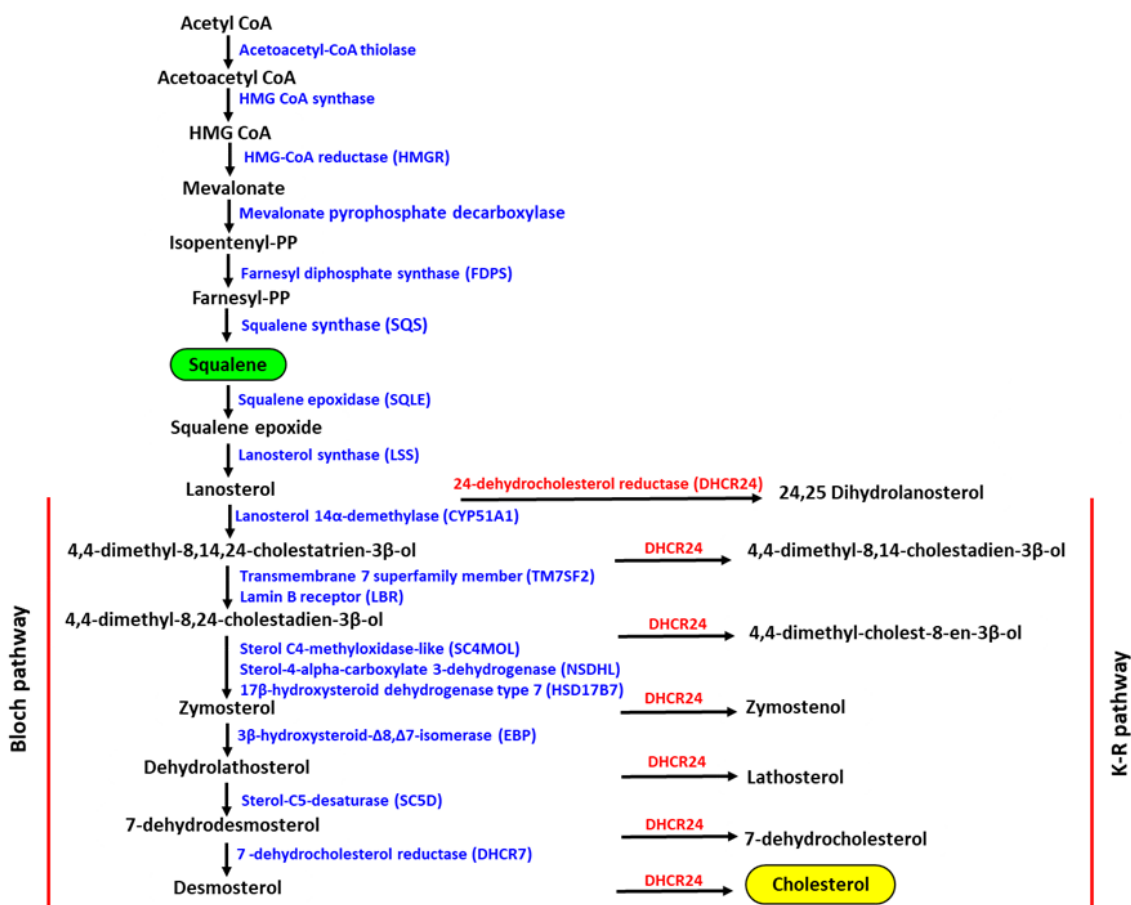


Figure 8. Bloch and K-R pathways in Chol biosynthesis.

The six double bonds in the isoprenoid structure protect cells from oxidative damage and microbial infection (177, 194). In the skin, squalene absorbs almost a quarter of its weight in oxygen, protecting against cutaneous flora and peroxidases (195), and reducing ultraviolet (UV)-induced nucleic acid damage (160).

In addition, squalene has anti-cancer activity by down-regulating HMGR towards Chol synthesis, as well as intermediate steps via MVA, where FPP is involved in the farnesylation and geranylgeranylation of proteins, including small guanosine triphosphate (GTP)-binding proteins such as Ras (196-198), by suppressing these proteins, which then inhibit the signaling involved in the proliferation and differentiation of malignant cells (168, 178, 199), or by regulating the metabolism of

Introduction

carcinogenic xenobiotics, or by preventing mutagenesis and carcinogenesis caused by nucleic acid oxidation by scavenging free radicals and ROS (178). Squalene may also inhibit NASH-related HCC (200, 201), which is interrupted by elevated cholesteryl ester concentrations.

Squalene also retains detoxifying activities via stimulation of hepatic P450 enzymes (202), together with the non-polar nature of the triterpene which provides an affinity for detoxification of non-ionized xenobiotics (194).

Erythrodiol

Erythrodiol (5 α -olean-12-ene-3 β , 28-diol, homo-olestranol, C₃₀H₅₀O₂) (Figure 9), is a pentacyclic triterpene with a molecular mass of 442.7.

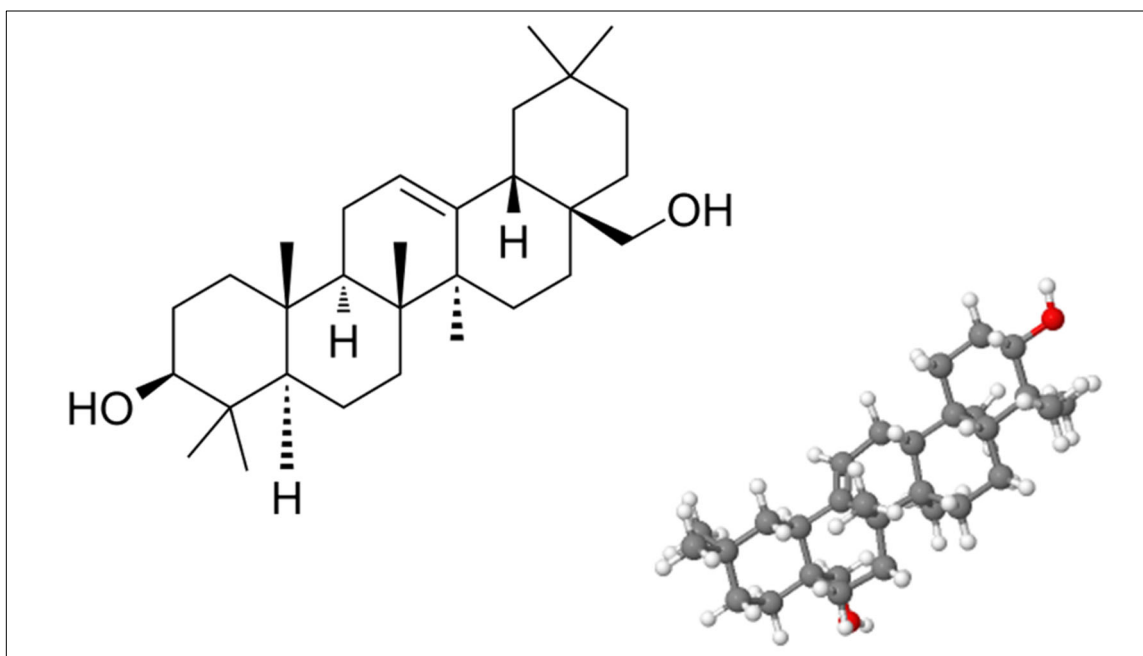


Figure 9. Erythrodiol chemical structure. Adapted from <https://chemfaces.com/natural/Erythrodiol-CFN98914.html> (<https://www.molinstincts.com/molar-mass/Erythrodiol-mowt-CT1001736412.html>)

In olive oil, the concentration of erythrodiol varies depending on the cultivation, quality and handling of the olive oil (161, 203) in a range of 26-90 mg/kg (204, 205), with higher levels in olive pomace oil (158, 161), where the dialcohol is 500 mg/kg compared to 75 mg/kg in EVOO (206, 207). Erythrodiol is also present in olive leaves and its content varies during leaf ontogeny (208), ranging from 0.6-1.8 mg/g (209), representing practically 60% of the their triterpenic content (207). In addition, the triterpenoid is widely distributed from other plant sources, including leaves of *Ficus mysorensis* (210),

Introduction

Celastrus kusanoi stems (211), stem bark of Erythrina indica (212), birch bark trees (213) and leaves of Maytenus ilicifolia (214).

Erythrodiol is an oxygenated derivative of β -amyirin and a precursor of oleanolic and maslinic acids by cyclization of 2,3-oxidosqualene via the non-steroidal triterpenoid biosynthetic pathway (215, 216).

The triterpenoid is involved in antioxidant activities and ROS production (217) by modulating primary proteins of oxidative stress and inflammation including nuclear factor kappa B (NF- κ B) and COX-2, as well as the non-enzymatic antioxidants glutathione and nicotinamide adenine dinucleotide phosphate hydrogen (NADPH), and antioxidant enzymes including glutathione peroxidase, glutathione reductase, glucose-6-phosphate dehydrogenase and 6-phosphogluconate dehydrogenase (215, 218). In addition to its anticarcinogenic and antiproliferative properties (215). Its proapoptotic potential associated with ROS and c-Jun N-terminal kinase (JNK) activation has also been reported (211, 219, 220). Other biological activities include anti-inflammatory potentials via modulation of cytokine secretion (158).

The triterpene also protects against portal vein thrombosis and has vasorelaxant activities (221-223) and may improve endothelial function (157, 224, 225).

In addition, the triterpene promotes wound healing by increasing the production of actin filopodia, lamellipodia and stress fibers through the activation of Rho GTPases (213), and has antiplatelet properties by suppressing adenosine diphosphate (ADP) activity (226).

Animal Models

Mus musculus (NCBI: txid39442)

The domestic mouse has been associated with humans since the beginning of civilization and has become the model animal of choice in several fields of research (227). The model has several intrinsic advantages over other models, including low cost, ease of maintenance, rapid reproductive rates (228-230), short life cycles (231, 232), the small size of animal (227), which is 2500 times smaller than humans, resulting in the mouse having a basal metabolic rate seven times faster than an average sized human (228). Mice fall under the jurisdiction of the local ethics committees (233). For the mouse genome, an

extensive amount of data is available for chromosomal mapping and gene linkage analysis (228-230) and the draft sequence of the mouse genome is now available (227).

The mouse is the most widely used mammalian model for studying genetic interactions and pathogenesis in human disorders. Data from the Human Genome Project and the sequencing of the *Mus musculus* genome, followed by comparative analysis of the genomes of the two models (228), all showed outstanding genetic homology between humans and mice (228). Both models share almost 99% of genes and gene expression is quite similar, with an average of 85% identical protein-coding regions (227), while there is considerable variation in the regulatory networks that modulate immune response, stress and metabolic functions and human physiology (228, 234, 235).

Chol transport and metabolism are relatively similar between the two species (236). Mice are therefore used to study obesity, hypertension and MetS. However, some strains do not develop all the components (237). In particular, wild-type mouse LP profiles contain atheroprotective HDL, whereas normal human LP profiles contain atherogenic LDL (234). In particular, the wild-type mouse has a high HDL/LDL ratio, which is maintained even when mice are fed a high-fat diet (HFD). Unlike humans, who have the majority of their plasma Chol in LDL (236). Also, the adipokine adipisin, which is elevated in human MetS, is lower in rodents (234). Mice do not always develop hypertension (234), making the translation of rodent data to humans difficult. However, this discrepancy can be overcome using biotechnology by genetic manipulation to develop a variety of knockout and transgenic strains (228) in a reasonable amount of time (229).

Apolipoprotein E knock-out (*ApoE* KO), *ApoE* (-/-) mice

APOE is a 34 kDa polymorphic glycoprotein synthesized by the liver (238-240) and various peripheral tissues and cell types, including macrophages. The most common isoforms of APOE are APOE2, APOE3 and APOE4 (240).

The apolipoprotein is a major component of TG and Chol-rich LPs, VLDL and chylomicron, and HDL (240, 241). APOE has two main structural features, an LDL receptor (LDLR)-binding domain at the amino-terminus and a lipid-binding domain at the carboxy-terminus (239).

Functionally, APOE is a ligand for cell surface receptors involved in the removal of chylomicrons and VLDL remnants after lipolysis in the circulation (241), including LDLR, VLDL receptor (VLDLR), LDL receptor-related protein (LRP) and heparan sulphate proteoglycan (HSPG) receptor. These receptors then mediate the endocytosis and degradation of LPs, releasing Chol and TGs into the hepatocytes, thereby reducing their levels in the plasma (238-240, 242-244).

In 1992, *ApoE*-KO mice were generated in embryonic stem (ES) cells by gene targeting via homologous recombination. This model has defective clearance of plasma LPs and their plasma Chol levels are 5 times higher than those of wild-type animals. When fed standard chow, they develop spontaneous hypercholesterolemia and atherosclerosis that is similar to that in humans (241, 245). A HFD can further exacerbate and accelerate this process (246), as well as hepatic inflammation with mild steatosis (247).

Although these mice lack ligands to remove remnant LPs, a HFD affects gene expression and the Chol balance is normal. This is because induced hepatic lipase mediates the uptake of LPs in *ApoE*-deficient mice (241).

Apolipoprotein A1 knock-out (KO) mice (*Apoa1* (-/-)) mice

APOA1 is a 28 kDa apolipoprotein (239) that is synthesized in both the intestine and the liver (248, 249). It consists of ten transmembrane amphipathic α -helices (239) and serves as a recognition site for most proteins that interact with HDL, including ATP-binding cassette A1 (ABCA1) (250) and scavenger receptor BI (SR-BI) (251). APOA1 is a major structural component of HDL (252) and accounts for approximately 70% of HDL proteins (248, 249). Functionally, it mediates the reverse efflux of Chol and phospholipids from cells via the ABCA1 transporter (239, 253). Accordingly, the LP plays a key role in the biogenesis, remodeling and catabolism of HDL (254), as well as in the inflammatory and immunoregulatory response (255). The *Apoa1* gene has the same evolutionary origin as the *ApoE* gene, due to duplication and diversification of a basic genetic motif (256-259).

Apoa1 KO mice were developed in ES cells by gene targeting (260, 261). Mutations in human APOA1 reduce circulating HDL levels (262). Also, *Apoa1* KO mice fail to produce normal HDL particles and show a 70-80% reduction in plasma Chol and HDL levels.

Introduction

These mice also show increased diet-induced TG deposition, IR and a high risk of NAFLD (263).

HDL are amphipathic LPs with lipid-loaded and hydrophobic agent-incorporating properties, in addition to protein-protein interactions, heterogeneity and small size, and are therefore used as efficient drug delivery vehicles (264). This structure lends itself well to carrying cholesteryl esters and lipophilic substances, including drugs, in its core compartment (264). In this sense, the APOA1-lacking model can be used to study the effects of HDL deficiency on drug delivery.

Oryctolagus cuniculus (NCBI: txid9986)

Rabbits are an economical, non-aggressive animal model (233), easy to handle (265) of medium size and with a short life cycle (233). They have a longer life span than rodents and are more genetically related to humans (266). In addition to their ability to carry some pathogens, they are therefore more susceptible to simulating human pathogen infections (267, 268).

Oryctolagus cuniculus is the scientific name for the European rabbit, also known as the domestic rabbit. The New Zealand rabbit is a strain of domestic rabbit. It is the most commonly used strain in the laboratories. The animal weighs between 2-5 kg (269) and is less aggressive with fewer health problems compared to other rabbit strains (233). This strain can be genetically modified (269). They are actively used as animal models for human disease research, including cardiovascular disease, cancer (270) and metabolic disorders (271). Both have similar LP metabolism and chemical composition of apolipoprotein APOB100, as well as high baseline levels of cholesteryl ester transfer protein (CETP) and high LDL levels (166, 272). Rabbits have high absorption and hepatic accumulation of dietary Chol (269, 273). As a result, the liver produces high levels of LDL and VLDL that remain in the circulation for a prolonged period, and the lack to increase sterol excretion, results in hypercholesterolemia after a few days of dietary administration, with early progression to macrophage-induced lesions similar to those seen in humans, although in rabbits the lesions do not develop as tissue plaques (269). On the other hand, hepatotoxicity induced by long-term high Chol diets leads to animal mortality, limiting the usefulness of the animals. In addition, the massive inflammatory response in the rabbit body does not reflect human pathophysiology (269).

Sus scrofa (NCBI: txid9823)

Pigs belong to the genus *Sus* and the family Suidae (274). They are one of the most common domestic animals in the world. Compared with other domestic animals and primates, the pig model has a rapid growth rate and short generation intervals (275). Pigs are classified as large animals, which require additional approval from central ethics committees (233). The pig model is inextricably linked to humans through anatomical and physiological similarities, as well as similar body and organ sizes (276, 277). In addition, the pig genome is more comparable to the human genome than the mouse genome. The complete pig genome sequence is now available (*Sus scrofa* Build 10), allowing gene manipulation. In addition, naturally occurring and genetically modified pig models are used by the biomedical community as human models. All this makes the pig the animal model for human health and disease (276). A disadvantage is their high cost compared to small animals, which can limit experimental sample sizes (234). In terms of metabolic properties, pigs show all the clinical signs of carbohydrate and lipid metabolic diseases (278) in a short period of time (279), in addition to the analogy of lipid disposition (280), as well as LP metabolism and the physiopathology of liver lesions (281). MetS can be induced in variant strains of pigs, with overt symptoms appearing within 12 weeks of feeding a high-fat, high-sugar diet (282) and adipose lesions appearing within about 6 months (283, 284). Porcine models account for about 10% of publications on metabolic disorders (234). They are also the non-rodent model of choice for toxicological research, particularly because of their close response to drugs and because both oral and parenteral dosing are similar to humans (276). The crossbreeding system of Large White x Landrace domestic pigs is used to produce a strain with good fertility (285, 286). Despite the genetic resistance of commercial crosses to the production of NAFLD as a result of extended selection to convert all intake to muscle weight gain (287). Nevertheless, this strain was able to develop NAFLD that progress to NASH using a short-term steatosis diet (279, 288).

Cell Culture

Cell culture refers to the *in vitro* growth of cells under controlled physiological conditions (289, 290). This assay was first tested on chicken embryos maintained in warm

saline for several days (290). Some cells require liquid suspension culture (291) to grow without attaching to a surface, while others are adherent cells that require a solid or semi-solid growth substrate (289).

Culture cells are categorized as:

- Primary cell lines are finite cells obtained from a precise tissue biopsy and are the best model of the tissue of origin (289). They therefore more closely resemble *in vivo* cells (292, 293). These cells are the standard model for studying hepatocyte morphology (292), regulation of carbohydrate and lipid metabolism (293) and pharmacotoxicology (294). Disadvantages include limited availability, especially from human sources (293, 294), short time span (293, 294), variability in preparation (293), limited *in vitro* proliferative capacity, instability (293) and eventual loss of hepatic phenotypes (292).
- Transformed cell lines are genetically engineered immortalized cells with high growth rates, produced spontaneously or by genetic manipulation (289). Several immortalization strategies are available, including viral oncogenes, human telomerase reverse transcriptase, plasmid transfection, viral transduction and human artificial chromosomes (294). Cells offer many advantages, including the ability to manipulate genes and molecular pathways, and the homogeneity of cell line populations, which eliminates genotypic or environmental variation, resulting in highly reproducible and consistent results. However, 15-35% of cell lines are cross-contaminated with other cell lines and mycoplasmas, and high serial passage numbers can cause genetic and phenotypic changes (289, 295). Immortal hepatocyte cell lines model exhibit liver-like functions (292) and are used to study gene function (296), gene therapy (294), drug metabolism, hepatotoxicity (294, 296), protein synthesis (296), carbohydrate and lipid metabolism (292, 293), fatty liver disease (294) and neoplasia (294, 296). However, the metabolic gene expression profile and phenotypes of neoplastic-derived cells such as HepG2 differ from those of healthy hepatocytes (292, 293) and are closer to liver cancer than primary cells (292), and HepG2 is derived from a Caucasian male,

Introduction

which alters glucose and FA metabolic pathways (293). Immortalized hepatic cell lines derived from healthy liver have more advantages than HepG2 cells in terms of metabolic functions. The murine hepatocyte cell line AML12 is derived from the livers of transgenic mice overexpressing transforming growth factor (TGF) and is used to study lipid metabolism and NAFLD progression, but the expression of gluconeogenic and hepatokine genes differ from *in vivo* cells (293).

Analytical Procedures

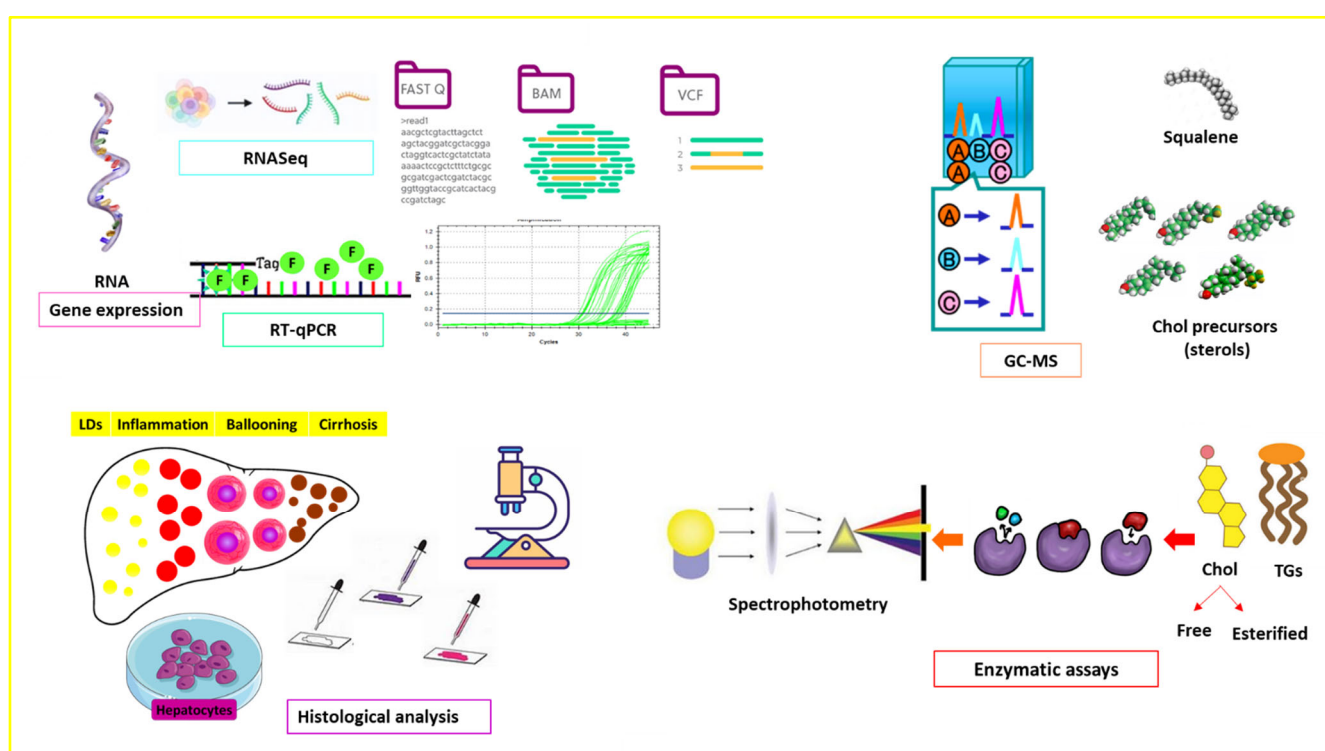


Figure 10. Summary of techniques used

Histological Analysis

Histological analysis is a microscopic study that allows visualization of the structure (297, 298) and any characteristic changes in the tissue (298), by chemical fixation to preserve the tissue formation and protect it from irreversibly cross-linked proteins, followed by dehydration to further harden the tissue. The tissue is then embedded to optimize the extraction of cellular structures prior to light microscopy (297, 298). Antigen retrieval is sometimes performed to retrieve antigens that may have cross-linked during the fixation and embedding steps (297, 298). In terms of proper histological staining, one

Introduction

of the most common stains is hematoxylin and eosin (H&E), the hematoxylin is a blue basic dye that targets acidic structures called basophils, which stand for nucleic acid and RER, followed by the pink acidic eosin dye that targets basic structures called eosinophils, including cytoplasm. Another common stain is Masson's trichrome, which stains collagen fibers blue. In microscopy, the light microscope is used for the examination of live or dead specimens. The electron microscope is used to view intracellular components that are not visible by light microscopy, with a 100 to 300 times higher magnification (298).

Functional Analysis

Functional analysis predicts pathogenesis and response to stimuli by examining diagnostic markers, such as RNA levels via gene expression assays and metabolite networks via metabolomics (299).

Transcriptomics

The process of transcription gives rise to different cell sets and activities from the same set of genes. The transcriptome is the sum set of all RNA transcripts, including coding and non-coding regions. RNAs can be broadly classified into protein-coding RNAs and non-protein-coding RNAs (ncRNAs). In the case of the human genome, more than 93% is transcribed into RNAs, of which only 98% is noncoding regions. Noncoding regions includes house-keeping and regulatory regions. House-keeping ncRNAs include transfer RNAs (tRNAs) and ribosomal RNAs (rRNAs), involved in protein synthesis, small nuclear RNAs (snRNAs) involved in pre-messenger RNA (mRNA) splicing, small nucleolar RNAs (snoRNAs) involved in rRNA modification and processing and guide RNAs (gRNAs) involved in RNA editing. Regulatory ncRNAs are divided into small ncRNAs of 17-35 base pair (bp), including microRNAs (miRNAs), which regulate gene expression, and small interfering RNA (siRNA) and piwi-interacting RNA (piRNA), which are involved in gene regulation and genomic stability, while long ncRNAs (lncRNAs) (>200 bp) regulate gene expression (300).

The transcriptome profile reflects the transient state of the cell (301). Transcriptomics is the study of an organism's transcriptome, which involves determining the structure of genes in terms of post-transcriptional modifications, mainly start sites, 5' and 3' ends and

splicing patterns, and quantifying the change in expression of each transcript under specific biological conditions (302), providing information on the regulation of gene expression and the function of gene products, followed by further insights into the regulatory network of biological processes involved in areas of diagnosis and therapy (300). A number of high-throughput technologies have been developed to analyze the transcriptome (302):

Early sequencing techniques used Sanger sequencing technology and expressed sequence tags (ESTs) generated from a single RNA transcript, but due to low throughput, digital tag-based sequencing approaches using optimized double-stranded oligodeoxynucleotide tags, adapters and PCR primers were developed (301-303), including serial analysis of gene expression (SAGE) by Sanger sequencing of long strands of concatenated 3' complementary DNA (cDNA) tags fragmented by restriction enzymes (301, 304), cap analysis of gene expression (CAGE) which is a variant of SAGE that sequences tags from the 5' end of transcripts (300, 304) and massively parallel signature sequencing, where transcripts are captured on single microbeads by short cDNA signature sequences generated by restriction and ligation reactions (300), although short-tag sequencing assays may not be specific particularly for isoforms (302). These methods have largely been replaced by high-throughput whole transcript sequencing, which provides additional information on genome structure (301). Initially, the microarray or chip method was used (300). This method is based on cDNA hybridization to a large set of complementary oligonucleotide probes attached to a solid support to simultaneously quantify the expression of specific transcripts (301). Advanced arrays have been developed that detect different spliced isoforms using probes spanning exon junctions, while whole genome mapping is achieved using tiling arrays. However, this approach relies on existing knowledge of the genome sequence and has limited dynamic range due to high background from cross-hybridization and signal saturation at high expression levels (302).

RNA Sequencing (RNA-seq)

RNA-seq uses massively parallel sequencing, also known as next-generation sequencing (NGS) (305, 306) to map and characterize the abundance of the entire transcriptome (307), to determine post-transcriptional modifications and single

nucleotide polymorphisms (SNPs), for simultaneous high-resolution RNA editing (305, 308), and for computational reconstruction of RNA by aligning reads to a reference genome or aligning reads to each other (*de novo* assembly) without the use of a reference genome (301).

RNA-seq offers several key advantages, most notably high sensitivity, which can be increased by enriching classes of target RNAs and depleting unwanted RNAs (301), excellent reproducibility, a large dynamic range not limited by signal saturation, and the ability to reconstruct known and novel transcripts at the single base level and to detect transcripts from organisms with previously undetermined genomic sequences (305, 309). In addition, mapping the RNA sequence to the target genome removes experimental noise (309).

Sequencing is divided into paired and single end sequencing. The former involves sequencing both ends of the cDNA rather than just one end (310), which allows the size of the gap between the two ends to be estimated, providing an accurate alignment (311). However, paired-end sequencing requires twice as much sequencing as single-end sequencing (312).

In brief, long RNAs are first converted into a library of cDNA fragments by either DNA fragmentation or RNA fragmentation and cDNA synthesis. Approximately 50 bp reads are sufficient for mapping mammalian RNA, but longer reads increase the likelihood of capturing splice sites within the reads (313). The average length is around 100 bp, depending on the method (301). This step is followed by end repair of the cDNA library and ligation of adaptors. The short reads are then amplified by clonal PCR to produce tens of thousands to millions of bundles of the same sequence, followed by sequencing from random positions of the input RNA using a high-throughput platform. The resulting sequence reads are demultiplexed, aligned and computationally mapped against the reference genome and classified as exonic reads, junction reads and polyadenylated (poly-A) end reads to generate a base-resolution expression profile for each gene (302, 305, 314). Analysis of the raw reads requires a combination of bioinformatics software tools. For quality control, the raw data is checked for base call scores, guanine-cytosine distribution, k-mers and read duplication rates. Sequence aligners control alignment speed, intron splice detection and read mapping.

Quantitative tools use dedicated software at the gene, exon or transcript level. Differential expression is determined by normalization, modelling and statistical analysis (301).

Reverse Transcription Quantitative Real-time PCR (RT-qPCR)

RT-qPCR is the preferred method for quantifying steady-state mRNA levels (315) of a small number of genes (316), and can provide a rapid, sensitive and accurate assessment of changes in gene expression (315, 317), which can be used to measure responses to experimental stimuli. It is also used to confirm data obtained from high-throughput transcriptomics (316), including microarray (318) and RNA seq, when the number of biological replicates used is small or when gene expression levels or differences in expression levels are small (316).

The assay quantifies the initial amount of nucleic acid by its amplification and by monitoring the amplicon at the end of each cycle using fluorogenic probes. If the reaction efficiency is optimal, twice the amount of amplicon will be present after each PCR cycle. The final product is exposed to increasing temperatures to determine when the double-stranded product melts. This melting point depends on the length of the amplicon and its nucleotide content (315). The fluorescence emitted is measured after each cycle and is proportional to the amount of amplicon synthesized (319). Amplification curves are plotted to determine the cycle time (CT) at which fluorescence reaches a threshold value. The CT value is inversely related to the concentration of the target sequence (315). There are two common methods for quantification: relative and absolute quantification. Relative quantification uses the $\Delta\Delta\text{CT}$ method to measure changes in steady-state levels of a gene of interest normalized to the expression ratio of a reference gene (320, 321). Absolute quantification uses a standard curve where a series of dilutions of known template concentration and unknown samples are compared to the standard curve (274, 322).

Several probes are available: SYBR green I, which fluoresces when it binds to double-stranded DNA (dsDNA), absorbing light at 480 nm and emitting light at 520 nm (315). It binds to the minor groove of dsDNA and emits 1,000 times more fluorescence than when it is free in solution (315). Specificity is a primary concern with SYBR Green fluorescence, but this drawback can be identified by determining the melting point of

the amplicon using the amplicon dissociation curve. Several compatible sequence-specific hydrolysis probes, also known as 5'-nuclease probes, are inherently less prone to non-specific amplification. They consist of two fluorophore-labelled DNA oligonucleotides, called a quencher and a reporter. Prior to amplification, the fluorophores are attached in close proximity to the same short oligonucleotide. During amplification, they move away from each other, releasing the reporter from the quencher and allowing measurable fluorescence (315). Other classes are hybridization probes, which use donor and acceptor fluorophores (315). The most common are hairpin oligonucleotide probes called molecular beacons, which show distinct fluorescence in the presence and absence of the target sequence, and binary probes, which consist of two fluorescently labelled oligonucleotide strands that bind to adjacent regions of their target and produce distinct fluorescence (323). Another is a peptide nucleic acid (PNA) probe, to which thiazole orange fluorophores are attached to give a stronger signal when DNA binds (315).

Metabolite Analysis

Metabolites are intermediates of cellular metabolism (324) that are involved in biological activities such as signaling, stimulatory and inhibitory functions (325). Metabolite analysis is the identification and quantification of a metabolite and the relative analysis of the correlation between that metabolite and biological changes (326, 327). Recent analytical platforms include gas chromatography-mass spectrometry (GC-MS), high-performance liquid chromatography (HPLC), ultra-performance liquid chromatography (UPLC), capillary electrophoresis coupled with nuclear magnetic resonance and mass spectrometry (MS) methods (327).

Spectrophotometry Based Techniques

Spectrophotometry measures the electromagnetic radiation absorbed or reflected by analytes in relation to the intensity of light at a specific wavelength (328). The primary spectrophotometric techniques are based on the absorption of radiation at specific wavelengths of light to obtain the absorption spectrum, or depend on the reflectance of specific spectra of a given material within the UV and visible (VIS) regions of the electromagnetic radiation spectrum (328). In terms of wavelength, spectrophotometry is

divided into two types: UV-VIS spectrophotometers, which use light in the UV (185 - 400 nm) and VIS (400 - 700 nm) regions of the electromagnetic spectrum, and infrared spectrophotometers (328, 329). Inorganic analysis uses the UV-VIS region, while organic analysis uses the UV region (329). The main components of UV-VIS spectrophotometers are a beam in the 190-800 nm spectral range, a monochromator, a sample holder, a detector and an interpreter (330). In most cases, the resulting measurements are determined using the standard curve technique (329).

Chromatography Based Techniques

Chromatography is a biophysical technique to separate, identify and purify analyte components for qualitative and quantitative analysis. The principle is based on the separation of components of a mixture by transfer from a stable solid or liquid stationary phase to a liquid or gaseous mobile phase, depending on adsorption, partitioning, affinity or molecular weight. Because of these differences, some components stick more to the stationary phase and take longer time to pass through the system, while others are more soluble in the mobile phase and exit the system more quickly (331).

Mass Spectrometry

MS determines the mass-to-charge ratio of ions. A beam of high energy electrons is used to ionize the analyte and produce these ions. The mass analyzer then receives the gas phase ions and separates them - in space or time - based on their mass-to-charge ratio (m/z). An ion detector measures the separated ions in space or time and generates electrical signals. These signals are processed to produce mass spectra, which reveal the number of ions with different m/z values that correspond to the original molecules, their fragments or other species formed during the ionization process (332).

Gas Chromatography-Mass Spectrometry (GC-MS)

GC is a method of separating different types of molecules on the basis of their weight (333). The technique consists of a liquid stationary phase adsorbed on the surface of an inert solid column, while the mobile phase is an inert gas, such as nitrogen, helium or hydrogen, which is passed through the column under high pressure. When a mixture of

Introduction

substances is injected at the column inlet, it is vaporized and is carried towards the detector by the mobile carrier gas (334).

GC-MS identifies different analytes by combining the volatile separation properties of GC based on retention time, with the mass-based fragmentation detection properties of MS (333). This spectrometry is one of the most effective and consistent analytical platforms for volatile (335) and low molecular weight metabolomics via various derivatization approaches. The technique typically employs electron impact (EI) and chemical ionization approaches (333). High reproducibility of retention time and mass spectra, improved molecular ion and increased sensitivity, especially for difficult analytes, are the main advantages of GC-MS (333, 336). Results are usually expressed in mass units (333).

III. OBJECTIVES

As shown, erythrodiol and squalene are supposed to play important biological actions *in vivo*. To characterize in further detail using hepatic transcriptomic changes, the following objectives have been established:

1. Analyze the long-term administration of erythrodiol on hepatic transcriptome through RNA sequencing approach. Establish the influence of sex, dose and genetic background.
2. To assess the effect of squalene on the hepatic transcriptome through RNA sequencing in male New Zealand rabbits. Verify the impact of post squalene metabolites on the gene expression changes.
3. To evaluate the effect of squalene on the hepatic transcriptome by using RNA sequencing in two groups of male Large White x Landrace pigs developing nonalcoholic steatohepatitis.

III. OBJETIVOS

Como se ha mostrado, el eritrodiol y el escualeno pueden desempeñar importantes acciones biológicas *in vivo*. Para caracterizar con mayor detalle mediante los cambios transcriptómicos hepáticos implicados, se han establecido los siguientes objetivos:

1. Analizar la administración a largo plazo de eritrodiol en el transcriptoma hepático mediante la secuenciación del ARN. Establecer la influencia del sexo, la dosis y el fondo genético.
2. Evaluar el efecto del escualeno sobre el transcriptoma hepático a través de la secuenciación de ARN en conejos machos de Nueva Zelanda. Verificar el impacto de los metabolitos post escualeno sobre los cambios en la expresión génica.
3. Evaluar el efecto del escualeno sobre el transcriptoma hepático mediante secuenciación de ARN en dos grupos de cerdos machos Large White x Landrace que desarrollaron esteatohepatitis no alcohólica.

IV. MATERIALS AND METHODS

i. Biological Samples

1. *In Vivo* Experiments

- ♣ *In vivo* experiments used in this thesis were carried out in accordance with the Guidelines for Laboratory Animals (European Union Directive 2010/63) for the protection of animals used for scientific purposes and the ARRIVE guidelines.
- ♣ The study protocols were approved by the Animal Research Ethics Committee of the University of Zaragoza (PI43/15, 9 October 2015 and PI35/18, 4 October 2018).

I. Animal Models

- ♣ The *ApoE*- and *ApoA1*- deficient mouse strains were 2-month-old, C57BL/6J genetic background, both bred at the Centro de Investigación Biomédica de Aragón. *ApoE*-KO mice were obtained from Charles River Laboratories (Barcelona, Spain) and *ApoA1*-deficient mice were obtained from Dr Nobuyo Maeda, University of North Carolina at Chapel Hill.
- ♣ 6-month-old New Zealand White rabbits, wild type, were obtained from the Animal Research Support Service (University of Zaragoza).
- ♣ Large White × Landrace pigs were produced by artificial insemination at the Cooperativa Ganadera de Caspe (Zaragoza, Spain) and transferred to the facilities of the Servicio General de Apoyo a la Investigación, División de Experimentación Animal, Facultad de Veterinaria, Universidad de Zaragoza.

II. Experiment Design

❖ Mice

The mice were housed in sterile filter-top cages in rooms with a controlled 12-hour light/12-hour dark and a controlled microclimate, with a minimum temperature of 20 °C and a maximum temperature of 23 °C, a minimum humidity of 50% and a maximum humidity of 60%. They had *ad libitum* access to food and water. The diets tested were

well tolerated. Fresh diets were prepared weekly, stored in an N₂ atmosphere at -20 °C and replaced daily.

Quality Control Management

Blood samples taken from the facial vein 4 hours after fasting were used to establish experimental groups with similar baseline plasma Chol levels. This was used as a rapid quality control for mouse identification. In this sense, *Apoe*-deficient mice were hypercholesterolemic and their plasma levels should be higher than 5 ± 1 mmol/l compared to 2.9 ± 0.5 mmol/l for the wild type (337). In the case of *Apoa1*-deficient mice and due to their hypocholesterolemia, they should have values of 0.8 ± 0.4 mmol/l (338). Any mouse that did not have these values was genotyped and excluded if not correctly identified (339). The absence of hepatic expression of *Apoe* and *Apoa1* in the corresponding mice was also verified by analyzing their presence or absence by RT-PCR. Animals with liver dysfunction as determined by histological analysis (cirrhosis, necrosis, hepatitis, etc.) were excluded.

Effect of Dietary 10 mg/kg Erythrodiol in a Western Diet on *Apoe*- and *Apoa1*-Deficient Mice

4 groups of *Apoe*-deficient mice were established: female (n=12) and male (n=14) control groups received a purified Western diet containing 0.15% Chol and 20% refined palm oil (Gustav Heess, S.L., Barcelona, Spain), and the other two groups, female (n=13) and male (n=15), received the same diet supplemented with 0.01% erythrodiol (Extrasynthese, Genay, France). At a daily intake of 3 g per mouse, this corresponds to a dose of 10 mg/kg per mouse. This dose was chosen on the basis of that previously used for oleanolic acid (340), which did not alter body weight while inducing liver gene expression. The animals were fed the experimental diets for 12 weeks. In *Apoa1*-deficient mice, the intervention lasted 4 weeks and included female (n=9) and male (n=14) control groups and female (n=9) and male (n=15) erythrodiol groups.

Effect of Different Doses of Erythrodiol in Western Diets on Male *Apoe*-Deficient Mice

4 groups were established. The control group (n=17) received the Western diet and 3 groups received the same diet formulated to provide doses of 0.5 (n=16), 1 (n=17) and

Materials and Methods

5 mg/kg erythrodiol (n =17). These doses, corrected for the metabolic rate of the mice, would correspond to the amount of erythrodiol ingested by humans consuming extra virgin olive oil or olive-pomace oil. The animals were fed the experimental diets for 12 weeks.

Diet Composition of Purified diets

Percentage of total diet content:	
Chol	0.15%
Fat (soybean & palm oil):	20.0%
Soybean oil	4%
Corn starch	46.57%
Casein	14%
Maltodextrin	15.5%
Sucrose	10%
Vitacel	5%
Minerals mix	3.5%
Multivitamins	1%
Choline	0.25%
Cystine	0.18%
FAs	
Caprylic acid (C8:0)	0.01%
Capric acid (C10:0)	0.01%
Lauric acid (C12:0)	0.15%
Myristic acid (C14:0)	0.85%
Palmitic acid (C16:0)	38.5%
Palmitoleic acid (C16:1)	0.16%
Stearic acid (C18:0)	4.4%
Oleic acid (C18:1)	38.1%
Linoleic acid (C18:2 n6)	15.5%
Linolenic acid (C18:3 n3)	1.1%
Arachidic acid (C20:0)	0.6%
Gadoleic acid (C20:1)	0.22%

Somatometric Analyses

Body mass, diets consumption and survival rates were monitored throughout the experiment on weekly basis. At the end of the experiment, after a 4-hour fast, the mice were euthanized by CO₂ inhalation and the livers were removed and weighed. An aliquot was stored in neutral formaldehyde and the remaining organ was frozen in liquid nitrogen. Plasma samples were stored at -80 °C.

❖ Rabbits

Rabbits were housed in individual cages in rooms with a controlled 12-hour light/12-hour dark cycle with a controlled microclimate. They had ad libitum access to food and water. The diets were well tolerated. Fresh diets were prepared weekly, stored in an N₂ atmosphere at -20 °C and replaced every 2 days.

Quality Control Management

Animals with body weight of 1485 ± 201 g were used in the experiment. Blood samples were collected through the lateral ear vein. Animals with liver dysfunction were excluded as mentioned before.

Effect of 0.5% Squalene in a Control Diet Enriched with 1% Sunflower Oil

Animals were divided into two groups, the first receiving a control regular diet supplemented with 1% sunflower oil (n=5) and the second receiving the diet supplemented with 1% sunflower oil and 0.5% squalene (Sigma-Merck, Darmstadt, Germany) (n=5). 1% sunflower oil was used to dissolve the squalene and was found to incorporate perfectly into the diet. The initial body weights of the control and experimental groups were 1560 ± 201 g and 1410 ± 203 g, respectively. Taking into account food consumption and body weight, the squalene dose was equivalent to 0.6 mg/kg/day (341). The animals were fed the experimental diets for 4 weeks.

Control Diet Composition

Materials and Methods

Amounts of total diet content:	
Proteins	15.9%
Total oils and fats (Sunflower and olive)	3.62%
Ash	7.36%
Fibers	18.6%
Calcium	0.9%
Phosphorus	0.6%
Sodium	0.2%
Lignin	0.68%
Methionine	0.28%
Vitamin A	7,934 UD kg
Vitamin D	1,014 UD kg
Vitamin E	20 ppm
Iodine	0.5 ppm
Cobalt	3.24 ppm
Copper	13 ppm
Magnesium	15 ppm
Zinc	49 ppm
Selenium	0.10 ppm
Lysine monohydrochloride	0.05%
Ethoxyquin	124 ppm
FAs	
Myristic acid (C14:0)	0.1%
Palmitic acid (C16:0)	6.4%
Palmitoleic acid (C16:1)	0.1%
Heptadecanoic acid (C17:0)	≤ 0.05%
Stearic acid (C18:0)	3.9%
Oleic acid (C18:1)	23.6%
Linoleic acid (C18:2)	64.2%
Linolenic acid (C18:3)	0.1%
Arachidonic acid (C20:0)	0.3%
Eicosenoic acid (C20:1)	0.2%
Behenic acid (C22:1)	0.7%

Materials and Methods

Lignoceric acid (C24:0)	0.3%
-------------------------	------

Somatometric Analyses

Body mass, food consumption and survival rates were checked every 2 days. After the dietary intervention, the rabbits were fasted for 18 hours. Time was selected according to previous studies carried on these animals (341). Then they were weighed and euthanized by cervical dislocation, and the livers were collected. An aliquot of each sample was stored in neutral formaldehyde and the remainder immediately frozen in liquid nitrogen. Plasma samples were stored at -80 °C.

❖ Pigs

Pigs were housed in the facilities of the Animal Experimentation Unit of the General Research Support, of the University of Zaragoza. They had ad libitum access to food and water. The diets were well tolerated. Fresh diets were prepared monthly, stored in an N₂ atmosphere at -20 °C and replaced on weekly bases.

Quality Control Management

To establish the study groups, fasting blood samples were collected and animals were assigned to groups so that all had similar basal plasma Chol levels. Biopsies were taken under Propofol® (B/Braun-Vetcare, Rubí, Barcelona, Spain) induced and maintained anesthesia. Animals with liver dysfunction were excluded as mentioned before.

The Effect of 0.5% Squalene in a Steatotic Diet on the Progression of NASH

The experimental animals used were 24 male Large White x Landrace pigs. The pigs, weighing 38 ± 2.8 kg, were fed a steatotic diet, high in cholate, Chol, fructose and saturated fat and low in methionine and choline. The diet was prepared by the Veterinary Unit of the University of Zaragoza, and pigs were fed for one month (279). They were then biopsied and divided into two groups with equal hepatic TG and Chol levels. The first group (n = 12) was fed the steatotic diet and the second group (n = 12) was fed the same diet enriched with 0.5% squalene. Both groups continued on their diets for a further month. Taking into account the amount consumed and body weight, the

Materials and Methods

dose was equivalent to 135 mg/kg of squalene per animal per day. Squalene was purchased from the Molekula Group (Darlington, UK).

Steatotic Diet Composition

Percentage of total diet content:	
Chol	2%
Proteins	8.5%
Fibers	10%
CHO	53.2%
Sugars	33.4 %
Minerals mix	2.2%
Vitamins	0.4%
Choline	0.016%
Methionine	0.1%
Sodium cholate	0.5%
Fat: hydrogenated palm & sunflower oil	25.7%
FAs	
Caprylic acid (C8:0)	0.1%
Capric acid (C10:0)	0.04%
Lauric acid (C12:0)	0.5%
Myristic acid (C14:0)	1.0%
Palmitic acid (C16:0)	39.0%
Palmitoleic acid (C16:1)	0.2%
Stearic acid (C18:0)	8.7%
Oleic acid (C18:1)	32.7%
Linoleic acid (C18:2 n6)	12.6%
Linolenic acid (C18:3 n3)	0.1%
Arachidic acid (C20:0)	0.4%
Gadoleic acid (C20:1)	0.14%

Somatometric Analyses

Body weight, dietary consumption and survival were recorded on weekly basis. Liver and plasma samples were collected at the beginning and end of the experiments after an overnight fast. At termination, all pigs were euthanized with an overdose of propofol (B/Braun-Vetcare, Rubí, Barcelona, Spain). Liver biopsies were obtained by laparotomy. An aliquot of all liver samples was stored in neutral formaldehyde and the remainder were immediately frozen in liquid nitrogen. Plasma samples were stored at -80 °C.

2. *In Vitro* Assays

Both AML12 and HEPG2 cell lines were obtained from the ATCC collection (Manassas, VA, USA).

I. Cell Culture Conditions

❖ Preparing Strict Aseptic Environment

- ♣ Working area: All procedures were performed under laminar hood.
- ♣ Equipment and materials: To prevent microbial growth in the cell culture, all media, reagents and supplements were sterile; if not supplied sterile, filter sterilization was required. Pipette tips were purchased pre-autoclaved and DNA/RNA free and glass items used (Pasteur pipettes, flasks and bottles) were autoclaved before use.
- ♣ Handling procedures: Exposure of the cell culture to air was minimized. All surfaces were pre-sprayed with 70% ethanol prior to use. Pouring of media and reagents directly from bottles and flasks was avoided. Liquid waste and tips were discarded into a waste pot containing approximately 100 ml of 10% sodium hypochlorite, into which liquid waste and tips were carefully disposed of to prevent dripping and minimize the risk of contamination.

❖ Growth and Maintenance of the Cell Lines

- ♣ Fresh culture media components and reagents used were warmed in a 37 °C water bath for at least 30 minutes.
- ♣ Cells were maintained at 37 °C in a humidified atmosphere of 95% air and 5% CO₂.
- ♣ Culture media changes were every 2-3 days.

Materials and Methods

- ♣ Hepatic cell lines were grown on T25 flasks with a vented cap without the need for a specific matrix. This flask has a surface area of 25 cm² and is optimal for seeding a density of 0.7 × 10⁶ cells in a final volume of 5 ml. The average yield was approximately 2.5 × 10⁶ cells. A 1:10 split (0.07 × 10⁶ cells) was 90-100% confluent in 4-5 days.
- ♣ The experiments were performed in 6-well plates with a surface area of 9.6 cm² per well. The seeding density was 0.3 × 10⁶ cells per well and the average yield was 1.2 × 10⁶ cells.

II. Hepatocytes Cell Lines

❖ AML12 Cell Line Growth Medium

Reagents

- 1:1 Dulbecco's modified Eagle's minimum essential medium (DMEM) with glucose (4.5 g/l) (Thermo Fisher Scientific) and F12-Ham's medium with 1 mM L-glutamine (GE Healthcare Life Science)
- 10% fetal bovine serum (FBS) (Thermo Fisher Scientific)
- 1:500 insulin-transferrin-selenium (Corning, Bedford)
- 40 ng/ml dexamethasone (Sigma-Aldrich; Merck Millipore)
- 1% non-essential amino acids (Thermo Fisher Scientific)
- 100 U/ml penicillin (Thermo Fisher Scientific)
- 100 µg/ml streptomycin (Thermo Fisher Scientific)
- 2.5 µg/ml amphotericin B (Thermo Fisher Scientific)

❖ HEPG2 Cell Line Growth Medium

Reagents

- DMEM (4.5 g/l) (Thermo Fisher Scientific)
- 10% FBS (Thermo Fisher Scientific)
- 2% of 4 mM glutamine (Thermo Fisher Scientific)
- 1% of 100 mM sodium pyruvate (Thermo Fisher Scientific)
- 1% non-essential amino acids (Thermo Fisher Scientific)
- 100 U/ml penicillin (Thermo Fisher Scientific)

Materials and Methods

- 100 µg/ml streptomycin (Thermo Fisher Scientific)
- 2.5 µg/ml amphotericin B (Thermo Fisher Scientific)

III. Observing Cells

Optical microscopy was used to monitor cell viability, growth and contamination every 2-3 days:

- ♣ Healthy hepatocytes were typically found adherent to the bottom of the flask and had a bright and translucent appearance with a spherical, cuboidal or polygonal shape and a well-contrasted border.
- ♣ Damaged hepatocytes, on the other hand, formed dark, small, shrunken, round detached blebs in the plasma membrane.

IV. Subculture by Trypsinization

When cells reached 90-100% of confluence, they were sub-cultured to 6 well plates.

Reagents

- Phosphate buffered saline (PBS) (1 x):
 - PBS (10 x) (Thermo Fisher Scientific)
 - Fresh autoclaved distilled water
- Trypsin (1 x):
 - 7.7 ml of 10 mM ethylenediaminetetraacetic acid (EDTA) (372 mg in 100 ml) filtered through sterile Millex® PVDF syringe filters (pore size 0.22 µm, diameter 33 mm, sterile, hydrophilic) (Sigma Aldrich, Merk Milipore).
 - 5.5 ml of PBS (10 x) (Thermo Fisher Scientific).
 - 7.7 ml of 2.5% trypsin, 10 x (Thermo Fisher Scientific).
 - 56.1 ml fresh autoclaved distilled water.
- ♣ The cells were washed twice with 3 ml PBS (1 x).
- ♣ 1.5 ml of 1 x trypsin solution was added to the flask. It took almost 5 minutes at 37 °C with gentle agitation for the cells to detach.
- ♣ Once detached, the cells were homogenized in 5 ml of culture medium (FBS inactivates trypsin) and centrifuged at 300 g for 5 minutes.

Materials and Methods

- ♣ The culture medium was then removed by aspiration and the cell sediment was homogenized with fresh culture medium.
- ♣ The cell suspension was diluted (approximately 0.1×10^6 cells per well). The required volume of cells was aspirated into a 6-well plate with a final volume of 3 ml. It took approximately 4-5 days to reach 90-100% confluence.

V. Cell Freezing

Reagents

- Dimethyl sulfoxide (DMSO) (Sigma Aldrich; Merck Millipore)
- Fresh cell culture medium
- ♣ Steps were similar to those for trypsinisation.
- ♣ The cell pellet (with a maximum concentration of 2.5×10^6 cells) was resuspended in 1 ml of media to which very cold 10% DMSO was added drop by drop.
- ♣ The mixture was stored in freezing 2 ml microtubes and progressively frozen at $-80\text{ }^{\circ}\text{C}$ in an isopropanol container (5100 Cryo $1\text{ }^{\circ}\text{C}$ freezing container, Mr Frosty).
- ♣ The vials were then stored in nitrogen liquid until needed.

VI. Cell Thawing

- ♣ Tubes of frozen cells were removed from the liquid nitrogen storage container and the cap was slightly reduced to lower the internal pressure.
- ♣ Cells were thawed in a $37\text{ }^{\circ}\text{C}$ water bath for 1-2 minutes.
- ♣ Cells were then resuspended at high density in T25 flask to optimize recovery and pre-warmed growth medium was slowly added.
- ♣ The next day, two $1 \times$ PBS washes followed by fresh growth medium were required to remove DMSO.

VII. The Effect of Cholesterol Precursors on Hepatic Gene Expression (AML12 Cell Lines):

Reagents

Materials and Methods

- 200 μ M squalene (Sigma-Merck) in ethanol.
- 200 nM lanosterol, 200 nM dihydrolanosterol, 200 nM zymostenol, 200 nM desmosterol (Avanti Polar lipids, Alabaster, AL, USA) in ethanol.
- Fresh prepared culture media without FBS, insulin-transferrin-selenium or amphotericin B
- 1 x PBS
- Absolute ethanol

Protocol

- ♣ When the cells reached 90-100% confluence, the medium was removed and the cells were washed twice with 1 x PBS. The cells were then starved for 48 hours by adding medium without FBS, insulin-transferrin-selenium or amphotericin B.
- ♣ Cells were washed twice with 1 x PBS and then were incubated for 6 hours with 200 μ M squalene, 200 nM lanosterol, dihydrolanosterol, zymostenol or desmosterol versus ethanol as a negative control.
- ♣ Each condition was tested in 6 replicates.
- ♣ Media was removed and cells were washed twice with PBS.
- ♣ Total RNA was extracted using Tri-Reagent solution (Ambion).
- ♣ DNA contaminants were removed by TURBO deoxyribonuclease (DNase) treatment using a DNA Removal kit (Ambion).
- ♣ Squalene and sterol effects were investigated at the mRNA level by RT-qPCR assays.

VIII. The Effect of Squalene on Hepatic Gene Expression (AML12 and HEPG2 Cell Lines):

Reagents

- 0.1% polylactic-co-glycolic acid (PLGA) nanoparticles
- 30 μ M squalene (Sigma-Merck) carried in 0.1% PLGA nanoparticles
- 1 x PBS
- Fresh prepared culture medium without FBS and amphotericin B

Preparation of PLGA-Based Squalene-Loaded Nanoparticles

- Pluronic powder (F68) (Nanoscience Aragon)
- Ethyl acetate (99.6% ACS reagent) (Sigma-Aldrich, Merck Millipore)

Materials and Methods

- Resomer RG 503 H (PLGA-COOH, Mw 24–38 kDa) (Sigma-Aldrich; Merck Millipore)
- 2.05 M squalene (Sigma-Aldrich, Merck Millipore)
- Milli-Q water
- Sterile 1 × PBS (Thermo Fisher Scientific)

Protocol

- ♣ In two sterile beakers, 50 mg of PLGA and 150 mg of Pluronic powder were dissolved in 5 ml of ethyl acetate per beaker and then were placed in an ultrasonic bath to complete the dissolution.
- ♣ For the PLGA with squalene preparation, 50 µL of 2.05 M squalene was added to one of the beakers.
- ♣ 10 ml of Milli-Q water was added to both beaker and the contents were sonicated in an ice bath for 25 seconds at 80% amplitude.
- ♣ The organic solvent was evaporated under sterile conditions for 3 hours of rotating at 600 rpm with beakers open.
- ♣ Nanoparticles were transferred to sterile Falcon tubes and centrifuged at $12,350 \times g$ for 15 min at 10 °C and the supernatant was collected in sterile Falcon tubes and then re-centrifuged at $15,000 \times g$ for 15 min at 10 °C and the supernatant was dissolved in sterile PBS in an ultrasonic bath.
- ♣ 20 µl of both PLGA and PLGA with squalene were saved for quantification.
- ♣ Nanoparticles were aliquoted to 1 ml per Eppendorf tube and frozen at -20 °C.

Cellular Incubations

- ♣ When the cells were 90-100% confluent, the medium was removed and the cells were washed twice with 1 × PBS. The cells were then starved by adding medium without FBS and amphotericin B for 48 hours.
- ♣ Cells were washed twice with 1 × PBS and then were incubated for 72 hours with 30 µM squalene (Sigma-Merck) carried in 0.1% PLGA versus unloaded PLGA nanoparticles as a negative control.
- ♣ Each condition was tested in triplicate in two experiments.

Materials and Methods

- ♣ Media was removed and cells were washed twice with 1 x PBS and cells were collected.
- ♣ Total RNA was extracted using Tri-Reagent Solution (Ambion).
- ♣ DNA contaminants were removed by TURBO DNase treatment using DNA Removal Kit (Ambion).
- ♣ Squalene effect was investigated at the mRNA level by RT-qPCR assays for target genes.

ii. Gene Expression Experiments

1. Good Laboratory Practices for RNA Extraction and Handling

Reagents

- RNAase free water or diethylpyrocarbonate (DEPC)-treated water. Water treated with 0.05% (v/v) DEPC, autoclaved for 1 hour at 100 °C
- 70% Ethanol in DEPC-treated water

Practices

- ♣ Reagents used were free of ribonucleases (RNases) to prevent degradation of RNA and interference with the analysis.
- ♣ Work surfaces, instruments and equipment were disinfected and wiped with 70% ethanol and RNaseZap™ RNase Decontamination Solution (Invitrogen).
- ♣ Sample handling equipment were cleaned between samples with 70% ethanol, DEPC-treated water and RNaseZap™.
- ♣ Commercially available consumables such as pipette tips, PCR tubes, microcentrifuge tubes were sterile and free of nuclease.
- ♣ All samples, including tissues, cells and extracted RNA, were kept on ice to prevent RNA degradation.

2. Total RNA Extraction

❖ Extraction by Phenol-Guanidine Isothiocyanate (GITC)-Based Solution

Reagents

- Phenol- GITC-based solution. TRI Reagent (Life Technologies)
- Chloroform

Materials and Methods

- Absolute isopropanol
- 70% Ethanol in DEPC-treated water
- RNAase free water.
- DEPC-treated water

Samples Preparation

- ♣ For liver samples, a frozen aliquot of approximately 50 mg was immediately homogenized with 1 ml of TRI Reagent in a sterile and RNase-free ULTRA-TURRAX® homogenizer, followed by incubation for 5 minutes at 2-8 °C for complete degradation of nucleoproteins.
- ♣ For cell culture, cell pellet was homogenized in TRI Reagent by repeated pipetting (1ml TRI Reagent/ 5–10 ×10⁶ cells), followed by incubation for 5 minutes at 2-8 °C.

Phase Separation

- ♣ 0.2 ml of chloroform was added to each ml of TRI reagent used, the samples were shaken vigorously by inversion for 15 seconds and allowed to stand for 10-15 minutes.
- ♣ The samples were then centrifuged at 12,000 × g for 15 minutes at a temperature of 2-8 °C. Centrifugation separates the mixture into 3 phases: a reddish organic phase containing protein, a whitish intermediate phase containing DNA and a colorless upper aqueous phase containing RNA.

RNA Precipitation

- ♣ The aqueous phase was transferred to a new Eppendorf tube, to which 0.5 ml of isopropanol was added. The mixture was then thoroughly mixed by inverting the tube and was incubated for 10 minutes at 2–8 °C. The mixture was then centrifuged at 12,000 × g for 10-15 minutes at same temperature.
- ♣ The RNA pellet was collected and washed with 1 ml of 75% ethanol.
- ♣ The RNA pellet was air dried or subjected to vacuum for 5-10 minutes, then dissolved by adding the required volume of RNase-free water, and gently mixing by pipetting.
- ♣ Average RNA yields ranged from 6-10 mg RNA per mg tissue to 8-15 mg RNA per 10⁶ cells.

Materials and Methods

- ♣ RNA samples were used immediately or stored frozen at -80 °C.
- ❖ **Silica-Membrane Based Spin Column Technology (Quick-RNA™ Miniprep Kit)**

Reagents

- Quick-RNA™ Miniprep Kit (ZYMO Research):
 - RNA lysis buffer
 - 24 ml RNA wash buffer: 96 ml absolute ethanol
 - RNA preparation buffer
 - 250 U lyophilized DNase I: 275 µl nuclease-Free Water
 - DNA digestion buffer
 - RNase free water

Samples Preparation

- ♣ For liver samples, a frozen aliquot of approximately 50 mg was immediately homogenized with 600 µl of RNA Lysis Solution in a sterile and RNase-free ULTRA-TURRAX® homogenizer.
- ♣ For cell culture, cell pellet was homogenized in RNA Lysis solution by repeated pipetting (600 µl ml RNA Lysis Solution / 5×10^6 - 10^7 cells).
- ♣ The lysed homogenate was centrifuged at 16,000 x g for 1 minute at 2-8 °C to remove debris and the supernatant was transferred to a new Eppendorf tube.

RNA Purification

- ♣ The lysed sample was transferred to a Spin-Away™ filter in a Collection Tube and centrifuged at 16,000 x g for 1 minute at 2-8 °C to remove the DNA.
- ♣ 600 µl of absolute ethanol was added to the pass-through, mixed well by pipetting and transferred to a Spin™ IICG column filter in a Collection Tube at 16,000 x g for 1 minute at 2-8 °C.
- ♣ 400 µl of RNA Wash Buffer was added to the column filter and the column was then centrifuged for 1 min at room temperature.
- ♣ 5 µl DNase: 75 µl DNA Digestion Buffer was added to the column filter and allowed to stand at 20-30 °C for 15 minutes.
- ♣ 400 µl of RNA Preparation Buffer was added to the column filter and the column was then centrifuged for 1 min at room temperature.

Materials and Methods

- ♣ The filter was washed twice with 700 µl followed by 400 µl RNA Wash Buffer and centrifuged for 1-2 minutes to remove residual ethanol.
- ♣ ≥ 50 µl of RNAase-free water was added directly to the filter and centrifuged at 2-8 °C for 1 minute.
- ♣ RNA samples were used immediately or stored frozen at -80 °C.

3. RNA Quantification

- ♣ The RNA concentration was determined using a Nanodrop ND-1000 UV/Vis Spectrophotometer by analyzing the absorbance at 260 nm and 280 nm. The concentration was calculated based on the Beer-Lambert law, according to the equation: RNA concentration (µg/ml) = (optical density at 260 nm (OD₂₆₀)) × (dilution factor) × (40 µg RNA/ml) / (1 OD₂₆₀ unit).
- ♣ RNA purity was assessed using the 260/280 and 260/230 ratios. Pure RNA had a 260/280 ratio between (1.8 to 2.0). In general, a high ratio indicates a poor-quality blank. A low 260/280 ratio is due to contamination with proteins, phenol, guanidine. Pure RNA had a 260/230 ratio between (2.0 to 2.2). A higher ratio indicates contamination with guanidine isothiocyanate or very diluted RNA and a lower ratio indicates contamination with organic compounds.

4. Gel Electrophoresis

The quality of the extracted RNA was validated by size-based separation of RNA by agarose gel electrophoresis

Reagents

- UltraPure Agarose (Thermo Fisher Scientific)
- 1% Tris-borate-EDTA (TBE) buffer (9 mM Tris base, 50 mM EDTA (pH 8) and 90 mM boric acid)
- DEPC-treated water
- 10 mg/ml ethidium bromide (EtBr) stock solution (Sigma Aldrich; Merck Millipore)
- Nucleic acid ladder 1000 bp (Thermo Fisher Scientific)
- 6X DNA loading Dye (containing bromophenol blue and xylene cyanol FF dyes) (Thermo Fisher Scientific)

Gel Preparation

- ♣ 1% Agarose gel. 0.5 g of agarose in 1X TBE (50 ml) was heated to dissolution, then cooled for a few seconds and mixed with 2-3 μ l of EtBr stock solution.
- ♣ The mixture was then poured into a gel mold using combs to make wells sufficiently large to contain at least 10 μ l of samples. The gel was then allowed to solidify.
- ♣ The gel was assembled in the tank, and then covered with 1X TBE running buffer until to a depth of a few mms above the gel. Once the gel had solidified, the combs were then removed.

Loading of Samples

- ♣ The wells were loaded with 1X loading dye and 500 ng of RNA.
- ♣ 5 μ l of 1000 bp nucleic acid ladder was loaded into one well of each lane of the gel.

Running the Gel

- ♣ Electrophoresis was run at 70-80 V for 20-25 minutes until the bromophenol blue (a fast-tracking dye) had migrated two-thirds of the length of the gel.

RNA Imaging by UV Transilluminator

- ♣ The stained gel was then visualized under UV light. The different size fragments for ribosomal RNA (rRNA) 5S, 18S and 28S are approximately 0.12, 1.9 and 5.0 kb respectively.
- ♣ Intact total RNA has sharp 28S and 18S bands and the 28S band is 2:1 more intense than the 18S band.
- ♣ Slightly degraded RNA exhibits a smeared appearance, with a 2:1 ratio of 28S to 18S bands.
- ♣ Fully degraded RNA exhibits a very low molecular weight smeared appearance.

5. Removal of DNA Contamination

Reagents

- TURBO DNA-free™ Ki TURBO DNA-free™ Kit (Thermo Fisher Scientific):
- TURBO DNase™ Enzyme (2 units/ μ l)
- 10 x TURBO DNase™ Buffer

Materials and Methods

- DNase Inactivation Reagent
- RNase-free water

Protocol

- ♣ If the RNA samples contained > 200 µg of RNA, they were diluted to ≤ 200 µg before use (Up to 50 µg DNA/ml RNA).
- ♣ In a 0.5 ml tube, 5 µl of 10 x TURBO DNase™ Buffer and 1 µl of TURBO DNase™ Enzyme were gently mixed with 10 µg of RNA in a 50 µl reaction volume and incubated at 37° C for 20-30 minutes.
- ♣ DNase Inactivation Reagent was resuspended by vortexing and 5 µl was added to the previous mixture and mixed well to be then incubated for 5 minutes at ambient temperature, with flicking 2–3 times to keep the DNase Inactivation Reagent suspended.
- ♣ The tubes were centrifuged at 10,000 × g for 1.5 minutes and the supernatant containing the RNA was transferred to another tube.
- ♣ The concentration, purity and integrity of the cleaned RNA sample were reassessed.

6. RNA Sequencing

Library construction and sequencing (RNA-seq) was carried out by BGI service (Shenzhen, China)

I. Experiment Workflow

- ❖ **Assessment of Total RNA Quality and Integrity** (Agilent 2100 Bio analyzer).

Reagents

- Agilent RNA 6000 Nano Kit (Agilent Technologies)

Concept

- ♣ The RNA integrity number (RIN) algorithm produces an electropherogram of the length (peak intensity) of RNA subunits (28S, and 18S) over time. If the RNA is highly intact, the RIN value will be between 8 and 10. For moderately intact RNA with some degradation, the RIN value is between 6 and 8. Highly degraded RNA is typically associated with RIN values between 1 and 5.

- ♣ The 28S/18S ratio measures the relative abundance of the two subunits. The ideal ratio is 2:1.
- ♣ The fragment length distribution provides information about the size and abundance of each rRNA subunit.

❖ Library Construction

- ♣ **mRNA enrichment:** poly-A-containing mRNA was purified using poly-T oligo-attached magnetic beads.
- ♣ **RNA fragmentation:** mRNA was fragmented into small pieces using divalent cations at elevated temperatures.
- ♣ **Reverse transcription:** cleaved RNA fragments were copied into first-strand cDNA using reverse transcriptase and random primers, followed by second-strand cDNA synthesis using DNA polymerase I (Pol I) and RNase H.
- ♣ **End repair:** by filling in the sticky ends of any single strand fragment.
- ♣ **3'Adenylation (A tailing):** by adding a single adenine ('A') base at the 3' end.
- ♣ **Adaptor ligation:** adaptors containing a single thymine ('T') were ligated to the ends of these 3' adenylated cDNA fragments.
- ♣ **PCR amplification:** multiple rounds of PCR amplification were performed to enrich the purified cDNA template.
- ♣ **Cyclization:** the PCR product was denatured by heating and the DNA was cyclized using splint oligo and DNA ligase.
- ♣ The PCR product was quantified using the Qubit Fluorometer and then pooled to form a single-stranded DNA (ssDNA) circle, which gave the final library.
- ♣ **Synthesis of DNA nanoballs (DNBs):** DNBs were generated from the ssDNA circle by Rolling Circle Replication (RCR) to enhance fluorescence signals during sequencing.
- ♣ **Sequencing on the DNBSEQ platform:** DNBs were loaded onto the patterned nanoarrays and pair-end reads of 100 bp were read on the DNBseq platform.

II. Bioinformatics Workflow

- ♣ **Reads filtering:** Sequencing reads containing low quality reads, reads with adapters and reads with unknown (N) bases were removed to obtain the clean reads, which were stored in FASTQ format (342).
- ♣ **Genome mapping:** Clean reads were mapped to the reference genome (*Mus musculus*, GRCm39) (*Oryctolagus cuniculus* GCA_000003625.1) (*Sus scrofa*11.1 (GCA_000003025.6)) using hierarchical indexing for spliced alignment of transcripts (HISAT2) (343). Bam files were used for the genome mapping result.
- ♣ **Prediction of novel transcripts:** Transcripts were reconstructed using StringTie (344) and the reconstructed transcripts were compared to the reference annotation using Cuffcompare (CPC) (345). CPC was used to predict the coding potential of novel transcripts, followed by merging coded novel transcripts with reference transcripts to obtain a complete reference.
- ♣ **SNP and INDEL detection:** GATK (346) was used to call SNP and INDEL and the unreliable sites were filtered.
- ♣ **Detection of differentially spliced genes (DSGs):** After genome mapping, rMATS (347) was used to detect DSGs between samples. DSGs were regulated by alternative splicing events, including skipped exon (SE), alternative 5' splicing site (A5SS), alternative 3' splicing site (A3SS), mutually exclusive exon (MXE) and retained intron (RI), which allow the production of multiple isoforms of a single gene. False discovery rate (FDR) ≤ 0.05 was defined as a significant difference.
- ♣ **Gene expression analysis:** After novel transcript detection, transcripts were merged with reference transcripts to obtain a complete reference, then clean reads were mapped using Bowtie2 (348), then gene expression levels were calculated for each sample using RSEM (349).
- ♣ The complete databases have been deposited in the Gene Expression Omnibus (GEO) database (GSE155163), (GSE191236) and (GSE214732).

- ♣ **Gene ontology (GO) classification and functional enrichment of DEGs:** GO included the molecular biological function, the cellular component and the biological process. Significant enrichment was defined as $FDR \leq 0.01$.

7. Reverse Transcription

- PrimeScript™ reverse transcription (RT) Reagent Kit: (Components per sample in a 10 μ l volume reaction)
- 2 μ l of 5 x PrimeScript Buffer containing deoxynucleotide triphosphates (dNTPs) and Mg^{2+}
- 0.5 μ l PrimeScript RT and RNase Inhibitor
- 0.5 μ l 50 μ M Oligo dT Primer
- 0.5 μ l 100 μ M Random 6 mers
- Nuclease Free water

Protocol

- ♣ The above reaction mixture was prepared on ice.
- ♣ 10% extra volume was prepared to allow for pipetting errors.
- ♣ Approximately 500 ng RNA/10 μ l reaction was gently mixed with the premix and then was incubated in a thermal cycler as follows:

Step	Temperature	Time
RT	37 °C	15 minutes
RT inactivation	85 °C	5 second
Hold	4 °C	

8. Good Laboratory Practices for PCR Work

- ♣ Reagents used were free of DNase, which can degrade DNA and interfere with the analysis.
- ♣ Work surfaces, instruments and equipment were disinfected and wiped with 70% ethanol.

- ♣ DNA-OFF was used to eliminate DNA from work surfaces, instruments, and equipment. DNA contamination in PCR work area can cause DNA amplification artifacts.
- ♣ Consumables used were sterile and nuclease-free, e.g., pipettor tips, PCR tubes, microcentrifuge tubes.
- ♣ When working with SYBR Green, light exposure was minimized before and during the reaction to ensure accurate results. This is because SYBR Green is a fluorescent dye that intercalates between DNA bases.

9. Primer Design and Optimization

- ♣ For primers design, the RNA transcript sequence was selected to have an exon-to-exon spanning region of 70-300 bp in length, the primer length was 18-24 bases, the GC content was 40-60% and the difference in melting temperature (T_m) between forward and reverse primers was ± 5 °C.
- ♣ Primers were designed using NCBI. Gene specificity and full variant coverage were checked using basic local alignment search tool (BLAST) (NCBI), Kyoto encyclopedia of genes and genomes (KEGG) and Ensemble genome browser. (Tables 1,2,3).
- ♣ On completion of RT, a pool of cDNA samples was prepared and serial dilutions (1:2, 1:4, 1:8, 1:16, 1:32, 1:64) were performed to generate a standard curve for primer optimization. The cDNA dilution factor for each primer was chosen to give C_t values between 24 and 29 in response to the standard curve of the pool serial dilution. Primer efficiency should be in the range of 90-110%. The characteristics of the primers used in RT-quantitative PCR (qPCR) were in accordance with the minimum information for publication of quantitative real-time PCR experiments (MIQE) guidelines (350).

10. Real-Time Quantitative PCR

Reagents

- Half volume of (2X) Power Up™ SYBR™ Green Master Mix (Thermo Fisher Scientific)

Materials and Methods

- Forward and reverse primers (amount depends on primer optimization in the range (0.05-0.2 μM))
- Fresh autoclaved distilled water
- 96-well reaction optical plates (Thermo Fisher Scientific)
- 384-well reaction optical plates (Thermo Fisher Scientific)

Assay

- ♣ Each qPCR reaction was run in duplicate.
- ♣ To detect contamination, the non-template control was run in duplicate.
- ♣ The reaction mixture was prepared on ice.
- ♣ An additional 10% volume has been prepared to allow for pipetting errors.
- ♣ For 96-well reaction plate: 2 μl cDNA and 18 μl premix were added per well
- ♣ For 384-well reaction plate 1 μl cDNA and 9 μl premix were added per well
- ♣ Plate was sealed with optical adhesive cover.
- ♣ Components were mixed thoroughly and the plate was spined down to eliminate air bubbles.
- ♣ The real-time instruments used were the Step One Plus Real-Time PCR System for 96-well plates and the ViiA7 Real-Time PCR System for 384-well plates.
- ♣ The plate was loaded into the real-time PCR instrument using the following programs:

Conditions for thermal cycling

Step	Temperature	Time	N° of cycles
Uracil-DNA glycosylase activation	50 °C	2 minutes	1
DNA polymerase activation	95 °C	10 minutes	1
Denaturation	95 °C	15 seconds	40
Annealing	60 °C	1 minute	

Melting curve conditions

Ramp rate	Temperature	Time
1.6 °C/second	95 °C	15 seconds
1.6 °C/second	60 °C	1 minute
0.15 °C/second	95 °C	15 seconds

- ♣ The SYBR Green, once bound to the minor groove of the DNA double helix, emits a fluorescent signal at 520 nm when excited at 497 nm. The intensity of the emitted fluorescence is proportional to the number of copies of the amplicon.
- ♣ Ct values for amplification curves were calculated using the qPCR instrument software. Non-specific amplification was defined using dissociation curves.
- ♣ Relative quantification was calculated using the comparative Ct method ($2^{-\Delta\Delta Ct}$ method), which compares the Ct values of target and reference genes between different samples.
- ♣ Relative expression values were normalized by dividing their values by the average relative expression of the control group.
- ♣ Reference genes were selected as those whose expression does not change under different study conditions, including *Ppib* and *Tbp* for mice, *Ppib* for the AML12 cell line, *GAPDH* for the HEPG2 cell line, *PPIB* and *GAPDH* for rabbits and *UBA52* for pigs.

iii. Histological Examination of the Liver

1. Preparation of liver tissue blocks

Reagents

- 10% paraformaldehyde in PBS (40 g paraformaldehyde powder was dissolved in 800 mL pre-warmed 1 × PBS, 1 N NaOH was added drop by drop until the solution was clear. The solution was cooled, filtered and made up to 1 L with 1 × PBS.
- Absolute ethanol
- Paraffin
- Distilled water
- Tissue Cassettes

Protocol

- ♣ Histological analysis was performed on liver samples from all animals.
- ♣ Fixation to preserve morphology and chemical composition of cells and tissues: Immediately after obtaining the samples, they were fixed in 10%

Materials and Methods

paraformaldehyde for 1-4 days, depending on the size of the piece, to avoid autolysis. The volume of fixative was twenty times that of the fixed sample.

- ♣ Sections no thicker than 1 cm were cut with a scalpel blade and placed in cassettes. Sections were washed in running water for 30 minutes.
- ♣ Using an automated tissue processor, samples were embedded in liquid paraffin, with a melting point of 56 °C, which was then solidified. This process included:
 - ♣ Samples were dehydrated gradually with increasing concentration of ethanol (40%, 50%, etc.) until 100% was reached. For at least 1 hour each time.
 - ♣ Alcohol clearance was achieved by immersing the samples in 1:1 ethanol: xylene for 1 hour followed by 2 hours of xylene twice.
 - ♣ The samples were transferred to the liquid paraffin, which gradually replaced the bleaching agent and filled all intra- and extracellular spaces.
 - ♣ After removal from the processor, the samples were placed in a paraffin station (57-60 °C) for approximately 3 hours to allow complete paraffin infiltration of the tissue sections.

2. Deparaffinization of Liver Tissue Sections

Reagents

- Xylene
- Absolute ethanol
- Distilled water
- Slides and coverslips

Protocol

- ♣ Paraffin-embedded blocks were placed on ice before prior to sectioning, which allowed thinner sections to be obtained. The microtome was used to trim 10-30 µm to expose the tissue surface, then sections of approximately 4-5 µm thickness were cut, with the first section discarded due to holes created during trimming.
- ♣ Sections were removed with tweezers, softened and flattened out in a 37 °C water bath and then cut into individual sections.
- ♣ After dehydration, the sections were placed on numbered slides, which had previously been coated with Mayer albumin.

Materials and Methods

- ♣ Slides were stored upright in a slide rack which was then placed in an oven and sections dried at 37 °C overnight or 60 °C for 30 minutes to evaporate water.
- ♣ Specimens were prepared for deparaffinization, hydration and staining with the stain of interest.
- ♣ Sections were washed twice for 10 minutes in a xylene bath.
- ♣ Sections were hydrated twice in absolute ethanol followed by 95%, 90%, 85%, 70%, 50% and 30% ethanol. Each step was carried out for 3 minutes at room temperature.
- ♣ Sections were washed twice in running distilled water for 5 minutes.
- ♣ Slides were then ready for further processing such as staining.
- ♣ After staining, very clean coverslips, with a drop of mounting medium on each were placed on the section to prevent the formation of air bubbles. The most commonly used mounting medium is balsam of Canada. The balsam was allowed to dry and the specimen can now be viewed under the microscope.

3. Hematoxylin and Eosin Staining

This staining (H&E) staining was used to quantify LDs in the liver of the animal models in all experiments and to estimate the activity index and SAF score of NASH in porcine samples.

Reagents

- Hematoxylin stain (0.5 g hematoxylin, 0.1 g potassium iodate, 25 g potassium alum (Aluminum potassium sulfate may also be used), 100 ml glycerol, 400 ml distilled water). Potassium alum was dissolved in 200 ml of boiled distilled water, followed by haematoxylin and stirred until dissolved. Potassium iodate and the remaining water were added to the mixture. Finally, glycerol was added and the mixture was allowed to cool.
- Eosin stain (1% eosin in distilled water)

Protocol

- ♣ Deparaffined sections attached to slides were placed in a metal staining rack.

- ♣ These slides were immersed in filtered haematoxylin stain for 15 minutes, followed by a low flow of distilled water for 10 minutes to remove excess haematoxylin.
- ♣ Slides were then immersed in a rack of filtered eosin stain for approximately 15 seconds and then washed in running water as above.
- ♣ Slides dehydrated by rapid immersion in 96% ethanol, absolute ethanol, then cleared by rapid immersion in xylene. Twice for each step.
- ♣ Stained slides were observed using a Nikon light microscope (Eclipse E200) and were photographed with a Nikon digital camera (DS-Fi1) attached to the microscope.

4. LD Area

Protocol

- ♣ Using these photographs, LDs were selected from the toolbar of Adobe Photoshop CS3 (Adobe Inc., San Jose, CA, USA) and their areas were measured.
- ♣ The percentage of LDs was calculated by dividing the total area of the selected droplets by the total area of the liver section and then multiplying by 100%.

5. NASH Activity Index and SAF Score

- ♣ **Steatosis** was based on the percentage of hepatocytes containing large and medium-sized lipid droplets, using a scale of 0 to 3 (0: < 5%; 1: 5-33%; 2: 34-66% and 3: > 67%).
- ♣ **Ballooning** was graded on a scale of 0 to 2 (0: normal hepatocytes; 1: groups of rounded hepatocytes with pale cytoplasm and size similar to normal hepatocytes; and 2: as grade 1, but with at least one enlarged ballooned hepatocyte (2 times the size of normal cells within a group of grade 1 hepatocytes)).
- ♣ **The inflammatory response** was assessed by counting the number of inflammatory foci (≥ 2 cells per lobule) at 20 x magnification. Inflammation was scored as 0 for none, 1 for less than 2 foci per lobule and 2 for at least 2 foci per lobule.
- ♣ **Activity score** is the sum of the ballooning and lobular inflammation grades.

- ♣ **Fibrosis** was graded on a scale of 0 to 4 based on the location and number of fibers present. Grade 0 indicates the absence of fibrosis, grade 1 indicates the presence of fibrosis confined to the perisinusoidal or periportal regions, grade 2 indicates the presence of perisinusoidal and periportal fibrosis without flange, grade 3 indicates the presence of flanged fibrosis and grade 4 indicates the presence of cirrhosis.
- ♣ **The Steatosis Activity Fibrosis (SAF) score** is the sum of the steatosis, activity and fibrosis scores.

6. Masson's Trichrome Stain

The stain was used to quantify the area in the liver where collagen fibers were stained dark blue.

Reagents

- Wiegert haematoxylin stain (1:1 of A and B):
A: 1 g of haematoxylin in 1 ml of 96% ethanol
B: 4 ml of 29% ferric chloride, 1 ml hydrochloric acid and 95 ml distilled water
- 1% fuchsin
- 5% phosphotungstic acid
- 1% aniline blue
- 1% acetic acid (10 g of glacial acetic acid in 1000 ml water)
- Distilled water

Protocol

- ♣ Slides with sections were placed in a metal staining rack.
- ♣ Slides were immersed in filtered Wiegert haematoxylin for 5 minutes, followed by a low flow of distilled water for 10 minutes.
- ♣ Slides were dipped in 1% fuchsin for 15 minutes and washed in 1% acetic acid solution for 5 minutes.
- ♣ Slides were immersed in 5% phosphotungstic acid for 5 minutes and then in 1% acetic acid solution for a further 5 minutes.
- ♣ Sections were immersed in 1% aniline blue for 30 seconds to 1 minute and washed again with 1% acetic acid as before.
- ♣ Finally, the sections were dehydrated.

- ♣ Stained slides were viewed using a Nikon light microscope as for H&E.

iv. Enzyme-Based Hepatic Lipid Assays

Reagents

- 1% PBS buffer (pH 7.4) (136 mM NaCl, 0.2 g/l KCl, 1.44 g/l Na₂HPO₄ and 0.24 g/l KH₂PO₄ and autoclaved distilled water)
- 2:1 Chloroform: Methanol solvent
- Infinity™ Cholesterol Liquid Stable Reagent (Thermo Fisher Scientific)
- Infinity™ Triglycerides Liquid Stable Reagent (Thermo Fisher Scientific)

1. Lipids Extraction

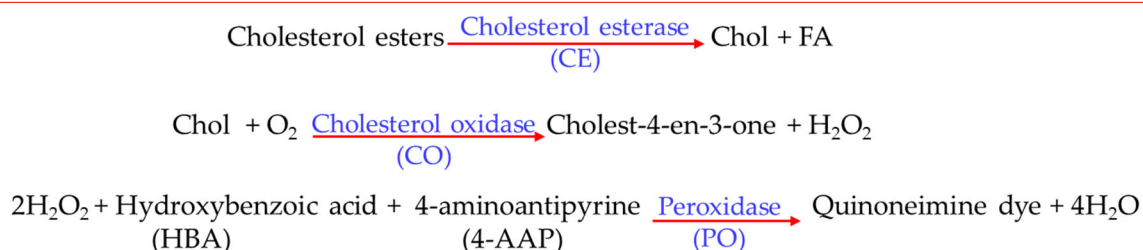
Protocol

- ♣ A frozen aliquot of approximately 20 mg was weighed and then homogenised in 1 ml PBS using a potter's homogeniser until complete disintegration of the tissue and then transferred to a glass tube.
- ♣ Lipid extraction: 3 ml of 2:1 chloroform: methanol solvent was mixed with lysate and then was centrifuged at 500 g for 5 minutes according to Folch's method (351).
- ♣ After centrifugation, the lower organic phase containing solubilized lipids, was collected with sterile Pasteur pipette and then transferred to a glass tube.
- ♣ This extraction procedure was repeated with 1.5 ml of the chloroform: methanol mixture and centrifuged as before, with the remaining organic phase collected and added to the previous extraction from the previous centrifugation.
- ♣ The chloroform was evaporated in a bath at 50 °C under a nitrogen stream to prevent oxidation of the lipids, which were then dissolved in 200 µl of isopropanol.
- ♣ The extracted lipids were available for the determination of TG and Chol levels.

2. Cholesterol Quantification

Materials and Methods

- ♣ The protocol used was based on enzymatic reactions involved in the conversion of cholesterol to a coloured quinone with a maximum absorbance of 550 nm.
- ♣ Enzymatic reaction used to assay Chol:

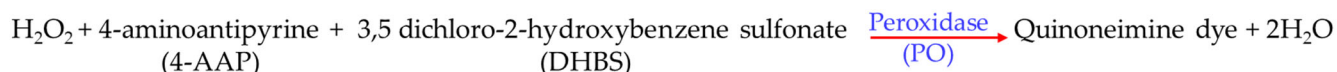


- ♣ Each unknown and control sample was run in duplicate.
- ♣ For quality control, Chol calibrator with a concentration of 200 mg/dl was included, in addition to a sample without Chol as a negative control.
- ♣ 2 µl of each sample was incubated with 100 µl of Chol reagent for 30 minutes at room temperature.
- ♣ Absorbance at 510 nm was performed using the SPECTRO star Nano Microplate Reader (BMG Labtech).
- ♣ Background was corrected by subtracting the values obtained from the negative control.

3. Triglyceride Quantification

- ♣ Protocol and absorbance reading conditions were the same as for Chol. In addition to a glycerol calibration curve with concentrations from 0.625 to 10 mM.
- ♣ Enzymatic reaction used to assay TGs:

Materials and Methods



4. Unesterified and Esterified Fractions of Cholesterol

Reagents

- Amplex® Red Chol Assay Kit:
- 20 mM Amplex® Red Reagent Stock Solution in DMSO.
- 200 U/ml horseradish peroxidase (HRP) in 1 x reaction buffer.
- 1/5 of 5 x reaction buffer (0.5 M potassium phosphate, pH 7.4, 0.25 M NaCl, 25 mM cholic acid, 0.5% Triton® x -100) with deionized water.
- 20 mM H₂O₂ in deionized water.
- 200 U/mL Chol oxidase solution in 1 x reaction buffer.
- 200 U/mL Chol esterase solution in 1 x reaction buffer.
- 2 mg/ml (5.17 mM) Chol reference standard.

Protocol

- ♣ For the Chol standard curve, the reference standard was diluted with 1 x buffer to give concentrations of 0.25-10 μM and 0 μM for the negative control. For the positive control 20 mM H₂O₂ was diluted with 10 μM in 1 x reaction buffer.
- ♣ Samples and controls were run in duplicate.
- ♣ All samples were diluted in 1 x reaction buffer.
- ♣ **For total Chol:** the working solution contained 300 μM Amplex® Red Reagent containing 2 U/ml HRP, 2 U/ml Chol oxidase and 0.2 U/ml Chol esterase.
- ♣ **For non-esterified Chol:** the working solution was as above but without Chol esterase.

- ♣ 50 μl of the diluted samples and the control were added to the wells of the microtiter plate, and mixed with 50 μl of the master mix and then incubated for 30 minutes at 37 °C in the dark and the fluorescence was measured in a fluorescence microplate reader (Spectrostar OMEGA instrument) using excitation at 550 nm and emission detection at 590 nm.
- ♣ A standard curve was generated and background fluorescence for both calibrators and samples and sample dilution factors were corrected.
- ♣ Esterified Chol was calculated by subtracting unesterified Chol from total Chol.

v. Analyses of Metabolites

1. Squalene

II. Squalene Extraction

Reagents

- 1 mM 5 α -cholestane sigma (Sigma) dissolved in cyclohexane
- Cyclohexane (Honeywell)
- Sterile 1 x PBS (Thermo Fisher Scientific)
- 5 g silica
- 50 μM squalane (Merck) dissolved in in cyclohexane
- Sterile glass tubes
- Hamilton syringes and needles
- 2 ml glass screw-necked vials with 200 μl inner vial.
- All reagents used were GC-MS qualified.

Protocol

- ♣ 100 mg aliquot of the frozen liver was weighed using a precision balance, transferred to a sterile falcon tube and homogenized in 1 ml PBS, 10 μl of 1 mM 5 α -cholestane (50 μM) as internal standard solution to determine the efficiency of the extraction.

Materials and Methods

- ♣ 2 ml of cyclohexane was added to the mixture and vortexed for 1 minute until an emulsion of the organic and inorganic phases was obtained, then centrifuged at 2200 g for 10 minutes.
- ♣ The organic phase was transferred to a new Falcon tube.
- ♣ This process was repeated with the addition of 1.5 ml more cyclohexane to recover the remaining organic phase for efficient extraction.
- ♣ 0.5 g of silica was used to prepare a highly porous and partially hydrated silica gel, previously activated at 160 °C for at least 1 night, to remove other lipids and thus reduce the chromatogram background, especially for samples with low squalene concentrations and those with high lipid content. The silica was loaded in Falcon tube.
- ♣ The collected organic phases and the silica were vortexed and centrifuged as above
- ♣ The extract was transferred to a sterile glass tube and dried in a thermostatic bath at 55 °C under a stream of N₂.
- ♣ The dried sample was dissolved in 200 µl of 50 µM squalene as a secondary internal standard solution using a precision Hamilton syringe, the tube was capped and completely dissolved by sonication in an ultrasonic bath for 3 minutes.
- ♣ Samples were transferred to the 200 µl inner vials of the 2 ml glass screw-necked vials for chromatographic analysis or were frozen at -20 °C until further processing.
- ♣ For accurate squalene quantification, it was important to consider the amount of extract used and recovered.
- ♣ A standard calibration line was prepared using squalene at concentrations of 0, 1, 10, 100 and 1000 µM and the two internal standards at a concentration of 50 µM using a precision Hamilton syringe.

III. Gas Chromatography-Mass Spectrometry (GC-MS)

Squalene was analysed using 7890A GC and a 5975C MS acquisition parameter unit (Agilent Technologies).

Materials and Methods

GC-MS Parameters	
Injector	7683B
Carrier Gas	Helium
Flow Rate	1 ml/minute
Column	J&W122-5532
Nominal Length	30 m
Diameter	0.25 mm
Width	0.1 μ m
Oven Temperature	From 280 to 290 °C in 15 minutes with a ramping time (5-13 minutes)
Retention Time	Squalane (9.8 minutes) Squalene (11.3 minutes) 5 α -Cholestane (12.2 minutes)
Ion Mass Patron	Squalane (113 m/z) Squalene (69.1 m/z) 5 α -Cholestane (217.2 m/z)
Analysis	Peak identification is achieved by comparing the retention times of sample peaks with the external and internal standards used (squalene, squalane, and 5 α -cholestane)
	The linear calibration curve for the determination of squalene consisted of the 0, 1, 10, 100, and 1000 μ M concentrations.

5

2. Sterols

1. Sterol Extraction

Reagents

- 1 M NaOH
- Distilled tertiary butyl methyl ether (TBME)
- 5 mg primary-secondary amine (PSA)
- 10 µg/ml 5 α -cholestane
- N-trimethylsilylimidazole (TSIM)
- 9:1 N-methyl-N-trimethylsilyltrifluoroacetamide: trimethylsilylimidazole
- Hamilton syringes
- Sterile glass tubes
- 2 ml glass screw-necked vials with 200 µL inner vial.
- All reagents used are GC-MS qualified.

Protocol

- ♣ In a sterile Falcon tube, a 100 mg sample aliquot was homogenized in 1 ml PBS and the homogenate was mixed with 1 ml of 1 M NaOH and incubated at 70 °C for 1 hour.
- ♣ 50 µl of 10 µg/ml cholestane internal standard and 700 µl TBME were added to the previous Falcon tube and mixed vigorously for 1 minute and then centrifuged at 9200 × g for 5 minutes.
- ♣ The extraction was repeated as before using 750 µl of TBME.
- ♣ The supernatant was mixed vigorously with 35 mg sodium sulphate and 5 mg PSA and centrifuged as before.
- ♣ The organic extract was transferred to a glass tube and then was dried under a stream of N₂ and then dissolved in 950 µl of TBME and 50 µl of TSIM, followed by silylation (9:1 N-methyl-N-trimethylsilyltrifluoroacetamide: trimethylsilylimidazole) for 1 hour at room temperature.
- ♣ Samples were transferred to the 200 µl inner vials of the 2 ml glass vials and were now ready for chromatographic analysis or frozen at -20 °C.

II. Gas Chromatography-Mass Spectrometry (GC-MS)

Sterols were analysed using 6890N GC and 5975 MS equipments (Agilent Technologies).

Materials and Methods

GC-MS Parameters	
Injector	Spitless (injection volume 2 μ l)
Carrier Gas	Helium
Flow Rate	1 ml/minute
Column	DB-5 ms
Nominal Length	30 m
Diameter	0.25 mm
Width	0.1 μ m
Inlet Temperature	260 $^{\circ}$ C
Oven	55 $^{\circ}$ C for 2 minutes 260 $^{\circ}$ C for 10 minutes at a rate of 55 $^{\circ}$ C/minute 310 $^{\circ}$ C at a rate of 7 $^{\circ}$ C/minute
MS Detector	Selective ion monitoring (SIM) mode
Retention Time/ Ion mass Patron	MS is operated in full scan mode 7–9.5 minutes 60–450 m/z and 9.5–12.0 minutes 100–550 m/z and 70 electron volts (eV)
Analysis	Peak identification was done by comparison of retention with that of individual standards and normalized to internal standard (5- α Cholestane)

vi. Quality Control and Statistics

- ♣ Samples in the quantitative assays were run in duplicate and the coefficient of variation was calculated for each. Duplicates with a coefficient of variation of higher than 3% were discarded and retested.
- ♣ Statistical analyses were performed using GraphPad Prism (GraphPad Software, San Diego, CA, USA). The Shapiro-Wilk test was used for the analysis of distribution type and the Bartlett's F test for the analysis of homogeneity of

Materials and Methods

variance. When any of these parameters failed, the results were analyzed using the non-parametric one-tailed Mann-Whitney's U test. Differences between the two groups were considered significant when $p < 0.05$.

- ♣ Correlations between all parameters tested were analysed using the two-tailed Spearman correlation coefficient according to the Statistical Package for Social Sciences version 25 (IBM, Armonk, NY, USA), and those with $p < 0.02$ were considered.
- ♣ Receiver operating characteristic (ROC) curves were generated using GraphPad Prism 8.0 for quantitative values. This software also reports the area under the curve (AUC), which defines how well the measured parameter can discriminate between the groups tested for each parameter.

Materials and Methods

Characteristics of primers used in RT-qPCR according to MIQE guidelines

Primers used in manuscript 1

Gene symbol	Accession		Sequence	Amplicon length	Exons	[μ M]	Efficiency
<i>Mus musculus</i>							
<i>H4c17</i>	NM_001195421.1	Sense	CAAAGTGCTGCGCGATAACA	83	1	0.2	94%
		Antisense	AGATGCGCTTCACTCCTCC				
<i>LOC100862456</i>	XM_006537451.3	Sense	TTGTGGAGAGTGTACACCG	121	1	0.05	92%
		Antisense	TCGAGCATCAAAAACCACCA				
<i>Ccl19-ps2</i>	XM_006536385.3	Sense	GTAGGAGCCTCGACCTCTCA	142	1	0.2	94%
		Antisense	GGAAGGTCCAGAGAACCAGC				
<i>Ctrb1</i>	NM_025583.2	Sense	CACCACCATGGCATTCTTT	126	1/2	0.075	94%
		Antisense	GCATCCTCTCCGTTGACGAT				
<i>Cyp2b10</i>	NM_009999.4	Sense	ATGTTTGTAGTGGAGGAACTGCGG	81	3/4	0.1	103%
		Antisense	ATATTGGCCGTGATGCACTG				
<i>Zfp969</i>	XM_017319408.2	Sense	ATGAAAGAGAAACCCTATGAATGC	112	1	0.2	96%
		Antisense	ACACCCCTGTATCCTCTTGA				
<i>Zfp965</i>	NM_001242944.1	Sense	CTTCACTCAGGAAGAGTGGGC	243	2/4	0.1	95%
		Antisense	TGCCTTTGACTACGACTCTGA				
<i>Ttn</i>	NM_011652.3	Sense	GCCACTGCTGTGGTAGAAGT	129	245/246	0.2	98%
		Antisense	CTTAGACCCGCCATCGTCTC				
<i>Rbm14-rbm4</i>	NM_001290127.1	Sense	AATGTTCGATGGGGCGGATAC	74	1	0.2	106%
		Antisense	CAGCTCATGACCGTGCCATA				
<i>Sec61g</i>	XM_003085302.1	Sense	TTGTTGAGCCAAGTCAGCGG	120	1/2	0.05	105%
<i>Gm15266</i>		Antisense	TGATAGCAAATCCTATCGTTGTGG				
<i>LOC102637269</i>							
<i>Rbm24</i>	NM_001081425.1	Sense	TGCAGCCAGTTTTGCCTTT	166	2/4	0.2	95%
		Antisense	ATGTACGGTGTGGTGAAGCC				
<i>Tmem81</i>	NM_029025.3	Sense	TGGCCTTGGCTACAAGGAAG	266	2	0.1	93%
		Antisense	AATTGGCTCGGAAGGGTCTG				
<i>Rnase2a</i>	NM_053113.2	Sense	GAGCCTATCCCCGATGTGATG	218	2	0.1	93%
		Antisense	ATGACTGGCCGGAGTTGTG				
<i>Sult2a2</i>	NM_009286.2	Sense	ACCTCCCATCTTCCCATCCA	73	2/3	0.1	95%
		Antisense	TCATGAGATAGATCGCCTTGG				
<i>Ndufb4b</i>	XM_001478443.6	Sense	TGAAAATCCCGGGGAGTCAA	102	1	0.2	94%
		Antisense	CGGAGACACGTCATACTCGG				

Materials and Methods

<i>Dmbt1</i>	NM_001347632.2	Sense	CACCACCAATCTCCTTTGTCAG	207	44/46	0.1	99%
		Antisense	GTCTCGTTGTCAGCCTGTTTGA				
<i>Cyp2b13</i>	NM_007813.2	Sense	CTCATGCTGAGTCACTTCCCTCTT	52	9	0.1	91%
		Antisense	ACAGACCACAGAGTGTGAAGTTGG				
<i>Prtn3</i>	NM_011178.2	Sense	CAATTACAACCCCGAGGAGAAC	51	3/4	0.1	95%
		Antisense	TTTAGCTGGAGGAGAAGCACGT				
<i>Amy2a5</i>	NM_001042711.2	Sense	TGCTTTCCTCATTGGGTTTC	101	1	0.1	93%
		Antisense	AATATCAACCCAGCGCCACT				
<i>Cyp2b9</i>	NM_010000.2	Sense	ACCAGATCTACTTCTTAGCCCGCT	151	9	0.1	104%
		Antisense	GAGAACAACAGTAGAAGGAAGGGTG				
<i>Mup1</i>	NM_001163011.1	Sense	TAAGAACAAGCAAAGGGGCTGG	127	1	0.1	97%
		Antisense	TCAGTCCCAAACACAGCAGCA				
<i>Apoa1</i>	NM_009692.4	Sense	GCTGAACCTGAATCTCCTGGAA	52	3/4	0.1	93%
		Antisense	ACTAACGGTTGAACCCAGAGTGTC				
<i>ApoE</i>	NM_009696.4	Sense	CTTGTTTCGGAAGGAGCTGACT	92	1/3	0.1	97%
		Antisense	AGGCATCCTGTCAGCAATGTG				
<i>Tbp</i>	NM_013684.3	Sense	GTGAGTTGCTTGCTCTGTGC	359	8	0.2	104%
		Antisense	GCTGCGTTTTTGTGCAGAGT				
<i>Pipb</i>	NM_011149	Sense	GGAGATGGCACAGGAGGAA	72	3/4	0.1	103%
		Antisense	GTAGTGCTTCAGCTTGAAGTTCTCAT				

Materials and Methods

Primers used in manuscript 2

Gene symbol	Accession		Sequence	Amplicon length	Exons	[μ M]	Efficiency
<i>Oryctolagus cuniculus</i>							
LOC100344375	XM_017339423.1	Sense	GTTGAGAAGGGCTCAACCGT	126	4/5	0.3	97%
		Antisense	CAGACGTCTCAACACAAGCC				
LOC100344884	XM_017339724.1	Sense	CCTTCTACGGGGAGCATGAC	169	5	0.3	96%
		Antisense	TACCCGCGAACGCATATCTC				
GCK	XM_008261818.2	Sense	AGACATCGACAAGGGCATCC	79	4/5	0.3	90%
		Antisense	CCCCACGATGTTGTTCCCTT				
LOC103351691	XR_001795369.1	Sense	AACCAGCCCAGAAGATGACTG	136	NA	0.3	100%
		Antisense	CCTGTGGTCTTCCTTTGCTCT				
TFCP2L1	XM_008251077.2	Sense	CGAAGAGACGCTGACCTACC	212	2/4	0.3	93%
		Antisense	CAATGTCCAGGATGCGGTCT				
ACACB	XM_017339196.1	Sense	GGCCATCCGGTTTGTAGTCA	125	3/4	0.3	99%
		Antisense	CCACGTTGGCGTAGTTGTTG				
ASCL1	XM_002711229.3	Sense	TTGGTGCGAATGGACTTTGG	70	1/2	0.3	94%
		Antisense	CGTCACTGACCAGAAAGCAC				
ACSS2	XM_002710791.3	Sense	AACAGGGCATTTCGAAAGGGT	127	4/5	0.3	98%
		Antisense	GCAGAGAAGCCTGCAAACAC				
LOC108177690	XM_017346007.1	Sense	CTGTGTGGAGGCAGTGTAGG	113	1	0.3	98%
		Antisense	GAGAACGACGAGCAGGAAGA				
FAM91A1	XM_002710763.3	Sense	CAAGGTGGACTTGCAGCATT	236	20/22	0.3	99%
		Antisense	CAAGAGGAACCCAGTCTGCC				
MYH6	XM_017348206.1	Sense	GACACTGGCAAAGGCAAAGG	234	NA	0.3	104%
		Antisense	CTTCCTGCAGATGCGAATGC				
OMD	NM_001101695.1	Sense	TCAACCCCTGAAAATAACGC	157	1/2	0.3	103%
		Antisense	CCTCACTTGGGTCTTGGTCAT				
LRRC39	XM_002715469.3	Sense	ACGAGGGAGGATGGAAGAGT	219	3	0.4	96%
		Antisense	AGTGAGCAGTCCAATTCCTCG				
LOC108176846	XR_001793580.1	Sense	TCTGGGGACCTTACGGAGTC	107	NA	0.3	93%
		Antisense	TCAGCTCCTGAGAAAGTGCG				
TTN	XM_017343215.1	Sense	TGCCAAGTGACCAACCTTGT	186	271/272	0.3	93%
		Antisense	GGCTAAGGTTCGACTGTCT				
GLT1D1	XM_008251202.1	Sense	AGAGTCAAGGCATCACCACG	89	2/4	0.3	91%
		Antisense	GTCGTCAGCACTCCGGTTA				

Materials and Methods

<i>TREH</i>	NM_001082290.1	Sense	CACCCTGTGAGAGCCAGATT	81	1/2	0.3	99%
		Antisense	GCTTATCGTCCGGGTAGAGC				
<i>GAPDH</i>	NM_001082253.1	Sense	TCGGAGTGAACGGATTTGGC	146	NA	0.3	105%
		Antisense	GCCGTGGGTGGAATCATACT				
<i>PIIB</i>	XM_002718143.4	Sense	TCCCAGTTCCTTCATCACCACAG	83	4	0.3	94%
		Antisense	TCCATGCCCTCCAGAACTTT				

Mouse AML12 cell line

<i>Fam91a1</i>	NM_145959.3	Sense	TGGCGCCTCTTACCAATGAG	124	16/17	0.1	99%
		Antisense	CCTTGCCCAGTGACATGGTA				
<i>Acss2</i>	NM_019811.3	Sense	GCCATATGCTGACCCCTCTC	103	12/13	0.3	100%
		Antisense	TCCCCGGACTCATT CAGGAT				
<i>Pnpla3</i>	NM_054088.3	Sense	CTTCCTGGGCTTCTACCACG	152	1/2	0.3	103%
		Antisense	CCATTATACGGCCGAGAGGG				
<i>Pipb</i>	NM_011149.2	Sense	GGAGATGGCACAGGAGGAA	72	3/4	0.1	103%
		Antisense	GTAGTGCTTCAGCTTGAAGTTCTCAT				

Materials and Methods

Primers used in manuscript 3

Gene symbol	Accession		Sequence	Amplicon length	Exons	[μ M]	Efficiency
<i>Sus scrofa</i>							
PPP1R1B	XM_021067044.1	Sense	GGCACCACCTCAAGTCGAAG		99	NA	0.08
	XM_021067045.1	Antisense	TGATGGACTGCAGGTGAGAC				
	XM_021067046.1						
	XM_021067047.1						
OASL	NM_001031790.1	Sense	GTGTGGTTGGTCGAGGAAGT		98	2	0.08
		Antisense	CTGTAGGCAGGCATGATGGT				
PPP4R4	XM_021099655.1	Sense	ATATGCCTGTCTCCCACACG		115	NA	0.2
	XM_021099656.1	Antisense	TGAAGCTGCCTTTTGCACAG				
	XM_021099657.1						
	XM_021099658.1						
	XM_021099659.1						
	XM_021099660.1						
	XM_021099661.1						
	XM_021099662.1						
HES4	XM_003481929.4	Sense	GAAAGAGAGTTCCCGCCACT		181	NA	0.2
		Antisense	GACCAGGAATCGGTTACCT				
NEURL3	XM_003124839.5	Sense	CATGGATCCTACAGCCAGCG		203	NA	0.2
		Antisense	GGCATTGGCCGTGTCCTTTG				
HTD2	XM_003132274.4	Sense	GTGGGGTTGGACTGAATGCT		97	NA	0.2
	XM_021069097.1	Antisense	ATGTCCAAGGGTAAGGCAGC				
	XM_021069098.1						
	XM_003132275.4						
CYP2C32	XM_013983597.2	Sense	GCCCCGATGGAGCTATTTTT		115	NA	0.08
		Antisense	CGTGGCTGAACCCACTATAAAA				
AFP	NM_214317.1	Sense	AGAGGAACAACCTTGAGGCCG		107	13/14	0.1
		Antisense	TCAGTGCTGGACCCTCTCT				
TMEM45B	XM_021063152.1	Sense	TTGTGCTGGAGCTTTTCCGA		109	NA	0.2
	XM_021063153.1	Antisense	TTCTGGTCCCATTTCAGGTGC				
	XM_021063154.1						

Materials and Methods

	XM_021063155.1						
	XM_021063156.1						
ENPEP	NM_214017.1	Sense	TATCTGTGCAGCGGTAGTGG	286	1	0.1	102%
		Antisense	GGAGATGTTCACTGTCCCCG				
LOC110256649	XM_021072807.1	Sense	ACAACACGGCTGAAGGTAGG	199	NA	0.2	102%
		Antisense	TCTGAGGTGGGATCAAAAGG				
CYP2J34	NM_001244633.1	Sense	AGCGGTTTGACTACCAGGATG	91	4/5	0.2	100%
		Antisense	AGCTGGACCTGCACTGATGTG				
LOC100526118	XM_003128792.4	Sense	GGTTATCCGGTGGCTTCTGG	152	NA	0.1	101%
		Antisense	TCTGGACCAACTTCATGCCA				
S100A2	XM_001929556.5	Sense	GGTTGCCACCTTCCACAAGTA	203	NA	0.08	102%
SPRY3	XM_013986552.2	Sense	CAGCATTACGCCCTCACCTT	96	NA	0.2	100%
FOXG1	XM_021099188.1	Sense	TATGAGAAGCCCGGTCAG	171	NA	0.2	100%
GTSE1	XM_003126205.6	Sense	AGCCCTGCAAGCAACATAGT	87	NA	0.2	98%
	XM_005663861.3	Antisense	TGGCAGAACATACGGCAGAG				
SQLE	NM_001101026.1	Sense	GCAGCTATTCTCCAGGCCAA	191	8/10	0.2	99%
		Antisense	AGCGCAACTGGACCACTAAT				
CHL1	XM_021069243.1	Sense	CTGCAAACAATGACCCTGTGT	154	NA	0.2	102%
	XM_021069244.1	Antisense	GGAGGCAGCCCAGAAAGAAT				
	XM_021069246.1						
	XM_013981901.2						
	XM_021069247.1						
	XM_021069248.1						
	XM_021069249.1						
	XM_021069250.1						
UBA52	NM_214211.1	Sense	CTGCCGCAAGTGTTATGCTC	100	4/5	0.2	102%
		Antisense	TTTGACCTTCTTCTTGGGGCG				

Materials and Methods

<i>Homo sapiens</i> cell line							
PPP1R1B	NM_032192	Sense	GGGCACCATCTCAAGTCGAA	126	4/5	0.2	92%
	NM_181505	Antisense	TGAGGCCTGGTTCTCATTCA				
AFP	NM_001134.3	Sense	CTTTGGGCTGCTCGCTATGA	176	5/6	0.2	91%
	NM_001354717	Antisense	ATGGCTTGAAAGTTCGGGT		6/7		
TMEM45B	NM_001331210.2	Sense	CTCTGTTCCGAGGGTGTGTT	158	5/6	0.2	95%
	NM_138788.5	Antisense	GTCCCATTCGGGTGTCCAA		4/5		
	NM_001331211.2				5/6		
	NM_001331212.2				5/6		
ENPEP	NM_001977.4	Sense	GAAGAGCTTACCCCCAGCAG	120	1	0.4	100%
	NM_001379611.1	Antisense	GACTTGTCGGTTCTCCGTGT				
	NM_001379612.1						
	NM_001379613.1						
SPRY3	NM_005840.4	Sense	TGAACAGCTGCGCTCTACTC	237	2	0.4	98%
	NM_001304990.2	Antisense	GCAGTGGTGCTATGGGACAT		3		
	NM_001394353.1				4		
	NM_001394354.1				4		
	NM_001394355.1					4	
SQLE	NM_003129.4	Sense	GCCTGCCTTTCATTGGCTTC	90	1/2	0.2	99%
		Antisense	TTCCTTTTCTGCGCCTCCTG				
GAPDH	NM_002046.7	Sense	CAAATTCCATGGCACCCTCA	132	4/5	0.2	95%
	NM_001256799.3	Antisense	GACTCCACGACGTACTCAGC		3/4		
	NM_001289745.3				4/5		
	NM_001289746.2				3/4		

Materials and Methods

Mouse cell line							
<i>Ppp1r1b</i>	NM_144828.2	Sense	CCCAACCCCTGTGCCTATAC	119	4/5	0.3	90%
	NM_001313970.1	Antisense	TCCCGAAGCTCCCCTAACTC				
<i>Afp</i>	NM_007423.4	Sense	AGTTTCCAGAACCTGCCGAG	145	4/5	0.1	100%
		Antisense	ACCTTGTCGTACTIONGAGCAGC				
<i>Tmem45b</i>	NM_144936.1	Sense	TCGGGATAACATCGTGCTGG	115	4/5	100	0.2%
		Antisense	GTCCCATTCTGGCCTTCCAA				
<i>Enpep</i>	NM_007934.3	Sense	GCAAACCCACTCGTGACCTA	188	1	0.2	97%
		Antisense	CAGCCGATAGACACTGTCCC				
<i>Spry3</i>	NM_001030293.3	Sense	GCTCTCCCACGCAGTATCAG	111	4	0.2	98%
	NM_001401849.1	Antisense	TTGATCAGAGGCAGTGGTGC				
	NM_001401850.1						
	NM_001401851.1						
<i>Sqle</i>	NM_009270.3	Sense	TACCTCAGTGTGACCTCGT	92	2	0.2	99%
		Antisense	TGGAGAGAACTGCTGCCAAG				
<i>Ppib</i>	NM_011149.2	Sense	GGAGATGGCACAGGAGGAA	72	3/4	0.1	103%
		Antisense	GTAGTGCTTCAGCTTGAAGTTCTCAT				

V. RESULTS

i. Dietary Erythrodiol Modifies Hepatic Transcriptome in Mice in a Sex and Dose-Dependent Way

Abstract: Erythrodiol is a terpenic compound found in a large number of plants. To test the hypotheses that its long-term administration may influence hepatic transcriptome and this could be influenced by the presence of APOA1-containing high-density lipoproteins (HDL), Western diets containing 0.01% of erythrodiol (10 mg/kg dose) were provided to *ApoE*- and *ApoA1*-deficient mice. Hepatic RNA-sequencing was carried out in male *ApoE*-deficient mice fed purified Western diets differing in the erythrodiol content. The administration of this compound significantly up-regulated 68 and down-regulated 124 genes at the level of 2-fold change. These genes belonged to detoxification processes, protein metabolism and nucleic acid related metabolites. Gene expression changes of 21 randomly selected transcripts were verified by RT-qPCR. *Ccl19-ps2*, *Cyp2b10*, *Rbm14-rbm4*, *Sec61g*, *Tmem81*, *Prtn3*, *Amy2a5*, *Cyp2b9* and *Mup1* showed significant changes by erythrodiol administration. When *Cyp2b10*, *Dmbt1*, *Cyp2b13*, *Prtn3* and *Cyp2b9* were analyzed in female *ApoE*-deficient mice, no change was observed. Likewise, no significant variation was observed in *ApoA1*- or in *ApoE*-deficient mice receiving doses ranging from 0.5 to 5 mg/kg erythrodiol. Our results give evidence that erythrodiol exerts a hepatic transcriptional role but this is selective in terms of sex and requires a threshold dose.

Keywords: erythrodiol; mice; liver; apolipoprotein E; olive oil; transcriptome

1. Introduction

A preeminent health-promoting traditional eating pattern commonly known as The Mediterranean diet (MedDiet) has occupied a wide framework of global research efforts for decades due to the very low-cardiovascular disease mortality rates regardless of lifestyle, poverty or any geographical differences between countries who have traditionally consumed as was evidenced by The Seven Countries study [1]. Further epidemiological studies revealed that this pattern was also associated with lower mortality rates and thus provided a healthy and extended life-span [2]. Recent evidence

Results

has proved that an intervention using this diet is able to reduce cardiovascular mortality [3]. A review of these aspects can be found in [4].

Virgin olive oil, directly extracted from fresh olive fruits, stands out as the major source of lipids in the MedDiet [5, 6]. Pomace olive oil is a blend obtained from remainder of the olives, skin, and pits used organic solvents [7] and is also consumed in this geographical area. Both have similar fatty acid composition [5, 8], but vary in phytosterols, waxes, tocopherols and triterpenes (uvaol, maslinic and erythrodiol) with higher content in pomace than in virgin olive oil [9]. Several recent studies have shown that continuous consumption of pomace olive oil protects against carcinogenic activities [10], hepatic steatosis [9], atherosclerosis [6], cardiovascular problems (CHD and stroke), inflammation and type 2 diabetes mellitus [5]. The latter was associated with positive antioxidant properties [11] or reduction in blood pressure [5].

Erythrodiol (18b-olean-12-ene-3b,28diol) [7], a 30-carbon atom pentacyclic triterpene (Figure 1) is biosynthesized by a cascade of cyclizations and rearrangements from oxidosqualene [10, 12, 13]. The alcohol is present in virgin olive oil at a concentration of 75 mg/kg [9, 13], with more presence in the unsaponifiable fraction of this oil [14] at a concentration of 500 mg/kg [9]. Erythrodiol is also detected in olive leaves [10, 15], leading to approximately 60% of their triterpenic content [13]. This alcohol is widely distributed through other plant species including leaves of *Ficus mysorensis* [12], *Conyza canadensis* [16], *Celastrus kusanoi* stems [17], stem bark of *Erythrina indica* [18], birch bark trees [19] and leaves of *Maytenus ilicifolia* [20].

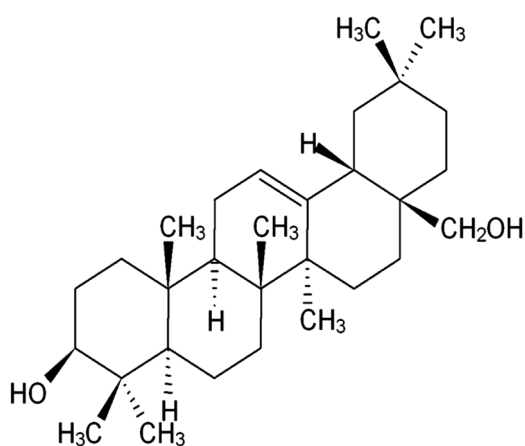


Figure 1. Erythrodiol chemical structure.

Results

Several studies have shown favorable properties of erythrodiol including diverse endogenous anti oxidative activities [11], antiproliferative, proapoptotic actions against colon adenocarcinoma HT-29 cells [10], histolytic lymphoma (U937) cells [21], breast cancer [21], gastric cancer [16] and astrocytoma [22]. The triterpenoid is also related to several antioxidant, antithrombotic and vasorelaxant benefits against cardiovascular problems [23, 24], combined with the ability to reduce cardiac hypertrophy and block profibrotic effects of angiotensin II [24]. Other biological activities include anti-inflammatory, immunomodulatory and anti-edematous properties by reducing neutrophil infiltration [8, 14, 25] and its ability to protect from neuroinflammation [25]. Erythrodiol was found to induce wound healing by increasing the production of actin filopodia, lamellipodia and stress fibers through activating Rho GTPases [19] and has provided antiplatelet properties when inhibiting ADP-induced activation [15].

Significant modifications on hepatic gene expression were found after long-term administration of pomace olive oil fraction-enriched diets with erythrodiol among other compounds [9]. Since the changes were not observed by its single administration, a new experiment was required to single out its action. In this regard, the long-term effect of erythrodiol needed to be addressed in order to understand and assess molecular functions and pharmacogenetic pathways of this triterpene.

2. Results

2.1. Somatometric Parameters

A long-term administration of a 10 mg/kg erythrodiol-supplemented Western diet was carried out in two mouse models of both sexes: *Apo1*- and *ApoE*-deficient mice. In the former group, erythrodiol administration for 4 weeks significantly increased body weight gain in males (4.2 ± 1.6 vs. 5.9 ± 1.4 g, $p < 0.01$ for control and erythrodiol, respectively). In contrast, in the second model, the administration of the triterpene for 12 weeks caused a decrease in body weight gain (4.5 ± 5.0 vs. 3.1 ± 3.3 g, $p < 0.05$ for control and erythrodiol, respectively) with a marked decrease in liver mass (1.6 ± 0.6 vs. 1.3 ± 0.5 g, $p < 0.05$ for control and erythrodiol, respectively). No effect was observed in females of both genetic models.

2.2. Histological Analyses

Mice lacking APOE are models of spontaneous hepatic steatosis as shown in Figure 2A. To explore the influence of erythrodiol administration on this parameter, histological

Results

analyses of livers were carried out. Male *Apoe*-deficient mice consuming 10 mg/kg erythrodiol-enriched Western diet for 12 weeks showed decreased lipid droplets (Figure 2B). When the fat areas were quantified, the group receiving erythrodiol exhibited a non-significant ($P < 0.06$) trend to a lesser accumulation than control group, as shown in Figure 2C.

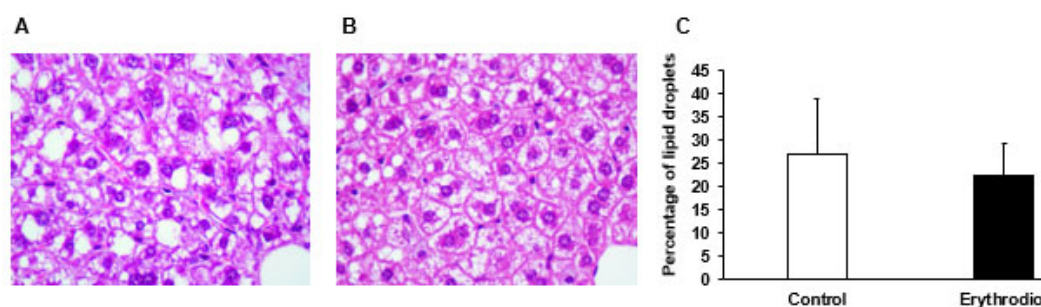


Figure 2. Hepatic histological analyses in male *Apoe*-deficient mice fed the different diets. Representative liver micrographs at $\times 400$ magnification from consuming Western diet (A) and consuming 10 mg/kg erythrodiol-containing Western diet (B). Liver sections ($4 \mu\text{m}$) from each mouse were stained with hematoxylin and eosin and blind evaluated. Morphometric changes of hepatic fat surface in mice consuming the different diets (C) where data are means \pm SD for each group ($n = 14$ and $n = 15$, respectively for control and erythrodiol). Statistical analyses were done according to Mann-Whitney's U-test.

2.3. Hepatic Gene Expression of *Apoe*-Deficient Male Mice Fed for 12 Weeks on a 10 mg/kg Erythrodiol-Containing Western Diet

To determine the impact of erythrodiol intake on hepatic transcriptome, seven RNA pools from fifteen animals receiving the above diet and another seven from fourteen mice receiving the Western control diet were sequenced using next generation sequencing. From each library, clean reads sequences ($46765 \times 10^3 \pm 7189 \times 10^3$), filtered from contaminants, adaptors, low quality regions, and reads with unknown bases, were mapped onto reference genome, followed by gene prediction. In both groups, the mapping ratio was 74% for a transcript number of $31,369 \pm 3,051$. Splicing patterns contributed to a variety of differentially splicing genes with a total of 14,920 novel transcripts, 13,439 coding and 1,481 non coding transcripts. Coding genes showed 11,605 previously unknown splicing events for known genes and 1,834 coding transcripts previously unknown. Globally, the erythrodiol administration did not significantly modify single nucleotide polymorphisms. In this regard, transversions A-G were $3172 \pm$

Results

1019 vs 3835 ± 155 for control and erythrodiol groups, respectively and those corresponding to C-T were 3113 ± 1024 vs 3787 ± 133 . No significant changes were observed for transversions either (A-C, 609 ± 209 vs 743 ± 47 ; A-T 796 ± 335 vs 988 ± 61 ; C-G, 576 ± 217 vs 726 ± 23 and G-T, 578 ± 200 vs 708 ± 28 for control and erythrodiol groups, respectively).

When alternative splicing events were screened, erythrodiol administration had no significant effect. Skipped exons were 6432 ± 1526 vs 7178 ± 344 for control and erythrodiol groups; alternative 5' splicing sites, 1568 ± 368 vs 1789 ± 42 ; alternative 3' splicing sites: 2181 ± 522 vs 2503 ± 62 ; mutually exclusive exons, 696 ± 102 vs 732 ± 48 and retained introns, 1504 ± 265 vs 1688 ± 20 in control and erythrodiol groups, respectively.

Differentially expressed genes, shown in Figure 3A, were 554 in the control and 488 in the erythrodiol group. According to their gene ontology classification, Figure 3B, all kinds of biological processes were involved, being cellular processes the category that included the highest number of genes. Using more stringent criteria of 2-fold change and false discovery rate of $P < 0.001$, 68 up-regulated genes and 124 down-regulated as reflected in the volcano plot of Figure 4A. As reflected in Figure 4 panels B, C and D, these genes were sorted into three main categories: detoxification processes, protein metabolism and nucleic acid related compounds. An example of genes modified at the level 2.9-fold change (\log_2 fold change 1.5 or -1.5) is reflected in Tables 1 and 2. Twenty-nine transcripts were up-regulated (Table 1) and sixty-three were down-regulated according to this criterion (Table 2).

Results

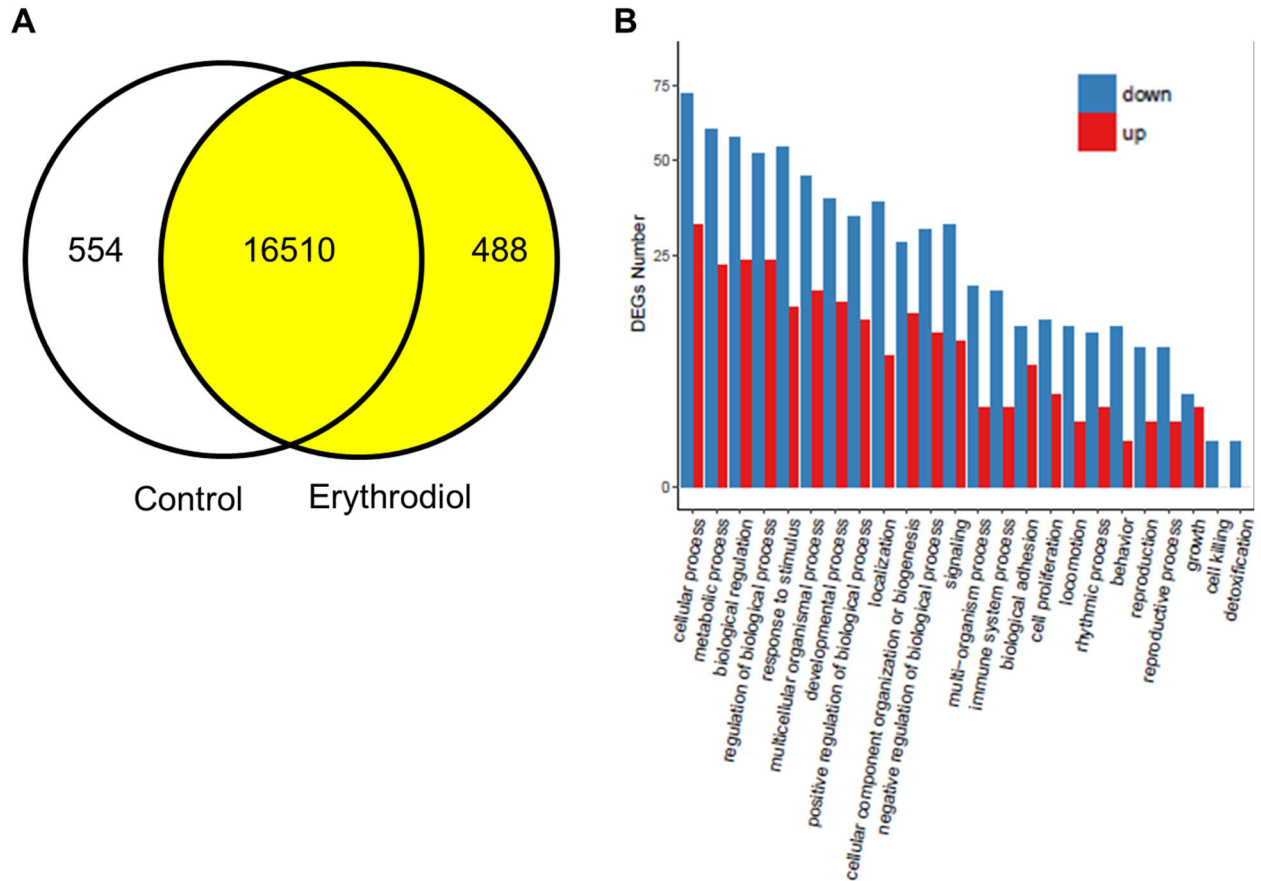


Figure 3. Differentially expressed genes. A, Venn diagram analysis. Control expressed 17064 while erythrodiol 16998 genes. Functional enrichment analysis of differentially expressed genes. B, Gene ontology (GO) classification of biological processes of liver transcriptome by erythrodiol administration. X axis represents GO term. Y axis represents the amount of up/down-regulated genes. DEGs, differentially expressed genes.

Results

NA	XM_01732 1851.2	Extensin-like isoform X2	<i>Gm40365</i>	2.7	0.000
Chromosomal stability	NM_17821 2.3	H2A clustered histone 19	<i>H2ac19/Hist2h2 aa2</i>	2.6	0.000
Aminopeptidase activity	NM_02900 8.1	Laeverin	<i>Lvrn</i>	2.5	0.001
G protein-coupled receptor signaling	NM_14633 7.1	Olfactory receptor 1396	<i>Olf1396</i>	2.5	0.001
Proteolysis	NM_02558 3.2	Chymotrypsinogen B1	<i>Ctrb1</i>	2.4	0.000
NA	XM_01731 3070.1	Predicted gene/ coiled- coil domain containing 168	<i>Gm8251/Ccdc16 8</i>	2.2	0.000
Ion transmembrane transport	NM_00109 9298.3	Sodium channel, voltage-gated, type II, alpha	<i>Scn2a</i>	2.2	0.000
Cell adhesion	NM_00103 3364.3	Cadherin-related family member 2	<i>Cdhr2</i>	2.0	0.000
Short-term neuronal synaptic plasticity	NM_17273 7.4	Shisa family member7	<i>Shisa7</i>	2.0	0.0003
Regulation of immune response	NM_17878 6.4	Selection and upkeep of intraepithelial T cells 4	<i>Skint4</i>	1.9	0.001
Chromatin organization	NM_13921 8.1	Developmental pluripotency- associated 3	<i>Dppa3</i>	2.0	0.001
Transcription factor	NM_00102 9933.3	Zinc finger protein 114	<i>Zfp114</i>	1.9	0.001
Ubiquitin-protein transferase activity	NM_02770 8.1	F-box protein 24	<i>Fbxo24</i>	1.8	0.0002
Protein glycosylation and carbohydrate metabolism	NM_00805 1.6	Fucosyltransferase 1	<i>Fut1</i>	1.8	0.000
G protein-coupled receptor	NM_00101 1852.2	Olfactory receptor 1029	<i>Olf1029</i>	1.7	0.001
NA	NA	Predicted gene, 40600	<i>Gm40600</i>	1.7	0.0001
Cell adhesion	NM_17868 5.5	Protocadherin 20	<i>Pcdh20</i>	1.7	0.000
Metal ion binding	NM_00122 0499.3	Ring finger 223	<i>Rnf223</i>	1.7	0.001
NA	NM_02960 8.1	Family with sequence similarity 209	<i>Fam209</i>	1.6	0.0003
P450 pathways	NM_00999 9.4	Cytochrome P450, family 2, subfamily b, polypeptide 10	<i>Cyp2b10</i>	1.6	0.000

Results

NA	NM_02751 1.1	Histidine rich carboxyl terminus 1	<i>Hrct1</i>	1.6	0.001
Cell adhesion	NM_03358 5.2	Protocadherin gamma subfamily A, 2	<i>Pcdhga2</i>	1.5	0.000
Retinoic acid binding	NM_02995 8.1	Lipocalin 12	<i>Lcn12</i>	1.5	0.0001

NA, not available.

Table 2. Hepatic transcripts differentially down-regulated by the administration of erythrodiol at the level of signal \log_2 ratio < -1.5 and false discovery rate < 0.001 in male *ApoE*-deficient mice according to RNAseq.

Biological Process	GenBank	Name	Gene Symbol	SL ₂ R	P-value
Transcription factor	XM_017319408.2	Zinc finger protein 969	<i>Zfp969</i>	-6.7	0.0000
Transcription factor	NM_001242944. 1	Zinc finger protein 965	<i>Zfp965</i>	-6.5	0.0000
Muscle structure	NM_011652.3	Titin	<i>Ttn</i>	-5.8	0.0000
Transcription factor	NM_001290127. 1	RNA binding motif protein 14(Rbma4) and RNA binding motif protein 4 (Rbm4)	<i>Rbm14- rbm4</i>	-5.2	0.0000
Protein transmembrane transporter activity	NM_011343.3	Translocase Sec61 gamma subunit	<i>Sec61g</i>	-5.1	0.0000
Cell differentiation	NM_001081425	RNA binding motif protein 24	<i>Rbm24</i>	-4.9	0.0001
NA	NM_029025.3	Transmembrane protein 81	<i>Tmem81</i>	-4.7	0.0002
NA	NA	Nuclear body protein SP140-like	LOC1052 47075	-4.5	0.001
Metal ion binding, nucleic acid binding	NM_053113.2	Ribonuclease, RNase A family, 2A (liver, eosinophil-derived neurotoxin)	<i>Rnase2a</i>	-4.5	0.001
Sulfotransferase activity	NM_009286.2	Sulfotransferase family 2A, member 2	<i>Sult2a2</i>	-4.4	0.001
Response to oxidative stress	XM_001478443.6	Predicted NADH:ubiquinone oxidoreductase subunit B4B	<i>Ndufb4b</i>	-4.3	0.0000
Sulfation of steroids and bile acids	NM_001111296. 2	Sulfotransferase family 2A, member 1	<i>Sult2a1</i>	-4.0	0.0000

Results

Hydrogen peroxide catabolic process and oxygen transport	NM_001278161.1	Hemoglobin, beta adult major chain	<i>Hbb-b1</i>	-4.0	0.0000
NA	NA	Small nuclear ribonucleoprotein F	<i>Gm13092</i>	-4.0	0.0000
Ion transport	XM_006509537.4	Predicted solute carrier family 5 (sodium iodide symporter),	<i>Slc5a5</i>	-3.9	0.0002
Cell differentiation and protein transport	NM_001347632.2	Deleted in malignant brain tumors 1	<i>Dmbt1</i>	-3.9	0.0000
P450 pathway	NM_007813.2	Cytochrome P450, family 2, subfamily b, polypeptide 13	<i>Cyp2b13</i>	-3.7	0.0000
G protein-coupled receptor signaling pathway	NM_010999.3	Olfactory receptor 56p	<i>Olfr56</i>	-3.3	0.0000
Cation transport	NM_172583.3	Transmembrane protein 63c	<i>Tmem63c</i>	-3.2	0.0000
Regulation of GTPase activity	NM_011178.2	Proteinase 3	<i>Prtn3</i>	-3.2	0.0000
Ions and reactive oxygen species responses	NM_134066.3	Aldo-keto reductase family 1, member C18	<i>Akr1c18</i>	-3.0	0.0000
NA	NA	Circumsporozoite protein-like	<i>LOC108167857</i>	-2.7	0.0007
Cell adhesion and blood coagulation	NM_001001999.1	Glycoprotein Ib, beta polypeptide	<i>Gp1bb</i>	-2.7	0.0001
NA	NM_001013773.3	Neurexophilin and PC-esterase domain family, member 5	<i>Nxpe5</i>	-2.6	0.0005
Signaling pathway	NM_001101656.2	CD300 molecule like family member D4	<i>Cd300ld4</i>	-2.6	0.0000
Regulation of transcription	NG_065348.1	Coiled-coil-helix-coiled-coil-helix domain containing 2, pseudogene on chromosome 4	<i>Chchd2-ps</i>	-2.6	0.0000
Carbohydrate catabolism	NM_001042711.2	Amylase 2a5	<i>Amy2a5</i>	-2.5	0.0000
Cell-matrix adhesion	NM_080457.3	Mucin 4	<i>Muc4</i>	-2.3	0.0006
Transcription		Predicted gene 3055	<i>Gm3055</i>	-2.3	0.001

Results

	NM_001346707				
G-protein coupled receptor signaling pathway	NM_013564.7	Insulin-like 3	<i>Insl3</i>	-2.2	0.0000
Immune response	NM_011280.2	Tripartite motif-containing 10	<i>Trim10</i>	-2.2	0.0001
Signaling pathway	NM_010014.3	Disabled 1	<i>Dab1</i>	-2.1	0.0000
Cell growth and differentiation	NM_010052.5	Delta like non-canonical Notch ligand 1	<i>Dlk1</i>	-2.1	0.0002
Regulation of cell adhesion	NM_001351947.1	Olfactomedin 4	<i>Olfm4</i>	-2.1	0.0000
Ion transport	NM_172469.3	Chloride intracellular channel 6	<i>Clic6</i>	-2.1	0.0000
Oxidoreductase activity	NM_021509.5	Monoxygenase, DBH-like 1	<i>Moxd1</i>	-2.0	0.0000
P450 pathway	NM_010000.2	Cytochrome P450, family 2, subfamily b, polypeptide 9	<i>Cyp2b9</i>	-2.0	0.0000
Ion binding	NM_009789.2	S100 calcium binding protein G	<i>S100g</i>	-2.0	0.0000
Immune response	NM_001013832.2	G protein-coupled receptor 31, D17Leh66b region	<i>Gpr31b</i>	-2.0	0.0003
Proteolysis	NM_010810.5	Matrix metalloproteinase 7	<i>Mmp7</i>	-2.0	0.0000
Oxidation process	NM_019545.4	Hydroxyacid oxidase 2	<i>Hao2</i>	-1.9	0.0000
Visual perception.	NM_021352.3	Crystallin, beta B3	<i>Crybb3</i>	-1.9	0.0000
Iron-binding	NM_008522.3	Lactotransferrin	<i>Ltf</i>	-1.9	0.0000
Glycolytic process	NM_001025388.2	Enolase 1B	<i>Eno1b</i>	-1.9	0.0000
Chromatin organization	NM_178187.4	H2A clustered histone 8	<i>Hist1h2ae</i>	-1.7	0.0000
Signaling pathway and hydrogen peroxide catabolism	NM_001362755.1	Dual oxidase 2	<i>Duox2</i>	-1.7	0.0000
mRNA splicing	NM_183024.1	Ribonucleoprotein, PTB-binding 2	<i>Raver2</i>	-1.7	0.0000
Cytoplasmic translation	NM_026517.3*	Ribosomal protein L22 like 1	<i>Rpl22l1</i>	-1.7	0.00000
Keratinization	NM_009264.2	Small proline-rich protein 1A	<i>Sprr1a</i>	-1.6	0.0000

Results

Carbohydrate and MHC class I protein binding	NM_133203.5	Killer cell lectin-like receptor, subfamily A, member 17	<i>Klra17</i>	-1.6	0.001
Modulation of synaptic transmission	NM_023716.2	Tubulin, beta 2B class IIB	<i>Tubb2b</i>	-1.6	0.0000
Ion transmembrane transport	NM_146017.3	Gamma-aminobutyric acid (GABA) A receptor, pi	<i>Gabrp</i>	-1.6	0.0002
G protein-coupled receptor activity	NM_001104614.1	Vomerolnasal 2, receptor 3	<i>Vmn2r3</i>	-1.6	0.0000
Sulfotransferase activity	NM_001184981.2	Sulfotransferase family 2A, member 7	<i>Sult2a7</i>	-1.6	0.0000
Interferon response	NM_011579.3	T cell specific GTPase 1	<i>Tgtp1</i>	-1.5	0.0000
Transcription factor	NM_001033123.3	Predicted gene 14288	<i>Gm14288</i>	-1.5	0.0000
Binding monosaccharides	NM_001134644.1	Major urinary protein 13	<i>Mup13</i>	-1.5	0.0000
Regulation of gene expression, protein kinase B signaling	NM_001163011.1	Major urinary protein 1	<i>Mup1</i>	-1.5	0.0000

NA, not available.

To confirm the RNAseq data carried out on seven hepatic RNA pools of each group, 21 transcripts were randomly chosen from Tables 1 and 2 to design their RT-qPCR assays. The latter were carried out on individual hepatic RNA samples of each mouse. Selected transcripts were: *H4c17*, *LOC100862456*, *Ccl19-ps2*, *Ctrb1*, *Cyp2b10*, *Zfp969*, *Zfp965*, *Ttn*, *Rbm14-rbm4*, *Sec61g*, *Rbm24*, *Tmem81*, *Rnase2a*, *Sult2a2*, *Ndufb4b*, *Dmbt1*, *Cyp2b13*, *Prtn3*, *Amy2a5*, *Cyp2b9* and *Mup1*. The expression of these transcripts normalized to the average of *Ppib* and *Tbp* reference genes is depicted in Table 3. Only 9 (*Ccl19-ps2*, *Cyp2b10*, *Rbm14-rbm4*, *Sec61g*, *Tmem81*, *Prtn3*, *Amy2a5*, *Cyp2b9* and *Mup1*) out of 21 showed significant changes by the administration of erythrodiol. Association analyses of individual values obtained by RT-qPCR of these genes (Figure 4E) revealed a significant association between *Cyp2b13* and *Cyp2b9* and between *Cyp2b13* and *Prtn3*, suggesting a certain co-regulation or overlapping in biological activities.

Results

Table 3. Changes in selected hepatic gene expressions of male *Apoe*-deficient mice receiving 10 mg/kg erythrodiol according to RT-qPCR assay.

Gene Symbol	Control (n=14)	Erythrodiol (n=15)	Fold Change	SL ₂ R
<i>H4c17</i>	1.1 ± 0.5	1.0 ± 0.3	0.85	-0.23
<i>LOC100862456</i>	1.0 ± 0.3	1.1 ± 0.9	1.1	0.13
<i>Ccl19-ps2</i>	1.0 ± 0.2	0.7 ± 0.3*	0.67	-0.58
<i>Ctrb1</i>	2.5 ± 3.4	100 ± 341	40	5.32
<i>Cyp2b10</i>	1.5 ± 1.4	2.3 ± 5.4*	1.46	0.55
<i>Zfp969</i>	1.9 ± 2.0	2.5 ± 1.3	1.34	0.42
<i>Zfp965</i>	1.2 ± 0.6	1.5 ± 0.7	1.55	0.63
<i>Ttn</i>	1.3 ± 0.8	1.1 ± 0.7	0.90	-0.16
<i>Rbm14-rbm4</i>	1.0 ± 0.2	0.8 ± 0.3*	0.77	-0.37
<i>Sec61g</i>	4.6 ± 9.4	0.1 ± 0.01*	0.01	-6.54
<i>Rbm24</i>	1.9 ± 3.4	0.8 ± 0.7	0.44	-1.19
<i>Tmem81</i>	1.1 ± 0.5	0.6 ± 0.2*	0.49	-1.02
<i>Rnase2a</i>	1.8 ± 2.2	1.4 ± 1.5	0.79	-0.34
<i>Sult2a2</i>	4.6 ± 13	2.1 ± 3.9	0.45	-1.15
<i>Ndufb4b</i>	1.1 ± 0.6	1.1 ± 0.5	0.97	-0.04
<i>Dmbt1</i>	1.4 ± 2.0	0.01 ± 0.01	0.01	-6.81
<i>Cyp2b13</i>	46 ± 105	6.2 ± 19	0.14	-2.89
<i>Prtn3</i>	7.4 ± 17	0.3 ± 0.2*	0.04	-4.79
<i>Amy2a5</i>	1.1 ± 0.4	0.4 ± 0.1*	0.41	-1.28
<i>Cyp2b9</i>	21 ± 31	1.0 ± 1.9*	0.05	-4.36
<i>Mup1</i>	1.4 ± 0.8	0.6 ± 0.5*	0.44	-1.19

Results are expressed as means and standard deviations normalized to the average of *Ppib* and *Tbp* as reference genes. Statistical analysis was carried out according to Mann-Whitney U-test and *, $P < 0.05$.

Using the \log_2 ratio of fold changes obtained by RNAseq and RT-qPCR for the twenty-one selected transcripts, a correlation analysis was carried out. As shown in

Results

Figure 5A, a non-significant low correlation coefficient of 0.3 was obtained. Indeed, as shown in Figure 5B, there were important discrepancies between both methods. To explore the reason of such lack of agreement, both methods were critically revised. When transcripts of RNAseq showing either zero counts or without counts in more than 60% of samples were excluded, a significant agreement ($r = 0.9$, $P < 0.0008$) between both methods was observed (Figure 5C) and all samples were properly categorized (Figure 5D). Only 9 out the 21 chosen genes tested by RT-qPCR show good correlation with the RNA seq data.

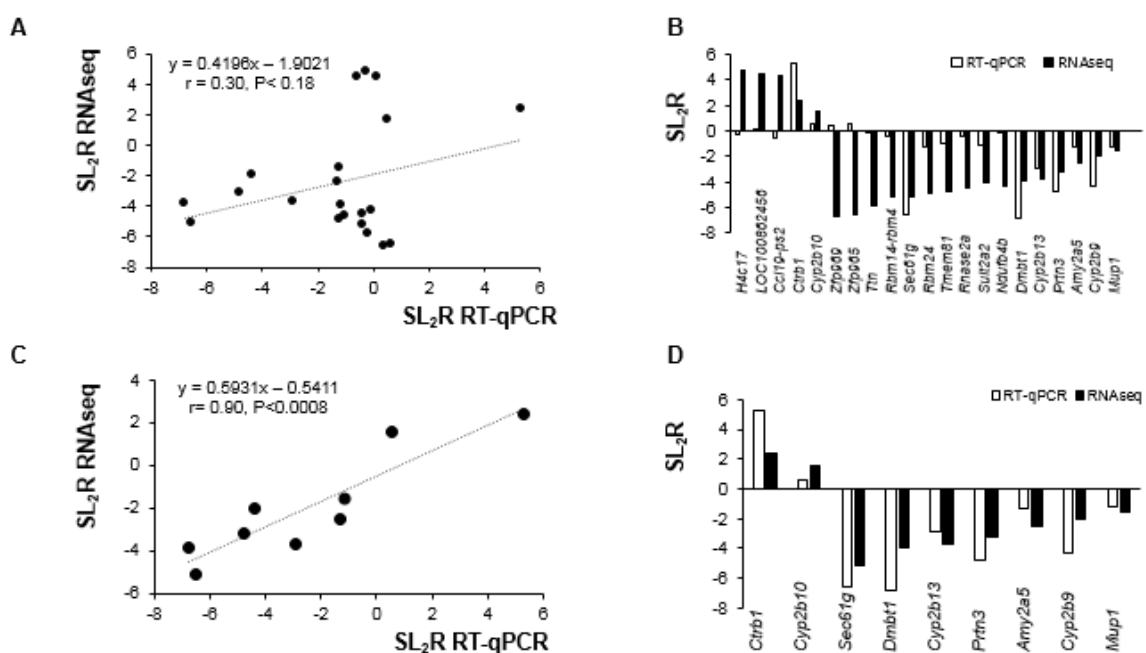


Figure 5. Concordance between used methods of RNA analysis. A) Correlation analysis of 21 selected genes between RNAseq and RT-qPCR normalized to the invariant *Pipb* and *Tbp* genes. The mean values obtained for signal log₂ ratio (SL₂R) from individual analyses (Table 3) were plotted against the RNAseq which used partially pooled samples (Tables 1 and 2). Poor agreement between the procedures was seen ($r=0.3$, $P<0.18$). B) Changes in values of SL₂R expression of both methods for the 21 selected genes. C) SL₂R correlation analysis between between RNAseq and RT-qPCR results normalized to the invariant *Pipb* and *Tbp* of 9 filtered genes after excluding those without counts in more than 60% of samples. Good agreement between the procedures was observed ($r=0.9$, $P<0.0008$). D) Changes in values of SL₂R expression of both methods for the 9 after removing those with low counts.

2.4. Hepatic Gene Expression in the Livers of Female *Apoe*-Deficient Mice Fed on a 10 mg/kg Erythrodiol-Containing Western Diet for 12 Weeks

To explore, a sex-related response, five transcripts (*Cyp2b10*, *Dmbt1*, *Cyp2b13*, *Prtn3* and *Cyp2b9*) showing high expression changes in male *Apoe*-deficient mice were used as

Results

subrogated markers of erythrodiol administration and quantified their expression in the female livers. Results showed no significant changes (Table 4). This finding points out to a sex-specific hepatic gene expression in response to erythrodiol.

Table 4. Hepatic changes in selected gene expressions of female. *Apoe*-deficient mice receiving 10 mg/kg erythrodiol.

Gene Symbol	Control (n=12)	Erythrodiol (n=13)
<i>Cyp2b10</i>	1.6 ± 1.4	1.4 ± 1.5
<i>Dmbt1</i>	1.9 ± 2.8	6.5 ± 9.6
<i>Cyp2b13</i>	19 ± 18	17 ± 17
<i>Prtn3</i>	1.4 ± 1.4	1.5 ± 1.0
<i>Cyp2b9</i>	5.7 ± 4.1	5.2 ± 4.3

Results as arbitrary units according to RT-qPCR assay normalized to *Ppib* and *Tbp* are expressed as means and standard deviations. Statistical analysis was carried out according to Mann-Whitney U-test.

2.5. Influence of Erythrodiol Dose on Selected Hepatic Gene Expressions in Male *Apoe*-deficient Mice Fed on Erythrodiol-Containing Western Diets for 12 Weeks.

A putative dose–response relationship was examined in males for the five selected genes, *Cyp2b10*, *Dmbt1*, *Amy2a5*, *Prtn3* and *Cyp2b9*. Several doses ranging from 0.5 to 5 mg/kg were tested in male *Apoe*-deficient mice. Interestingly, none showed a significant change in gene expression (Table 5). Genes such as *Cyp2b10* at 0.5 mg/kg and *Dmbt1* at 1 mg/kg showed no normal distributions with individual highly responders that skew the standard deviation and force the statistical analysis to a non-parametric approach. Despite the significant odd increases of *Cyp2b9* at 0.5 mg/kg and *Prtn3* at 1 mg/kg, no general trend of more pronounced changes was observed when a higher dose was used. These results suggest that 10 mg/kg is the lower effective dose contributing to induce hepatic gene expression changes.

Results

Table 5. Hepatic changes in selected gene expressions of male *Apoe*-deficient mice receiving different doses of erythrodiol.

Gene Symbol	Control (n=17)	0.5 mg/kg erythrodiol (n=16)	1 mg/kg erythrodiol (n=17)	5 mg/kg erythrodiol (n=17)
<i>Cyp2b10</i>	1.2 ± 0.7	11.1 ± 41.3	1.6 ± 1.1	1.7 ± 1.8
<i>Dmbt1</i>	4.5 ± 15	2.5 ± 4.3	8.5 ± 27.0	1.7 ± 2.5
<i>Amy2a5</i>	1.0 ± 0.2	1.3 ± 0.2	1.1 ± 0.2	1.1 ± 0.4
<i>Prtn3</i>	1.9 ± 2.9	1.1 ± 1.2	3.2 ± 7.8*	1.2 ± 1.0
<i>Cyp2b9</i>	1.6 ± 1.3	3.0 ± 2.6*	2.2 ± 1.9	2.1 ± 1.7

Results are expressed as means and standard deviations according to RT-qPCR assay normalized to *Ppib* and *Tbp*. Statistical analysis was carried out according to One-way ANOVA and Mann-Whitney's U-test for pair wise comparisons. *, P < 0.05 vs control.

2.6. Influence of *Apoa1*-Deficiency on Selected Hepatic Gene Expressions on Mice Consuming the 10 mg/kg Erythrodiol-Containing Western Diet for 4 weeks.

Absence of APOA1 is a genetic model of HDL deficiency. In mice lacking this protein from both sexes, the impact of erythrodiol-containing Western diet on hepatic gene regulation was assessed by measuring the expressions of *Cyp2b10*, *Dmbt1*, *Cyp2b13*, *Prtn3* and *Cyp2b9* as subrogate genes. Results showed no significant change in any of the genes in either sex following erythrodiol administration (Table 6). These results may imply that APOA1-containing HDL may not participate in delivering erythrodiol to the liver.

Table 6. Effect of 10 mg/kg erythrodiol on selected gene expressions in *Apoa1*-deficient mice according to sex.

Gene Symbol	Males		Females	
	Control (n=14)	Erythrodiol (n=15)	Control (n=9)	Erythrodiol (n=9)
<i>Cyp2b10</i>	30 ± 110	1.2 ± 1.8	7.2 ± 19	0.9 ± 0.9
<i>Dmbt1</i>	5.0 ± 10.8	7.3 ± 19	9.8 ± 21	87 ± 156
<i>Cyp2b13</i>	4.2 ± 6.3	4.5 ± 9.8	1.3 ± 0.9	1.9 ± 1.1
<i>Prtn3</i>	1.2 ± 0.8	1.1 ± 0.8	1.2 ± 0.9	5.3 ± 8.1
<i>Cyp2b9</i>	2.4 ± 3.8	1.6 ± 1.9	1.1 ± 0.5	1.2 ± 0.7

Results are expressed as means and standard deviations according to RT-qPCR assay normalized to *Ppib* and *Tbp*. Statistical analysis was carried out according to One-way ANOVA and Mann-Whitney's U-test for pair wise comparisons. *, P < 0.05 vs control.

3. Discussion

The present nutrigenomic approach was carried out to determine the effect of erythrodiol on hepatic transcriptome in male *Apoe*-deficient mice as a hepatic

Results

steatosis-prone model. Using RNAseq, erythrodiol administration did not modify single nucleotide polymorphisms, nor created errors in transcription, nor influenced global alternative splicing events. Results indicate that this compound mainly modified hepatic expression of clusters of genes involved in xenobiotics, protein and nucleic acid metabolisms. These findings were accompanied by a trend to decrease accumulation of lipids in cytoplasmic lipid droplets and decreased hepatic mass. A comparison between RNAseq and RT-qPCR revealed that due to their different methodological approaches, special care should be applied in order to compare their outcomes. Nine randomly selected genes (*Ccl19-ps2*, *Cyp2b10*, *Rbm14-rbm4*, *Sec61g*, *Tmem81*, *Prtn3*, *Amy2a5*, *Cyp2b9* and *Mup1*) showing good agreement between both methods were significantly modified in males by the administration of erythrodiol. An association of expressions among *Cyp2b13*, *Cyp2b9* and *Prtn3* was observed. When these gene expressions together with that of *Cyp2b10* and *Dmbt1* were tested in female mice receiving erythrodiol, a different sex-response was observed. Used to explore the minimal required dose, they evidenced a minimum 10 mg/kg, to observe male responses. Used as markers of erythrodiol delivery to the liver in absence of APOA1-HDL, no influence was observed in this setting. Overall, dietary erythrodiol administration is safe and induces hepatic gene changes that are sex-specific and dose-dependent and APOA1- containing HDL may not participate in its delivery to the liver.

Due to the fact that the high-throughput sequencing technology for transcriptomic purposes provides huge amounts of data about differentially expressed genes and additional analyses including polymorphisms, alternative spliced variants, low-expressed genes, and novel transcripts, has been proposed as an attractive choice, superseding quantitative transcript profiling by microarray [26]. Using this approach, we have proved that erythrodiol administration induced differentially expressed genes without modifying single nucleotide polymorphisms, creating errors in transcription or influencing global alternative splicing events. This fact, the lack of death mice receiving this agent at 10 mg/kg for 12 weeks and the normal hepatic morphology indicate that erythrodiol administration is safe for males and females.

Results

In our technical approach for RNA seq, a strategy of pooling was adopted. This may raise two drawbacks, bias and loss of biological variability, but it also has advantages in terms of cost and complexity of analysis [26,27]. Undoubtedly, this approach requires confirmation by an independent procedure, and RT-qPCR was selected and applied to 21-randomly chosen genes that were analyzed using individual samples. The initial correlation between RNAseq and RT-qPCR was rather poor (Figure 5A). A profound analysis of both methods considering primer design used in RT-qPCR that corresponded to most read exons, and establishing an unambiguous limit of detection in RNAseq showed a robust agreement between both procedures ($r=0.9$, $P<0.0008$) (Figure 5C). Thereby, pooling assays are a reliable screening approach that saves samples, is more economic and straightforward as it was for microarrays [9,28,29] and in this particular case it also facilitates the finding of targets of erythrodiol. RNAseq provides an unsurpassed overview of genome activity. Although preliminary, this finding is also suggesting that bioinformatic tools for analyzing RNAseq data should be refined to reinforce its specificity displaying quantified transcripts and taking into consideration their limits of detection. One potential limitation of our approach is the search in the range of the highest changes where some control samples did not express and did contribute to an increased erythrodiol/control ratio. For that reason, only 9 out 21 chosen genes show good correlation. Furthermore, it should also be taken into consideration that depending on the chosen primers, different transcripts are analyzed [30]. These caveats warrant more research in the future.

A cluster of genes involved in xenobiotics metabolism has been influenced by erythrodiol administration. In this regard, one gene with induced expression was *Cyp2b10*. It belongs to cytochrome P450 components of phase I response involved in NADPH-dependent electron transport. It oxidizes steroids, fatty acids, and xenobiotics, leading to detoxification of approximately 10% of drugs [31]. Erythrodiol as an alcohol was able to induce it, as did ethanol [32]. However, other members of phase I response, *Cyp2b9* and *Cyp2b13*, were found decreased by erythrodiol administration. This represents a unique pattern differing from the response to oleanolic acid-diet that also induced *Cyp2b9* expression [28] and that of

Results

maslinic acid administration that induced the triad (*Cyp2b9*, *Cyp2b10* and *Cyp2b13*) [29] or the lineal triterpene, squalene (*Cyp2b10* and *Cyp2c55*) [33]. These facts clearly indicate different responses depending on the administered triterpene. This particular hepatic response to erythrodiol may escape of the consequences observed when these three *Cyp* genes were deleted, namely fatty liver disease progression [34]. Indeed, our results do not support an increased lipid droplet accumulation in the liver.

Regarding protein metabolism, particularly interesting are the findings of *Prtn3* changes and their association with those of *Cyp2b9* and *Cyp2b13* (Figure 4E). *Prtn3* encodes for a proteinase 3 with proteolytic activities and reactive oxygen species responses. *Prtn3* deficiency is strongly correlated with fewer incidences of liver steatosis and adipose tissue inflammation and thus reduced risk of NAFLD and obesity-related steatosis [35]. High PRTN3 levels are also correlated with poor survival rates in pancreatic cancer [36]. In this regard, *Prtn3* suppression by erythrodiol may be a potent hepatic therapy against steatosis. *Mup1* is a member of the lipocalin family that regulates metabolic homeostasis by controlling expression of gluconeogenic and lipogenic genes in the liver. Its down-regulation has been shown to induce hyperglycemia, impaired insulin secretion, glucose intolerance and hyperlipidemia [37, 38]. Accordingly, erythrodiol could carry deleterious effects when repressing MUP1 gene. On the other hand, SEC61g over-expression is considered a parameter of bad glioblastoma prognosis [39]. TMEM81 is overexpressed in hepatocellular carcinoma [40]. In addition, a frameshift deletion mutation of RBM14-RBM4 chimera was screened in liver cancer, considering this mutation a putative marker for hepatic neoplasia [41]. The decreased expressions of these three genes by erythrodiol might contribute to explain its antineoplastic properties [22].

When comparing gene expression patterns of our study with those observed using olive oil components, *Dmbt1*, an extracellular receptor, showed reduced expression in animals consuming a pomace olive diet [9]. This pattern was reproduced by erythrodiol but not by other terpenic compounds. Thus, the gene

could be a unique marker for erythrodiol intake. Its significance on liver damage needs to be explored [42].

The sex-differences noted in gene expression changes observed by erythrodiol administration are particularly striking. Our results again reinforce the previously noted differences between sexes in the liver [43], particularly when a Western diet was administered [30]. Indeed, *Cyp2b9* gene expressions have been particularly sensitive to sex differences [34,44,45], β -estradiol [46] and prolactin [47]. Thus, hepatic drugs should be specially tested for females. A threshold dose was also required to elicit male hepatic changes in gene expression confirming a dose-dependent pattern of other erythrodiol-related actions [10, 25], and a potential cytotoxic effect at high doses [48]. APOA1 is the most abundant protein constituent of HDL produced by the liver and the intestine [49]. To test the hypothesis whether this type of HDL could be involved in delivering erythrodiol to the liver, mice lacking *Apoa1* gene were used as models of HDL absence. As suspected, no notable changes were observed for tested genes. The same results were obtained with oleanolic acid administration [28], which is consistent with the fact that both triterpenes may not be vehicled by APOA1-containing HDL in their route to the liver. Overall, the hepatic gene expression profile induced by erythrodiol is a multistep, complicated process of integrated factors, particularly dose and sex. To translate these results into humans, its bioavailability has to be proved, something that has only been observed in rats [50]. Based on the present work and the different metabolic rates of mice and humans a 1 mg/kg dose should be explored in the latter. Consuming a daily 50 ml of extra-virgin olive oil, a human would be exposed to a 53 μ g/kg erythrodiol dose, but using the same amount of pomace olive oil [51] the exposition would be 500 μ g/kg, close to the predicted active dose in humans. A potential sex-differential response is required to be tested in our species.

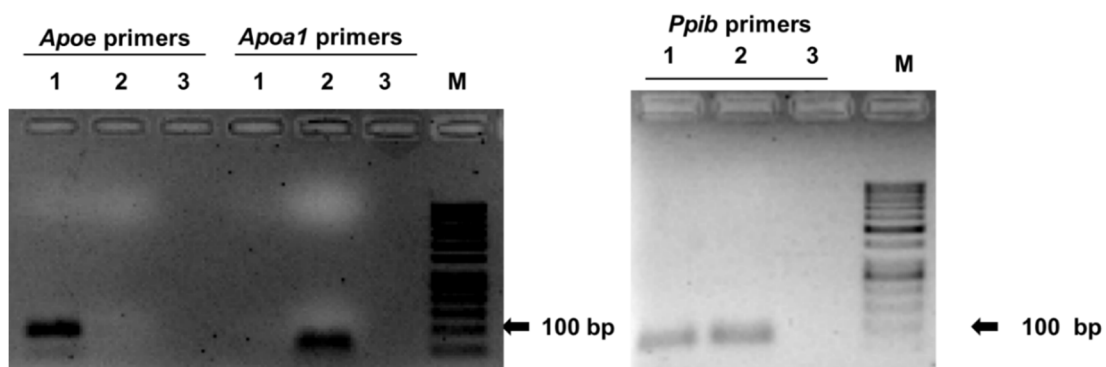
4. Materials and Methods

4.1. Animal Models

The experimental animals used were two-month-old, homozygous *ApoE*-deficient mice on C57BL/6J genetic background, obtained from Charles River

Results

Laboratories (Barcelona, Spain) and *Apoa1*-deficient mice on C57BL/6J genetic background, generously provided by Dr. Nobuyo Maeda from the University of North Carolina at Chapel Hill. Both were bred at the *Centro de Investigación Biomédica de Aragón*. Blood samples obtained from the facial vein 4h after a fasting period were used to establish experimental groups with similar baseline plasma cholesterol. This was used as a quick additional quality control of mouse identification. In this sense, *ApoE*-deficient mice on C57BL/6J background are hypercholesterolemic and their plasma levels should be higher than 5 ± 1 mmol/L [52] compared to 2.9 ± 0.5 mmol/L for wild-type. Any mouse not showing these values were genotyped and if their identification was correct were excluded due to hepatic dysfunctionality. In the case of *Apoa1*-deficient mice and due to their hypocholesterolemia [53], they should show values of 0.8 ± 0.4 mmol/l [54]. As in the case of *ApoE*-deficient mice, any discrepant mouse is genotyped as described [55]. The lack of *ApoE* and *Apoa1* hepatic expressions in these mice, respectively, was also verified by analyzing their presence or absence by RT-PCR (Supplementary Figure 1).



Supplementary Figure 1. PCR products obtained from hepatic RNA by RT-PCR. *Apoa1*-deficient mice do not express *Apoa1* and *ApoE*-deficient mice do not express *ApoE*. Lane 1, *Apoa1*-deficient mice; lane 2, *ApoE*-deficient mice and lane 3, negative control, no cDNA input. M, DNA ladder. PCR products were run into a 2% agarose gel and stained with ethidium bromide.

Mice were housed in sterile filter-top cages in rooms supplied with monitored 12-hour light/12-hours dark cycle and had ad libitum access to food and water. The experiments were carried out in accordance with the EU Directive 2010/63 on the protection of animals used for scientific purposes and the study protocol was

approved by the Ethics Committee for Animal Research of the University of Zaragoza (PI43/15 and PI35/18).

4.2. Experimental Designs

4.2.1. Effect of Dietary 10 mg/kg Erythrodiol in a Western Diet on *ApoE*- and *ApoA1*-Deficient Mice.

Four study groups were established: female (12) and male control (n = 14) groups received a purified Western diet containing 0.15% cholesterol and 20% refined palm oil (Gustav Heess, S.L., Barcelona, Spain), and the other two groups female (13) and male (n = 15) were fed with the same diet containing 0.01% erythrodiol (Extrasynthese, Genay, France). Assuming a daily intake of 3 g for each mouse, this is equivalent to a dose of 10 mg/kg mouse. This dose was chosen based on that previously used of oleanolic acid [28] that did not modify body weight and elicited hepatic gene expressions. Fresh diets were prepared weekly, kept under N₂ atmosphere at – 20 °C and replaced daily. The animals were fed the experimental diets for 12 weeks and both were well tolerated.

A similar design was used for *ApoA1*-deficient mice, the size of groups was female (9) and male (14) controls and female (9) and male (15) erythrodiol groups. In this case, the intervention lasted for 4 weeks.

4.2.2. Effect of Different Doses of Erythrodiol in Western Diets on Male *ApoE*-Deficient Mice.

Four groups were established. Control group (17) received the Western diet and three groups receiving the same diet formulated to receive lower doses of 0.5 (n = 16), 1 (n = 17) and 5 mg/kg erythrodiol (n = 17), respectively. As mentioned above and once corrected by mouse metabolic rate, these doses would represent the amount of erythrodiol received by humans consuming extra-virgin olive oil or pomace olive oil. The animals were fed the experimental diets for 12 weeks.

4.3. Somatometric Analyses

During the experiment, body weight and survival rate were monitored. At the end of the experiment, following 4-hour fast mice were euthanized by CO₂

inhalation, and the livers obtained and weighed. An aliquot was stored in neutral formaldehyde and the remaining organ frozen in liquid nitrogen.

4.4. Liver Histology Analyses

Sections (4 μm) of the livers stored in neutral formaldehyde were stained with hematoxylin and eosin and observed using a Nikon microscope. Hepatic fat content was evaluated by quantifying the area of lipid droplets in each section and expressed as percentage of total liver section [56].

4.5. RNA Isolation

Total RNA of each liver was isolated using Tri Reagent from Ambion® (Life Technologies, Carlsbad, CA, USA) following the manufacturer's instructions. DNA contaminants were removed by TURBO DNase treatment of 5 μg of total RNA using the DNA Removal Kit from Invitrogen (Cat.No:AM1907, Carlsbad, CA, USA). RNA was quantified by absorbance at A260/280 using Nanodrop Spectrophotometer and the ratio was greater than 1.75. The integrity of the 28S and 18S ribosomal RNAs was verified by 1% agarose gel electrophoresis followed by ethidium bromide staining and the 28S/18S ratio was greater than 2.

4.6. RNAseq and Data Analyses

For RNA sequencing, 6 pools of control mice were prepared using equal amounts of hepatic total RNA of two mice and in the seventh the total RNA from three mice was used. Another 7 pools were prepared for erythrodiol-treated mice combining total RNA from two or three mice per pool. The resulting 14 samples were sent to BGI (Shenzhen, China) service. Their total RNA quality was tested using Agilent 2100 Bioanalyzer (Agilent RNA 6000 Nano Kit, Santa Clara, CA, USA), then library construction was initiated by purifying the poly-A containing mRNA molecules using oligo-dT attached to magnetic beads. The mRNA was fragmented, copied into cDNA, linked to an adapter, purified and amplified by PCR. PCR yield was quantified by Qubit, and pooled samples together to make a single strand DNA circle (ssDNA circle), which gave the final library. DNA nanoballs (DNBs) were generated with the ssDNA circle by rolling circle replication (RCR) to enlarge the

fluorescent signals at the sequencing process, the DNBs were loaded into the patterned nanoarrays and pair-end reads of 100 bp were read through the BGISEQ-500 platform. Sequencing reads which contained low-quality, adaptor-polluted and high content of unknown base reads were removed before downstream analyses. After read filtering, genome mapping of clean reads to reference genome was performed using HISAT (Hierarchical Indexing for Spliced Alignment of Transcripts) generating a Bioinformatics flow of about 4.73 Gb per sample with an average genome mapping rate of 92.76%. After genome mapping, StringTie was used to reconstruct transcripts [57], with genome annotation information, novel transcripts were identified by using Cuffcompare (a tool of Cufflinks) [58] and the coding ability of those new transcripts was predicted using Coding Potential Calculator [59]. In total, 14,920 novel transcripts were identified. GATK (Broad Institute, Inc, Boston, MA, USA) was then used to call SNP and INDEL variants for each sample. RMATS [60] was used to detect differentially splicing genes between samples. After novel transcript detection, novel coding transcripts were merged with reference transcripts to get complete reference, then clean reads were mapped to it using Bowtie2 [61]. Then gene expression level for each sample was calculated with RSEM [62]. The complete datasets were deposited in the GEO database (Accession number GSE155163).

4.7. Quantification of mRNA

To verify the most striking observed changes by the administration of erythrodiol using RNAseq, represented by signal \log_2 ratio > 1.5 or < -1.5 and false discovery rate < 0.001 for up-regulated and down-regulated, respectively, 21 genes fulfilling these criteria were chosen. Their gene structure was analyzed using Ensembl Genome Browser and primers representative of the main hepatic transcripts according to Mouse Genome Informatics were prepared. The reverse transcriptase quantitative PCR (RT-qPCR) assays of these transcripts were optimized in terms of primer and input cDNA concentrations to obtain similar efficiencies and analyzed on individual samples. Basically, equal amounts of DNA-free RNA (500 ng) from each liver were reverse transcribed into cDNA using PrimeScript RT Reagent Kit (Cat. No: RR037A, Takara, Kutsatsu, Shiga, Japan). The

used primers were designed using NCBI and Primer 3 software [63] and checked by BLAST (NCBI) and KEGG to verify gene specificity and coverage of all variants for a specific gene. Tables for the primers in the Material and Method section show their characteristics. Quantitative real time was carried out according to manufacturer's instructions (SYBR Green PCR Master Mix, Applied Biosystems, Foster city, CA, USA) on a Step One Real Time PCR System (Applied Biosystem). The relative amount of mRNA was calculated using the comparative $2^{-\Delta\Delta Cq}$ method and normalized to the reference *Ppib* and *Tbp* expressions and reported as signal \log_2 ratio of erythrodiol/control.

4.8. Quality Control and Statistics

PCR duplicates for samples were carried out and their coefficient of variation obtained. Samples displaying values higher than 3% were discarded and assayed again. Statistical analyses were performed using GraphPad Prism (GraphPad Software, San Diego, CA). Data were checked for normal distribution by Shapiro-Wilk test and homogeneity of variance by Bartlett F-test. When any of these failed, results were analyzed by Mann-Whitney U test. Differences between both groups were considered significant when $P < 0.05$. Correlation between gene expressions was analyzed using Spearman correlation coefficient.

5. Conclusion

Through transcriptomic profiling and selecting a procedure previously validated by our group, erythrodiol has proved to act as a transcriptional modulator of hepatic gene expression dependent on sex. At 10 mg/ kg, erythrodiol modulates expression of hepatic genes involved in detoxification and tumor processes, and shows a trend to decrease the percentage of area occupied by lipid droplets. In this aspect, erythrodiol could be a potential candidate to halt the evolution of fatty liver into hepatocarcinoma.

Supplementary Materials: The following are available online at <https://www.mdpi.com/1422-0067/21/19/7331/s1>. Figure S1 and Table S1.

Funding: This research was supported by grants (CIBEROBN, CB06/03/1012) from CIBER Fisiopatología de la Obesidad y Nutrición as initiative of FEDER- ISCIII, Ministerio de

Results

Ciencia e Innovación-Fondo Europeo de Desarrollo Regional (SAF2016-75441-R and PID2019-104915RB-I00) and Fondo Social Europeo-Gobierno de Aragón (B16_20R).

Acknowledgments: We thank Silvia Garcés and M^a Pilar Lierta for their help in maintaining the mice, and David Banks for his critical reading.

Conflicts of Interest: there is no conflict of interest.

References

1. Keys, A. Mediterranean diet and public health: Personal reflections. *Am J Clin Nutr* 1995, 61, 1321S-1323S.
2. Trichopoulou, A.; Costacou, T.; Bamia, C.; Trichopoulos, D. Adherence to a mediterranean diet and survival in a greek population. *N Engl J Med* 2003, 348, 2599-2608.
3. Estruch, R.; Ros, E.; Salas-Salvado, J.; Covas, M.I.; Corella, D.; Aros, F.; Gomez-Gracia, E.; Ruiz-Gutierrez, V.; Fiol, M.; Lapetra, J., et al. Primary prevention of cardiovascular disease with a mediterranean diet supplemented with extra-virgin olive oil or nuts. *N Engl J Med* 2018, 378, e34.
4. Martínez-González, M.A.; Gea, A.; Ruiz-Canela, M. The mediterranean diet and cardiovascular health. *Circulation Research* 2019, 124, 779-798.
5. Foscolou, A.; Critselis, E.; Panagiotakos, D. Olive oil consumption and human health: A narrative review. *Maturitas* 2018, 118, 60-66.
6. Lou-Bonafonte, J.M.; Arnal, C.; Navarro, M.A.; Osada, J. Efficacy of bioactive compounds from extra virgin olive oil to modulate atherosclerosis development. *Mol Nutr Food Res* 2012, 56, 1043-1057.
7. Habib, L.; Jraij, A.; Khreich, N.; Charcosset, C.; Greige-Gerges, H. Effect of erythrodiol, a natural pentacyclic triterpene from olive oil, on the lipid membrane properties. *J Membr Biol* 2015, 248, 1079-1087.
8. de la Puerta, R.; Martinez-Dominguez, E.; Ruiz-Gutierrez, V. Effect of minor components of virgin olive oil on topical antiinflammatory assays. *Z Naturforsch C J Biosci* 2000, 55, 814-819.
9. Acín, S.; Navarro, M.A.; Perona, J.S.; Surra, J.C.; Guillen, N.; Arnal, C.; Sarría, A.J.; Arbonés-Mainar, J.M.; Carnicer, R.; Ruiz-Gutiérrez, V., et al. Microarray analysis of hepatic genes differentially expressed in the presence of the unsaponifiable fraction of olive oil in apolipoprotein e-deficient mice. *Br J Nutr* 2007, 97, 628-638.
10. Juan, M.E.; Wenzel, U.; Daniel, H.; Planas, J.M. Erythrodiol, a natural triterpenoid from olives, has antiproliferative and apoptotic activity in ht-29 human adenocarcinoma cells. *Mol Nutr Food Res* 2008, 52, 595-599.
11. Perona, J.S.; Arcemis, C.; Ruiz-Gutierrez, V.; Catala, A. Effect of dietary high-oleic-acid oils that are rich in antioxidants on microsomal lipid peroxidation in rats. *J Agric Food Chem* 2005, 53, 730-735.

Results

12. Abbass, H.S.; Ragab, E.A.; El-Salam, A.; Mohammed, I.; El-Hela, A.A. Phytochemical and biological investigation of ficus mysorensis cultivated in egypt. *Journal of Pharmaceutical, Chemical and Biological Sciences* 2015, 3, 396-407
13. Abboud, R.; Charcosset, C.; Greige-Gerges, H. Tetra- and penta-cyclic triterpenes interaction with lipid bilayer membrane: A structural comparative study. *J Membr Biol* 2016, 249, 327-338.
14. Marquez-Martin, A.; De La Puerta, R.; Fernandez-Arche, A.; Ruiz-Gutierrez, V.; Yaqoob, P. Modulation of cytokine secretion by pentacyclic triterpenes from olive pomace oil in human mononuclear cells. *Cytokine* 2006, 36, 211-217.
15. Kontogianni, V.G.; Tsoumani, M.E.; Kellici, T.F.; Mavromoustakos, T.; Gerotheranassis, I.P.; Tselepis, A.D.; Tzakos, A.G. Deconvoluting the dual antiplatelet activity of a plant extract. *J Agric Food Chem* 2016, 64, 4511-4521.
16. Liu, K.; Qin, Y.H.; Yu, J.Y.; Ma, H.; Song, X.L. 3-beta-epsilon-rythrodiol isolated from conyza canadensis inhibits mkn45 human gastric cancer cell proliferation by inducing apoptosis, cell cycle arrest, DNA fragmentation, ros generation and reduces tumor weight and volume in mouse xenograft model. *Oncol Rep* 2016, 35, 2328-2338.
17. Chen, H.L.; Lin, K.W.; Huang, A.M.; Tu, H.Y.; Wei, B.L.; Hour, T.C.; Yen, M.H.; Pu, Y.S.; Lin, C.N. Terpenoids induce cell cycle arrest and apoptosis from the stems of celastrus kusanoi associated with reactive oxygen species. *J Agric Food Chem* 2010, 58, 3808-3812.
18. Nkengfack, A.E.; Azebaze, A.G.; Waffo, A.K.; Fomum, Z.T.; Meyer, M.; van Heerden, F.R. Cytotoxic isoflavones from erythrina indica. *Phytochemistry* 2001, 58, 1113-1120.
19. Ebeling, S.; Naumann, K.; Pollok, S.; Wardecki, T.; Vidal, Y.S.S.; Nascimento, J.M.; Boerries, M.; Schmidt, G.; Brandner, J.M.; Merfort, I. From a traditional medicinal plant to a rational drug: Understanding the clinically proven wound healing efficacy of birch bark extract. *PLoS One* 2014, 9, e86147.
20. Xiaoli, L.; Naili, W.; Sau, W.M.; Chen, A.S.; Xinsheng, Y. Four new isoflavonoids from the stem bark of erythrina variegata. *Chem Pharm Bull (Tokyo)* 2006, 54, 570-573.
21. Allouche, Y.; Warleta, F.; Campos, M.; Sanchez-Quesada, C.; Uceda, M.; Beltran, G.; Gaforio, J.J. Antioxidant, antiproliferative, and pro-apoptotic capacities of pentacyclic triterpenes found in the skin of olives on mcf-7 human breast cancer cells and their effects on DNA damage. *J Agric Food Chem* 2011, 59, 121-130.
22. Martin, R.; Ibeas, E.; Carvalho-Tavares, J.; Hernandez, M.; Ruiz-Gutierrez, V.; Nieto, M.L. Natural triterpenic diols promote apoptosis in astrocytoma cells through ros-mediated mitochondrial depolarization and jnk activation. *PLoS One* 2009, 4, e5975.
23. Allouche, Y.; Beltran, G.; Gaforio, J.J.; Uceda, M.; Mesa, M.D. Antioxidant and antiatherogenic activities of pentacyclic triterpenic diols and acids. *Food Chem Toxicol* 2010, 48, 2885-2890.
24. Martin, R.; Miana, M.; Jurado-Lopez, R.; Martinez-Martinez, E.; Gomez-Hurtado, N.; Delgado, C.; Bartolome, M.V.; San Roman, J.A.; Cordova, C.; Lahera, V., et al. Diol

Results

triterpenes block profibrotic effects of angiotensin ii and protect from cardiac hypertrophy. *PLoS One* 2012, 7, e41545.

25. Martin, R.; Hernandez, M.; Cordova, C.; Nieto, M.L. Natural triterpenes modulate immune-inflammatory markers of experimental autoimmune encephalomyelitis: Therapeutic implications for multiple sclerosis. *Br J Pharmacol* 2012, 166, 1708-1723.

26. Rajkumar, A.P.; Qvist, P.; Lazarus, R.; Lescai, F.; Ju, J.; Nyegaard, M.; Mors, O.; Borglum, A.D.; Li, Q.; Christensen, J.H. Experimental validation of methods for differential gene expression analysis and sample pooling in rna-seq. *BMC Genomics* 2015, 16, 548.

27. Peng, X.; Wood, C.L.; Blalock, E.M.; Chen, K.C.; Landfield, P.W.; Stromberg, A.J. Statistical implications of pooling rna samples for microarray experiments. *BMC Bioinformatics* 2003, 4, 26.

28. Gabas-Rivera, C.; Martinez-Beamonte, R.; Rios, J.L.; Navarro, M.A.; Surra, J.C.; Arnal, C.; Rodriguez-Yoldi, M.J.; Osada, J. Dietary oleanolic acid mediates circadian clock gene expression in liver independently of diet and animal model but requires apolipoprotein a1. *J Nutr Biochem* 2013, 24, 2100-2109.

29. Guillen, N.; Acin, S.; Surra, J.C.; Arnal, C.; Godino, J.; Garcia-Granados, A.; Muniesa, P.; Ruiz-Gutierrez, V.; Osada, J. Apolipoprotein e determines the hepatic transcriptional profile of dietary maslinic acid in mice. *J Nutr Biochem* 2009, 20, 882-893.

30. Herrera-Marcos, L.V.; Sancho-Knapik, S.; Gabas-Rivera, C.; Barranquero, C.; Gascon, S.; Romanos, E.; Martinez-Beamonte, R.; Navarro, M.A.; Surra, J.C.; Arnal, C., et al. Pgc1a is responsible for the sex differences in hepatic cidec/fsp27beta mrna expression in hepatic steatosis of mice fed a western diet. *Am J Physiol Endocrinol Metab* 2020, 318, E249-E261.

31. Zhao, M.; Zhao, H.; Lin, L.; Wang, Y.; Chen, M.; Wu, B. Nuclear receptor co-repressor rip140 regulates diurnal expression of cytochrome p450 2b10 in mouse liver. *Xenobiotica* 2020, 1-10.

32. Koga, T.; Yao, P.L.; Goudarzi, M.; Murray, I.A.; Balandaram, G.; Gonzalez, F.J.; Perdew, G.H.; Fornace, A.J., Jr.; Peters, J.M. Regulation of cytochrome p450 2b10 (cyp2b10) expression in liver by peroxisome proliferator-activated receptor-beta/delta modulation of sp1 promoter occupancy. *J Biol Chem* 2016, 291, 25255-25263.

33. Gabás-Rivera, C.; Jurado-Ruiz, E.; Sánchez-Ortiz, A.; Romanos, E.; Martínez-Beamonte, R.; Navarro, M.A.; Surra, J.C.; Arnal, C.; Rodríguez-Yoldi, M.J.; Cristina Andrés-Lacueva, C., et al. Dietary squalene induces cytochromes cyp2b10 and cyp2c55 independently of sex, dose and diet in several mouse models. *Mol Nutr Food Res* 2020.

34. Heintz, M.M.; Kumar, R.; Rutledge, M.M.; Baldwin, W.S. Cyp2b-null male mice are susceptible to diet-induced obesity and perturbations in lipid homeostasis. *J Nutr Biochem* 2019, 70, 125-137.

35. Mirea, A.M.; Stienstra, R.; Kanneganti, T.D.; Tack, C.J.; Chavakis, T.; Toonen, E.J.M.; Joosten, L.A.B. Mice deficient in the il-1beta activation genes prtn3, elane, and casp1 are protected against the development of obesity-induced nafld. *Inflammation* 2020, 43, 1054-1064.

Results

36. Hu, D.; Ansari, D.; Zhou, Q.; Sasor, A.; Said Hilmersson, K.; Andersson, R. Low p4ha2 and high prtn3 expression predicts poor survival in patients with pancreatic cancer. *Scand J Gastroenterol* 2019, 54, 246-251.
37. Zhou, Y.; Jiang, L.; Rui, L. Identification of mup1 as a regulator for glucose and lipid metabolism in mice. *J Biol Chem* 2009, 284, 11152-11159.
38. Fan, Y.; Fang, X.; Tajima, A.; Geng, X.; Ranganathan, S.; Dong, H.; Trucco, M.; Sperling, M.A. Evolution of hepatic steatosis to fibrosis and adenoma formation in liver-specific growth hormone receptor knockout mice. *Front Endocrinol (Lausanne)* 2014, 5, 218.
39. Liu, B.; Liu, J.; Liao, Y.; Jin, C.; Zhang, Z.; Zhao, J.; Liu, K.; Huang, H.; Cao, H.; Cheng, Q. Identification of sec61g as a novel prognostic marker for predicting survival and response to therapies in patients with glioblastoma. *Med Sci Monit* 2019, 25, 3624-3635.
40. Chen, J.; Qian, Z.; Li, F.; Li, J.; Lu, Y. Integrative analysis of microarray data to reveal regulation patterns in the pathogenesis of hepatocellular carcinoma. *Gut Liver* 2017, 11, 112-120.
41. Sultana, N.; Rahman, M.; Myti, S.; Islam, J.; Mustafa, M.G.; Nag, K. A novel knowledge-derived data potentizing method revealed unique liver cancer-associated genetic variants. *Hum Genomics* 2019, 13, 30.
42. Mollenhauer, J.; Wiemann, S.; Scheurlen, W.; Korn, B.; Hayashi, Y.; Wilgenbus, K.K.; Poustka, A. Dmbt1, a new member of the srcr superfamily, on chromosome 10q25.3-26.1 is deleted in malignant brain tumours. *Nature genetics* 1997, 17.
43. Kwekel, J.C.; Desai, V.G.; Moland, C.L.; Branham, W.S.; Fuscoe, J.C. Age and sex dependent changes in liver gene expression during the life cycle of the rat. *BMC Genomics* 2010, 11, 675.
44. Xie, X.; Miao, L.; Yao, J.; Feng, C.; Li, C.; Gao, M.; Liu, M.; Gong, L.; Wang, Y.; Qi, X., et al. Role of multiple micrnas in the sexually dimorphic expression of cyp2b9 in mouse liver. *Drug Metab Dispos* 2013, 41, 1732-1737.
45. Kumar, R.; Mota, L.C.; Litoff, E.J.; Rooney, J.P.; Boswell, W.T.; Courter, E.; Henderson, C.M.; Hernandez, J.P.; Corton, J.C.; Moore, D.D., et al. Compensatory changes in cyp expression in three different toxicology mouse models: Car-null, cyp3a-null, and cyp2b9/10/13-null mice. *PLoS One* 2017, 12, e0174355.
46. Jarukamjorn, K.; Sakuma, T.; Nemoto, N. Discriminating activation of cyp2b9 expression in male c57bl/6 mouse liver by beta-estradiol. *Biochem Biophys Res Commun* 2000, 279, 288-292.
47. Sato, Y.; Kaneko, Y.; Cho, T.; Goto, K.; Otsuka, T.; Yamamoto, S.; Goto, S.; Maruyama, H.; Narita, I. Prolactin upregulates female-predominant p450 gene expressions and downregulates male-predominant gene expressions in mouse liver. *Drug Metab Dispos* 2017, 45, 586-592.
48. Sanchez-Quesada, C.; Lopez-Biedma, A.; Warleta, F.; Campos, M.; Beltran, G.; Gaforio, J.J. Bioactive properties of the main triterpenes found in olives, virgin olive oil, and leaves of olea europaea. *J Agric Food Chem* 2013, 61, 12173-12182.

Results

49. Arbonés-Mainar, J.M.; Navarro, M.A.; Acín, S.; Guzmán, M.A.; Arnal, C.; Surra, J.C.; Carnicer, R.; Roche, H.M.; Osada, J. Trans-10, cis-12- and cis-9, trans-11-conjugated linoleic acid isomers selectively modify hdl-apolipoprotein composition in apolipoprotein e knockout mice. *J Nutr* 2006, 136, 353-359.
50. Gimenez, E.; Juan, M.E.; Calvo-Melia, S.; Planas, J.M. A sensitive liquid chromatography-mass spectrometry method for the simultaneous determination in plasma of pentacyclic triterpenes of *olea europaea* l. *Food Chem* 2017, 229, 534-541.
51. Acin, S.; Navarro, M.A.; Perona, J.S.; Arbones-Mainar, J.M.; Surra, J.C.; Guzman, M.A.; Carnicer, R.; Arnal, C.; Orman, I.; Segovia, J.C., et al. Olive oil preparation determines the atherosclerotic protection in apolipoprotein e knockout mice. *J Nutr Biochem* 2007, 18, 418-424.
52. Surra, J.C.; Guillen, N.; Arbones-Mainar, J.M.; Barranquero, C.; Navarro, M.A.; Arnal, C.; Orman, I.; Segovia, J.C.; Osada, J. Sex as a profound modifier of atherosclerotic lesion development in apolipoprotein e-deficient mice with different genetic backgrounds. *J Atheroscler Thromb* 2010, 17, 712-721.
53. Li, H.; Reddick, R.L.; Maeda, N. Lack of apo-a-i is not associated with increased susceptibility to atherosclerosis in mice. *Arterioscler Thromb* 1993, 13, 1814-1821.
54. Gabas-Rivera, C.; Barranquero, C.; Martinez-Beamonte, R.; Navarro, M.A.; Surra, J.C.; Osada, J. Dietary squalene increases high density lipoprotein-cholesterol and paraoxonase 1 and decreases oxidative stress in mice. *PLoS One* 2014, 9, e104224.
55. Carnicer, R.; Navarro, M.A.; Arbones-Mainar, J.M.; Arnal, C.; Surra, J.C.; Acin, S.; Sarria, A.; Blanco-Vaca, F.; Maeda, N.; Osada, J. Genetically based hypertension generated through interaction of mild hypoalphalipoproteinemia and mild hyperhomocysteinemia. *J Hypertens* 2007, 25, 1597-1607.
56. Guillen, N.; Acin, S.; Navarro, M.A.; Perona, J.S.; Arbones-Mainar, J.M.; Arnal, C.; Sarria, A.J.; Surra, J.C.; Carnicer, R.; Orman, I., et al. Squalene in a sex-dependent manner modulates atherosclerotic lesion which correlates with hepatic fat content in apo-e-knockout male mice. *Atherosclerosis* 2008, 197, 72-83.
57. Pertea, M.; Pertea, G.M.; Antonescu, C.M.; Chang, T.-C.; Mendell, J.T.; Salzberg, S.L. Stringtie enables improved reconstruction of a transcriptome from rna-seq reads. *Nature Biotechnology* 2015, 33, 290-295.
58. Trapnell, C.; Roberts, A.; Goff, L.; Pertea, G.; Kim, D.; Kelley, D.R.; Pimentel, H.; Salzberg, S.L.; Rinn, J.L.; Pachter, L. Differential gene and transcript expression analysis of rna-seq experiments with tophat and cufflinks. *Nature Protocols* 2012, 7, 562-578.
59. Kong, L.; Zhang, Y.; Ye, Z.-Q.; Liu, X.-Q.; Zhao, S.-Q.; Wei, L.; Gao, G. Cpc: Assess the protein-coding potential of transcripts using sequence features and support vector machine. *Nucleic acids research* 2007, 35, W345-W349.
60. Shen, S.; Park, J.W.; Lu, Z.-x.; Lin, L.; Henry, M.D.; Wu, Y.N.; Zhou, Q.; Xing, Y. Rmats: Robust and flexible detection of differential alternative splicing from replicate rna-seq data. *Proceedings of the National Academy of Sciences* 2014, 111, E5593-E5601.

Results

61. Langmead, B.; Salzberg, S.L. Fast gapped-read alignment with bowtie 2. *Nature Methods* 2012, 9, 357-359.
62. Li, B.; Dewey, C.N. Rsem: Accurate transcript quantification from rna-seq data with or without a reference genome. *BMC Bioinformatics* 2011, 12, 323.
63. Untergasser, A.; Cutcutache, I.; Koressaar, T.; Ye, J.; Faircloth, B.C.; Remm, M.; Rozen, S.G. Primer3—new capabilities and interfaces. *Nucleic Acids Research* 2012, 40, e115-e115.

ii. Squalene through its Post-Squalene Metabolites is a Modulator of Hepatic Transcriptome in Rabbits.

Abstract: Squalene is a natural bioactive triterpene and an important intermediate in the biosynthesis of sterols. To assess the effect of this compound on the hepatic transcriptome, RNA-sequencing was carried out in two groups of male New Zealand rabbits fed either a diet enriched with 1% sunflower oil or the same diet with 0.5% squalene for 4 weeks. Hepatic lipids, lipid droplet area, squalene, and sterols were also monitored. The Squalene administration downregulated 9 transcripts and upregulated 13 transcripts. The gene ontology of transcripts fitted into the following main categories: transporter of proteins and sterols, lipid metabolism, lipogenesis, anti-inflammatory and anti-cancer properties. When the results were confirmed by RT-qPCR, rabbits receiving squalene displayed significant hepatic expression changes of *LOC100344884* (*PNPLA3*), *GCK*, *TFCP2L1*, *ASCL1*, *ACSS2*, *OST4*, *FAM91A1*, *MYH6*, *LRRC39*, *LOC108176846*, *GLT1D1* and *TREH*. A squalene-enriched diet increased hepatic levels of squalene, lanosterol, dihydrolanosterol, lathosterol, zymostenol and desmosterol. Strong correlations were found among specific sterols and some squalene-changed transcripts. Incubation of the murine AML12 hepatic cell line in the presence of lanosterol, dihydrolanosterol, zymostenol and desmosterol reproduced the observed changes in the expressions of *Acss2*, *Fam91a1* and *Pnpla3*. In conclusion, these findings indicate that the squalene and post-squalene metabolites play important roles in hepatic transcriptional changes required to protect the liver against malfunction.

Keywords: squalene; virgin olive oil; rabbits; murine; AML12 cell line; lipid droplets; transcriptome; liver; hepatic; RNA sequencing

1. Introduction

The Seven Countries Study and subsequent epidemiological studies have linked the Mediterranean diet to natural occurring longevity, welfare and low rates of metabolic disorders [1,2]. There are some geographical modifications in the pattern of the Mediterranean diet; however, all of them use virgin olive oil (VOO) as a principal source of energy and as a health-promoting component [3]. Briefly, the consumption of VOO positively modulates the lipid metabolism, lipogenic response, insulin resistance,

Results

immune-inflammatory pathways, antithrombotic effect, blood pressure control, detoxification of reactive species and endothelial functions [3–6]. A substantial part of this effect has been attributed mainly to the minor unsaponifiable fraction [7,8], which represents about 0.5 to 1.5% of the oil and is composed of phytosterols, phenolic compounds, triterpenes and hydrocarbons. The latter accounts for almost 50% of the unsaponifiable composition [9,10], with squalene as the preeminent component [7]. This polyunsaturated terpenoid is made up of six units of isoprene (Figure 1) and is present in VOO at a concentration of 1.5 to 10.1 g per kg depending on cultivars, agronomical issues and olive fruit processing [11].

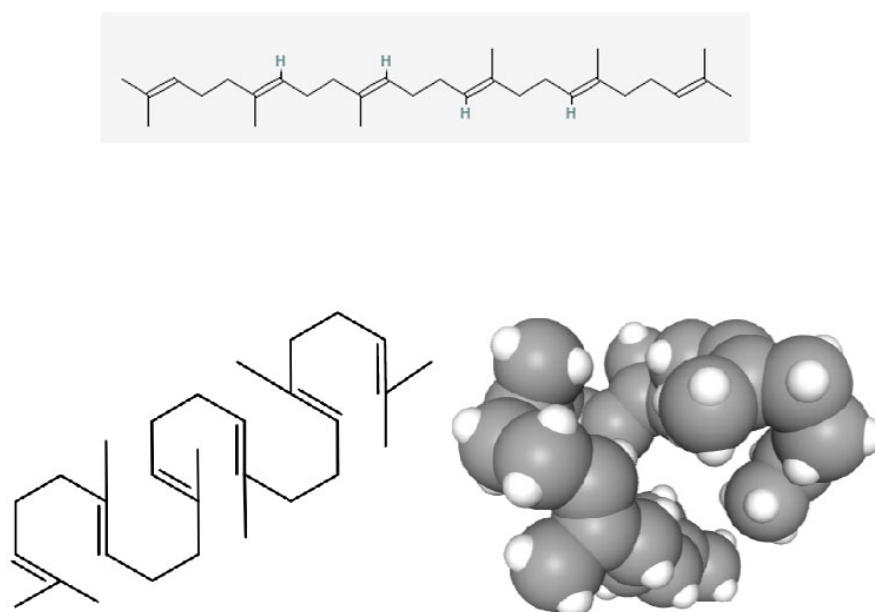


Figure 1. Squalene chemical structures.

Obtained from: <https://pubchem.ncbi.nlm.nih.gov/compound/638072#section=2D-Structure>, and <https://www.lipidmaps.org/databases/lmsd/LMPR0106010002?LMID=LMPR0106010002>, accessed on 9 February 2022.

Several assays have tested favorable properties of squalene as a strong antioxidant, anti-inflammatory and highly effective oxygen scavenger against cell deterioration, senescence, neoplasm and chemotherapy-induced side-effects and as an enhancer of immune response to various associated antigens [11,12]. In humans, the estimated squalene intake ranges from 30 to 400 mg per day [13], with high oral absorption efficiency at rates from 60 to 85% compared to 42% in animals [14,15]. Dietary squalene is transported by chylomicrons into circulation, followed by hepatic uptake prior to conversion into sterols and bile acids or re-secreted into the bloodstream into very low-

density lipoproteins (VLDL) and low-density lipoproteins (LDL) and distributed to various tissues [15].

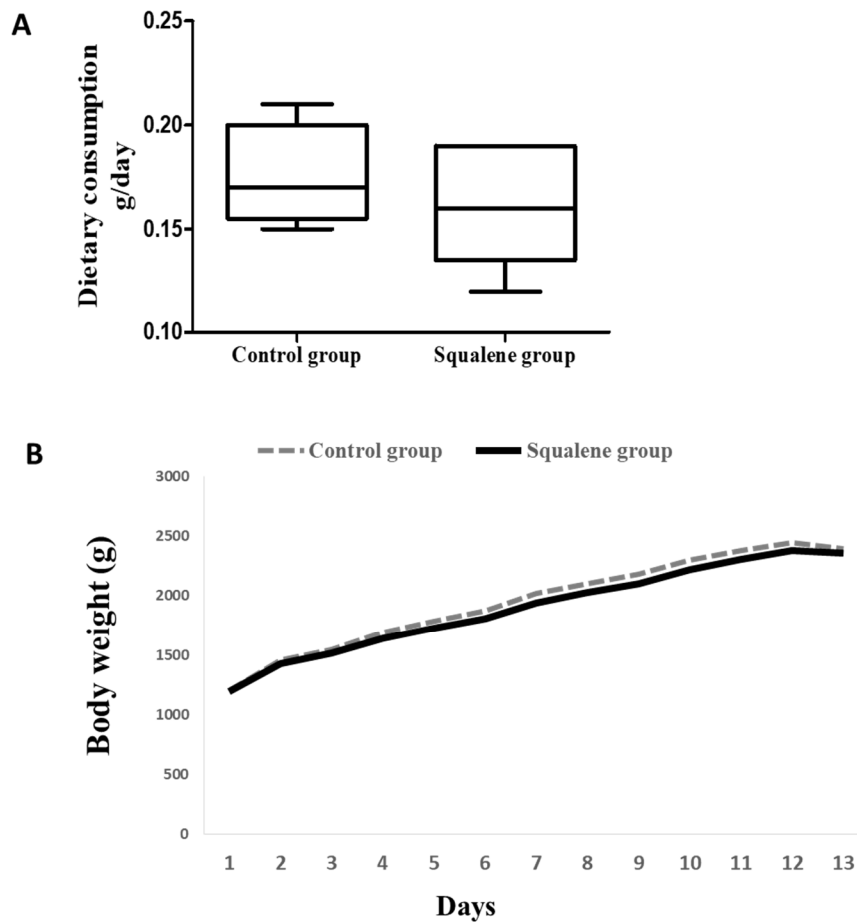
Oryctolagus cuniculus represents an excellent laboratory model for its high absorption and responsiveness to dietary cholesterol [16] and its high cholesteryl ester transfer protein activity [17]. In addition, the liver secretes apolipoprotein APOB100 [18] and plasma APOB100-containing particles have similar chemical components to humans [11]. Several studies have tested the hepatic biological effects caused by dietary squalene. Kritchevsky et al. [19] were the first to prove that a diet enriched in squalene caused an increase in mass and unsaponifiable material in the liver. Recently, it has been observed that exogenous squalene fed to these animals results in an increase in the hepatic content of squalene in the rough endoplasmic reticulum, the nucleus and expanded lipid vesicle size [20,21]. These authors have also found a hepatic accumulation of non-esterified cholesterol and of sterol precursors in the modified Kandutsch–Russell pathway [21]. This initial complexity may point out a complex network of gene expressions being involved. To address this hypothetical setting, an RNA-sequencing approach was tackled in rabbits consuming squalene and murine cell lines treated with cholesterol precursors were used in an attempt to clarify sterol's ability to modulate *in vivo* gene expression changes.

2. Results

2.1. Body Weight and Hepatic Parameters

Rabbits receiving the squalene-supplemented diet did not change body weight, despite a slight decline in food intake (Supplementary Figure S1). In addition, hepatic lipid droplet area was augmented ($p < 0.01$) (Figure 2), with an increase in the contents of non-esterified cholesterol content ($p < 0.02$), squalene ($p < 0.01$) and sterol metabolites such as lanosterol, dihydrolanosterol, zymosterol, lathosterol and desmosterol (for all $p < 0.01$), however, no significant change in triglycerides nor in esterified cholesterol was detected (Figure 3).

Results



Supplementary figure 1. Body weight difference in response to dietary consumption. A, Food consumption of both groups. Statistical analysis was done according to Mann-Whitney's U-test. $P > 0.05$. B, Body weight for control and squalene groups was compared among different days of assay.

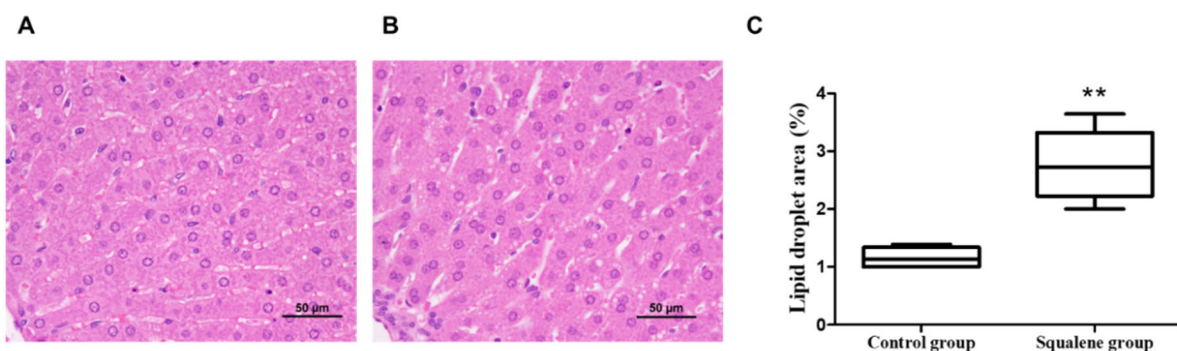


Figure 2. Hepatic histological analyses in rabbits fed with different diets. Representative liver micrographs when consuming control containing sunflower-oil diet (A) vs. 0.6 g/kg squalene-enriched control diet (B). Liver sections from each animal were stained with hematoxylin and eosin and evaluated blindly. Morphometric difference in amount of lipid droplet area in both control and squalene groups (C). Data are means and 10–90 percentiles for each group. Statistical analyses were performed according to Mann-Whitney's U-test. **, $p < 0.01$.

Results

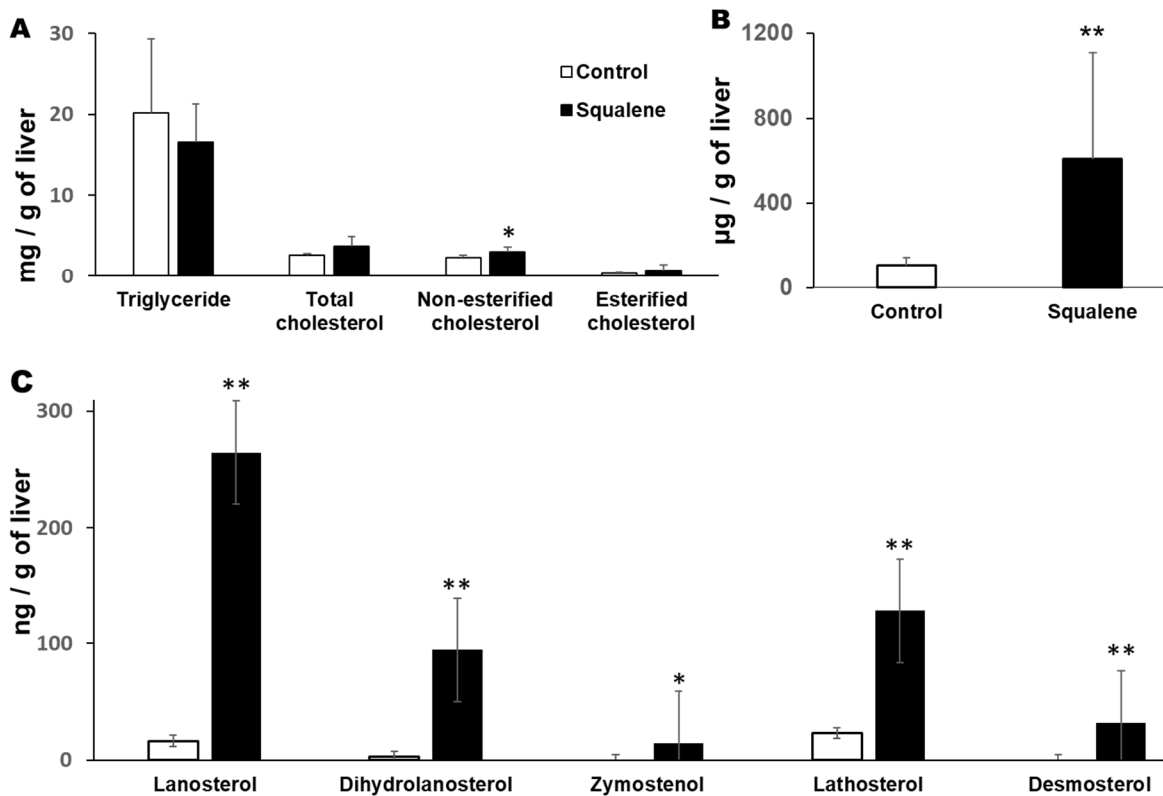


Figure 3. Hepatic lipid composition. (A) Triglyceride and cholesterol. (B) Squalene level. (C) Cholesterol biosynthesis intermediate sterols. Unfilled bar, control diet; filled bar, squalene-supplemented diet. Data are means \pm SD. Statistical analyses were performed according to Mann–Whitney’s U-test. * $p < 0.05$, ** $p < 0.01$ vs. control.

2.2. Hepatic Gene Expression

To determine the response of squalene intake to the hepatic transcriptome, RNA was extracted from five animals receiving the squalene-supplemented diet and from five receiving the control diet and sequenced by next-generation sequencing using the DNBseq platform. From each library, clean read sequences represented an average of $45.8 \pm 26 \times 10^6$ with a ratio of coverage of 91.60%. On average, 87.69% of the reads were mapped with the reference genome, and the uniformity of the mapping results for each sample suggests that the samples were uniform. In total, 19,163 genes were identified, of which 18,561 were known and 720 were new. Dietary squalene did not influence single nucleotide polymorphisms. Regarding transition, A-G were 55.6 ± 5.4 vs. 50.9 ± 5.9 and C-T were 55.7 ± 5.5 vs. 50.9 ± 5.9 for control and squalene groups, respectively. Regarding transversions, A-C were 9.2 ± 0.9 vs. 8.6 ± 0.7 ; A-T were 6.6 ± 0.8 vs. 6.4 ± 0.4 ; C-G were

Results

10.8 ± 1.1 vs. 9.9 ± 1.0 and finally, G-T were 9.2 ± 1.0 vs. 8.6 ± 0.6 for control and squalene groups, respectively.

When alternative splicing events were tested, squalene administration had a significant influence on splicing events, alternative 5' splicing, alternative 3' splicing site and retained introns (data not shown), while no effect was found on skipped exons or mutually exclusive exons. Splicing patterns led to a variety of differentially splicing genes and a variety of different isoforms from one gene, with a total of 10,924 novel transcripts, of which 8562 were previously anonymous splicing events for known genes, 720 were novel coding transcripts without any known features, and the rest were 1642 long noncoding RNA. Differentially expressed genes were 18,485 in the squalene group and 18,186 in the control group as shown in Figure 4A. Gene ontology of upregulated and downregulated genes involves molecular, biological functions and cellular components. The latter required a larger number of genes, as revealed in Figure 4C. Summary of DEGs and volcano plot show DEGs distribution are displayed in Figure 4B, D. Using more stringent conditions (\log_2 fold change higher than 1.5 or less than -1.5) and a false discovery rate of $p < 0.001$, nine transcripts were downregulated (Table 1) and 13 transcripts were upregulated (Table 2). The biological function of some of these genes fitted into the following five main categories: hepatic transport of sterols and proteins, lipid metabolism, lipogenesis, anti-inflammatory and anti-cancer processes.

Results

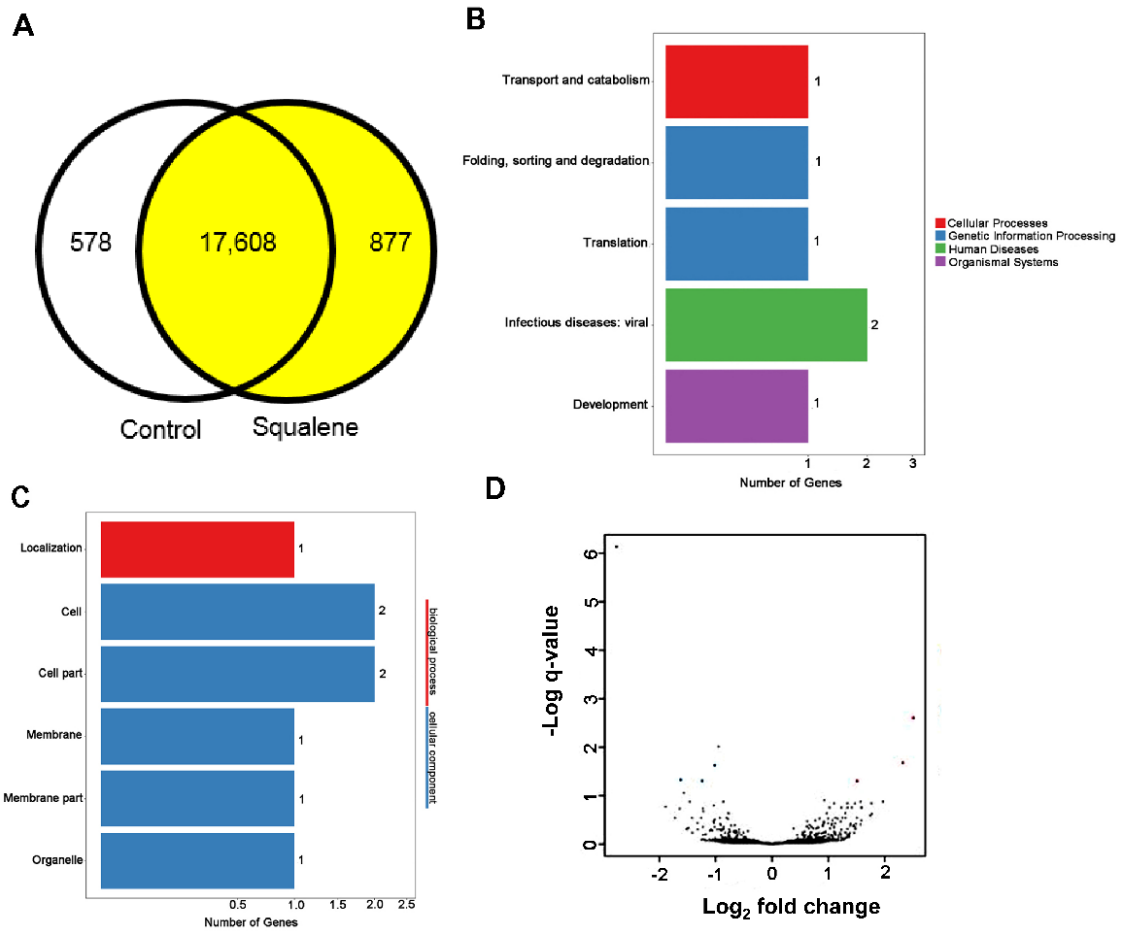


Figure 4. Differentially expressed genes (A) Venn diagram analysis. Control expressed 18,186 transcripts vs. 18,485 in squalene group. (B) Pathway classification of DEGs, X axis; number of DEG. Y axis; functional classification of KEGG. (C) GO classification of DEGs, axis represents number of DEG. Y axis represents GO term. (D) Volcano plot of DEGs. X axis, \log_2 transformed fold change. Y axis; $-\log_{10}$ of false discovery rate.

Table 1. Hepatic transcripts differentially downregulated by the administration of squalene at the level of signal \log_2 ratio < -1.5 and false discovery rate < 0.001 in male *Oryctolagus cuniculus* according to RNAseq.

Biological Process	GenBank	Name	Gene Symbol	Signal \log_2 Ratio	p -Value
Intracellular protein transport	XM_017339423.1	B-cell receptor-associated protein 29, BCAP29	<i>LOC100344375</i>	-2.8	0.00000
Hydrolysis of triglycerides	XM_017339724.1	Patatin-like phospholipase domain-containing protein 3, PNPLA3	<i>LOC100344884 (PNPLA3)</i>	-1.9	0.00018
	XM_008252198.2				
	XM_008252200.2				
	XM_017339725.1				
Glucose metabolism	XM_008252201.2	Glucokinase	<i>GCK</i>	-1.7	0.00061
XM_008261818.2					

Results

LncRNA	XR_001795369.1 XR_001795370.1 XR_519422.2	Uncharacterized LOC103351691	<i>LOC103351691</i>	-1.6	0.00026
Regulation of transcription	XM_008251077.2	Transcription factor CP2 like 1	<i>TFCP2L1</i>	-1.6	0.00001
Fatty acid biosynthesis	XM_017339196.1	Acetyl-CoA carboxylase beta	<i>ACAB</i>	-1.6	0.00004
Transcription activity	XM_002711229.3	Achaete-scute family bHLH transcription factor 1	<i>ASCL1</i>	-1.5	0.00246
NA	XM_017348395.1	E3 ubiquitin-protein ligase HERC2-like	<i>LOC108178363</i>	-1.5	0.00225
Acetate-CoA ligase activity	XM_002710791.3 XM_002710792.3	Acyl-CoA synthetase short chain family member 2	<i>ACSS2</i>	-1.5	0.00273

Table 2. Hepatic transcripts differentially upregulated by the administration of squalene at the level of signal \log_2 ratio > 1.5 and false discovery rate < 0.001 in male *Oryctolagus cuniculus* according to RNAseq.

Biological Process	GenBank	Name	Gene Symbol	Signal \log_2 Ratio	<i>p</i> -Value
Protein glycosylation	XM_017346007.1	Dolichyl- diphosphooligosaccharide-- protein glycosyltransferase subunit 4, OST4	<i>LOC108177690</i> (<i>OST4</i>)	2.5	2.60 ⁻⁷
Intracellular protein transport, vesicle tethering to Golgi	XM_002710763.3 XM_008255883.2 XM_008255884.2 XM_017341515.1	Family with sequence similarity 91 member A1	<i>FAM91A1</i>	2.3	4.39 ⁻⁶
NA	XR_515397.2	Uncharacterized LOC103345531	<i>LOC103345531</i>	2	0.00009
Actin binding, ATP binding	XM_017348206.1	Myosin-6	<i>MYH6</i>	1.8	0.00041
Regulate bone mineralization	NM_001101695.1	Osteomodulin	<i>OMD</i>	1.8	0.00013
Negative Regulation of translational initiation	NM_001204114.1	Eukaryotic translation initiation factor 4E binding protein 3	<i>EIF4EBP3</i>	1.7	0.00046
Integral component of membrane	XM_008249188.2 XM_017337996.1 XM_008249187.2 XM_008249192.2	Leucine rich repeat and Ig domain containing 1	<i>LINGO1</i>	1.7	0.00022

Results

	XM_008249193.2 XM_008249194.2				
NA	XM_002715469.3	Leucine rich repeat containing 39	<i>LRRC39</i>	1.6	0.00086
Nucleoside triphosphate catabolic process, immune response	XM_008263526.2 XM_017345377.1	Ectonucleotide pyrophosphatase/phosphod iesterase 3	<i>ENPP3</i>	1.6	0.00022
lncRNA	XR_001793580.1 XR_001793581.1	Uncharacterized LOC108176846	<i>LOC108176846</i>	1.6	0.00009
Muscle contraction	XM_017343215.1	Titin	<i>TTN</i>	1.6	0.00133
Glycosylation	XM_008251202.1	Glycosyltransferase 1 domain containing 1	<i>GLT1D1</i>	1.5	0.00002
Trehalose metabolism	NM_001082290.1	Trehalase	<i>TREH</i>	1.5	0.00057

To confirm the RNAseq data, 17 transcripts with log₂ fold change higher than 1.5 or lower than -1.5 were randomly selected from Tables 1 and 2, including *LOC100344375*, *LOC100344884* (*PNPLA3*), *GCK*, *LOC103351691*, *TFCP2L1*, *ACAB*, *ASCL1*, *ACSS2*, *OST4*, *FAM91A1*, *MYH6*, *OMD*, *LRRC39*, *LOC108176846*, *TTN*, *GLT1D1* and *TREH*. Their RT-qPCR assays were set up and verified on individual hepatic samples. A correlation study between RNAseq and RT-qPCR by assessing log₂ fold change values of transcripts showed a significant agreement ($r = 0.8$, $p < 0.0001$) (Figure 5A) and all samples were properly classified (Figure 5B). In rabbits receiving squalene (Table 3), twelve transcripts displayed significant expression changes (*LOC100344884* (*PNPLA3*), *GCK*, *TFCP2L1*, *ASCL1*, *ACSS2*, *OST4*, *FAM91A1*, *MYH6*, *LRRC39*, *LOC108176846*, *GLT1D1* and *TREH*).

Results

Table 3. Changes in selected hepatic gene expressions of male *Oryctolagus cuniculus* receiving 0.5% squalene according to RT-qPCR assay for genes with signal log₂ ratio < -1.5 or >1.5.

Gene Symbol	Control (n = 5)	Squalene (n = 5)	Fold Change	Signal log ₂ Ratio
<i>ASCL1</i>	2.4 ± 3.4	0.1 ± 0.2 *	0.1	-4.2
<i>ACAB</i>	2.3 ± 3.3	0.5 ± 0.3	0.2	-2.3
<i>GCK</i>	1.5 ± 1.4	0.3 ± 0.2 *	0.2	-2.2
<i>LOC100344884</i> (<i>PNPLA3</i>)	1.2 ± 0.6	0.3 ± 0.3 *	0.3	-1.9
<i>ACSS2</i>	1.0 ± 0.2	0.3 ± 0.2 **	0.3	-1.8
<i>TFCP2L1</i>	1.0 ± 0.2	0.4 ± 0.2 **	0.4	-1.3
<i>LOC100344375</i>	1.5 ± 1.1	0.9 ± 0.5	0.6	-0.7
<i>LOC103351691</i>	2.0 ± 2.1	1.9 ± 1.7	1.0	0.0
<i>FAM91A1</i>	1.1 ± 0.6	2.0 ± 0.9 *	1.8	0.8
<i>LOC108177690</i> (<i>OST4</i>)	1.1 ± 0.5	2.2 ± 0.8 *	2.0	1.0
<i>LRRC39</i>	1.1 ± 0.4	2.0 ± 0.9 *	1.9	1.0
<i>LOC108176846</i>	1.4 ± 1.2	3.6 ± 1.9 *	2.6	1.4
<i>GLT1D1</i>	1.4 ± 1.2	4.4 ± 2.3 *	3.2	1.7
<i>MYH6</i>	2.2 ± 1.9	11.2 ± 9.7 *	5.1	2.3
<i>OMD</i>	4.1 ± 5.6	19.7 ± 28.2	4.8	2.3
<i>TTN</i>	1.0 ± 2.1	5.8 ± 5.3	5.6	2.6
<i>TREH</i>	1.4 ± 1.1	16.3 ± 15.2 *	11.7	3.6

Results are expressed as means and standard deviations normalized to *PPIB* and *GAPDH*. Statistical analyses were carried out according to Mann–Whitney U-test and *, $p < 0.05$, ** $p < 0.01$ vs. control.

Results

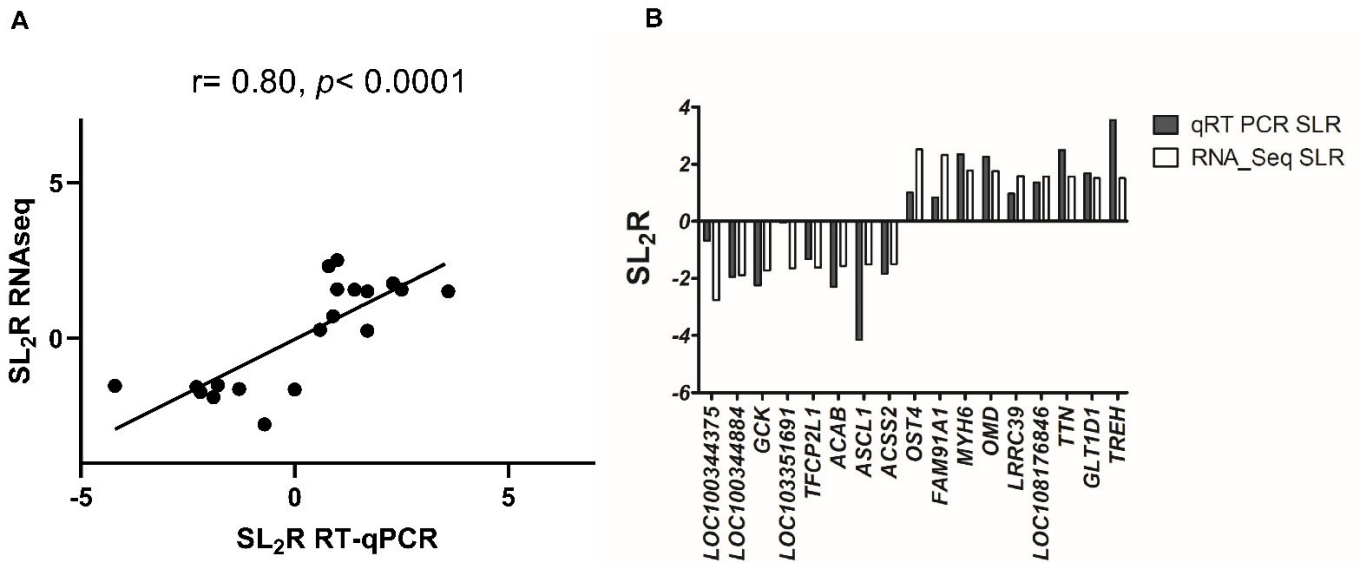


Figure 5. Concordance between used methods of RNA analysis. (A) Correlation analysis of 17 selected genes between RNAseq and RT-qPCR normalized to the invariant *PIPB* and *GAPDH* genes. The mean values obtained for signal log₂ ratio (SL₂R) from individual analyses (Table 3) were plotted against the RNAseq which used partially pooled samples (Tables 1 and 2). Good agreement between the procedures was observed ($r = 0.8, p < 0.0001$). (B) Difference in results of SL₂R expression of both procedures of the 17 selected genes.

Network correlations obtained from RT-qPCR results revealed significant association among key transcripts (Figure 6). *OST4* and *TFCP2L* were hubs and correlated with *LOC100344884* (*PNPLA3*), *GCK*, *ACSS2*, *MYH6*, *LRR39*, *LOC108176846*, *GLT1D1* and *TREH*.

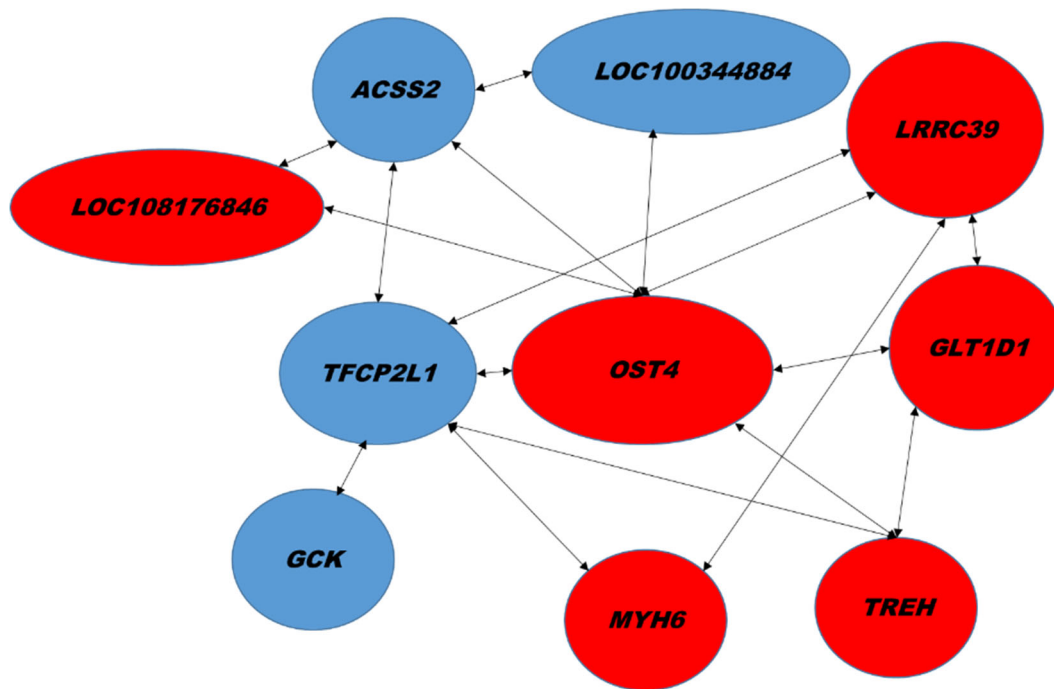


Figure 6. Network of hepatic transcripts. A, Association among transcript changes assayed by RT-qPCR. Red, up regulation. Blue, down regulation. Significant Spearman's correlations ($p < 0.02$).

Likewise, significant associations were observed among several transcripts and the hepatic content of metabolites in cholesterol biosynthetic pathways, including lanosterol, dihydrolanosterol, and desmosterol (Figure 7A). In this regard, down regulations of *TFCP2L1* and *ACSS2* were associated with sterols in the Kandutsch–Russell pathway and with increased hepatic lipid droplet area (Figure 7B). The increase in *FAM91A1* and the decrease in *LOC100344884* (*PNPLA3*) were associated with sterols in the Bloch pathway.

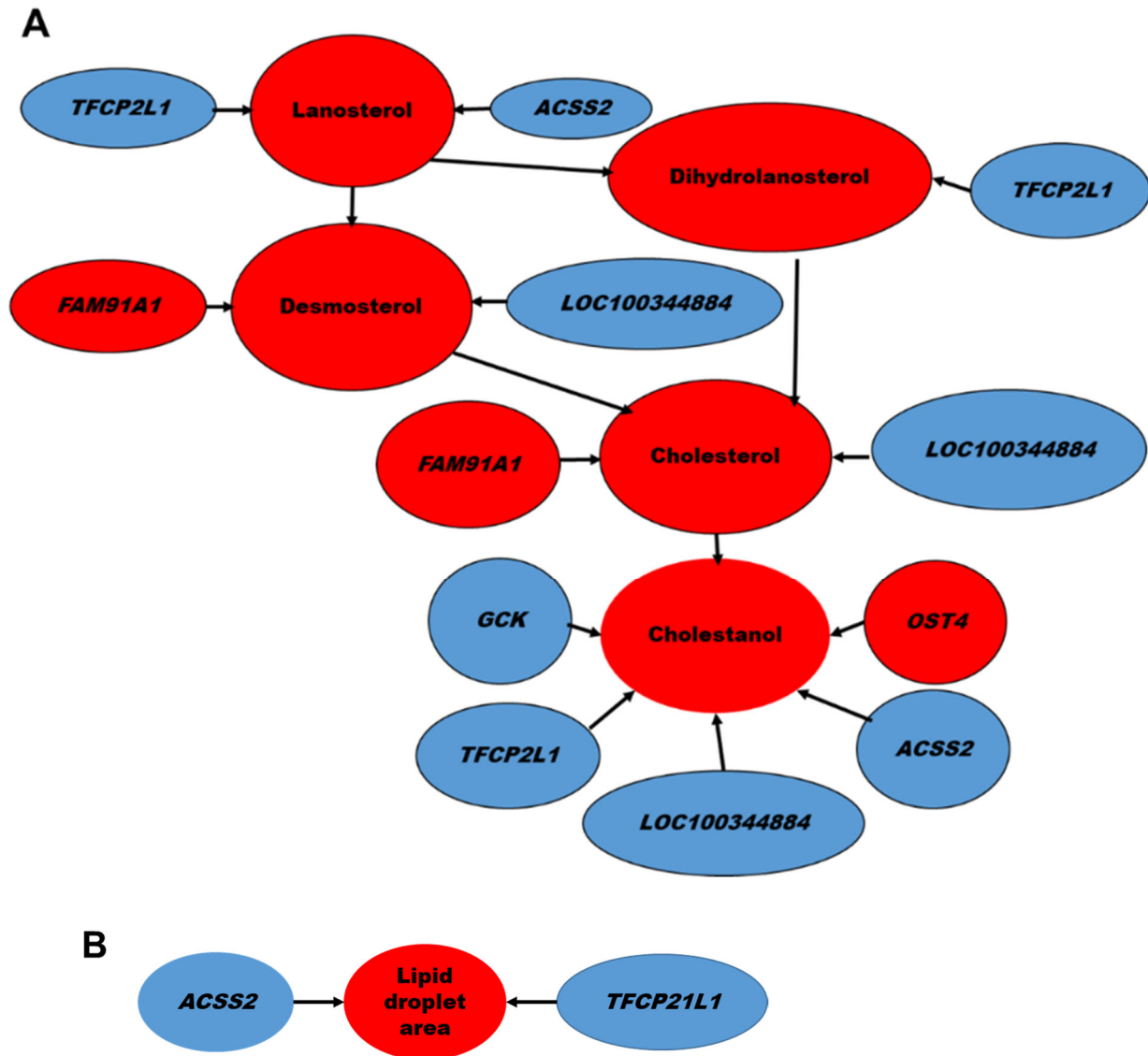


Figure 7. Correlation between hepatic transcripts and biological parameters in response to squalene intake. (A) transcripts associated with sterol precursors in the Kandutsch–Russell pathway. (B) transcripts related to lipid droplet area. Red; up regulation. Blue; down regulation. Significant ($p < 0.02$) Spearman’s correlations are shown.

To verify those associations, a murine AML12 hepatic cell line was incubated with 200 μ M squalene and 200 nM of lanosterol, dihydrolanosterol, zymostenol or desmosterol for 6 h. In the assayed conditions, only *Acss2*, *Fam91a1* and *Pnpla3* expressions reproduced the pattern observed in rabbit’s livers (Figure 8).

Results

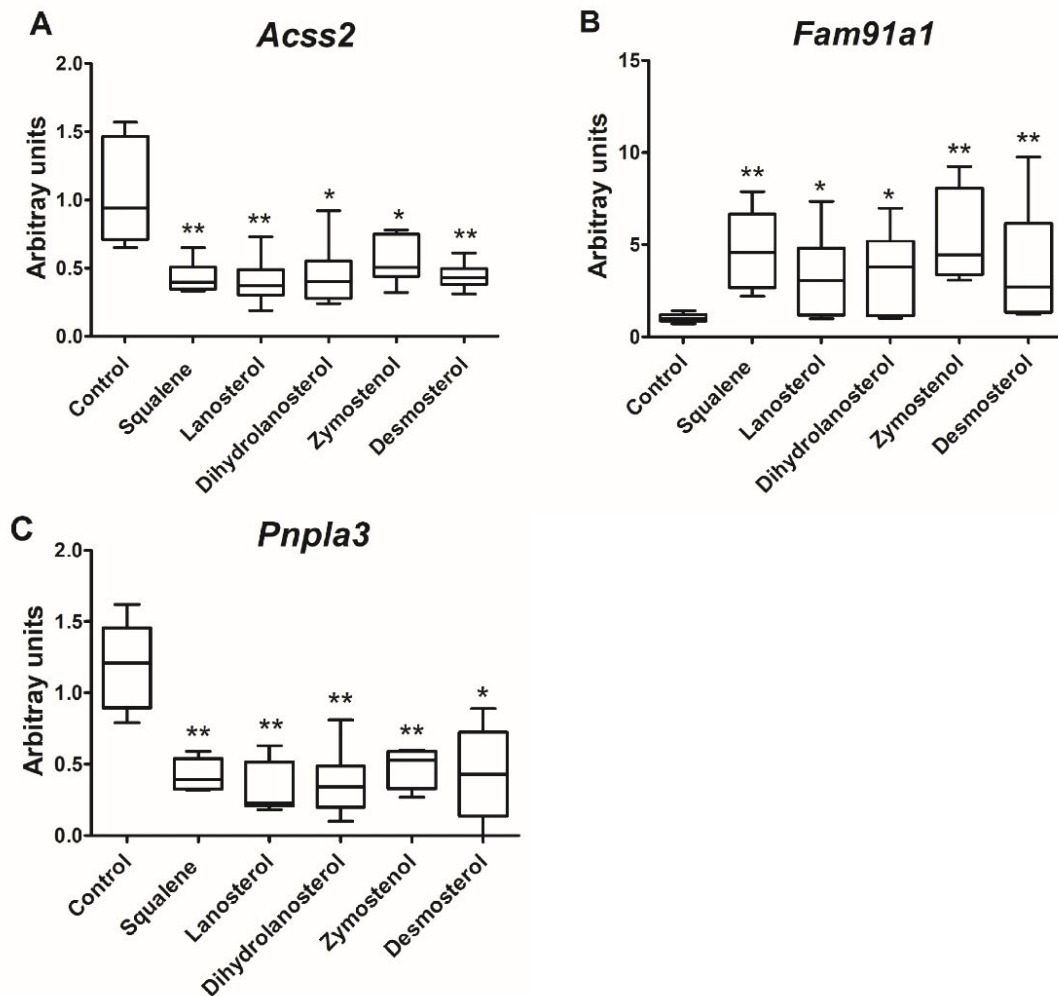


Figure 8. Effect of in vitro incubation of cholesterol precursors on selected gene expressions. AML12 cells were incubated in presence of 0.1% ethanol (control) or 200 μ M squalene, 200 nM lanosterol, dihydrolanosterol, zymostenol or desmosterol dissolved in 0.1% ethanol for 6 h. The experiment was performed in triplicate, with $n = 6$ in each experiment for control and treated cells. Panels (A–C) correspond to *Acss2*, *Fam91a1* and *Pnpla3* mRNA levels normalized to *Pipb* by RT-qPCR, respectively. Data are means and 10–90% percentiles. Statistical analyses were performed according to Mann–Whitney’s U-test. * $p < 0.05$, ** $p < 0.01$ vs. control.

3. Discussion

The nutrigenomic approach was carried out through transcriptomic analysis of the liver in male wild-type white rabbits (*Oryctolagus cuniculus*) following 0.5% squalene intake (0.6 g/kg). The administration induced increased hepatic squalene accumulation and elevated levels of post-squalene metabolites of cholesterol biosynthesis, lanosterol, dihydrolanosterol, lathosterol, zymostenol and desmosterol. Using RNA sequencing, squalene intake did not modify single nucleotide polymorphisms; however, the terpene induced alternative splicing patterns, both at 5’ and 3’ sites and retained introns. Rabbits receiving squalene displayed significant hepatic expression changes of *LOC100344884*

Results

(*PNPLA3*), *GCK*, *TFCP2L1*, *ASCL1*, *ACSS2*, *OST4*, *FAM91A1*, *MYH6*, *LRRC39*, *LOC108176846*, *GLT1D1* and *TREH*. Post-squalene metabolite levels were also associated with transcript levels. Moreover, the modified expression of *Acss2*, *Fam91a1* and *Pnpla3* was modified in the murine AML12 hepatic cell line by incubation with squalene and post-squalene intermediates in cholesterol biosynthesis such as lanosterol, dihydrolanosterol, zymostenol and desmosterol. These findings indicate that transcriptional changes are not only dependent on squalene but also its downstream metabolites.

The absence of changes in body weight in animals receiving dietary squalene compared to control rabbits and the normal histomorphometric evaluation of hepatocytes (Figure 2) implies the nontoxic accumulation of the triterpene in small lipid droplets, unlike mice, where it accumulates in larger droplets [20,21]. Interestingly, a similar pattern of droplets was observed with oleanic acid triterpene [22]. These droplets could accumulate lipids in the form of non-esterified cholesterol [21], acting as energy storage depots and barriers against lipotoxicity, preventing cellular membrane defects, mitochondrial dysfunction, and errors in signaling pathways [23]. In contrast to previous studies in mice, squalene administration in rabbits did not decrease hepatic triglyceride content. Nor were there observed changes in *CYP2B* and *CYP2C* expressions (data not shown) using a similar dose to mice [9]. The length of treatment, animal model and experimental designs are crucial differences that could be responsible for the discrepant results.

Squalene mainly modified the hepatic expression for gene clusters involved in the hepatic transport of lipids and proteins, lipid metabolism, lipogenesis, protective effects against inflammation and neoplasm. These findings might contribute to explaining the absence of inflammation even in the presence of increased content of non-esterified cholesterol and increased caspase1 levels [21].

FAM91A1, a poorly understood gene, seems to play a regulatory role in golgin-mediated vesicle capturing in order to process, package and transport proteins and lipid molecules [24,25]. *FAM91A1* expression was not correlated to the increased squalene content (data not shown), which might be explained by the fact that this triterpene is also distributed in further subcellular organelles, including nuclear and plasma membranes

Results

and rough endoplasmic reticulum [20]. The reduced expression of *ACSS2* and *TFCP2L1* was associated with elevated lipid droplet areas in the liver (Figure 7B). The reduced expression of *GCK*, *ACSS2* and *LOC100344884* and the increased expression of *TREH* are of interest regarding the squalene-modified hepatic lipid profile. *GCK* activates lipogenesis, increases cellular triglyceride content, and regulates glucose disposal [26,27]. Reduced-*GCK* activity lowers mRNA levels for triglyceride synthesis enzymes but also for insulin receptors, leading to insulin resistance [27,28,29], suggesting that *GCK* inhibition by squalene may be useful in the treatment against fatty liver. *ACSS2* is a metabolic gene that promotes fat storage. *ACSS2* deficiency inhibits activity of lipid transporters and fatty acid oxidation genes, which then lowers dietary lipid absorption, reduces triglyceride content [29], and lessens hepatic fibrosis [30]. *LOC100344884*, the ortholog for *Pnpla3*, expresses lipase activity towards triglycerides in hepatocytes and retinyl esters in hepatic stellate cells [31] and was strongly associated with hepatic cholesterol content (Figure 7), fibrosis and steatosis [31,32]. *TREH* is the least studied membrane-bound α -glucosidase that hydrolyzes trehalose. Its transcript is normally expressed in intestine [33,34] and to a lesser amount in liver (<https://gtexportal.org/home/gene/TREH>, accessed on 1 March 2022). Squalene increased expression of *TREH* that could drive glucose metabolism [35]. Regarding protein modification, squalene-upregulated *OST4* may play a key role in promoting co-translational N-glycosylation by stabilizing STT3A-containing *OST* isoforms present in high amounts in liver cells [36]. Glycosylation deficiency interferes with protein functions and drug disposition [37,38] and reduces low-density lipoprotein cholesterol [39]. Two transcripts, *MYH6* and *LRRC39*, mainly expressed in muscle, were upregulated in the liver in response to squalene intake. Hepatocytes showed very low expression (1.6 transcripts per million vs. a median of 3.3) [40]. Interestingly, both transcript levels were associated (Figure 6) and share a function in cell signaling by protein dephosphorylation. Overexpression of (*Myh6/Ghrl*) in transgenic rats lessened oxidative stress and prevented fat dietary-induced hyperglycemia [41]. Squalene might modulate lipid and glucose metabolism through the expression of these genes.

Rabbits receiving squalene increased the hepatic content of cholesterol precursors including lanosterol, dihydrolanosterol, lathosterol and zymostenol via the Kandutsch-

Results

Russell path and desmosterol via the Bloch path. In addition, strong correlations linked squalene-modified transcript levels with increased hepatic quantities of cholesterol precursors. In this sense, the reduced expression of *TFCP2L1* was strongly associated with the accumulation of lanosterol and dihydrolanosterol, as did *ACSS2* in regard to lanosterol. The increased expression of *FAM91A1* and the decreased expression of *LOC100344884* were associated with desmosterol. These associations indicate that the observed actions of squalene could be executed through its post-squalene precursors in the cholesterol biosynthesis pathway and may differ from those observed when squalene is not metabolized [42]. Squalene accumulation in cholesterol auxotrophic lymphomas prevents oxidative cell death [42]. To solve this dilemma, the AML12 hepatic cell line was incubated with lanosterol, dihydrolanosterol, zymostenol or desmosterol, followed by analyses of *Acss2*, *Fam91a1* and *Pnpla3* transcripts. Obtained results (Figure 8) displayed the same expression changes that those observed *in vivo* by squalene administration. In consequence, a direct hepatic transcriptional effect of lanosterol, dihydrolanosterol, zymostenol and desmosterol is involved.

Previous studies have demonstrated that squalene shows protective anti-tumor activities [43]. *ACSS2* captures acetate as a carbon source for the proliferation of hepatocellular carcinoma [28,29]. Adult mice lacking *ACSS2* exhibit reduced hepatic tumor burdens [29]. *TFCP2L1*, a transcription factor required in germ cell specification and cholangiocyte-to-hepatocyte differentiation [44], is strongly correlated with several transcripts modulated by squalene, including *OST4*, *TREH*, *GCK*, *ACSS2*, *MYH6* and *LRRC39* (Figure 6). *TFCP2L1* is down regulated in renal and thyroid cancer cells [45]. Besides, *GLT1D1* is a tumor suppressor gene and is highly expressed in hepatocellular carcinoma [46].

In conclusion, dietary squalene accumulates in the liver and functions as a modulator of the hepatic transcriptome in wild-type *Oryctolagus cuniculus*. Concomitantly, increased levels of post-squalene metabolites of cholesterol biosynthesis, including lanosterol, dihydrolanosterol, lathosterol, zymostenol and desmosterol, were noted. Significant hepatic expression changes of *LOC100344884* (*PNPLA3*), *GCK*, *TFCP2L1*, *ASCL1*, *ACSS2*, *OST4*, *FAM91A1*, *MYH6*, *LRRC39*, *LOC108176846*, *GLT1D1* and *TREH* were observed in rabbits receiving squalene. Many of these changes were

correlated with post-squalene metabolite levels. Furthermore, incubation of the murine AML12 hepatic cell line in the presence of lanosterol, dihydrolanosterol, zymostenol and desmosterol modified *Acss2*, *Fam91a1* and *Pnpla3* expressions. These findings indicate that squalene and post-squalene metabolites play important roles in hepatic transcriptional changes.

4. Materials and Methods

4.1. Animal Models and Experimental Design

The experimental animals used were 10 male wild-type New Zealand white rabbits obtained from Servicio de Apoyo a la Investigación Animal (Universidad de Zaragoza). Animals were divided into two groups, the first fed a control diet enriched with 1% of sunflower oil ($n = 5$) and the second fed a diet containing 1% of sunflower oil and 0.5% of squalene (Sigma-Merck, Darmstadt, Germany) ($n = 5$). Initial body weight for control and experimental groups was 1560 ± 201 and 1410 ± 203 g, respectively. Taking into account consumed food and body weight, the dose was equivalent to 0.6 mg/kg/day [20]. Fresh diets were prepared weekly and changed each 2 days to reduce oxidation of squalene. The animals were fed the experimental diets for 4 weeks and they were well tolerated.

Body mass and dietary intake were recorded every 2 days. After dietary intervention, rabbits were starved for 18 h, then weighed and euthanized by cervical dislocation, and livers were obtained. An aliquot of each sample was stored in neutral formaldehyde and the remaining was frozen immediately in liquid nitrogen.

4.2. Liver Histology Analyses

The liver samples stored in formaldehyde were then embedded in paraffin wax 4 μm sections were stained with hematoxylin and eosin and observed under Nikon microscope. Lipid droplets were estimated by quantifying as percentage of total liver section with Adobe Photoshop CS3 (Adobe Inc., San Jose, CA, USA).

4.3. Quantification of Hepatic Lipids

10 mg sections of liver were used to extract and quantify lipids as previously mentioned [21].

4.4. Quantification of Hepatic Sterols

Sterol extraction and quantification by gas chromatography and mass spectrometry was performed as previously described [47].

4.5. Quantification of Hepatic Squalene

Results

Squalene was isolated and quantified by solid phase extraction, gas chromatography and mass spectrometry (GC-MS) as mentioned [20].

4.6. RNA Extraction

Total liver RNA was extracted using Quick-RNA MiniPrep Kit (Cat. No: R1055, ZYMO Research, Irvine, CA, USA) following manufacturer's instructions. Extracted RNA was quantified by absorbance at $A_{260/280}$ with Nanodrop Spectrophotometer. The purity was determined by analysis of absorbance at A_{260}/A_{280} the ratio was ~ 2 . The integrity of both 28S and 18S ribosomal RNAs was verified by agarose gel electrophoresis followed by ethidium bromide staining and the 28S/18S ratio was higher than 2.

4.7. RNAseq and Data Analyses

4.7.1. Library Construction and Sequencing Was Carried Out by BGI (Shenzhen, China) Service

Briefly, poly-A containing mRNA molecules were purified using poly-T oligo-attached magnetic beads. Following purification, mRNA was fragmented into small pieces using divalent cations under elevated temperatures. Cleaved RNA fragments were copied into first-strand cDNA using reverse transcriptase and random primers. This was followed by second-strand cDNA synthesis using DNA polymerase I and RNase H. These cDNA fragments then have the addition of a single 'A' base and subsequent ligation of the adapter. The products were then purified and enriched with PCR amplification. Then PCR yield was quantified using Qubit samples then pooled together to make a single-strand DNA circle (ssDNA circle), which gave the final library. DNA nanoballs (DNBs) were generated with the ssDNA circle by rolling circle replication (RCR) to enlarge the fluorescent signals at the sequencing process. The DNBs were loaded into the patterned nanoarrays, and pair-end reads of 100 bp were read through on the DNBseq platform for the following data analysis study. For this step, the DNBseq platform combines the DNA nanoball-based nanoarrays and stepwise sequencing using Combinational Probe-Anchor Synthesis Sequencing Method.

4.7.2. Bioinformatics Workflow

Sequencing reads containing low-quality, adaptor-polluted and high amounts of unknown base reads were removed, then these reads were mapped onto reference genome (*Oryctolagus cuniculus* GCA_000003625.1) using HISAT2 followed with novel gene prediction using StringTie to reconstruct transcripts, and Cuffcompare to compare

Results

reconstructed transcripts to reference annotation. Moreover, CPC was used to predict coding potential of novel transcripts, followed by merging coding novel transcripts with reference transcripts to obtain a complete reference. With genome mapping results, GATK was used to call SNP and INDEL for each sample, then filter out the unreliable sites results in final SNP and INDEL report. RMATS was also used to detect differentially splicing genes (DSG) between samples. After novel transcript detection, novel coding transcripts were merged with reference transcripts to obtain complete reference, then clean reads were mapped to reference using Bowtie and gene expression level for each sample was calculated with RSEM. This was followed by clustering analysis and functional annotations. The complete database was deposited in the GEO database (GSE191236).

4.8. Quantification of mRNA

RNAseq transcripts displaying signal \log_2 ratio > 1.5 or < -1.5 and false discovery rate < 0.001 were selected for confirmation and 18 out of 22 genes fulfilling these criteria assayed by reverse transcriptase quantitative PCR (RT-qPCR) assay. Primers for specific sequences were designed using NCBI and then were checked for gene specificity and full variant coverage by BLAST (NCBI), KEGG and Ensemble Genome Browser. Equal amounts of (500 ng) DNA-free RNA was used to synthesize complementary DNA using PrimeScript RT Reagent Kit (Cat. No: RR037A, Takara, Kutsatsu, Shiga, Japan) following manufacturer's instructions. Primers' concentrations and cDNA input were optimized to obtain efficiencies in the range of 90% to 110%. Primer characteristics are listed in the primer tables shown in section of Materials and Methods. Quantitative real-time was carried out using SYBR Green dye master mix (Applied Biosystems, Foster City, CA, USA) according to manufacturer's instructions, utilizing Step One Real-Time PCR System (Applied Biosystems, Foster City, CA, USA). Analysis of relative gene expression data was calculated using the $2^{(-\Delta\Delta CT)}$ method and normalized to the average of both reference genes *PPIB* and *GAPDH* for rabbits. *Ppib* was used as a reference gene for the murine AML12 cell line.

4.9. AML12 Cell Culture

Hepatic cell line of murine origin was grown in a humidified atmosphere of 5% CO₂ at 37 °C in DMEM (Thermo Fisher Scientific, Waltham, MA, USA): F12-Ham's medium (GE Healthcare Life Science, South Logan, UT, USA) enriched with fetal bovine serum

Results

and insulin/transferrin/selenium. When cells reached a confluence of 90–100%, medium was removed, cells were washed twice with phosphate buffered saline followed by addition of medium free of fetal bovine serum, insulin, transferrin and selenium. Cells were then incubated for 6 h with 200 μ M squalene (Sigma-Merck, Darmstadt, Germany) or with 200 nM lanosterol, dihydrolanosterol, zymostenol or desmosterol (Avanti Polar lipids, Alabaster, AL, USA). Each condition was tested in six replicates. Media were removed, cells were washed twice with phosphate buffered saline then collected and total RNA was extracted using Tri-Reagent Solution (Ambion, Austin, TX, USA). DNA contaminants were removed by TURBO DNase treatment using DNA Removal Kit (Ambion, Austin, TX, USA). Squalene and sterol effects were investigated at mRNA level by RT-qPCR assays. Primers are included in Materials and Methods.

4.10. Quality Control and Statistics

Samples in quantitative real time were tested in duplicate and their coefficient of variation obtained. Duplicates showing coefficient of variation higher than 3% were discarded and tested again. Statistical analyses were performed with GraphPad Prism (GraphPad Software, San Diego, CA, USA). Data was analyzed for normal distribution by Shapiro-Wilk's test and homogeneity of variance by Bartlett's F-test. When any of these parameters failed, results were analyzed by Mann-Whitney's U test. Differences in both groups were considered significant if $p < 0.05$. Correlation among tested results was analyzed using Spearman's ρ correlation coefficient.

Supplementary Materials: The following supporting information can be downloaded at: <https://www.mdpi.com/article/10.3390/ijms23084172/s1>.

Funding: This research was funded by Ministerio de Ciencia e Innovación-Fondo Europeo de Desarrollo Regional (PID2019-104915RB-I00 and RTI2018- 098113-B100), Fondo Social Europeo-Gobierno de Aragón (B16_20R) and the European Regional Development Fund Interreg-SUDOE (Redvalue, SOE1/PI/E0123) from the European Union. CIBER de Fisiopatología de la Obesidad y Nutrición (CIBEROBN, CB06/03/1012 and CB06/03/0021) is an initiative of ISCIII.

Institutional Review Board Statement: Experiments were executed in accordance with the Directive (2010/63/UE) for the protection of animals used for scientific aims and the study protocols were authorized by the Ethics Committee for Animal Research of the University of Zaragoza (PI47/10)

Informed Consent Statement: Not applicable

Data Availability Statement: Data is contained within the article and supplementary material and RNA seq dataset is deposited at GEO (GSE191236).

Results

Acknowledgments: We would like to thank SAEA (Servicio de Ayuda a la Experimentación Animal) for their help in maintaining the rabbits.

Conflicts of Interest: The authors declare no conflict of interest.

References

1. Keys, A.; Menotti, A.; Karvonen, M.J.; Aravanis, C.; Blackburn, H.; Buzina, R.; Djordjevic, B.S.; Dontas, A.S.; Fidanza, F.; Keys, M.H.; et al. The diet and 15-year death rate in the seven countries study. *Am. J. Epidemiol.* 1986, 124, 903–915. <https://doi.org/10.1093/oxfordjournals.aje.a114480>.
2. Martinez-Gonzalez, M.A.; Salas-Salvado, J.; Estruch, R.; Corella, D.; Fito, M.; Ros, E.; Predimed, I. Benefits of the Mediterranean Diet: Insights from the PREDIMED Study. *Prog. Cardiovasc. Dis.* 2015, 58, 50–60. <https://doi.org/10.1016/j.pcad.2015.04.003>.
3. Gaforio, J.J.; Visioli, F.; Alarcon-de-la-Lastra, C.; Castaner, O.; Delgado-Rodriguez, M.; Fito, M.; Hernandez, A.F.; Huertas, J.R.; Martinez-Gonzalez, M.A.; Menendez, J.A.; et al. Virgin Olive Oil and Health: Summary of the III International Conference on Virgin Olive Oil and Health Consensus Report, JAEN (Spain) 2018. *Nutrients* 2019, 11, 2039. <https://doi.org/10.3390/nu11092039>.
4. Soto-Alarcon, S.A.; Valenzuela, R.; Valenzuela, A.; Videla, L.A. Liver protective effects of extra virgin olive oil: Interaction between its chemical composition and the cell-signaling pathways involved in protection. *Endocr. Metab. Immune Disord.-Drug Targets (Former. Curr. Drug Targets-Immune Endocr. Metab. Disord.)* 2018, 18, 75–84. <https://doi.org/10.2174/1871530317666171114120552>.
5. Vitaglione, P.; Savarese, M.; Paduano, A.; Scalfi, L.; Fogliano, V.; Sacchi, R. Healthy virgin olive oil: A matter of bitterness. *Crit. Rev. Food Sci. Nutr.* 2015, 55, 1808–1818. <https://doi.org/10.1080/10408398.2012.708685>.
6. Foscolou, A.; Critselis, E.; Panagiotakos, D. Olive oil consumption and human health: A narrative review. *Maturitas* 2018, 118, 60–66. <https://doi.org/10.1016/j.maturitas.2018.10.013>.
7. Lou-Bonafonte, J.M.; Arnal, C.; Navarro, M.A.; Osada, J. Efficacy of bioactive compounds from extra virgin olive oil to modulate atherosclerosis development. *Mol. Nutr. Food Res.* 2012, 56, 1043–1057. <https://doi.org/10.1002/mnfr.201100668>.
8. Covas, M.-I.; Ruiz-Gutiérrez, V.; De La Torre, R.; Kafatos, A.; Lamuela-Raventós, R.M.; Osada, J.; Owen, R.W.; Visioli, F. Minor Components of Olive Oil: Evidence to Date of Health Benefits in Humans. *Nutr. Rev.* 2006, 64, 20–30. <https://doi.org/10.1301/nr.2006.oct.S20-S30>.
9. Gabas-Rivera, C.; Jurado-Ruiz, E.; Sanchez-Ortiz, A.; Romanos, E.; Martinez-Beamonte, R.; Navarro, M.A.; Surra, J.C.; Arnal, C.; Rodriguez-Yoldi, M.J.; Andres-Lacueva, C.; et al. Dietary Squalene Induces Cytochromes Cyp2b10 and Cyp2c55 Independently of Sex, Dose, and Diet in Several Mouse Models. *Mol. Nutr. Food Res.* 2020, 64, e2000354. <https://doi.org/10.1002/mnfr.202000354>.
10. Lanzon, A.; Albi, T.; Cert, A.; Gracian, J. The Hydrocarbon Fraction of Virgin Olive Oil and Changes Resulting from Refining.pdf. *J. Am. Oil Chem. Soc.* 1994, 71, 285–291. <https://doi.org/10.1007/BF02638054>.
11. Martinez-Beamonte, R.; Sanclemente, T.; Surra, J.C.; Osada, J. Could squalene be an added value to use olive by-products? *J. Sci. Food Agric.* 2020, 100, 915–925. <https://doi.org/10.1002/jsfa.10116>.

Results

12. Reddy, L.H.; Couvreur, P. Squalene: A natural triterpene for use in disease management and therapy. *Adv. Drug Deliv. Rev.* 2009, 61, 1412–1426. <https://doi.org/10.1016/j.addr.2009.09.005>.
13. Ramírez-Torres, A. Squalene: Current Knowledge and Potential Therapeutical Uses; Nova Science Publishers, Incorporated: Hauppauge, NY, USA, 2011.
14. Tilvis, R.S.; Miettinen, T.A. Absorption and metabolic fate of dietary 3H-squalene in the rat. *Lipids* 1983, 18, 233–238. <https://doi.org/10.1007/BF02534554>.
15. Gabas-Rivera, C.; Barranquero, C.; Martinez-Beamonte, R.; Navarro, M.A.; Surra, J.C.; Osada, J. Dietary squalene increases high density lipoprotein-cholesterol and paraoxonase 1 and decreases oxidative stress in mice. *PLoS ONE* 2014, 9, e104224. <https://doi.org/10.1371/journal.pone.0104224>.
16. Yang, B.C.; Phillips, M.I.; Mohuczy, D.; Meng, H.; Shen, L.; Mehta, P.; Mehta, J.L. Increased Angiotensin II Type 1 Receptor Expression in Hypercholesterolemic Atherosclerosis in Rabbits. *Arterioscler. Thromb. Vasc. Biol.* 1998, 18, 1433–1439. <https://doi.org/10.1161/01.atv.18.9.1433>.
17. Brousseau, M.E.; Hoeg, J.M. Transgenic rabbits as models for atherosclerosis research. *J. Lipid Res.* 1999, 40, 365–375. [https://doi.org/10.1016/S0022-2275\(20\)32440-8](https://doi.org/10.1016/S0022-2275(20)32440-8).
18. Fan, J.; Kitajima, S.; Watanabe, T.; Xu, J.; Zhang, J.; Liu, E.; Chen, Y.E. Rabbit models for the study of human atherosclerosis: From pathophysiological mechanisms to translational medicine. *Pharmacol. Ther.* 2015, 146, 104–119. <https://doi.org/10.1016/j.pharmthera.2014.09.009>.
19. Kritchevsky, D.; Moyer, A.W.; Tesar, W.C.; Logan, J.B.; Brown, R.A.; Richmond, G. Squalene feeding in experimental atherosclerosis. *Circ. Res.* 1954, 2, 340–343. <https://doi.org/10.1161/01.res.2.4.340>.
20. Martinez-Beamonte, R.; Alda, O.; Sanclemente, T.; Felices, M.J.; Escusol, S.; Arnal, C.; Herrera-Marcos, L.V.; Gascon, S.; Surra, J.C.; Osada, J.; et al. Hepatic subcellular distribution of squalene changes according to the experimental setting. *J. Physiol. Biochem.* 2018, 74, 531–538. <https://doi.org/10.1007/s13105-018-0616-2>.
21. Martinez-Beamonte, R.; Sanchez-Marco, J.; Felices, M.J.; Barranquero, C.; Gascon, S.; Arnal, C.; Burillo, J.C.; Lasheras, R.; Busto, R.; Lasuncion, M.A.; et al. Dietary squalene modifies plasma lipoproteins and hepatic cholesterol metabolism in rabbits. *Food Funct.* 2021, 12, 8141–8153. <https://doi.org/10.1039/d0fo01836h>.
22. Gabas-Rivera, C.; Martinez-Beamonte, R.; Rios, J.L.; Navarro, M.A.; Surra, J.C.; Arnal, C.; Rodriguez-Yoldi, M.J.; Osada, J. Dietary oleanolic acid mediates circadian clock gene expression in liver independently of diet and animal model but requires apolipoprotein A1. *J. Nutr. Biochem.* 2013, 24, 2100–2109. <https://doi.org/10.1016/j.jnutbio.2013.07.010>.
23. Seebacher, F.; Zeigerer, A.; Kory, N.; Krahmer, N. Hepatic lipid droplet homeostasis and fatty liver disease. *Semin. Cell Dev. Biol.* 2020, 108, 72–81. <https://doi.org/10.1016/j.semcdb.2020.04.011>.
24. Fromme, J.C.; Munson, M. Capturing endosomal vesicles at the Golgi. *Nat. Cell Biol.* 2017, 19, 1384–1386. <https://doi.org/10.1038/ncb3649>.
25. Barr, F.A.; Short, B. Golgins in the structure and dynamics of the Golgi apparatus. *Curr. Opin. Cell Biol.* 2003, 15, 405–413. [https://doi.org/10.1016/s0955-0674\(03\)00054-1](https://doi.org/10.1016/s0955-0674(03)00054-1).

Results

26. Kawano, Y.; Cohen, D.E. Mechanisms of hepatic triglyceride accumulation in non-alcoholic fatty liver disease. *J. Gastroenterol.* 2013, 48, 434–441. <https://doi.org/10.1007/s00535-013-0758-5>.
27. Guo, T.; Mao, Y.; Li, H.; Wang, X.; Xu, W.; Song, R.; Jia, J.; Lei, Z.; Irwin, D.M.; Niu, G.; et al. Characterization of the gene expression profile of heterozygous liver-specific glucokinase knockout mice at a young age. *Biomed. Pharmacother.* 2012, 66, 587–596. <https://doi.org/10.1016/j.biopha.2012.07.002>.
28. Kargbo, R.B. Inhibition of ACSS2 for Treatment of Cancer and Neuropsychiatric Diseases. *ACS Med. Chem. Lett.* 2019, 10, 1100–1101. <https://doi.org/10.1021/acsmchemlett.9b00295>.
29. Huang, Z.; Zhang, M.; Plec, A.A.; Estill, S.J.; Cai, L.; Repa, J.J.; McKnight, S.L.; Tu, B.P. ACSS2 promotes systemic fat storage and utilization through selective regulation of genes involved in lipid metabolism. *Proc. Natl. Acad. Sci. USA* 2018, 115, E9499–E9506. <https://doi.org/10.1073/pnas.1806635115>.
30. Xu, H.; Luo, J.; Ma, G.; Zhang, X.; Yao, D.; Li, M.; Loo, J.J. Acyl-CoA synthetase short-chain family member 2 (ACSS2) is regulated by SREBP-1 and plays a role in fatty acid synthesis in caprine mammary epithelial cells. *J. Cell Physiol.* 2018, 233, 1005–1016. <https://doi.org/10.1002/jcp.25954>.
31. Trepo, E.; Romeo, S.; Zucman-Rossi, J.; Nahon, P. PNPLA3 gene in liver diseases. *J. Hepatol.* 2016, 65, 399–412. <https://doi.org/10.1016/j.jhep.2016.03.011>.
32. Kawaguchi, T.; Sumida, Y.; Umemura, A.; Matsuo, K.; Takahashi, M.; Takamura, T.; Yasui, K.; Saibara, T.; Hashimoto, E.; Kawanaka, M. Genetic polymorphisms of the human PNPLA3 gene are strongly associated with severity of non-alcoholic fatty liver disease in Japanese. *PLoS ONE* 2012, 7, e38322. <https://doi.org/10.1371/journal.pone.0038322>.
33. Packard, C.J.; Boren, J.; Taskinen, M.R. Causes and Consequences of Hypertriglyceridemia. *Front. Endocrinol.* 2020, 11, 252. <https://doi.org/10.3389/fendo.2020.00252>.
34. Oesterreicher, T.J.; Markesich, D.C.; Henning, S.J. Cloning, characterization and mapping of the mouse trehalase (Treh) gene. *Gene* 2001, 270, 211–220. [https://doi.org/10.1016/s0378-1119\(01\)00474-7](https://doi.org/10.1016/s0378-1119(01)00474-7).
35. Rui, L. Energy metabolism in the liver. *Compr. Physiol.* 2014, 4, 177–197. <https://doi.org/10.1002/cphy.c130024>.
36. Dumax-Vorzet, A.; Roboti, P.; High, S. OST4 is a subunit of the mammalian oligosaccharyltransferase required for efficient N-glycosylation. *J. Cell Sci.* 2013, 126, 2595–2606. <https://doi.org/10.1242/jcs.115410>.
37. Clarke, J.D.; Novak, P.; Lake, A.D.; Hardwick, R.N.; Cherrington, N.J. Impaired N-linked glycosylation of uptake and efflux transporters in human non-alcoholic fatty liver disease. *Liver Int.* 2017, 37, 1074–1081. <https://doi.org/10.1111/liv.13362>.
38. Mohanty, S.; Chaudhary, B.P.; Zoetewey, D. Structural Insight into the Mechanism of N-Linked Glycosylation by Oligosaccharyltransferase. *Biomolecules* 2020, 10, 624. <https://doi.org/10.3390/biom10040624>.
39. van den Boogert, M.A.W.; Larsen, L.E.; Ali, L.; Kuil, S.D.; Chong, P.L.W.; Loregger, A.; Kroon, J.; Schnitzler, J.G.; Schimmel, A.W.M.; Peter, J.; et al. N-Glycosylation Defects in Humans Lower Low-Density Lipoprotein Cholesterol Through Increased Low-Density Lipoprotein Receptor Expression. *Circulation* 2019, 140, 280–292. <https://doi.org/10.1161/CIRCULATIONAHA.118.036484>.

Results

40. Ehrlich, K.C.; Lacey, M.; Ehrlich, M. Epigenetics of skeletal muscle-associated genes in the ASB, LRRC, TMEM, and OSBPL gene families. *Epigenomes* 2020, 4, 1. <https://doi.org/10.3390/epigenomes4010001>.
41. Cappellari, G.G.; Zanetti, M.; Semolic, A.; Vinci, P.; Ruozi, G.; Falcione, A.; Filigheddu, N.; Guarnieri, G.; Graziani, A.; Giacca, M. Unacylated ghrelin reduces skeletal muscle reactive oxygen species generation and inflammation and prevents high-fat diet-induced hyperglycemia and whole-body insulin resistance in rodents. *Diabetes* 2016, 65, 874–886. <https://doi.org/10.2337/db15-1019>.
42. Garcia-Bermudez, J.; Baudrier, L.; Bayraktar, E.C.; Shen, Y.; La, K.; Guarecuco, R.; Yucel, B.; Fiore, D.; Tavora, B.; Freinkman, E.; et al. Squalene accumulation in cholesterol auxotrophic lymphomas prevents oxidative cell death. *Nature* 2019, 567, 118–122. <https://doi.org/10.1038/s41586-019-0945-5>.
43. Smith, T.J. Squalene: Potential chemopreventive agent. *Expert Opin. Investig. Drugs* 2000, 9, 1841–1848. <https://doi.org/10.1517/13543784.9.8.1841>.
44. Wei, J.; Ran, G.; Wang, X.; Jiang, N.; Liang, J.; Lin, X.; Ling, C.; Zhao, B. Gene manipulation in liver ductal organoids by optimized recombinant adeno-associated virus vectors. *J. Biol. Chem.* 2019, 294, 14096–14104. <https://doi.org/10.1074/jbc.RA119.008616>.
45. Kotarba, G.; Krzywinska, E.; Grabowska, A.I.; Taracha, A.; Wilanowski, T. TFCP2/TFCP2L1/UBP1 transcription factors in cancer. *Cancer Lett.* 2018, 420, 72–79. <https://doi.org/10.1016/j.canlet.2018.01.078>.
46. Shastri, B. Functional Characterisation of Glycosyltransferase 1 Domain Containing 1 Gene in Mammary Carcinoma Cells. ResearchSpace@ Auckland. Dissertation Thesis, University of Auckland, Auckland, New Zealand, 2013.
47. Canfran-Duque, A.; Casado, M.E.; Pastor, O.; Sanchez-Wandelmer, J.; de la Pena, G.; Lerma, M.; Mariscal, P.; Bracher, F.; Lasuncion, M.A.; Busto, R. Atypical antipsychotics alter cholesterol and fatty acid metabolism in vitro. *J. Lipid Res.* 2013, 54, 310–324. <https://doi.org/10.1194/jlr.M026948>.

iii. Differentially Expressed Genes in Response to a Squalene-Supplemented Diet Are Accurate Discriminants of Porcine Non-Alcoholic Steatohepatitis

Abstract: Squalene is the major unsaponifiable component of virgin olive oil, the fat source of the Mediterranean diet. To evaluate its effect on the hepatic transcriptome, RNA sequencing was carried out in two groups of male Large White x Landrace pigs developing nonalcoholic steatohepatitis by feeding them a high fat/cholesterol/fructose and methionine and choline-deficient steatotic diet or the same diet with 0.5% squalene. Hepatic lipids, squalene content, steatosis, activity (ballooning + inflammation), and SAF (steatosis + activity + fibrosis) scores were analyzed. Pigs receiving the latter diet showed hepatic squalene accumulation and twelve significantly differentially expressed hepatic genes (\log_2 fold change > 1.5 or < -1.5) correlating in a gene network. These pigs also had lower hepatic triglycerides and lipid droplet areas and higher cellular ballooning. Glutamyl aminopeptidase (*ENPEP*) was correlated with triglyceride content, while alpha-fetoprotein (*AFP*), neutralized E3 ubiquitin protein ligase 3 (*NEURL3*), 2'-5'-oligoadenylate synthase-like protein (*OASL*), and protein phosphatase 1 regulatory inhibitor subunit 1B (*PPP1R1B*) were correlated with activity reflecting inflammation and ballooning, and *NEURL3* with the SAF score. *AFP*, *ENPEP*, and *PPP1R1B* exhibited a remarkably strong discriminant power compared to those pathological parameters in both experimental groups. Moreover, the expression of *PPP1R1B*, *TMEM45B*, *AFP*, and *ENPEP* followed the same pattern in vitro using human hepatoma (HEPG2) and mouse liver 12 (AML12) cell lines incubated with squalene, indicating a direct effect of squalene on these expressions. These findings suggest that squalene accumulated in the liver is able to modulate gene expression changes that may influence the progression of non-alcoholic steatohepatitis.

Keywords: squalene; virgin olive oil; pigs; murine AML12 cell line; human HEPG2 cell line; transcriptome; hepatic; RNA sequencing; *AFP*; *ENPEP*; *PPP1R1B*

1. Introduction

Nonalcoholic fatty liver disease (NAFLD), characterized by an imbalance between hepatic lipid output and input resulting in lipid droplet deposition [1], is the most common chronic liver metabolic disorder, with an estimated prevalence range of 6–35%

Results

worldwide and 25–26% in Europe [2]. Between 15% and 20% [3] or 15.9% and 68.3% [4] of NAFLD patients progress to nonalcoholic steatohepatitis (NASH). NASH, an inflammatory disease, is characterized by a combination of three histological features: fat accumulation or steatosis, ballooning of hepatocytes, and lobular inflammation, with or without fibrosis [5,6]. Approximately 20% of patients with chronic NASH develop cirrhosis [7] and about 85% of cirrhosis patients evolve to hepatocellular carcinoma (HCC) [8], leading to 12 times more HCC than in NAFLD [9]. In this metabolic disorder, hepatic gene transcriptome changes have been found to be involved [10,11].

Since the 1960s, the Mediterranean diet has been recognized as a healthy choice against major chronic degenerative diseases [12,13]. Virgin olive oil (VOO) is the main fat component in this diet [14]. VOO is not only composed of triglycerides containing monounsaturated fatty acids, but also of minor bioactive phytochemicals that have important health benefits [15]. The terpene squalene is one of the most abundant minor components present in a wide range (2.4 to 9.3 g/kg of VOO) depending on cultivar, climate, and ripeness of olive fruit [16]. This hydrocarbon is a precursor in the cholesterol biosynthesis [17], and its administration has been shown to exert anti-neoplastic, anti-inflammatory, and antioxidant properties, and to control glucose and lipid metabolisms [18,19].

Squalene received its name because it was first discovered in the livers of sharks [20]. Some species belonging to the family *Squalidae* can accumulate this compound in their livers up to 50–82% of their liver weight [21]. The lifespan of these sharks is currently unknown. Other sharks, such as *Somniosus microcephalus*, are known for having one of the longest lifespans among vertebrates (392 ± 120 years) [22]. However, the amount of squalene in their livers has not been measured [23]. In this way, the impact of squalene on hepatic content and lifespan remains uncertain. Thus, the effect of squalene on NASH pathogenesis also requires further investigation. Kritchevsky et al. [24] were the first to prove that dietary squalene accumulated in the rabbit liver. Recent studies, utilizing mouse and rabbit models, have shown distinct subcellular accumulation depending on the experimental model [25]. The first model accumulated squalene in large lipid droplets and smooth reticulum fractions, whereas the second did so in small-size vesicles and the rough endoplasmic reticulum. Furthermore, squalene modulated

Results

hepatic lipids, particularly triglycerides and cholesterol, with different outcomes in both models. In mice, hepatic triglyceride content was reduced, whereas this effect was not observed in rabbits [19,26]. Squalene administration induced important changes in hepatic proteins involved in lipid metabolism, oxidative stress, and lipoprotein secretion, which could explain the observed reduction in hepatic triglycerides in mice [27]. The accumulation of squalene in the liver of mice was associated with complex transcriptional and post-translational changes in gene expressions, including of *Mat1*, *Acox1*, *Casp1*, *Cyp2b10*, *Cyp2c55*, *Cpt1a*, and *Txndc5* [27–29]. In contrast, the hepatic changes in rabbit involved *PNPLA3*, *GCK*, *TFCP2L1*, *ASCL1*, *ACSS2*, *OST4*, *FAM91A1*, *MYH6*, *LRRC39*, *LOC108176846*, *GLT1D1*, and *TREH* [30]. These discrepant findings in animal models need further confirmation in different models and might indicate varied metabolic responses in humans. In this regard, the swine model represents an interesting approach due to its metabolic and physiological similarities to humans [31]. Our group has recently developed a model of porcine NASH using a dietary manipulation [32], and squalene has been shown to improve steatosis in this model despite an increase in the ballooning score. Furthermore, there were no changes in inflammation or fibrosis [33]. This experimental design provides an interesting approach to discover specific gene expression changes involved in controlling ballooning and steatosis. The current study was designed to identify the responsible molecular candidates through high-throughput RNA sequencing.

2. Results

2.1. Hepatic Histological Analyses

Pigs receiving both diets developed hepatic steatosis, as depicted in Figure 1A, B. The pigs receiving the squalene diet showed significantly decreased lipid droplet areas (Figure 1C). Likewise, the animals receiving squalene displayed a higher number of ballooned hepatocytes than the control group (Figures 1D and 1E respectively), with all animals reaching a value of 2 (Figure 1F). No significant changes were observed in fibrosis (Figure 1G–I) or in the presence of inflammatory foci by squalene administration (Figures 1J–L). When the latter parameter was considered together with ballooning as the activity index [5], the group of animals receiving squalene showed a significant increase (Figure 1M) due to the increase in the ballooning score. According to the fatty liver inhibition of progression (FLIP) algorithm [5], all the animals exhibited NASH.

Results

When using a semi-quantification of steatosis, activity, and fibrosis as the SAF score [5], the pigs consuming squalene showed a significantly increased SAF score (Figure 1N).

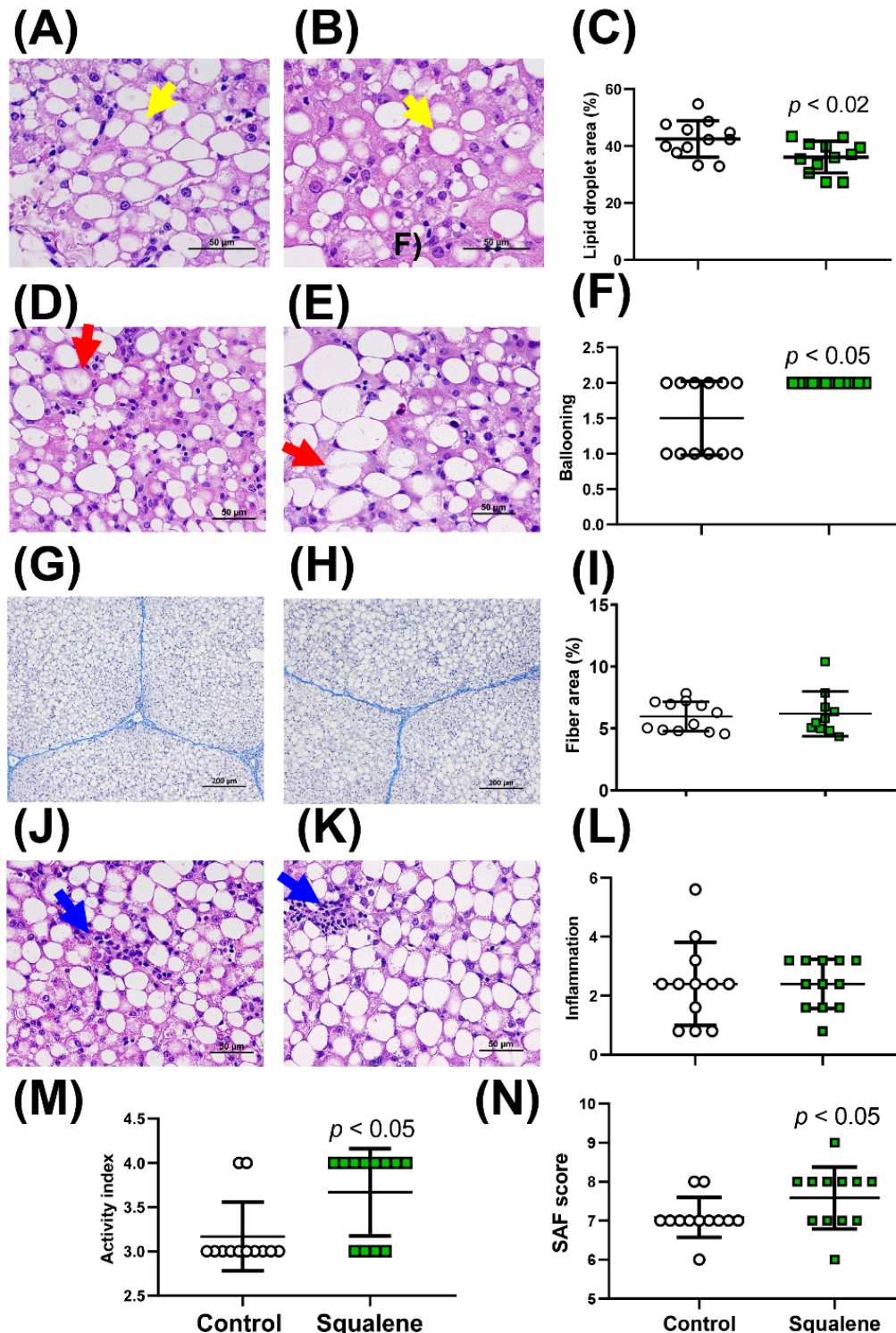


Figure 1. Histological analyses of male swine livers fed different diets. Representative hepatic micrographs of hematoxylin-eosin-stained sections (4 μ m) from control (A) and squalene (B) groups. Bar denotes 50 μ m. Morphometric changes in lipid droplet area expressed as percentage of total liver section (C). Selected fields displaying ballooned hepatocytes from control (D) and squalene (E) groups and quantification of ballooning (F). Bar denotes 50 μ m. Representative liver micrographs of Masson's trichrome-stained slides from control (G) and squalene groups (H). The

Results

scale bar represents 200 μm . Changes in fiber area (I) were assessed morphometrically and are expressed as a percentage of total liver section. Selected fields displaying inflammatory foci in control (J) and squalene (K) groups and quantification in all animals (L). Bar denotes 50 μm . The activity index (ballooning and inflammation) (M). The SAF score (steatosis grading, ballooning, inflammation, and fibrosis) (N). Lipid droplets, ballooned hepatocytes, and inflammatory foci are represented by yellow, red, and blue arrows, respectively. Data are individual results and their means and standard deviations of 12 pigs per group. Statistical analyses were performed according to the one-tailed Mann–Whitney U-test.

2.2. Hepatic Gene Expression

To investigate the effect of squalene intake on the hepatic transcriptome of pigs with NASH, total RNA was extracted from twelve animals receiving the squalene-enriched steatotic diet and the other twelve receiving the steatotic diet. Four pools made up of three samples for each condition were prepared and analyzed by next generation sequencing using the DNBseq platform. Clean reads (on average 45.8×10^6) were obtained from each library with a coverage of 91.60%. The resultant average mapping ratio with the reference genome (*Sus scrofa*11.1 (GCA_000003025.6)) was 93.51%. On average, 4.33 Gb bases per sample were generated and mapping results for each pool indicated that samples were uniform. A total of 20,430 genes were identified, out of which 20,331 were known and 104 were not previously characterized.

The analysis of transitions showed that A-G were $35,438.5 \pm 1884.6$ vs. $33,354 \pm 1187.5$, and C-T were $35,351.8 \pm 1844.2$ vs. $33,152.3 \pm 1089.4$ for the control and squalene groups, respectively. Regarding the transversions analyzed, the A-C transversions were 6252 ± 318.6 for the control group and 5886.5 ± 274.0 for the squalene group; A-T transversions were 4462.3 ± 249.5 for the control group and 4111.8 ± 154.7 for the squalene group; C-G transversions were 6728.8 ± 384.0 for the control group and 6297.3 ± 208.2 for the squalene group; and, finally, G-T transversions were 6272.5 ± 312.0 for the control group and 5884.3 ± 260.2 for the squalene group. In quantitative terms, the number of SNPs did not show a significant difference between both groups, thus suggesting that the level of these changes was not influenced by squalene administration.

Alternative splicing (AS) analyses evidenced five events were significantly modified, namely, 5' splicing (A5SS), 3' splicing site (A3SS), retained introns (RI), skipped exons (SE), and mutually exclusive exons (MXE) (data are not shown). Splicing patterns led to differential splicing of genes (DSGs), resulting in a variety of different

Results

isoforms from the same gene. Using reference genome annotation, a total of 10,973 novel transcripts were identified. Of these, 9866 represented previously unknown splicing events for known genes, 104 were novel coding transcripts without any known features, and the remaining 1003 were long noncoding RNA. Considering gene expression levels, the control group expressed 18,602 genes compared to 18,659 in the squalene group. There were 100 up-regulated and 40 down-regulated differentially expressed genes (DEGs) in control versus squalene groups (Figure 2A). The gene ontology (GO) classifications of DEGs/up- and down-regulated genes corresponding to biological and cellular processes are displayed in Figures 2B and 2C, respectively. According to the biological classification of GO, the main changes in expression corresponded to 116 genes involved in the cellular process, biological regulation, and its control (Supplementary Table S1). Based on the GO cellular classification, the main changes in expression corresponded to 95 genes involved in cellular anatomical entity, intracellular, and protein-containing complex (Supplementary Table S2). Pathway enrichment of DEGs analyzed according to the Kyoto encyclopedia of genes and genomes (KEGG) (Figure 2D and Supplementary Table S3) showed the main categories corresponding to genes involved in viral and anti-inflammatory responses. The volcano plot of statistical significance against log₂-fold change between the tested groups is displayed in Figure 2C. Using stringent conditions of signal log₂ ratio (SL₂R) above 1.5 or less than -1.5 with a false discovery rate (FDR) of $p < 0.001$, sixteen transcripts were up-regulated, namely, *PPP1R1B*, *OASL*, *PPP4R4*, *HES4*, *NEURL3*, *HTD2*, *CYP2C32*, *TMEM45B*, *AFP*, *ENPEP*, *LOC110256649*, *CYP2J34*, *LOC100526118*, *S100A2*, *SPRY3*, and *FOXG1*, and three were down-regulated, namely, *GTSF1*, *SQLE*, and *CHL1* (Table 1). The biological function of some of these genes could be classified in categories such as metabolism of lipids and xenobiotics, transmembrane transporters, and anti-inflammatory responses.

Results

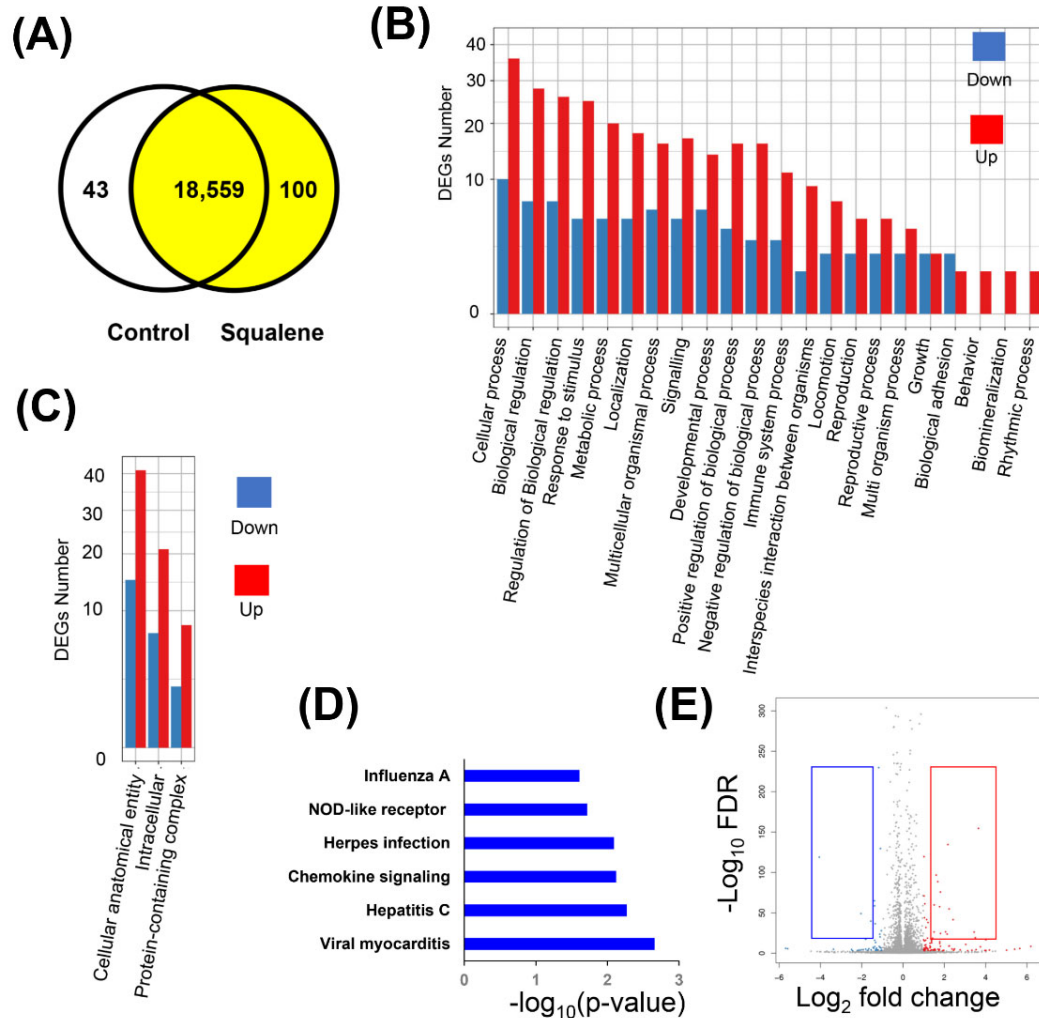


Figure 2. DEGs by the administration of squalene according to RNAseq of livers from a porcine model of dietary NASH development. **(A)** Venn diagram analysis showing the transcripts expressed in control and squalene groups on the steatotic diet with a fold change > 2 and false discovery rate $\text{FDR} < 0.001$. **(B)** Gene ontology (GO) classification of biological processes of up-regulated and down-regulated genes following squalene administration. The x -axis illustrates the GO term. The y -axis represents the number of up-/down-regulated genes. DEGs, differentially expressed genes. **(C)** GO classification of cellular processes of up-regulated and down-regulated genes by squalene administration. **(D)** Pathway enrichment of DEGs expressed as the $\log [-P]$ analyzed by KEGG. **(E)** Volcano plot representing DEGs. Each condition was performed on four pools, each pool consisting of three pig livers. Red and blue squares represent the selected genes shown in Table 1.

Results

Supplementary Table S1. Genes comprised in the main categories displayed in Figure 2B of gene ontology classification of biological processes of up- and down-regulated genes.

GO term	Regulation	Number of annotated genes	Gene symbols
Cellular process	Up	36	<i>AFP, ANO3, BORCS6, CBLC, CCL20, CDK1, CDK3, CLDN6, CXCL10, CXCL8, ENPEP, FOXG1, HTRA3, IFIT2, IFIT3, INHBB, ISG15, KCTD14, LIF, LOC100157935, LOC100516302, LOC110255217, MLC1, PKP3, PLP1, PLPPR2, PPP1R1B, RGS5, RSAD2, SDCBP2, SEMA3A, SERPINB2, SLITRK5, SPRY3, SYCE1L, TMIGD3</i>
	Down	10	<i>APOD, CA3, CRABP1, DEFB1, KCNJ3, LOC100621701, NPSR1, PIWIL2, RASL10A, SYT17</i>
Biological regulation	Up	28	<i>AFP, ANO3, CBLC, CCL20, CDK1, CDK3, CXCL10, CXCL8, ENPEP, FOXG1, HTRA3, IFIT3, INHBB, ISG15, LIF, LOC100516302, LOC110255217, MLC1, PKP3, PLP1, PLPPR2, RGS5, RSAD2, SEMA3A, SERPINB2, SLITRK5, SPRY3, TMIGD3</i>
	Down	7	<i>APOD, CRABP1, DEFB1, NPSR1, PIWIL2, RASL10A, SYT17</i>
Regulation of biological process	Up	26	<i>AFP, CBLC, CCL20, CDK1, CDK3, CXCL10, CXCL8, FOXG1, HTRA3, IFIT3, INHBB, ISG15, LIF, LOC100516302, LOC110255217, MLC1, PKP3, PLP1, PLPPR2, RGS5, RSAD2, SEMA3A, SERPINB2, SLITRK5, SPRY3, TMIGD3</i>
	Down	7	<i>APOD, CRABP1, DEFB1, NPSR1, PIWIL2, RASL10A, SYT17</i>
Response to stimulus	Up	25	<i>AFP, CBLC, CCL20, CDK1, CDK3, CXCL10, CXCL8, FOXG1, IFIT2, IFIT3, INHBB, ISG15, LIF, LOC100153139, LOC106504372, LOC110255217, MLC1, OASL, PLP1, PLPPR2, RGS5, RSAD2, SEMA3A, SLITRK5, SPRY3</i>
	Down	5	<i>APOD, CRABP1, DEFB1, LOC100525396, RASL10A</i>
Metabolic process	Up	20	<i>AFP, CBLC, CCL20, CDK1, CDK3, CXCL8, ENPEP, FOXG1, INHBB, ISG15, LIF, LOC100157935, LOC100516302, LOC100526118, MMP1, PKP3, PLP1, PLPPR2, RSAD2, TMIGD3</i>
	Down	5	<i>APOD, CA3, CRABP1, PIWIL2, SQLE</i>
Localization	Up	18	<i>AFP, ANO3, BORCS6, CCL20, CDK1, CXCL10, CXCL8, ENPEP, FOXG1, INHBB, LIF,</i>

Results

			<i>LOC100157935, MLC1, PKP3, RSAD2, SEMA3A, SYCE1L, TMIGD3</i>
	Down	5	<i>APOD, DEFB1, KCNJ3, NPSR1, SYT17</i>
Multicellular organismal process	Up	16	<i>AFP, CDK1, CDK3, CXCL10, CXCL8, ENPEP, FOXG1, GUCA1A, INHBB, ISG15, LIF, PLP1, RSAD2, SEMA3A, SLITRK5, SPRY3</i>
	Down	6	<i>APOD, CRABP1, DEFB1, LOC100621701, PIWIL2, SYT17</i>
Signaling	Up	17	<i>AFP, CBLC, CCL20, CDK3, CXCL10, CXCL8, INHBB, LIF, LOC110255217, PLP1, PLPPR2, PPP1R1B, RGS5, RSAD2, SEMA3A, SLITRK5, SPRY3</i>
	Down	5	<i>APOD, CRABP1, DEFB1, LOC100621701, RASL10A</i>
Developmental process	Up	14	<i>AFP, CDK1, CDK3, CXCL10, CXCL8, FOXG1, INHBB, ISG15, LIF, PLP1, RSAD2, SEMA3A, SLITRK5, SPRY3</i>
	Down	6	<i>APOD, CRABP1, DEFB1, LOC100621701, PIWIL2, SYT17</i>
Positive regulation of biological process	Up	16	<i>CCL20, CDK1, CDK3, CXCL10, CXCL8, FOXG1, INHBB, ISG15, LIF, LOC110255217, MLC1, PKP3, PLP1, RSAD2, SEMA3A, SLITRK5</i>
	Down	4	<i>DEFB1, NPSR1, PIWIL2, SYT17</i>
Negative regulation of biological process	Up	16	<i>CBLC, CDK1, CXCL10, CXCL8, FOXG1, IFIT3, INHBB, ISG15, LIF, LOC100516302, PKP3, RGS5, RSAD2, SEMA3A, SERPINB2, TMIGD3</i>
	Down	3	<i>APOD, NPSR1, PIWIL2,</i>
Immune system process	Up	11	<i>CCL20, CXCL10, CXCL8, IFIT3, ISG15, LIF, LOC100153139, LOC106504372, LOC110255217, OASL, RSAD2</i>
	Down	3	<i>APOD, DEFB1, LOC100525396</i>
Interspecies interaction among organisms	Up	9	<i>CCL20, CXCL10, CXCL8, IFIT3, ISG15, LOC110255217, OASL, RSAD2, SYCE1L</i>
	Down	1	<i>DEFB1</i>
Locomotion	Up	7	<i>CCL20, CXCL8, CXCL10, ENPEP, FOXG1, SEMA3A, TMIGD3</i>
	Down	2	<i>APOD, DEFB1</i>
Reproduction	Up	5	<i>AFP, CDK1, INHBB, LIF, SEMA3A</i>
	Down	2	<i>DEFB1, PIWIL2</i>
Reproductive process	Up	5	<i>AFP, CDK1, INHBB, LIF, SEMA3A</i>
	Down	2	<i>DEFB1, PIWIL2</i>
Multi-organism process	Up	4	<i>AFP, CDK1, INHBB, LIF</i>
	Down	2	<i>DEFB1, PIWIL2</i>
Growth	Up	2	<i>HTRA3, SEMA3A</i>
	Down	2	<i>APOD, SYT17</i>
Biological adhesion	Up	1	<i>CXCL8</i>

Results

	Down	2	<i>APOD, LOC100621701</i>
Behavior	Up	1	<i>SLITRK5</i>
	Down	-	-
Biomineralization	Up	1	<i>ISG15</i>
	Down	-	-
Rhythmic process	Up	1	<i>AFP</i>
	Down	-	-

Supplementary Table S2. Genes comprised in the main categories displayed in Figure 2C of gene ontology classification of cellular processes of genes.

GO term	Regulation	Number of annotated genes	Gene symbols
Cellular anatomical entity	Up	41	<i>AFP, ANO3, BORCS6, CBLC, CCL20, CDK1, CDK3, CLDN6, CXCL10, CXCL8, ENPEP, FOXG1, GUCA1A, HTRA3, IFIT3, INHBB, ISG15, LIF, LOC100153139, LOC100157935, LOC100516302, LOC106504372, LOC110255217, MLC1, MMP1, NRM, PI15, PKP3, PLP1, PLPPR2, RGS5, RSAD2, SDCBP2, SEMA3A, SERPINB2, SERPINB7, SLITRK5, SPRY3, SYCE1L, TMEM45B, TMIGD3</i>
	Down	15	<i>APOD, CA3, CPNE4, CRABP1, DEFB1, KCNJ3, LOC100525396, LOC100621701, NPSR1, PIWIL2, RASL10A, SHISA3, SQLE, SYT17, TECTB</i>
Intracellular	Up	21	<i>AFP, BORCS6, CBLC, CCL20, CDK1, CDK3, CXCL8, ENPEP, FOXG1, IFIT3, INHBB, LIF, LOC100157935, LOC110255217, MLC1, NRM, PKP3, RGS5, RSAD2, SDCBP2, SYCE1L</i>
	Down	7	<i>APOD, CA3, CRABP1, DEFB1, PIWIL2, SQLE, SYT17</i>
Protein-containing complex	Up	8	<i>BORCS6, CDK1, CDK3, LOC100153139, LOC100157935, LOC106504372, PKP3, SLITRK5</i>
	Down	3	<i>APOD, KCNJ3, PIWIL2</i>

Results

Supplementary Table S3. Genes comprised in the main categories displayed in Figure 2D according to Kyoto encyclopedia of genes and genomes (KEGG).

Pathways	Number of annotated genes	Differentially expressed genes
Viral myocarditis	5	<i>LOC110256649</i> , <i>LOC106504372</i> , <i>LOC100153139</i> , <i>LOC110258821</i> and <i>BGI_novel_G000045</i>
Hepatitis C	5	<i>IFIT1</i> , <i>IFIT3</i> , <i>IFIT2</i> , <i>CXCL8</i> and <i>CLDN6</i>
Chemokine signaling	6	<i>CXCL10</i> , <i>BGI_novel_G000048</i> , <i>LOC100525396</i> , <i>CCL20</i> , <i>CXCL8</i> and <i>LOC110255211</i>
Herpes infection	8	<i>IFIT1</i> , <i>IFIT3</i> , <i>IFIT2</i> , <i>LOC106504372</i> , <i>LOC100153139</i> , <i>CDK1</i> , <i>MAP3K7CL</i> and <i>SHISA3</i>
NOD-like receptor	5	<i>GVIN1</i> , <i>BGI_novel_G000048</i> , <i>LOC100525396</i> , <i>CXCL8</i> and <i>MAP3K7CL</i>
Influenza A	5	<i>CXCL10</i> , <i>RSAD2</i> , <i>LOC106504372</i> , <i>LOC100153139</i> and <i>CXCL8</i>

Table 1. The most striking hepatic transcripts regulated by 0.5% squalene in male pigs consuming the steatotic diet according to RNAseq.

Function	Gene ID	Name	Symbol	Control (FPKM)	Squalene (FPKM)	Log ₂ Fold Change Squalene/Control
Up-regulated						
Signal transduction	100736966	Protein phosphatase 1 regulatory inhibitor subunit 1B	<i>PPP1R1B</i>	63	785	3.7
Signal transduction	595119	2'-5'-oligoadenylate synthase-like protein	<i>OASL</i>	441	3611	3.0
Signal transduction	100737576	Protein phosphatase 4 regulatory subunit 4	<i>PPP4R4</i>	59	314	2.4
Transcription factor	100739264	Hes family bHLH transcription factor 4	<i>HES4</i>	569	2853	2.3

Results

Protein ubiquitination	10052479 7	Neuralized E3 ubiquitin protein ligase 3	<i>NEURL3</i>	98	456	2.2
Fatty acid biosynthesis	10051557 9	Hydroxyacyl-thioester dehydratase type 2, mitochondrial	<i>LOC100515579</i> (<i>HTD2</i>)	259	1155	2.2
Metabolism of xenobiotics	403106	Cytochrome P450, 2C32	<i>CYP2C32</i>	2165	8633	2.0
Membrane protein	10051699 1	Transmembrane protein 45B	<i>TMEM45B</i>	237	825	1.8
Fatty acid transport	397586	Alpha-fetoprotein	<i>AFP</i>	77	268	1.8
Peptide hormone metabolism	397080	Glutamyl aminopeptidase	<i>ENPEP</i>	191	647	1.8
Endogenous retrovirus C	11025664 9	Porcine endogenous retrovirus C gag protein	<i>LOC110256649</i>	337	1071	1.7
Metabolism of xenobiotics	10052475 0	Cytochrome P450, 2J34	<i>CYP2J34</i>	414	1249	1.6
Metabolism of xenobiotics	10052611 8	Glutathione S-transferase A1-like	<i>LOC100526118</i>	5125	15029	1.6
Cell cycle progression	10015272 9	S100 calcium binding protein A2	<i>S100A2</i>	1817	5171	1.5
ERK signaling	10051552 1	Sprouty RTK signaling antagonist 3	<i>SPRY3</i>	301	848	1.5
Transcription factor	11026157 9	Forkhead box G1	<i>FOXP1</i>	134	376	1.5
Down-regulated						
Control of transcription	10052149 5	Gametocyte specific factor 1	<i>GTSF1</i>	543	182	-1.6
Sterol biosynthesis	10011340 9	Squalene monooxygenase	<i>SQLE</i>	464	112	-2.0
Signal transduction	10051178 0	Cell adhesion molecule L1 like	<i>CHL1</i>	570	34	-4.1

Data are fragments per kilo base per million mapped (FPKM) reads. Only genes with SL₂R higher than 1.5 or lower than -1.5, FDR < 0.0001, and counts in more than 75% of samples have been taken into consideration. Annotations were carried out using https://www.ensembl.org/Pig/Search/Results?q=;site=ensembl;facet_species=Pig (accessed on 30 May 2023), <https://www.rnaatlas.org/> (accessed on 30 May 2023), and <https://blast.ncbi.nlm.nih.gov/Blast.cgi> (accessed on 30 May 2023) against Sus scrofa 11.1 reference annotation release 106 biological function obtained from <https://www.genecards.org/> (accessed on 30 May 2023) and <https://www.uniprot.org/uniprot/> (accessed on 30 May 2023).

To confirm sequencing results, all transcripts were individually tested by their corresponding reverse transcriptase quantitative PCR (RT-qPCR) assays (Table 2).

Results

Table 2. Changes in selected hepatic gene expressions in response to 0.5% squalene in male pigs consuming the steatotic diet according to RT-qPCR assay

Gene Symbol	Control (n = 12)	Squalene (n = 12)	Fold Change	Signal log ₂ Ratio (SL ₂ R)
<i>PPP1R1B</i>	2.2 ± 3.1	9.0 ± 10.5 *	4.2	2.1
<i>OASL</i>	0.8 ± 0.7	2.5 ± 1.4 *	3.1	1.6
<i>PPP4R4</i>	1.1 ± 0.8	6.7 ± 13.2 *	6.1	2.6
<i>HES4</i>	1.3 ± 1.3	7.2 ± 20.2	5.4	2.4
<i>NEURL3</i>	1.8 ± 2.2	11.3 ± 23.6 *	6.2	2.6
<i>LOC100515579 (HTD2)</i>	1.1 ± 0.4	1.1 ± 0.8	1.0	0.05
<i>CYP2C32</i>	2.8 ± 4.7	15.2 ± 24.6	5.3	2.4
<i>TMEM45B</i>	2.5 ± 4.7	11.1 ± 15.8 *	4.4	2.1
<i>AFP</i>	1.3 ± 0.9	5.4 ± 8.5 **	4.1	2.0
<i>ENPEP</i>	1.3 ± 0.7	6.3 ± 9.7 **	4.9	2.3
<i>LOC110256649</i>	1.6 ± 1.7	3.7 ± 3.2 *	2.4	1.2
<i>CYP2J34</i>	2.0 ± 1.6	4.9 ± 9.6	2.5	1.3
<i>LOC100526118</i>	1.4 ± 1.6	3.5 ± 4.8 **	2.5	1.3
<i>S100A2</i>	1.9 ± 1.9	4.4 ± 7.0	2.3	1.2
<i>SPRY3</i>	1.2 ± 0.7	4.3 ± 5.2 *	3.5	1.8
<i>FOXG1</i>	1.9 ± 2.2	6.8 ± 11.7	3.7	1.9
<i>GTSF1</i>	4.0 ± 5.7	1.7 ± 1.7	0.4	-1.2
<i>SQLE</i>	5.1 ± 14.5	2.7 ± 1.9 *	0.5	-0.9
<i>CHL1</i>	6.5 ± 11.9	0.2 ± 0.2 *	0.03	-4.8

Results are expressed as means and standard deviations normalized to *UBA52*. Twelve samples per group. Statistical analysis was carried out according to the Mann–Whitney U-test; *, $p < 0.05$ and **, $p < 0.01$.

A correlation study between RNAseq and RT-qPCR methods using the log₂ fold change of both procedures resulted in an excellent agreement ($r = 0.90$, $p < 0.0001$) (Figure 3A). Furthermore, all samples were correctly classified (Figure 3B). In pigs receiving squalene (Table 2), twelve transcripts (*PPP1R1B*, *OASL*, *PPP4R4*, *NEURL3*, *TMEM45B*, *AFP*, *ENPEP*, *LOC110256649*, *LOC100526118*, *SPRY3*, *SQLE*, and *CHL1*) underwent significant expression changes.

Results

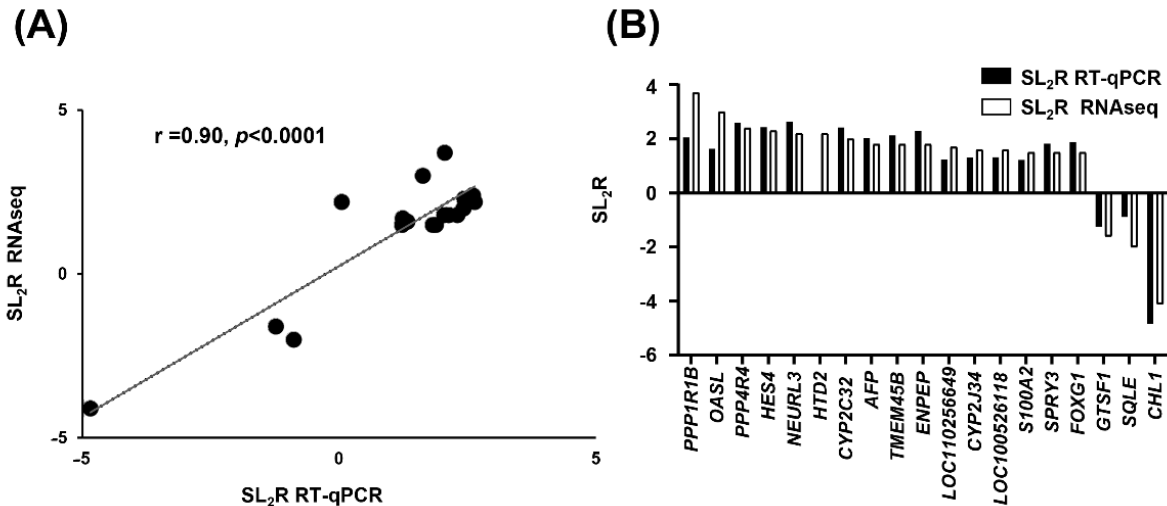


Figure 3. Concordance between used methods of RNA analysis. (A) Correlation analysis of 19 selected genes between RNAseq and RT-qPCR normalized to the constitutive *UBA52*. The mean values of SL_2R of selected genes from RT-qPCR individual analyses (Table 2) were plotted against SL_2R from RNAseq using pooled samples (Table 1). Twelve samples per group. Excellent agreement between assays was observed ($r = 0.90$, $p < 0.0001$). (B) Difference in expression of the 19 selected genes between both assays.

Network correlations obtained from RT-qPCR results revealed significant complex relationships among transcripts (Figure 4), particularly for *PPP1R1B*, *OASL*, *PPP4R4*, *NEURL3*, *TMEM45B*, *AFP*, *ENPEP*, and *SPRY3*.

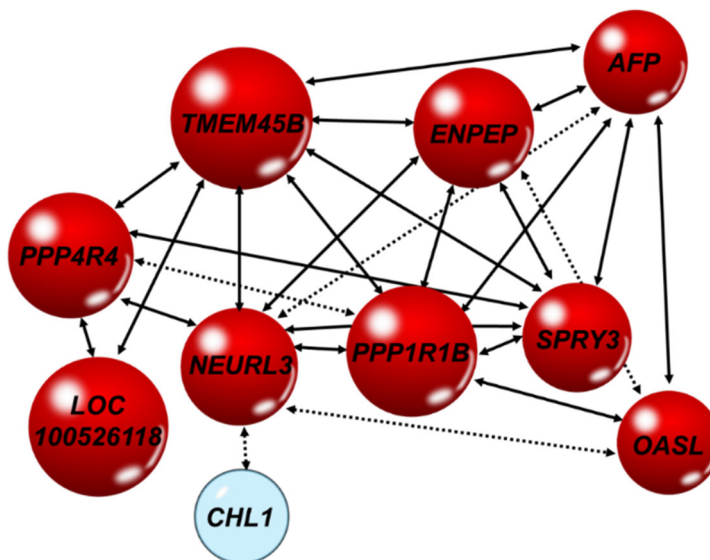


Figure 4. Network of hepatic transcripts in male swine consuming different diets. Significant bilateral Spearman's correlations of gene expressions analyzed by RT-qPCR. Red, up-regulation and blue, down-regulation. Solid line arrow, $p < 0.01$ and dotted arrow, $p < 0.02$.

2.3. Association among Gene Expression Changes and Pathological Features of NASH

Results

In order to explore the relevance of these gene changes in relation with the hallmarks of NASH, including lipid deposition, ballooning, and inflammation assessed as activity index, and steatosis, activity, and fibrosis as SAF score, correlation and receiver operating characteristic (ROC) curve analyses were carried out. Hepatic triglycerides were negatively associated ($\rho = -0.487$, $p < 0.025$) with *ENPEP* (Figure 5A) and lipid droplet areas were negatively associated ($\rho = -0.473$, $p < 0.026$) with *LOC100526118* expression (Figure 5D). Furthermore, changes in *ENPEP* and *LOC100526118* displayed higher discriminant power according to their area under the curve (AUC) values in their ROC curves compared to triglycerides (Figure 5B, C) and lipid droplet areas (Figure 5E, F). The activity index, reflecting the sum of ballooning and inflammation, was found to be positively associated with *AFP*, *NEURL3*, *OASL*, and *PP1R1B* and SAF score was positively associated with *NEURL3* (Figure 6A). Compared to the discriminant power indicated by their AUC values, either activity or SAF scores (Figure 6B, C) were surpassed by the values obtained for *PP1R1B* and *AFP* gene expression changes (Figure 6F, G).

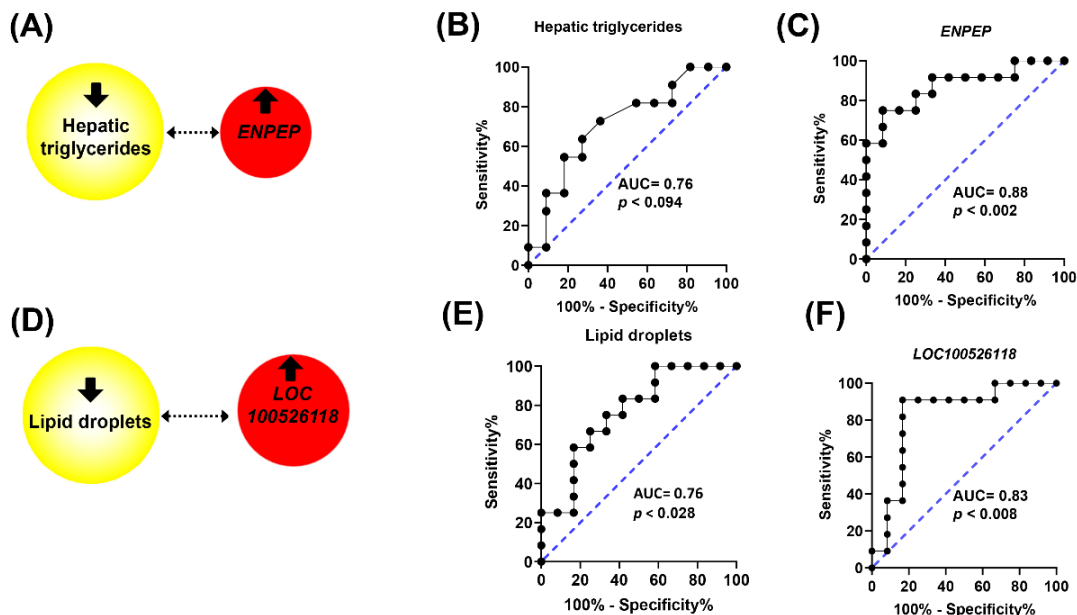


Figure 5. Association among hepatic triglycerides, lipid droplets, and gene expressions in response to squalene administration in pigs. Significant bilateral Spearman's correlations ($p < 0.02$). Red, up-regulation (A, D). ROC curves of hepatic triglycerides (B), *ENPEP* (C), lipid droplets (E), and *LOC100526118* (F).

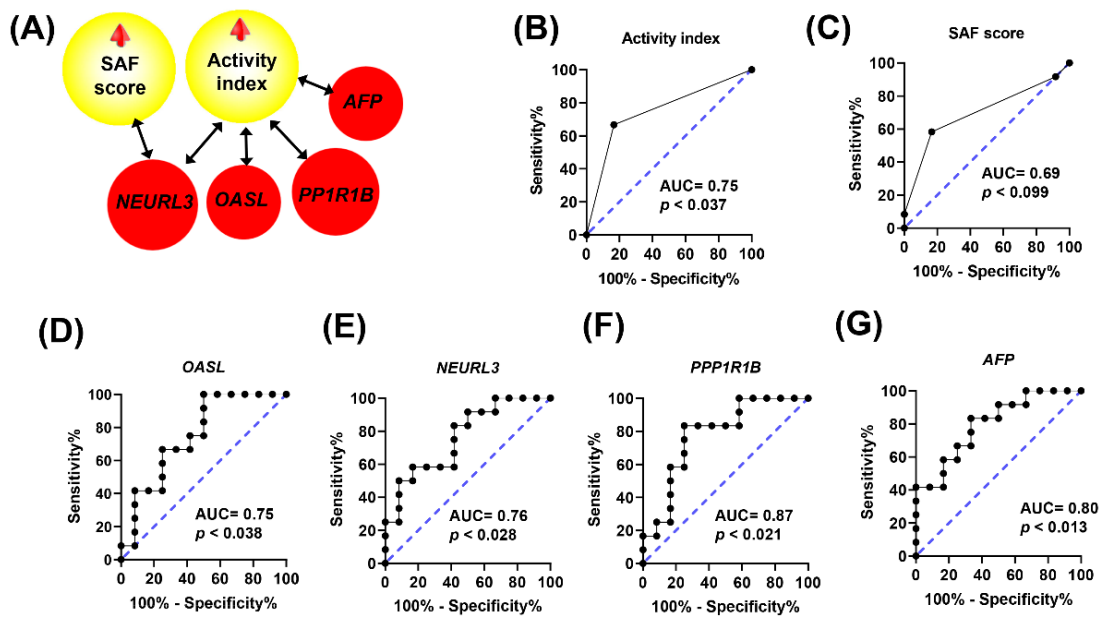


Figure 6. Histological findings and gene expressions in the livers of pigs receiving different diets. Association of NASH parameters with gene expressions (A). Significant Spearman’s correlations ($p < 0.02$) are shown. ROC curves of activity index (B), SAF score (C), hepatic expression of OASL (D), NEURL3 (E), PPP1R1B (F), and AFP (G).

2.4. Squalene Accumulates in the Liver and Is Responsible for the Changes in Gene Expressions

Pigs fed the squalene diet consumed, on average, more solid food than expected, resulting in a squalene intake per animal ranging from 135 to 240 mg/kg per day. The diet enriched with squalene led to a significant accumulation of this triterpene in swine livers (Figure 7A). The squalene content was found to be significantly associated with changes in *PPP1R1B*, *ENPEP*, *SPRY3*, *AFP*, and *TMEM45B* gene expressions, as shown in Figure 7B.

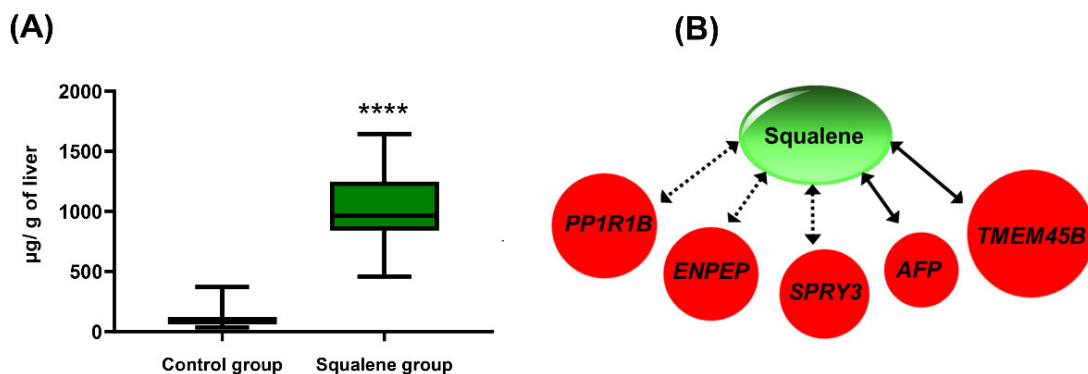


Figure 7. Squalene analyses in male swine consuming different diets. (A) Squalene content following dietary regimens. Data are means and 5–95 percentiles for each group of 12 pigs. Statistical analyses were performed according to the one-tail Mann–Whitney U-test. ****, $p < 0.0001$. (B) Correlations of hepatic squalene content with gene

Results

expression. Red; up-regulation. Significant Spearman's correlations. Solid line arrows, $p < 0.01$; dotted arrow, $p < 0.02$.

2.5. Squalene Is Responsible for the Changes in Genes Expression in Human Hepatoma G2 (HEPG2) and Murine Alpha Mouse Liver 12 (AML12) Cell Lines

To verify whether those changes and associations were a direct response of squalene, the human HEPG2 and the murine AML12 cell lines were incubated in the presence of 30 μM squalene for 72 h. This concentration carried in nanoparticles was particularly effective in controlling reactive oxygen stress in cell cultures [34]. Transcripts displaying significant correlation were assayed. Consistently, in the HEPG2 cell line, *PPP1R1B*, *TMEM45B*, *AFP*, *ENPEP*, and *SPRY3* matched the expression pattern observed in the livers of pigs consuming the squalene-enriched diet (Table 3). The same expression changes were observed in the AML12 cell line, except for *Spry3*, which showed the opposite expression pattern (Table 4).

Table 3. Changes in selected hepatic gene expressions in response to 30 μM squalene in HEPG2 cell line according to RT-qPCR assay.

Gene Symbol	Control (n = 6)	Squalene (n = 6)	Fold Change	Signal log ₂ Ratio
<i>PPP1R1B</i>	0.7 ± 0.2	0.9 ± 0.2 *	1.3	0.4
<i>TMEM45B</i>	1.0 ± 0.1	1.3 ± 0.1 **	1.3	0.4
<i>AFP</i>	0.8 ± 0.2	1.0 ± 0.1 *	1.2	0.2
<i>ENPEP</i>	0.8 ± 0.2	1.5 ± 0.3 *	1.9	0.9
<i>SPRY3</i>	0.8 ± 0.3	1.4 ± 0.3 *	1.8	0.8

Results are expressed as means and standard deviations normalized to *GAPDH*. Six replicates per group. Statistical analysis was carried out according to Mann–Whitney U-test. *, $p < 0.05$ and **, $p < 0.01$.

Table 4. Changes in selected hepatic gene expressions in response to 30 μM squalene in AML12 cell line according to RT-qPCR assay.

Gene Symbol	Control (n = 6)	Squalene (n = 6)	Fold Change	Signal log ₂ Ratio
<i>Ppp1r1b</i>	1.0 ± 0.1	1.5 ± 0.5 *	1.5	0.6
<i>Tmem45b</i>	1.0 ± 0.3	3.0 ± 1.7 *	3.0	1.6
<i>Afp</i>	1.0 ± 0.1	1.6 ± 0.8 *	1.6	0.7
<i>Enpep</i>	1.0 ± 0.1	1.4 ± 0.5 *	1.4	0.5
<i>Spry3</i>	1.2 ± 0.1	0.7 ± 0.1 *	0.7	-0.6

Results are expressed as means and standard deviations normalized to *Ppib*. Six replicates each group. Statistical analysis was carried out according to Mann–Whitney U-test; *, $p < 0.05$.

3. Discussion

The nutrigenomic approach aimed to characterize the hepatic transcriptomics of Large White x Landrace pigs developing a reproducible and reversible NASH following a steatotic diet and the changes induced by including 0.5% squalene in the diet. Pigs receiving the latter diet exhibited a noticeable squalene accumulation in their livers (Figure 7A) and significantly increased hepatic expressions of *PPP1R1B*, *OASL*, *PPP4R4*, *NEURL3*, *TMEM45B*, *AFP*, *ENPEP*, *LOC110256649*, *LOC100526118*, and *SPRY3*, as well as significantly decreased expressions of *CHL1* and *SQLE*. All of these transcripts were found to strongly interact in a complex hepatic network of gene expressions (Figure 4). These findings were accompanied by decreased hepatic triglycerides and lipid droplet areas, and an increased cellular ballooning, resulting in a higher NASH activity index and SAF score. However, there were no changes observed in inflammation or fibrosis. The DEGs were notably associated with some of these pathological parameters. In this sense, *ENPEP* was associated with hepatic triglyceride content; *LOC100526118* was associated with lipid droplet areas; *OASL*, *AFP*, *PPP1R1B*, and *NEURL3* were associated with activity index; and *NEURL3* was associated with activity and SAF score. Furthermore, *AFP*, *ENPEP*, and *PPP1R1B* ROC curves showed a great discriminant power according to their areas under the curves. Moreover, the squalene-dependent expression of *PPP1R1B*, *TMEM45B*, *AFP*, *ENPEP*, and *SPRY3* followed the same pattern in vitro using the human HEPG2 hepatic cell line incubated with squalene (Table 3). In murine AML12 cells, squalene induced the same expression profile for selected transcripts, except for *Spry3* (Table 4). These consistent findings suggest a direct effect of squalene on these hepatic transcripts, independent of the studied species. This represents a unique and uncharted territory of gene expression in liver pathology where ballooning is dissociated from steatosis.

The high-throughput RNA-sequencing technology provides raw data about DEGs in addition to polymorphisms, alternative splicing events, and low-expression and novel transcripts [35]. The squalene-modified DEGs were influenced by global alternative splicing events, including 5' and 3' sites, retained introns, skipped and mutually exclusive exons, with no change on single nucleotide polymorphisms. RNA pooling assay can be used as an effective tool to reduce the cost of large-scale assays. However,

Results

this may lead to random experimental errors in the forms of bias and loss of biological variability [35–37]. Therefore, this approach was confirmed by RT-qPCR using individual samples. Nineteen transcripts were analyzed using the stringent criteria of SL₂R more than 1.5 or less than –1.5 with a false discovery rate (FDR) of $p < 0.0001$. The robust linear association ($r = 0.90$, $p < 0.0001$) (Figure 3A) and the similitude of response (Figure 3B) verify the concordance between the two technologies and the high reliability of the results.

The steatotic diet used employs high amounts of saturated fat, cholesterol, cholate, and fructose, with low levels of methionine (1.1 g/kg) and choline (50 mg/kg), which are crucial for hepatic β -oxidation and the synthesis of very low-density lipoprotein (VLDL) [33,38]. In this way, the impairment of both metabolic pathways was critical to overcome the natural resistance of pig to develop fatty liver. Moreover, methionine-choline-deficient (MCD) diets lower glycogen stores and induce hepatic oxidative stress, apoptosis, and steatosis [38,39]. In the porcine model used in this study, the administration of the diet over a short period promoted NASH with an identical distribution of cellular ballooning grades 1 and 2, as determined by the steatosis activity fibrosis (SAF) score and FLIP algorithm [32]. The amount of squalene chosen was similar to that administered to rabbits, which induced changes in the hepatic transcriptome [30]. This amount would also represent an adapted metabolic rate of the 1% squalene-containing diets used in mice [29,40].

The porcine model has been used as a human alternative for studying NASH pathogenesis due to their high physiological, anatomical, metabolic, genetic, and liver size similarities [31,41]. The porcine expression map revealed global liver protein-coding and gene expression similarity for both species [42]. Squalene administration to the porcine model reproduced the accumulation seen in the liver of mice [29] and rabbits [25]. However, the latter models showed no change in hepatic triglyceride content despite a higher area of lipid droplets [25], in contrast to the results seen in male pigs. In the pig model, the squalene effect has been tested in animals with established non-alcoholic steatohepatitis. In cultured human hepatocytes, squalene modified the expression of lipid metabolism genes, leading to crucially lower triacylglycerols and cholesterol content, when cellular uptake of fatty acids was increased [43]. In other

Results

models, squalene has been found to influence a cluster of genes related to lipid content [29,30]. The difference in responses could be related to species-specific expression patterns or to experimental settings.

To address the meaning of these gene expressions, correlation analyses were conducted, revealing several pathological findings. In this regard, increased *ENPEP* expression was inversely related to the hepatic triglyceride level (Figure 5A). Controversial findings have been described regarding *ENPEP*. It codifies for a membrane glutamyl aminopeptidase whose hepatic levels increase with the progression of NAFLD and decrease upon treatment [44]. However, PPAR α modulators that are used as triglyceride-lowering agents induce hepatic expression of *ENPEP* [45,46] and *ENPEP* peptidase protects against hypertriglyceridemia [47]. Interestingly, *ENPEP* was associated with squalene levels and showed the same expression profile in hepatocytes, indicating a direct squalene effect. This was not the case of *LOC100526118*, which codifies for a glutathione S-transferase A1-like that is highly expressed in the liver. This is a highly polymorphic transcript that was activated in response to squalene and was associated with a reduced area of lipid droplets (Figure 5B), probably due to its triglyceride metabolic and antioxidant activities [48–50], in addition to detoxification properties due to conjugation of hydrophobic and electrophilic compounds with reduced glutathione (GSH). Decreased GSH has been linked to diminished lipid droplets [51]. *PPP4R4* over-expression was found to activate glucose metabolism [52], leading to lessen triglyceride content [53]. On the other hand, the squalene-reduced expression of *CHL1* impairs insulin secretion [54,55], thus activating the production of hepatic triglyceride-rich lipoproteins [56] and consequent NAFLD [57,58]. Considering the decreases in lipid droplet areas and triglyceride accumulation observed in squalene administration, these gene changes would be offset by the expression of other genes. These findings demonstrate the important involvement of all these genes in hepatic lipid metabolism and their intertwined network to achieve an effect in response to squalene administration.

The squalene accumulation was associated with the ballooning score and, in this way, with NASH activity and SAF score [33]. For this reason, the association of gene expressions with these indexes was examined. As shown in Figure 6, several genes,

Results

including *PPP1R1B*, *AFP*, *OASL*, and *NEURL3*, showed a significant association with those parameters. All these transcripts were noticeably interacting in a complex network, thus suggesting a functional association (Figure 4). *PPP1R1B* suppresses protein phosphatase 1 [59] and induces glycogenesis [60]. Glycogenesis in NAFLD patients is associated with higher ballooning score, despite the lower steatosis and fibrosis scores [61]. The same profile was observed in NASH liver in response to squalene. Furthermore, *AFP* is a fatty acid binding protein. Fatty acid composition triggers different responses to NAFLD and its synthesis is correlated with ballooning score [62]. In the liver, a lower stearic/palmitic fatty acid ratio and a higher palmitoleic/palmitic ratio increase ballooning and fibrosis scores [62], while the serum level of palmitoleic fatty acid is negatively correlated with NAFLD activity and ballooning scores [63]. Interestingly, in the squalene-NASH swine model, the plasma lipidomic showed a consistent decrease in palmitic fatty acid [33]. Moreover, *AFP* is essential in the SMADS signal transduction pathway against hepatic fibrosis, particularly for SMAD2 [64,65]. Both *PPP1R1B* and *AFP* showed the same expression profile *in vitro* in hepatocytes, indicating a direct squalene effect. Furthermore, *OASL* represses interferon type 1 activity [66], therefore reducing the polarization of macrophages, and consequently suppressing inflammation of NAFLD [67], reinforcing the anti-inflammatory role of intervention. Notably, *OASL* is positively regulated by PPAR α , which is inversely related to NAFLD activity score [68]. Finally, *NEURL3* enables ubiquitin protein ligase activity 3, which is involved in down-regulating NAFLD gene clusters [69,70], thus alleviating the progress of NAFLD. The combined induced expression of *PPP1R1B*, *AFP*, *OASL*, and *NEURL3* may play an important role in the development of this ailment. In fact, the obtained ROC curves suggest that *AFP* and *PPP1R1B* have a stronger discriminating value than classical indexes of NAFLD activity and SAF score. In humans, *PPP1R1B* and *AFP* are positively associated with ballooning score [60–62]. In this way, this model reproduces the human situation, but the expression of *ENPEP*, which lowers triglyceride levels [45–47], and that of *NEURL3* and *OASL*, which suppress inflammatory response [66,67], would create a unique setting of ballooning and no inflammatory or fibrotic changes, which merit further research.

Results

Previous studies showed that squalene exerts anti-neoplastic effects [30,71]. *PPP1R1B* is activated in colorectal liver metastasis [72]. *SPRY3* is a negative regulator of the RTK/Ras/MAPKS pathway. However, unlike *SPRY1*, *SPRY2*, and *SPRY4*, and despite its positive linkage with *SPRY1*, the expression level in HCC is not modified [73]. *TMEM45B* is a hub gene in hepatic differentiation [74] and is up-regulated in response to cirrhosis [75]. In addition, it has distinct neoplastic expression patterns, although none are of hepatic origin [76–79], so further studies are required to demonstrate the effect of *TMEM45B* on hepatic neoplasia. Both *SPRY3* and *TMEM45B* were induced by squalene administration (Table 2). On the other hand, *CHL1* is a modulator of the cell cycle through the p53 pathway, with frequent overexpression in liver cancers [80]. In this case, squalene administration decreased its expression, a phenomenon that seems to be independent of the previous expression since they were not connected in the proposed gene network (Figure 4). Therefore, the phenotype could be a balance of expression among these genes, which could play a role in the progression of NASH to cirrhosis and cancer.

In conclusion, feeding male Large White x Landrace pigs a squalene-supplemented steatotic diet resulted in squalene accumulation in the liver and acted as a modulator of the hepatic transcriptome. Transcripts including *PPP1R1B*, *OASL*, *PPP4R4*, *NEURL3*, *AFP*, *TMEM45B*, *ENPEP*, *LOC110256649*, *LOC100526118*, *SPRY3*, *CHL1*, and *SQLE* experienced significant changes, and their expression was significantly associated, suggesting an interacting network. Concomitantly, these findings were accompanied by decreased hepatic levels of triglycerides and lipid droplets, whereas cellular ballooning score, NASH activity, and SAF score increased. The associations of gene expression with pathological features indicate that *LOC100526118* was associated with hepatic lipid droplet areas; *ENPEP* with hepatic triglycerides; *OASL*, *AFP*, and *PPP1R1B* with NASH activity; and *NEURL3* with NASH activity and SAF scores. Moreover, *AFP*, *ENPEP*, *LOC100526118*, and *PPP1R1B* showed a strong discriminant power compared to those pathological parameters. Several transcripts, namely, *PPP1R1B*, *TMEM45B*, *AFP*, and *ENPEP*, showed the same expression pattern in vitro in a human cell line, indicating a hepatic direct relationship between squalene and these gene expressions. Overall, these

findings indicate that squalene accumulates in the liver and is able to modulate gene expression changes that may influence the fate of NASH.

4. Materials and Methods

4.1. Animal Models and Experimental Design

The experimental animals were 24 male Large White x Landrace pigs generated by artificial insemination at Cooperativa Ganadera de Caspe (Zaragoza, Spain). After one month of acclimation in the facilities of Servicio General de Apoyo a la Investigación, División de Experimentación Animal, Facultad de Veterinaria, Universidad de Zaragoza, pigs, weighing 38 ± 2.8 kg, received a steatotic diet of high cholate, cholesterol, fructose, and saturated fat, and low methionine and choline content, for 1 month [32]. Then, they were liver biopsied and divided into two groups of equal hepatic triglyceride and cholesterol contents. The first group ($n = 12$) was fed with the steatotic diet and the second ($n = 12$) was fed with the same diet enriched with 0.5% squalene. Both groups received their diets for one additional month. Dietary consumption was monitored on a weekly basis. Taking into account the amount consumed and body weight, the dose was equivalent to 135 mg/kg dose of squalene per animal per day. Squalene was purchased from Molekula Group (Darlington, UK). Animals had ad libitum access to feed and water. Following the experimental period and after an overnight fast, all pigs were euthanized by an overdose of Propofol (B/Braun-Vetcare, Rubí, Barcelona, Spain) and biological specimens were collected. Experiments were carried out according to the European Union guidelines for laboratory animals (Directive 2010/63/UE) and in compliance with ARRIVE guidelines. Study protocols were authorized by the Ethics Committee for Animal Research of the University of Zaragoza (PI43/15).

4.2. Liver Histological Analyses

A sample from each liver was stored in neutral formaldehyde and embedded in paraffin wax. Sections (4 μ m) were stained with hematoxylin-eosin or with Masson's trichrome staining and then images were captured using a Nikon microscope. Lipid droplet and fiber areas were quantified and expressed as percentage of total liver section with Adobe Photoshop CS3 (Adobe Inc., San Jose, CA, USA). Liver sections were blindly assessed by a single qualified pathologist. The fatty liver inhibition of progression (FLIP) algorithm and SAF score were used to categorize the histological stages of NASH [5]. Briefly, steatosis was based on the percentage of hepatocytes that contained large and

Results

medium lipid droplets, but no microvesicles, using a scale of 0 to 3 (0: <5%; 1: 5–33%, 2: 34–66% and 3: >67%). Ballooning was graded on a scale from 0 to 2 (0: normal hepatocytes; 1: groups of rounded hepatocytes with pale cytoplasm and the size similar to that of normal hepatocytes; and 2: as for grade 1, but where there was at least one enlarged ballooned hepatocyte (2-fold size compared with that of normal cells within a cluster of grade 1 hepatocytes)). Inflammation was assessed by counting the number of inflammatory foci ((2 or more cells)/lobule) at 20× magnification. The inflammation was graded 0 for none, 1 for less than 2 foci per lobule, and 2 for at least 2 foci per lobule. The activity score was calculated by adding the grades of ballooning and lobular inflammation. Fibrosis was classified on a scale from 0 to 4 based on the location and number of fibers present. Grade 0 indicated no fibrosis present, grade 1 indicated the presence of fibrosis limited to the perisinusoidal or periportal regions, grade 2 indicated the presence of perisinusoidal and periportal fibrosis without flanges, grade 3 indicated the presence of flanged fibrosis, and grade 4 indicated the presence of cirrhosis. The steatosis activity fibrosis (SAF) score was calculated by adding together the scores for steatosis, activity, and fibrosis.

4.3. Quantification of Hepatic Lipids and Squalene

Hepatic cholesterol and triglyceride extraction and analyses were carried out as previously described [32]. Squalene was extracted and quantified by solid phase extraction, gas chromatography, and mass spectrometry (GC-MS), as mentioned [25].

4.4. RNA Extraction

Total liver RNA was extracted using the Quick-RNA MiniPrep kit (Cat. No: R1055, ZYMO Research, Irvine, CA, USA), following the manufacturer's instructions. Both RNA quantity and purity were assessed using a Nanodrop1000 Spectrophotometer (Thermo Scientific, Waltham, MA, USA). RNA was quantified by measuring the absorbance at 260 nm. Purity was determined by analysis of the absorbance at A260/A280. The ratio was ~2. The integrity for both 28S and 18S ribosomal RNAs was verified by agarose gel electrophoresis with the 28S/18S ratio being greater than 2. The quality of RNAseq samples (RQI > 9) was checked using Bio-Rad Lab Chip technology (Hercules, CA, USA).

4.5. RNAseq and Data Analyses

Results

For both animal groups, four pools of three animals each were prepared using equal amounts of hepatic total RNA. RNA quantity and quality were tested by RIN value, 28S/18S, and fragment length distribution using an Agilent 2100 Bio analyzer (Agilent RNA 6000 Nano Kit, Santa Clara, CA, USA). Library construction and sequencing were carried out at the BGI service (Shenzhen, China) as previously described [81]. Sequencing reads containing low-quality, adaptor-polluted, and unknown base reads were filtered to obtain clean reads. These reads were mapped onto the reference genome (Sscrofa11.1 (GCA_000003025.6)) using HISAT2. The detailed bioinformatics workflow was previously described [32]. The complete database was deposited in the GEO database with the accession number GSE214732.

4.6. Reverse Transcriptase-Quantitative PCR (RT-qPCR)

RNAseq transcripts displaying a signal \log_2 ratio > 1.5 or < -1.5 and FDRs lower than 0.001 were selected for confirmation in individual samples by RT-qPCR. Primers were designed using NCBI and then checked for gene specificity and full variant coverage by BLAST (NCBI), KEGG and Ensemble Genome Browser. The primers are shown in the Materials and Methods. Equal amounts (500 ng) of DNA-free RNA were used to synthesize complementary DNA (cDNA) using PrimeScript RT Reagent Kit (Cat. No: RR037A, Takara, Kutsatsu, Shiga, Japan) following the manufacturer's instructions. Primer concentrations and cDNA input were optimized to obtain efficiencies between 95 and 105%. Quantitative real-time analysis was carried out using SYBR Green dye master mix (Applied Biosystems, Foster city, CA, USA) according to the manufacturer's instructions, utilizing a ViiA7 Real-TIME PCR System (Life Technologies, Carlsbad, CA, USA). Analysis of relative gene expression data was conducted using the $2^{-\Delta\Delta CT}$ method and normalized to the most stable reference genes: UBA52 for swine samples, *GAPDH* for the HEPG2 cell line, and *Ppib* for the AML12 cell line.

4.7. AML12 Cell Culture

The murine hepatic cell line was obtained from the ATCC collection (Manassas, VA, USA) and was grown in a humidified atmosphere of 5% CO₂ at 37 °C in DMEM with glucose (4.5 g/L) (Thermo Fisher Scientific Waltham, MA, USA), F12-Ham's medium with 1 mM l-glutamine (GE Healthcare Life Science, South Logan, UT, USA) enriched with 10% fetal bovine serum (Thermo Fisher Scientific Waltham, MA, USA), 1:500 insulin-transferrin-selenium (Corning, Bedford, MA, USA), 40 ng/mL dexamethasone

Results

(Sigma-Aldrich; Merck Millipore, Darmstadt, Germany), 1% non-essential amino acids (Thermo Fisher Scientific, Waltham, MA, USA), 100 U/mL penicillin; Thermo Fisher Scientific), 100 µg/mL streptomycin; Thermo Fisher Scientific, Waltham, MA, USA), and 2.5 µg/mL amphotericin B (Thermo Fisher Scientific, Waltham, MA, USA). When cells reached a confluence of 90–100%, the medium was removed and cells were washed twice with phosphate buffered saline followed by addition of medium free of fetal bovine serum and amphotericin B. Cells were then incubated for 72 h with 30 µM squalene (Sigma-Merck, Darmstadt, Germany), carried in 0.1% poly lactic-co-glycolic acid (PLGA) versus non-loaded PLGA nanoparticles as control [34]. Each condition was tested in triplicate in two experiments. Media were removed, and cells were washed twice with phosphate buffered saline and collected. Squalene effect was investigated at mRNA level for genes (*Ppp1r1b*, *Enpep*, *Afp*, *Tmem45b*, and *Spry3*), showing a significant association with hepatic squalene content in the swine model. The primers are shown in the Materials and Methods.

4.8. HEPG2 Cell Culture

The human hepatic cell line was obtained from the ATCC collection and was grown in a humidified atmosphere of 5% CO₂ at 37 °C in DMEM (4.5 g/L) (Thermo Fisher Scientific Waltham, MA, USA) supplemented with 10% fetal bovine serum (Thermo Fisher Scientific, Waltham, MA, USA), 2% of 4 mM glutamine, 1% of 100 mM sodium pyruvate, 1% non-essential amino acids (Thermo Fisher Scientific, Waltham, MA, USA), 100 U/mL penicillin; Thermo Fisher Scientific), 100 µg/mL streptomycin; Thermo Fisher Scientific, Waltham, MA, USA), and 2.5 µg/mL amphotericin B (Thermo Fisher Scientific, Waltham, MA, USA). When cells reached 90–100% confluence, the medium was removed and cells were washed twice with phosphate buffered saline followed by addition of the medium free of fetal bovine serum and amphotericin B. Cells were then incubated for 72 h with 30 µM squalene (Sigma-Merck, Darmstadt, Germany), carried in 0.1% poly lactic-co-glycolic acid (PLGA) versus non-loaded PLGA nanoparticles as control [34]. Each condition was tested in triplicate. Media were removed, and cells were washed twice with phosphate buffered saline and collected. Squalene effect was investigated at mRNA level for genes (*PPP1R1B*, *ENPEP*, *AFP*, *TMEM45B*, and *SPRY3*). The primers are shown in the Materials and Methods.

4.9. Quality Control and Statistics

Results

Samples in quantitative real-time analysis were run in duplicate and their coefficient of variation was obtained. Duplicates showing a coefficient of variation greater than 3% were discarded and repeated. Statistical analyses were carried out with GraphPad Prism 8.0 for Windows (GraphPad Software, San Diego, CA, USA). Data were analyzed for normal distribution using the Shapiro–Wilk test and for homogeneity of variance using Bartlett’s F-test. In most cases, the outcome of these parameters failed, and results were analyzed by the nonparametric one-tailed Mann–Whitney U-test. $p < 0.05$ was considered significant. Receiver operating characteristic (ROC) curves were generated using GraphPad Prism 8.0 for quantitative values. This software also reports the area under the curve (AUC), which defines how well the measured parameter can differentiate between tested groups for each parameter. Correlations among all parameters were analyzed using two-tailed Spearman’s correlation coefficient according to the Statistical Package for Social Sciences version 25 (IBM, Armonk, NY, USA), and those with $p < 0.02$ were considered.

Supplementary Materials: The supporting information can be downloaded at: <https://www.mdpi.com/article/10.3390/ijms241612552/s1>.

Funding: This research was funded by the Ministerio de Ciencia e Innovación-Fondo Europeo de Desarrollo Regional (MCIN/AEI/10.13039/501100011033, PID2019-104915RB-I00 and PID2022--104915RB-I00) and Fondo Social Europeo-Gobierno de Aragón (B16_23R). CIBER de Fisiopatología de la Obesidad y Nutrición (CIBEROBN, CB06/03/1012) is an initiative of ISCIII.

Institutional Review Board Statement: The animal study protocol was approved by the Ethics Committee for Animal Research of the University of Zaragoza (PI43/15) on March 2015.

Informed Consent Statement: Not applicable

Data Availability Statement: RNAseq data are available at GEO database with the accession number GSE214732. The rest will be provided on a reasonable request.

Acknowledgments: The editing of the English version was performed using the DeepL Pro translator (DeepL SE, Cologne, Germany). We thank Cristina Barranquero and Tania Herrero-Continente for their help in maintaining the laboratory. We thank the University of Zaragoza Veterinary Hospital for assistance with anaesthesia support and the Servicio General de Apoyo a la Investigación, División de Experimentación Animal, Universidad de Zaragoza for help in pig care.

Conflicts of Interest: There is no conflict of interest.

References

1. Di Ciaula, A.; Passarella, S.; Shanmugam, H.; Noviello, M.; Bonfrate, L.; Wang, D.Q.-H.; Portincasa, P. Nonalcoholic fatty liver disease (NAFLD). Mitochondria as players and targets of therapies? *Int. J. Mol. Sci.* 2021, 22, 5375.
2. Bellentani, S. The epidemiology of non-alcoholic fatty liver disease. *Liver Int.* 2017, 37, 81–84.

Results

3. Williams, C.D.; Stengel, J.; Asike, M.I.; Torres, D.M.; Shaw, J.; Contreras, M.; Landt, C.L.; Harrison, S.A. Prevalence of nonalcoholic fatty liver disease and nonalcoholic steatohepatitis among a largely middle-aged population utilizing ultrasound and liver biopsy: A prospective study. *Gastroenterology* 2011, 140, 124–131.
4. Dufour, J.-F.; Scherer, R.; Balp, M.-M.; McKenna, S.J.; Janssens, N.; Lopez, P.; Pedrosa, M. The global epidemiology of nonalcoholic steatohepatitis (NASH) and associated risk factors—A targeted literature review. *Endocr. Metab. Sci.* 2021, 3, 100089.
5. Bedossa, P.; Consortium, t.F.P. Utility and appropriateness of the fatty liver inhibition of progression (FLIP) algorithm and steatosis, activity, and fibrosis (SAF) score in the evaluation of biopsies of nonalcoholic fatty liver disease. *Hepatology* 2014, 60, 565–575. <https://doi.org/10.1002/hep.27173>.
6. Chalasani, N.; Younossi, Z.; Lavine, J.E.; Charlton, M.; Cusi, K.; Rinella, M.; Harrison, S.A.; Brunt, E.M.; Sanyal, A.J. The diagnosis and management of nonalcoholic fatty liver disease: Practice guidance from the American Association for the Study of Liver Diseases. *Hepatology* 2018, 67, 328–357.
7. Stine, J.G.; Wentworth, B.J.; Zimmet, A.; Rinella, M.E.; Loomba, R.; Caldwell, S.H.; Argo, C.K. Systematic review with meta-analysis: Risk of hepatocellular carcinoma in non-alcoholic steatohepatitis without cirrhosis compared to other liver diseases. *Aliment. Pharmacol. Ther.* 2018, 48, 696–703.
8. Ioannou, G.N.; Splan, M.F.; Weiss, N.S.; McDonald, G.B.; Beretta, L.; Lee, S.P. Incidence and predictors of hepatocellular carcinoma in patients with cirrhosis. *Clin. Gastroenterol. Hepatol.* 2007, 5, 938–945. e934.
9. Younossi, Z.M.; Koenig, A.B.; Abdelatif, D.; Fazel, Y.; Henry, L.; Wymer, M. Global epidemiology of nonalcoholic fatty liver disease—Meta-analytic assessment of prevalence, incidence, and outcomes. *Hepatology* 2016, 64, 73–84. <https://doi.org/10.1002/hep.28431>.
10. Peng, C.; Stewart, A.G.; Woodman, O.L.; Ritchie, R.H.; Qin, C.X. Non-alcoholic steatohepatitis: A review of its mechanism, models and medical treatments. *Front. Pharmacol.* 2020, 11, 603926.
11. Hasin-Brumshtein, Y.; Sakaram, S.; Khatri, P.; He, Y.D.; Sweeney, T.E. A robust gene expression signature for NASH in liver expression data. *Sci. Rep.* 2022, 12, 2571.
12. Trichopoulou, A.; Costacou, T.; Bamia, C.; Trichopoulos, D. Adherence to a Mediterranean diet and survival in a Greek population. *N. Engl. J. Med.* 2003, 348, 2599–2608.
13. Keys, A. Seven countries. In *Seven Countries*; Harvard University Press: Cambridge, MA, USA, 2013.
14. Estruch, R.; Ros, E.; Salas-Salvado, J.; Covas, M.I.; Corella, D.; Aros, F.; Gomez-Gracia, E.; Ruiz-Gutierrez, V.; Fiol, M.; Lapetra, J.; et al. Primary Prevention of Cardiovascular Disease with a Mediterranean Diet Supplemented with Extra-Virgin Olive Oil or Nuts. *N. Engl. J. Med.* 2018, 378, e34. <https://doi.org/10.1056/NEJMoa1800389>.
15. Herrera-Marcos, L.V.; Lou-Bonafonte, J.M.; Arnal, C.; Navarro, M.A.; Osada, J. Transcriptomics and the Mediterranean Diet: A Systematic Review. *Nutrients* 2017, 9, 472. <https://doi.org/10.3390/nu9050472>.
16. Martinez-Beamonte, R.; Sanclemente, T.; Surra, J.C.; Osada, J. Could squalene be an added value to use olive by-products? *J. Sci. Food Agric.* 2020, 100, 915–925. <https://doi.org/10.1002/jsfa.10116>.

Results

17. Tomkins, G.; Dauben, W.; Sheppard, H.; Chaikoff, I. Squalene as a precursor of cholesterol in liver. *J. Biol. Chem.* 1953, 202, 487–489.
18. Lou-Bonafonte, J.M.; Martinez-Beamonte, R.; Sanclemente, T.; Surra, J.C.; Herrera-Marcos, L.V.; Sanchez-Marco, J.; Arnal, C.; Osada, J. Current Insights into the Biological Action of Squalene. *Mol. Nutr. Food Res.* 2018, 8, e1800136. <https://doi.org/10.1002/mnfr.201800136>.
19. Martinez-Beamonte, R.; Sanchez-Marco, J.; Felices, M.J.; Barranquero, C.; Gascon, S.; Arnal, C.; Burillo, J.C.; Lasheras, R.; Busto, R.; Lasuncion, M.A.; et al. Dietary squalene modifies plasma lipoproteins and hepatic cholesterol metabolism in rabbits. *Food Funct.* 2021, 12, 8141–8153. <https://doi.org/10.1039/d0fo01836h>.
20. Tsujimoto, M. A highly unsaturated hydrocarbon in shark liver oil. *J. Ind. Eng. Chem.* 1916, 8, 889–896.
21. Wetherbee, B.M.; Nichols, P.D. Lipid composition of the liver oil of deep-sea sharks from the Chatham Rise, New Zealand. *Comp. Biochem. Physiol. Part. B Biochem. Mol. Biol.* 2000, 125, 511–521.
22. Nielsen, J.; Hedeholm, R.B.; Heinemeier, J.; Bushnell, P.G.; Christiansen, J.S.; Olsen, J.; Ramsey, C.B.; Brill, R.W.; Simon, M.; Steffensen, K.F.; et al. Eye lens radiocarbon reveals centuries of longevity in the Greenland shark (*Somniosus microcephalus*). *Science* 2016, 353, 702–704. <https://doi.org/10.1126/science.aaf1703>.
23. MacNeil, M.A.; McMeans, B.C.; Hussey, N.E.; Vecsei, P.; Svavarsson, J.; Kovacs, K.M.; Lydersen, C.; Treble, M.A.; Skomal, G.B.; Ramsey, M.; et al. Biology of the Greenland shark *Somniosus microcephalus*. *J. Fish. Biol.* 2012, 80, 991–1018. <https://doi.org/10.1111/j.1095-8649.2012.03257.x>.
24. Kritchevsky, D.; Moyer, A.W.; Tesar, W.C.; Logan, J.B.; Brown, R.A.; Richmond, G. Squalene feeding in experimental atherosclerosis. *Circ. Res.* 1954, 2, 340–343.
25. Martinez-Beamonte, R.; Alda, O.; Sanclemente, T.; Felices, M.J.; Escusol, S.; Arnal, C.; Herrera-Marcos, L.V.; Gascon, S.; Surra, J.C.; Osada, J.; et al. Hepatic subcellular distribution of squalene changes according to the experimental setting. *J. Physiol. Biochem.* 2018, 74, 531–538. <https://doi.org/10.1007/s13105-018-0616-2>.
26. Guillen, N.; Acin, S.; Navarro, M.A.; Perona, J.S.; Arbones-Mainar, J.M.; Arnal, C.; Sarria, A.J.; Surra, J.C.; Carnicer, R.; Orman, I.; et al. Squalene in a sex-dependent manner modulates atherosclerotic lesion which correlates with hepatic fat content in apoE-knockout male mice. *Atherosclerosis* 2008, 197, 72–83. <https://doi.org/10.1016/j.atherosclerosis.2007.08.008>.
27. Ramirez-Torres, A.; Barcelo-Batlloiri, S.; Martinez-Beamonte, R.; Navarro, M.A.; Surra, J.C.; Arnal, C.; Guillen, N.; Acin, S.; Osada, J. Proteomics and gene expression analyses of squalene-supplemented mice identify microsomal thioredoxin domain-containing protein 5 changes associated with hepatic steatosis. *J. Proteom.* 2012, 77, 27–39. <https://doi.org/10.1016/j.jprot.2012.07.001>.
28. Ramirez-Torres, A.; Barcelo-Batlloiri, S.; Fernandez-Vizarra, E.; Navarro, M.A.; Arnal, C.; Guillen, N.; Acin, S.; Osada, J. Proteomics and gene expression analyses of mitochondria from squalene-treated apoE-deficient mice identify short-chain specific acyl-CoA dehydrogenase changes associated with fatty liver amelioration. *J. Proteom.* 2012, 75, 2563–2575. <https://doi.org/10.1016/j.jprot.2012.02.025>.
29. Gabas-Rivera, C.; Jurado-Ruiz, E.; Sanchez-Ortiz, A.; Romanos, E.; Martinez-Beamonte, R.; Navarro, M.A.; Surra, J.C.; Arnal, C.; Rodriguez-Yoldi, M.J.; Andres-Lacueva, C.; et al. Dietary Squalene Induces Cytochromes Cyp2b10 and Cyp2c55 Independently of Sex, Dose,

Results

- and Diet in Several Mouse Models. *Mol. Nutr. Food Res.* 2020, 64, e2000354. <https://doi.org/10.1002/mnfr.202000354>.
30. Abuobeid, R.; Sánchez-Marco, J.; Felices, M.J.; Arnal, C.; Burillo, J.C.; Lasheras, R.; Busto, R.; Lasunción, M.A.; Rodríguez-Yoldi, M.J.; Martínez-Beamonte, R. Squalene through Its Post-Squalene Metabolites Is a Modulator of Hepatic Transcriptome in Rabbits. *Int. J. Mol. Sci.* 2022, 23, 4172.
 31. Bassols, A.; Costa, C.; Eckersall, P.D.; Osada, J.; Sabria, J.; Tibau, J. The pig as an animal model for human pathologies: A proteomics perspective. *Proteom. Clin. Appl.* 2014, 8, 715–731. <https://doi.org/10.1002/prca.201300099>.
 32. Herrera-Marcos, L.V.; Martínez-Beamonte, R.; Macias-Herranz, M.; Arnal, C.; Barranquero, C.; Puente-Lanzarote, J.J.; Gascon, S.; Herrero-Continente, T.; Gonzalo-Romeo, G.; Alastrue-Vera, V.; et al. Hepatic galectin-3 is associated with lipid droplet area in non-alcoholic steatohepatitis in a new swine model. *Sci. Rep.* 2022, 12, 1024. <https://doi.org/10.1038/s41598-022-04971-z>.
 33. Herrera-Marcos, L.V.; Martínez-Beamonte, R.; Arnal, C.; Barranquero, C.; Puente-Lanzarote, J.J.; Herrero-Continente, T.; Lou-Bonafonte, J.M.; Gonzalo-Romeo, G.; Mocciaro, G.; Jenkins, B. Dietary squalene supplementation decreases triglyceride species and modifies phospholipid lipidomic profile in the liver of a porcine model of non-alcoholic steatohepatitis. *J. Nutr. Biochem.* 2023, 112, 109207.
 34. Bidooki, S.H.; Alejo, T.; Sánchez-Marco, J.; Martínez-Beamonte, R.; Abuobeid, R.; Burillo, J.C.; Lasheras, R.; Sebastian, V.; Rodríguez-Yoldi, M.J.; Arruebo, M. Squalene Loaded Nanoparticles Effectively Protect Hepatic AML12 Cell Lines against Oxidative and Endoplasmic Reticulum Stress in a TXNDC5-Dependent Way. *Antioxidants* 2022, 11, 581.
 35. Rajkumar, A.P.; Qvist, P.; Lazarus, R.; Lescai, F.; Ju, J.; Nyegaard, M.; Mors, O.; Børghlum, A.D.; Li, Q.; Christensen, J.H. Experimental validation of methods for differential gene expression analysis and sample pooling in RNA-seq. *BMC Genom.* 2015, 16, 548.
 36. Sham, P.; Bader, J.S.; Craig, I.; O'Donovan, M.; Owen, M. DNA pooling: A tool for large-scale association studies. *Nat. Rev. Genet.* 2002, 3, 862–871.
 37. Peng, X.; Wood, C.L.; Blalock, E.M.; Chen, K.C.; Landfield, P.W.; Stromberg, A.J. Statistical implications of pooling RNA samples for microarray experiments. *BMC Bioinform.* 2003, 4, 26.
 38. Takahashi, Y.; Fukusato, T. Animal models of liver diseases. In *Animal Models for the Study of Human Disease*; Elsevier: Amsterdam, The Netherlands, 2017; pp. 313–339.
 39. Muriel, P.; Ramos-Tovar, E.; Montes-Páez, G.; Buendía-Montaño, L. Experimental models of liver damage mediated by oxidative stress. In *Liver Pathophysiology*; Elsevier: Amsterdam, The Netherlands, 2017; pp. 529–546.
 40. Gabas-Rivera, C.; Barranquero, C.; Martínez-Beamonte, R.; Navarro, M.A.; Surra, J.C.; Osada, J. Dietary squalene increases high density lipoprotein-cholesterol and paraoxonase 1 and decreases oxidative stress in mice. *PLoS ONE* 2015, 9, e104224. <https://doi.org/10.1371/journal.pone.0104224>.
 41. Prather, R.S.; Lorson, M.; Ross, J.W.; Whyte, J.J.; Walters, E. Genetically engineered pig models for human diseases. *Annu. Rev. Anim. Biosci.* 2013, 1, 203.

Results

42. Karlsson, M.; Sjöstedt, E.; Oksvold, P.; Sivertsson, Å.; Huang, J.; Álvez, M.B.; Arif, M.; Li, X.; Lin, L.; Yu, J. Genome-wide annotation of protein-coding genes in pig. *BMC Biol.* 2022, 20, 25.
43. Hoang, T.M.H.; Nguyen, C.H.; Le, T.T.; Hoang, T.H.Q.; Ngo, T.H.T.; Hoang, T.L.A.; Dang, D.H. Squalene isolated from *Schizochytrium mangrovei* is a peroxisome proliferator-activated receptor- α agonist that regulates lipid metabolism in HepG2 cells. *Biotechnol. Lett.* 2016, 38, 1065–1071.
44. Niu, L.; Geyer, P.E.; Wewer Albrechtsen, N.J.; Gluud, L.L.; Santos, A.; Doll, S.; Treit, P.V.; Holst, J.J.; Knop, F.K.; Vilsbøll, T. Plasma proteome profiling discovers novel proteins associated with non-alcoholic fatty liver disease. *Mol. Syst. Biol.* 2019, 15, e8793.
45. Raza-Iqbal, S.; Tanaka, T.; Anai, M.; Inagaki, T.; Matsumura, Y.; Ikeda, K.; Taguchi, A.; Gonzalez, F.J.; Sakai, J.; Kodama, T. Transcriptome analysis of K-877 (a novel selective PPAR α modulator (SPPARM α))-regulated genes in primary human hepatocytes and the mouse liver. *J. Atheroscler. Thromb.* 2015, 22, 754–772.
46. Fruchart, J.-C. Pemafibrate (K-877), a novel selective peroxisome proliferator-activated receptor alpha modulator for management of atherogenic dyslipidaemia. *Cardiovasc. Diabetol.* 2017, 16, 124.
47. Florentin, M.; Kostapanos, M.S.; Anagnostis, P.; Liamis, G. Recent developments in pharmacotherapy for hypertriglyceridemia: what's the current state of the art? *Expert. Opin. Pharmacother.* 2020, 21, 107–120.
48. Rosenblat, M.; Volkova, N.; Aviram, M. Pomegranate juice (PJ) consumption antioxidative properties on mouse macrophages, but not PJ beneficial effects on macrophage cholesterol and triglyceride metabolism, are mediated via PJ-induced stimulation of macrophage PON2. *Atherosclerosis* 2010, 212, 86–92.
49. Cichoż-Lach, H.; Michalak, A. Oxidative stress as a crucial factor in liver diseases. *World J. Gastroenterol. WJG* 2014, 20, 8082.
50. Lee, J.; Homma, T.; Kurahashi, T.; Kang, E.S.; Fujii, J. Oxidative stress triggers lipid droplet accumulation in primary cultured hepatocytes by activating fatty acid synthesis. *Biochem. Biophys. Res. Commun.* 2015, 464, 229–235.
51. Malott, K.F.; Reshel, S.; Ortiz, L.; Luderer, U. Glutathione deficiency decreases lipid droplet stores and increases reactive oxygen species in mouse oocytes. *Biol. Reprod.* 2022, 106, 1218–1231.
52. Guzmán, T.J.; Vargas-Guerrero, B.; García-López, P.M.; Gurrola-Díaz, C.M. Analysis of hepatic transcriptome modulation exerted by γ -conglutin from lupins in a streptozotocin-induced diabetes model. *Gene* 2020, 761, 145036.
53. Parhofer, K.G. Interaction between glucose and lipid metabolism: More than diabetic dyslipidemia. *Diabetes Metab. J.* 2015, 39, 353–362.
54. Jiang, H.; Liu, Y.; Qian, Y.; Shen, Z.; He, Y.; Gao, R.; Shen, M.; Chen, S.; Fu, Q.; Yang, T. CHL1 promotes insulin secretion and negatively regulates the proliferation of pancreatic β cells. *Biochem. Biophys. Res. Commun.* 2020, 525, 1095–1102.
55. Taneera, J.; Dhaiban, S.; Hachim, M.; Mohammed, A.K.; Mukhopadhyay, D.; Bajbouj, K.; Hamoudi, R.; Salehi, A.; Hamad, M. Reduced expression of Chl1 gene impairs insulin secretion by down-regulating the expression of key molecules of β -cell function. *Exp. Clin. Endocrinol. Diabetes* 2021, 129, 864–872.

Results

56. Chirieac, D.V.; Chirieac, L.R.; Corsetti, J.P.; Cianci, J.; Sparks, C.E.; Sparks, J.D. Glucose-stimulated insulin secretion suppresses hepatic triglyceride-rich lipoprotein and apoB production. *Am. J. Physiol. -Endocrinol. Metab.* 2000, 279, E1003–E1011.
57. Adiels, M.; Taskinen, M.-R.; Borén, J. Fatty liver, insulin resistance, and dyslipidemia. *Curr. Diabetes Rep.* 2008, 8, 60–64.
58. Tricò, D.; Natali, A.; Mari, A.; Ferrannini, E.; Santoro, N.; Caprio, S. Triglyceride-rich very low-density lipoproteins (VLDL) are independently associated with insulin secretion in a multiethnic cohort of adolescents. *Diabetes Obes. Metab.* 2018, 20, 2905–2910.
59. Khan, A.; Molitor, A.; Mayeur, S.; Zhang, G.; Rinaldi, B.; Lannes, B.; Lhermitte, B.; Umair, M.; Arold, S.T.; Friant, S. A Homozygous Missense Variant in PPP1R1B/DARPP-32 Is Associated With Generalized Complex Dystonia. *Mov. Disord.* 2022, 37, 365–374.
60. Brady, M.J.; Saltiel, A.R. The role of protein phosphatase-1 in insulin action. *Recent. Prog. Horm. Res.* 2001, 56, 157–174.
61. Allende, D.S.; Gawrieh, S.; Cummings, O.W.; Belt, P.; Wilson, L.; Van Natta, M.; Behling, C.A.; Carpenter, D.; Gill, R.M.; Kleiner, D.E. Glycogenosis is common in nonalcoholic fatty liver disease and is independently associated with ballooning, but lower steatosis and lower fibrosis. *Liver Int.* 2021, 41, 996–1011.
62. Yamada, K.; Mizukoshi, E.; Sunagozaka, H.; Arai, K.; Yamashita, T.; Takeshita, Y.; Misu, H.; Takamura, T.; Kitamura, S.; Zen, Y. Characteristics of hepatic fatty acid compositions in patients with nonalcoholic steatohepatitis. *Liver Int.* 2015, 35, 582–590.
63. Yoo, W.; Gjuka, D.; Stevenson, H.L.; Song, X.; Shen, H.; Yoo, S.Y.; Wang, J.; Fallon, M.; Ioannou, G.N.; Harrison, S.A. Fatty acids in non-alcoholic steatohepatitis: Focus on pentadecanoic acid. *PLoS ONE* 2017, 12, e0189965.
64. Xu, F.; Liu, C.; Zhou, D.; Zhang, L. TGF- β /SMAD pathway and its regulation in hepatic fibrosis. *J. Histochem. Cytochem.* 2016, 64, 157–167.
65. Zhou, G.; Lin, W.; Fang, P.; Lin, X.; Zhuge, L.; Hu, Z.; Jin, L. MiR-10a improves hepatic fibrosis by regulating the TGF β 1/Smads signal transduction pathway. *Exp. Ther. Med.* 2016, 12, 1719–1722.
66. Arimoto, K.I.; Miyauchi, S.; Stoner, S.A.; Fan, J.B.; Zhang, D.E. Negative regulation of type I IFN signaling. *J. Leukoc. Biol.* 2018, 103, 1099–1116.
67. Zhang, C.; Liu, S.; Yang, M. The Role of Interferon Regulatory Factors in Non-Alcoholic Fatty Liver Disease and Non-Alcoholic Steatohepatitis. *Gastroenterol. Insights* 2022, 13, 148–161.
68. Kersten, S.; Stienstra, R. The role and regulation of the peroxisome proliferator activated receptor alpha in human liver. *Biochimie* 2017, 136, 75–84.
69. Xu, M.; Tan, J.; Dong, W.; Zou, B.; Teng, X.; Zhu, L.; Ge, C.; Dai, X.; Kuang, Q.; Zhong, S. The E3 ubiquitin-protein ligase Trim31 alleviates non-alcoholic fatty liver disease by targeting Rbdf2 in mouse hepatocytes. *Nat. Commun.* 2022, 13, 1052.
70. Gawrieh, S.; Baye, T.M.; Carless, M.; Wallace, J.; Komorowski, R.; Kleiner, D.E.; Andris, D.; Makladi, B.; Cole, R.; Charlton, M. Hepatic gene networks in morbidly obese patients with nonalcoholic fatty liver disease. *Obes. Surg.* 2010, 20, 1698–1709.
71. Smith, T.J. Squalene: Potential chemopreventive agent. *Expert. Opin. Investig. Drugs* 2000, 9, 1841–1848.

Results

72. van Huizen, N.A.; van den Braak, R.R.C.; Doukas, M.; Dekker, L.J.; IJzermans, J.N.; Luiders, T.M. Up-regulation of collagen proteins in colorectal liver metastasis compared with normal liver tissue. *J. Biol. Chem.* 2019, *294*, 281–289.
73. Sirivatanauksorn, Y.; Sirivatanauksorn, V.; Srisawat, C.; Khongmanee, A.; Tongkham, C. Differential expression of sprouty genes in hepatocellular carcinoma. *J. Surg. Oncol.* 2012, *105*, 273–276.
74. Ghosheh, N.; Küppers-Munther, B.; Asplund, A.; Edsbacke, J.; Ulfenborg, B.; Andersson, T.B.; Björquist, P.; Andersson, C.X.; Carén, H.; Simonsson, S. Comparative transcriptomics of hepatic differentiation of human pluripotent stem cells and adult human liver tissue. *Physiol. Genom.* 2017, *49*, 430–446.
75. Chan, K.-M.; Wu, T.-H.; Wu, T.-J.; Chou, H.-S.; Yu, M.-C.; Lee, W.-C. Bioinformatics microarray analysis and identification of gene expression profiles associated with cirrhotic liver. *Kaohsiung J. Med. Sci.* 2016, *32*, 165–176.
76. Hu, R.; Hu, F.; Xie, X.; Wang, L.; Li, G.; Qiao, T.; Wang, M.; Xiao, H. TMEM45B, up-regulated in human lung cancer, enhances tumorigenicity of lung cancer cells. *Tumor Biol.* 2016, *37*, 12181–12191.
77. Zhao, L.-c.; Shen, B.-y.; Deng, X.-x.; Chen, H.; Zhu, Z.-g.; Peng, C.-h. TMEM45B promotes proliferation, invasion and migration and inhibits apoptosis in pancreatic cancer cells. *Mol. BioSystems* 2016, *12*, 1860–1870.
78. Shen, K.; Yu, W.; Yu, Y.; Liu, X.; Cui, X. Knockdown of TMEM45B inhibits cell proliferation and invasion in gastric cancer. *Biomed. Pharmacother.* 2018, *104*, 576–581.
79. Wang, G.; Guo, S.; Zhang, W.; Li, D.; Wang, Y.; Zhan, Q. Co-expression network analysis identifies key modules and hub genes implicated in esophageal squamous cell cancer progression. *Med. Omics* 2021, *1*, 100003.
80. Senchenko, V.N.; Krasnov, G.S.; Dmitriev, A.A.; Kudryavtseva, A.V.; Anedchenko, E.A.; Braga, E.A.; Pronina, I.V.; Kondratieva, T.T.; Ivanov, S.V.; Zabarovskiy, E.R. Differential expression of CHL1 gene during development of major human cancers. *PLoS ONE* 2011, *6*, e15612.
81. Abuobaid, R.; Herrera-Marcos, L.; Navarro, M.A.; Arnal, C.; Martinez-Beamonte, R.; Surra, J.; Osada, J. Dietary Erythrodiol Modifies Hepatic Transcriptome in Mice in a Sex and Dose-Dependent Way. *Int. J. Mol. Sci.* 2020, *21*, 21197331. <https://doi.org/10.3390/ijms21197331>.

VI. DISCUSSION

The present Thesis uses RNA sequencing approaches to widen the knowledge of biological properties of minor components of EVOO such as erythrodiol and squalene on the liver of several animal models (mice lacking *ApoE* and *ApoA1*, rabbits and pigs).

These findings led our research group to identify the mechanisms by which these compounds exert their effects. Minor triterpenic components of EVOO, including erythrodiol and squalene, were found to modulate the expression of several genes involved in complex hepatic metabolic pathways, such as lipogenesis and the metabolism of nucleic acids, proteins, xenobiotics, carbohydrates and lipids and to alter the hepatic lipid profile as well as the lipid droplet area occupied in hepatocytes. Several of these genes interact with each other and with the hepatic lipidomic changes to form a metabolic network of transcriptomic and post-transcriptional changes in response to these triterpenes in liver cells. Hepatocytes as main functional units of the liver are responsible for the major metabolic functions (2). Among the broad beneficial effects of the Mediterranean diet explained by the small fraction of EVOO, these terpenic compounds improve the metabolic properties of hepatocytes and protect against oxidative stress, malignancy and inflammatory responses (352, 353).

The first objective of analyzing the long-term administration of erythrodiol on hepatic transcriptome through RNA sequencing approach was addressed in the first manuscript of this Thesis entitled:

i. Dietary Erythrodiol Modifies Hepatic Transcriptome in Mice in a Sex and Dose-Dependent Way

Erythrodiol was used as a nutrigenomic approach to determine its effect on the hepatic transcriptome in male *ApoE*-deficient mice, an animal model prone to hepatic steatosis. The results indicate that this compound altered the hepatic expression of clusters of genes involved in xenobiotic, protein and nucleic acid metabolisms. These findings were accompanied by a trend to decrease accumulation of lipids in cytoplasmic LDs and decreased hepatic mass. A comparison between RNA-seq and RT-qPCR

Discussion

showed that special care should be taken when comparing results from different methods. The randomly selected genes (*Ccl19-Ps2*, *Cyp2b10*, *Rbm14-Rbm4*, *Sec61g*, *Tmem81*, *Prtn3*, *Amy2a5*, *Cyp2b9* and *Mup1*) (Table 3, manuscript 1) showed good agreement between the two assays (Figure 5C & D, manuscript 1). A complex network of *Cyp2b13*, *Cyp2b9* and *Prtn3* was defined by correlation assays (Figure 4E, manuscript 1). When these genes were tested together with *Cyp2b10* and *Dmbt1* in female *Apoe* KO mice on the same diet, a different sex response was observed (Table 4, manuscript 1). A dose-response study showed that a minimum of 10 mg/kg was required to observe male responses in male *Apoe* KO mice (Table 5, manuscript 1). Erythrodiol administration was tested in the absence of APOA1 and showed no differences (Table 6, manuscript 1).

Erythrodiol administration induced DEGs without altering SNPs, causing transcriptional errors or affecting the global profile of alternative RNA splicing events. This, together with the absence of mortality and the normal morphology of liver samples at a dose of 10 mg/kg for 12 weeks, suggests that erythrodiol intake is safe for both sexes.

The utility of the RNA sample pooling strategy has been adopted for RNA-seq to optimise sample cost and minimise the complexity of analysis (206, 340, 354), despite the bias and loss of biological variability (355, 356). RT-qPCR was selected as an independent method and used to confirm the result for 21 randomly selected genes tested as individual samples. Initial correlation between RNAseq and RT-qPCR was poor (Figure 5A & B, manuscript 1). A more detailed analysis of both methods, taking into account the primer design used in RT-qPCR, which corresponded to the most read exons, and the establishment of a clear limit of detection in RNAseq, showed a robust agreement between the two methods ($r = 0.9$, $p < 0.0008$) (Figure 5C, manuscript 1) and the similarity of the response (Figure 5D, manuscript 1). The results show that the pooling assay is a good way of screening the samples. They also show that the two methods agree with each other and that the results are very reliable. A potential limitation of our approach is the search in the top highest expressed changes, where some control samples did not show any expression and contributed to an increased erythrodiol/control ratio.

Erythrodiol modulated the expression of cytochrome P450 components of the phase I response, which are involved in NADPH-dependent electron transport that oxidizes

Discussion

steroids and FAs and detoxify about 10% of xenobiotics (357, 358). A gene with induced expression was *Cyp2b10*, as was induced by ethanol administration (359), while *Cyp2b9* and *Cyp2b13*, were found to be down expressed. This is a unique pattern that differs from the response to dietary oleanolic acid, which induced *Cyp2b9* expression (340), and maslinic acid, which induced the triad (*Cyp2b9*, *Cyp2b10* and *Cyp2b13*) (354), whereas squalene induced *Cyp2b10* and *Cyp2c55* (360). This suggests a different gene expression profile for different EVOO triterpenes.

Cyp2b genes are also involved in lipid metabolism. Their deletion led to an imbalance in lipid homeostasis (361). The *Cyp2b* profile in response to erythrodiol did not show signs of lipid accumulation, as indicated by a lower percentage of LDs, smaller liver size and lower body weight, which could be a cumulative effect of the modulated transcripts. *Cyp2b9* correlated with all of the above, while *Cyp2b10* correlated with LD area. In addition to the *Cyp2b* genes, *Ccl19-ps2* was also associated with LD area (Figure 11). The suppression of gene encoding CCL19 induced NAFLD by inhibiting TLR4/NF- κ B p65 signalling (362). While MUP1, a member of the lipocalin family, regulates glucose and lipid metabolism by controlling the expression of gluconeogenic and lipogenic genes in the liver, its downregulation induces beta-cell dysfunction, glucose intolerance, hyperglycaemia and hyperlipidaemia (363, 364) and was associated with reduced liver size in response to erythrodiol. This again suggests a combined effect of genes that modulate lipid accumulation in the liver.

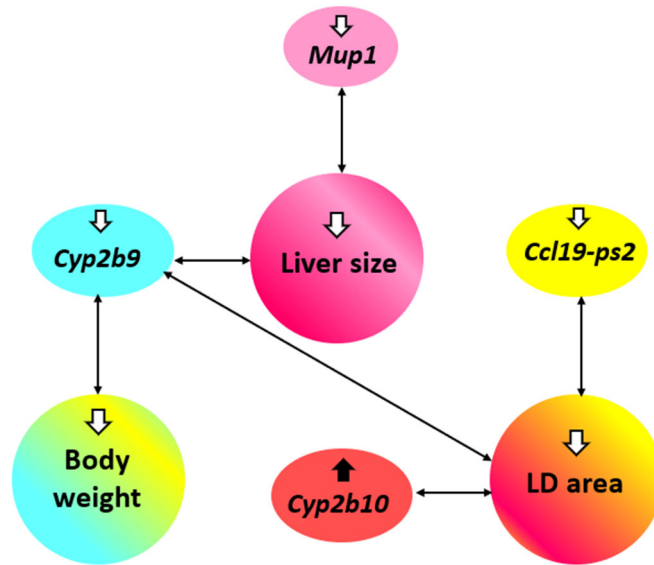


Figure 11. Network of association among hepatic transcripts and biological parameters in response to erythrodiol intake. Significant ($p < 0.02$) Spearman's correlations are shown.

In terms of protein metabolism, the finding of decreased *Prtn3* and its correlation with *Cyp2b9* and *Cyp2b13* is particularly interesting (Figure 4E, manuscript 1). *Prtn3* encodes a proteinase 3 with proteolytic activities and reactive oxygen species responses. *Prtn3* deficiency was associated with a lower incidence of hepatic steatosis and adipose tissue inflammation, and thus a reduced risk of NAFLD and obesity-related steatosis (365). In this context, *Prtn3* suppression by erythrodiol may be a potent hepatic therapy against steatosis.

In terms of malignancy, *Sec61g* is overexpressed in hepatocellular carcinoma (366), while the frameshift deletion mutation of the *Rbm14-rbm4* chimera was also investigated in liver cancer cells, as a putative marker of malignancy (367). The reduced expression of these three genes by erythrodiol may help to explain its antineoplastic properties (220).

Comparing the gene expression patterns of our study with those observed using olive oil components, *Dmbt1*, an extracellular receptor, showed reduced expression in animals consuming an olive pomace diet (206). This pattern is reproduced by erythrodiol but not by other terpenic compounds. Thus, *Dmbt1* may be a unique marker of erythrodiol intake. The gene was associated with liver damage, cancer and the repair mechanism (368). In cancer, *Dmbt1* is involved in the malignant transformation of

hepatic progenitor cells (369). Therefore, its relevance to liver damage needs to be investigated.

The sex differences in gene expression in response to erythrodiol are dramatically different. The results for those genes with high changes in expression confirm the previously observed sex differences in the liver (370), especially when a Western diet was administered (371). Studies have shown that *Cyp2b9* gene expression is particularly sensitive to sex differences (361, 372, 373), β -estradiol (374), and prolactin (375). It is therefore recommended that liver drugs be pre-tested for females.

A threshold dose was also required to induce hepatic gene expression changes in male mice, confirming a dose-dependent pattern of other erythrodiol-related effects (216, 376) and a possible cytotoxic effect at high doses (218).

Mice lacking the *Apoa1* gene were used as a model of HDL deficiency to test the hypothesis that APOA1 is required for the delivery of erythrodiol to liver cells. The results showed that there were no significant changes in the genes tested. The same results were obtained with oleanolic acid administration (340), consistent with both triterpenes being carried by non APOA1-containing HDL for transfer to the liver.

Overall, erythrodiol induces a dose- and sex-dependent hepatic transcriptome. To determine the hepatic gene expression pattern of erythrodiol in humans, it is first necessary to test its bioavailability, which has only been observed in rats (377). It is also necessary to test for a sex-specific response in our species. Consumption of 50 ml of EVOO per day would expose a person to a dose of 53 $\mu\text{g}/\text{kg}$ erythrodiol. Using the same amount of olive pomace oil (378), the exposure would be 500 $\mu\text{g}/\text{kg}$. A general overview of the findings is given in Figure 12.

Discussion

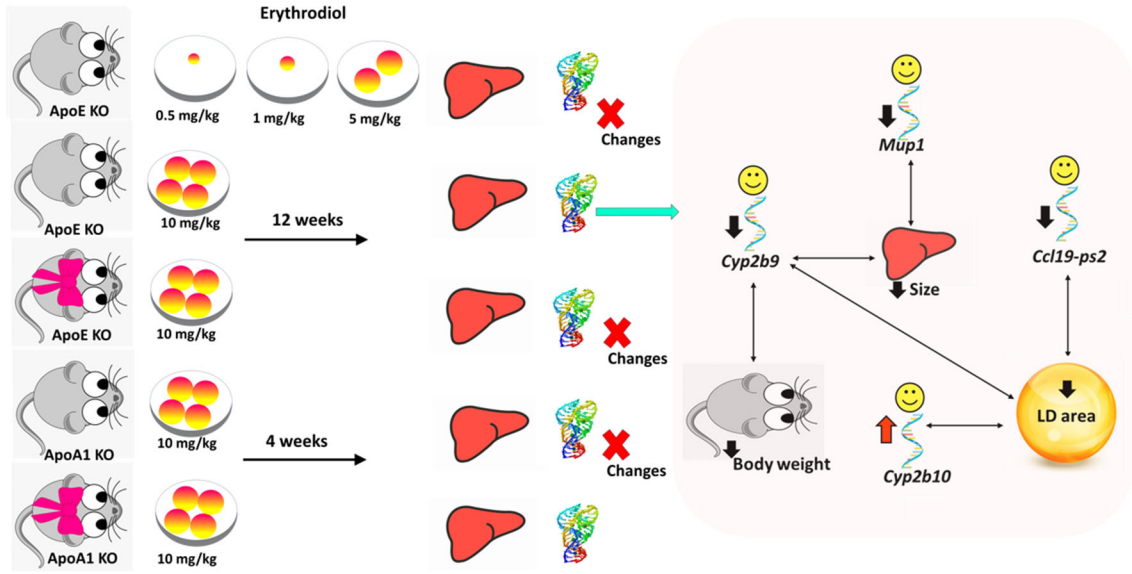


Figure 12. Summary of findings of erythrodiol experiments.

The second objective of assessing the effect of squalene on the hepatic transcriptome through RNA sequencing in male New Zealand rabbits was addressed in the second manuscript of this Thesis entitled:

ii. **Squalene through its Post-Squalene Metabolites is a Modulator of Hepatic Transcriptome in Rabbits.**

Dietary squalene was used as a nutrigenomic approach to determine its effect on the hepatic transcriptome in male wild-type white rabbits (*Oryctolagus cuniculus*) following a 0.5% squalene intake, equivalent to 0.6 g/kg. In general, the diet induced increased hepatic squalene accumulation (Figure 3B, manuscript 2) and increased levels of post-squalene metabolites of Chol biosynthesis including lanosterol, dihydrolanosterol, lathosterol, zymostenol and desmosterol (Figure 3C, manuscript 2). Using RNA-seq, squalene administration did not alter SNPs; however, the terpene induced AS events at both 5' and 3' sites and RIs. Rabbits treated with squalene showed significant changes in the hepatic expression of 12 transcripts: *LOC100344884 (PNPLA3)*, *GCK*, *TFCP2L1*, *ASCL1*, *ACSS2*, *OST4*, *FAM91A1*, *MYH6*, *LRRC39*, *LOC108176846*, *GLT1D1* and *TREH* (Table 3, manuscript2). These transcript levels correlated with hepatic LDs area and post-squalene metabolite levels (Figure 7, manuscript 2). Furthermore, incubation of murine hepatic AML12 with squalene and post-squalene intermediates of Chol biosynthesis, including lanosterol, dihydrolanosterol, zymostenol and desmosterol modified the expression of *ACSS2*, *FAM91A1* and *PNPLA3* (Figure 8, manuscript 2). These results indicate that the changes in transcriptional changes are not only dependent on squalene, but also on its downstream metabolites.

The utility of the RNAseq results was verified by RT-qPCR assay. The high correlation between the analyzed transcripts ($r = 0.8$, $p < 0.0001$) (Figure 5A, manuscript 2) and the similar pattern of the response (Figure 5B, manuscript 2) indicate that the two methods are consistent and the results are reliable.

The non-toxic accumulation of a similar dose of squalene in *ApoE*-KO mice has been demonstrated previously (341) and corresponds to the low toxicity of 90% w/w squalene in shark livers (379, 380). In rabbits, the absence of changes in body weight in animals receiving dietary squalene compared with the control group (Supplementary Figure S1,

Discussion

manuscript 2) and the normal histomorphometric assessment of hepatocytes (Figure 2, manuscript 2) suggest the non-toxic effect of the triterpene, which accumulates in small LDs, unlike in mice where it accumulates in larger droplets (341, 381). A similar droplet pattern has been observed for the triterpene oleanolic acid (340). These droplets accumulate lipids in the form of unesterified cholesterol (381) and thus act as energy stores and barriers against lipotoxicity, preventing cell membrane defects, mitochondrial dysfunction and errors in signalling pathways (33). In contrast to mice, squalene intake did not reduce hepatic TG levels in rabbits. Nor did it alter the expression of *CYP2B* and *CYP2C* (data not shown) at the same dose in mice (360). The duration of treatment, animal model and experimental design may explain these differences.

Squalene mainly altered the hepatic expression of gene clusters involved in lipid and protein transport, lipid metabolism, lipogenesis, anti-inflammatory effects and neoplasia. These findings may help to explain the absence of inflammation even in the presence of elevated levels of non-esterified Chol and increased levels of caspase1 (381). *FAM91A1*, a poorly understood gene, appears to play a regulatory role in Golgi-mediated vesicle capture for the processing, packaging and transport of proteins and lipids (382, 383). *FAM91A1* expression did not correlate with hepatic squalene accumulation (data not shown), possibly because the triterpene is distributed in other subcellular organelles, including nuclear and plasma membranes and the RER (341). With regard to LDs, the lower expression of *ACSS2* and *TFCP2L1* correlated with an increase in the hepatic area occupied by LDs (Figure 7B, manuscript 2). Regarding the liver lipid profile, the decreased expression of *GCK*, *ACSS2* and *LOC100344884* and the increased expression of *TREH* are of interest. *GCK* activates glycolysis, glycogen synthesis and lipogenesis and facilitates hepatic glucose uptake in hyperglycaemia. Suppression of *GCK* downregulates genes for TG synthesis enzymes, but also insulin receptors, leading to insulin resistance (384), suggesting that *GCK* inhibition by squalene may be useful in the treatment of NAFLD. *ACSS2* is a metabolic gene that induces lipid storage. When *ACSS2* is deficient, the activity of lipid transporters and FA oxidation genes is reduced. This in turn leads to reduced dietary lipid absorption, lower TG levels and reduced liver fibrosis (385, 386). *LOC100344884*, an ortholog of *Pnpla3*, shows lipase activity against hepatic TGs and retinyl esters in HSCs (387) and is strikingly correlated

Discussion

with hepatic Chol content (Figure 7A, manuscript 2), fibrosis and steatosis (387, 388). *TREH* is the least studied of the membrane-bound alpha-glucosidases that hydrolyse trehalose. Its transcript is typically expressed in the intestine (389, 390) and to a lesser extent in the liver (<https://gtexportal.org/home/gene/TREH>, accessed 1 March 2022). Trehalose inhibits cellular glucose and may be useful in the treatment of NAFLD via solute carrier family 2-member (SLC2A) transporters as a pathway for trehalose to stimulate autophagy via adenosine monophosphate activated protein kinase (AMPK) (391).

In terms of protein modification, *OST4* is an oligosaccharyltransferase subunit involved in the N-glycosylation of polypeptides in the lumen of the ER. Squalene-overexpressed *OST4* may promote co-translational N-glycosylation by stabilising STT3A-containing *OST* isoforms available in liver cells (392). Impaired glycosylation affects protein function and drug disposition (393, 394) and lowers LDL (395). *MYH6* and *LRRC39*, transcripts primarily expressed in muscle cells (396, 397), with very low expression (398, 399), were also overexpressed in the liver in response to squalene. Remarkably, both transcript levels were associated (Figure 6, manuscript 2) and share a function in cell signalling via protein dephosphorylation http://www.ensembl.org/Homo_sapiens/Gene/Ontologies/molecular_function?g=ENS [G00000197616;r=14:23381982-23408273](http://www.ensembl.org/Homo_sapiens/Gene/Ontologies/molecular_function?g=ENS), [LRRC39 Gene - GeneCards | LRC39 Protein | LRC39 Antibody](http://www.ensembl.org/Homo_sapiens/Gene/Ontologies/molecular_function?g=ENS). Overexpression of (*Myh6/Ghrl*) in transgenic rats reduces oxidative stress and prevents high-fat diet-induced hyperglycaemia (400). Through the expression of these genes, squalene appears to modulate lipid and glucose metabolism.

Squalene intervention increased hepatic levels of Chol precursors including lanosterol, dihydrolanosterol, lathosterol and zymostenol via the Kandutsch-Russell pathway and desmosterol via the Bloch pathway (Figure 3C, manuscript 2), all of which interestingly correlated strongly with squalene-modified transcript levels (Figure 7A, manuscript 2). In this sense, reduced *TFCP2L1* expression was strongly correlated with increased lanosterol and dihydrolanosterol accumulation, as was *ACSS2* for lanosterol. The increased expression of *FAM91A1* and the decreased expression of *LOC100344884* were associated with desmosterol. These associations suggest that the effects of squalene may be mediated by its post-squalene precursors in the Chol biosynthetic pathway, and

Discussion

that these effects may be different from those seen when squalene is not metabolised (401). The accumulation of squalene in Chol auxotrophic lymphoma alters the cellular lipid profile and prevents oxidative stress of cell death (401). To address this dilemma, the AML12 liver cell line was incubated with lanosterol, dihydrolanosterol, zymostenol or desmosterol, followed by analysis of *Acss2*, *Fam91a1* and *Pnpla3* transcripts. The results (Figure 8, manuscript 2) showed the same expression pattern as observed in vivo by squalene intake. This suggests that lanosterol, dihydrolanosterol, zymostenol and desmosterol have a direct hepatic transcriptional response.

With regard to the anti-cancer properties of squalene, previous studies have shown that squalene has these properties (178). *ACSS2* scavenges acetate as a carbon source for the proliferation of HCC (385, 402). Liver tumour burden was reduced in adult mice lacking *ACSS2* (385). *TFCP2L1*, a transcription factor required for germ cell specification and cholangiocyte-to-hepatocyte differentiation (403), was strongly associated with several transcripts modulated by squalene, including *OST4*, *TREH*, *GCK*, *ACSS2*, *MYH6* and *LRRC39* (Figure 6, manuscript 1). *TFCP2L1* expression is reduced in neoplastic kidney and thyroid cells (404). In addition, *GLT1D1* is a tumour suppressor gene and is highly expressed in HCC (405).

Overall, squalene accumulates in liver cells and modulates the hepatic transcriptome in wild-type *Oryctolagus cuniculus*. It also increases the levels of post-squalene metabolites of Chol biosynthesis, which are also able to modulate hepatic expression in the same pattern as squalene. The bioavailability of squalene has been demonstrated in cell culture, animal models and humans (168). It is recommended that the 0.5% dose of squalene be studied in humans. Consumption of 50 ml of EVOO per day would expose a person to a dose of 75 to 505 µg/kg. It is also necessary to test for a sex-specific response in our species (406). A general overview of what was found is given in Figure 13.

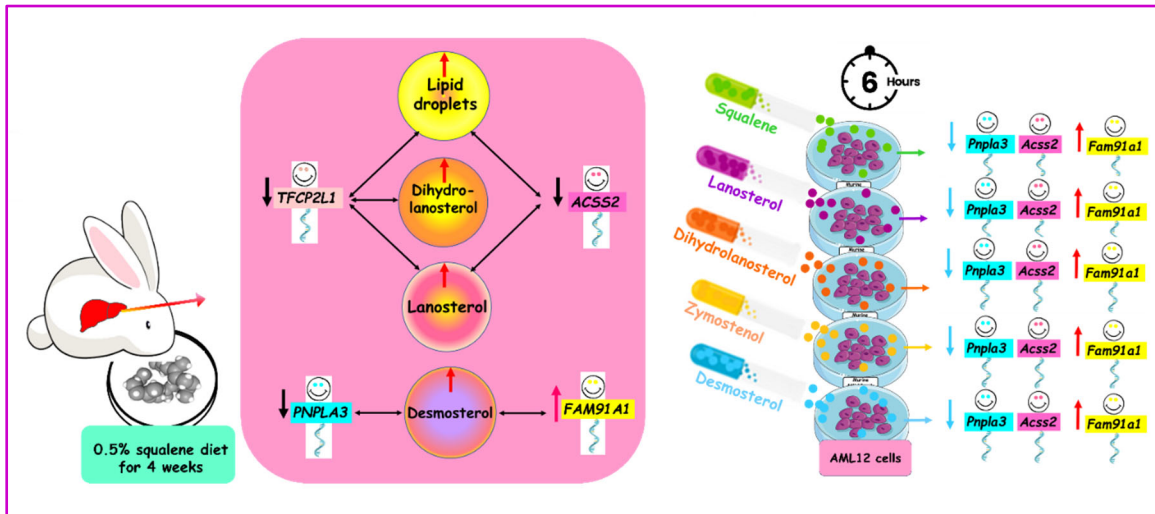


Figure 13. Summary of findings in this objective

The third objective of evaluating the effect of squalene on the hepatic transcriptome by using RNA sequencing in two groups of male Large White × Landrace pigs developing nonalcoholic steatohepatitis was addressed in the third manuscript of this Thesis entitled:

iii. Differentially Expressed Genes in Response to a Squalene-Supplemented Diet Are Accurate Discriminants of Porcine Non-Alcoholic Steatohepatitis

A 0.5% dietary squalene was used as a nutrigenomic approach to determine its effect on the hepatic transcriptome of Large White × Landrace pigs that developed reproducible and reversible NASH following a steatotic diet. Using RNA-seq, the modified DEGs were influenced by global AS events, including 5' and 3' sites, RIs, SEs and MXEs, with no change in SNPs. Pigs on this diet showed marked accumulation of squalene in their livers (Figure 7A, manuscript 3) and significantly increased hepatic expression of *PPP1R1B*, *OASL*, *PPP4R4*, *NEURL3*, *TMEM45B*, *AFP*, *ENPEP*, *LOC110256649*, *LOC100526118* and *SPRY3*, and significantly decreased expression of *CHL1* and *SQLE* (Table 2, manuscript 3). All these transcripts were part of a complex network of gene expression in the liver (Figure 4, manuscript 3). In addition to a reduced hepatic TG content and LDs areas and an increased cellular ballooning, results included increased NASH activity index and SAF score. There were no inflammatory responses or fibrotic changes (Figure 1, manuscript 3). Some of these changes were found to be particularly correlated with DEGs. *ENPEP* correlated with liver TG levels, *LOC100526118* with LD area, *OASL*, *AFP*, *PPP1R1B* and *NEURL3* with activity index and *NEURL3* with activity and SAF score. The ROC curves and areas under the curves of *AFP*, *ENPEP* and *PPP1R1B* showed a high discriminant power (Figure 5 & 6, manuscript 3). Furthermore, the modified transcripts that were correlated with hepatic squalene accumulation, including *PPP1R1B*, *TMEM45B*, *AFP*, *ENPEP* and *SPRY3* (Figure 7B, manuscript 3), followed the same pattern *in vitro* using the human hepatic HEPG2 cell line incubated with squalene (Table 3, manuscript 3) and in mouse AML12 cells without *Spry3* (Table 4, manuscript 3). This is an indication of a direct effect of squalene on these liver transcripts, independent of the species studied. Overall, this represents a unique

Discussion

and unexplored area of gene expression in liver pathology where ballooning is dissociated from steatosis.

The RNA pooling strategy for the RNAseq assay was confirmed by individual sample RT-qPCR. The robust linear association for the analyzed transcripts ($r = 0.90$, $p < 0.0001$) (Figure 3A, manuscript 3) and the similarity of the response (Figure 3B, manuscript 3) confirm that pooling is a reliable assay and demonstrate the concordance between the two methods and the high reliability of the results.

In terms of diet, the steatotic diet used was high in saturated fat, Chol, cholate and fructose and low in methionine (1.1 g/kg) and choline (50 mg/kg), which are essential for hepatic β -oxidation and VLDL biosynthesis (200, 407). Impairment of these two pathways was therefore critical in overcoming the natural resistance to the development of fatty liver. In addition, methionine-choline-deficient (MCD) diets reduce glycogen stores and induce hepatic oxidative stress, apoptosis and steatosis (407, 408). In the animal model studied, short-term administration of this diet induced NASH with an equal distribution of grade 1 and 2 hepatic ballooning as determined by the fatty liver inhibition of progression (FLIP) algorithm and SAF score (279). Regarding the level of squalene, the choice of 0.5% was similar to that tested in the rabbit model, which modulated gene expression and lipid profile in hepatocytes (409). This level would also represent an adapted metabolic rate of the 1% squalene diets used in the mouse model (338, 360).

The porcine model was used as a human alternative to test the squalene-induced transcriptome profile in NASH. This was due to the high physiological, anatomical, metabolic, genetic and liver size similarities (274, 410), as well as the similar hepatic transcriptomic and protein coding pattern with the human species (411).

In pigs with established NASH, the administration of 0.5% squalene reproduced the hepatic accumulation observed in mice (360) and rabbits (341). However, in contrast to pigs, both models didn't show any change in hepatic TG content, despite a higher area of LDs (341). In cultured human hepatocytes, squalene altered the expression of genes correlated with hepatic TG content (Figures 5A, manuscript 3) and activity index

Discussion

(Figures 6A, manuscript 3). In a previous study using the same cell type, squalene modified the expression of lipid metabolism genes, resulting in significantly lower TAG and Chol levels when FA uptake was increased (412). In other models, squalene modulated a cluster of genes that correlated with hepatic lipid content (360, 409). These differences in response may be due to species-specific expression differences or experimental conditions.

Correlation analyses were performed to determine the significance of the modulated gene expression. These analyses revealed various hepatic pathological findings. In this sense, *ENPEP*, a membrane glutamylaminopeptidase (<https://www.ncbi.nlm.nih.gov/gene/397080>), was inversely correlated with hepatic TG levels (Figure 5A, manuscript 3). PPAR α modulators used as TG-lowering agents induce hepatic expression of *ENPEP* (413, 414). The peptidase then protects against hypertriglyceridemia (415). However, it is controversial that its hepatic levels increase with progression of NAFLD and decrease upon treatment (416). Interestingly, *ENPEP* was related to squalene levels (Figure 7B, manuscript 3) and shared the same expression profile in hepatocytes (Tables 3 & 4, manuscript 3), suggesting a direct effect of the triterpene. However, *LOC100526118*, which encodes glutathione S-transferase A1-like (<https://www.ncbi.nlm.nih.gov/gene/?term=LOC100526118+pig>) and is highly expressed in the liver, was upregulated in response to squalene and was linked with reduced of LDs area (Figure 5D, manuscript 3), probably due to its TG metabolic and antioxidant properties (417-419), in addition to detoxification activities via conjugation of the hydrophobic and electrophilic compounds with reduced glutathione (GSH). Decreased GSH has been linked to diminished LDs (420). With regard to *PPP4R4*, which encodes for protein phosphatase 4 regulatory subunit 4 (<https://www.ncbi.nlm.nih.gov/gene/100737576>), its overexpression has been found to activate glucose metabolism (421), leading to lower TG levels (422). On the contrary, squalene reduced the expression of *CHL1*, which codifies for the cell adhesion molecule L1-like. This transcript impairs insulin secretion (423, 424), thereby promoting the production of hepatic TG-rich lipoproteins (425) and consequent NAFLD (426, 427). In view of the decrease in LD areas and TG accumulation observed with squalene administration, these gene changes would be compensated by the expression of other

Discussion

genes. The results indicate that all of these genes play a crucial role in the hepatic lipid metabolism and are interconnected to produce an effect in response to squalene administration.

In the context of NASH, squalene accumulation correlated with the ballooning score and thus with NASH activity and the SAF score (200). The correlations between the genes affected by squalene and these indexes were tested and found that some of them, including *PPP1R1B*, *AFP*, *OASL* and *NEURL3*, had a significant direct correlation with these parameters (Figure 6, manuscript 3). As shown in (Figure 4, manuscript 3), these transcripts form a complex network of interactions, indicating that they are functionally related. *PPP1R1B* is a protein phosphatase 1 regulatory subunit that suppresses protein phosphatase 1 activity (428) and induces glycogenesis (429). This condition was associated with a higher ballooning score in NAFLD patients, despite a lower level of steatosis and fibrosis (430). A similar pattern was observed in the NASH liver when exposed to squalene. Regarding *AFP*, the alpha fetoprotein binds to FAs (431) and their composition affects the progression of NAFLD. FA synthesis in liver cells was correlated with the ballooning score (432). For example, a lower estearic/palmitic acid ratio and a higher palmitoleic/palmitic acid ratio worsen ballooning and fibrosis scores (432), while blood levels of palmitoleic acid are negatively associated with NAFLD activity and ballooning scores (433). It is interesting to note that in the squalene NASH pig model, blood levels of palmitic acid are consistently lower (200). In addition, *AFP* plays a key role in the SMADS signaling pathway that protects against liver fibrosis, in particular for SMAD2 (434, 435). The expression of *PPP1R1B* and *AFP* in hepatocytes *in vitro* was similar, suggesting a direct effect of squalene (Tables 3 & 4 manuscript 3). In addition, *OASL* inhibits the activity of type 1 interferons (436), which are involved in macrophage polarization and the inflammation in NAFLD (437). This suggests that the intervention has an anti-inflammatory effect. Notably, *OASL* is a target gene of PPAR α , which was negatively correlated with NAFLD activity score (438). Finally, *NEURL3* activates ubiquitin protein ligase activity 3, an enzyme that helps to reduce the expression of genes associated with NAFLD (439, 440). This may slow the progression of NAFLD. The increased expression of the four genes: *PPP1R1B*, *AFP*, *OASL*, and *NEURL3*, may have a significant impact on the progression of this disease. In fact, the ROC curves show that

Discussion

AFP and *PPP1R1B* discriminate between different stages of NAFLD better than conventional measures of NAFLD activity and the SAF score. In humans, both *PPP1R1B* and *AFP* were positively associated with ballooning score (429, 430, 432), so this model mimics the human condition but also has some unique features. *ENPEP*, which reduces TG levels (413-415), and *NEURL3* and *OASL*, two genes that reduce inflammatory responses (436, 437). These genes may create a unique environment for ballooning without inflammatory or fibrotic changes. This is an interesting situation that requires further investigation.

Squalene has been shown to have anti-cancer properties (178, 409). *PPP1R1B* is turned on in colorectal liver metastasis (441). *SPRY3* (sprouty RTK signaling antagonist 3) (<https://www.ncbi.nlm.nih.gov/gene/?term=SPRY3+pig>) acts as a negative feedback regulator of the receptor tyrosine kinase (RTK)/ Ras GTPase/ MAP kinase (MAPK) (RTK/Ras/MAPKS) signaling pathway that is involved in cell growth and survival. However, unlike *SPRY1*, *SPRY2* and *SPRY4*, and despite its positive association with *SPRY1*, its expression level is not altered in HCC (442). *TMEM45B* (transmembrane protein 45B) (<https://www.ncbi.nlm.nih.gov/gene/?term=TMEM45B++pig>) plays a central role in hepatic differentiation (443) and its expression is increased in cirrhosis (444). Also, the expression of this gene is not the same in all types of cancer, but none is of hepatic origin (445-448). Therefore, more research is needed to understand how *TMEM45B* affects liver cancer. *PPP1R1B*, *SPRY3* and *TMEM45B* were all induced by squalene administration (Table 2, manuscript 3). On the other hand, *CHL1* (cell adhesion molecule L1 like) (<https://www.ncbi.nlm.nih.gov/gene/?term=CHL1+pig>) affects the cell cycle through the p53 pathway, and it is often overexpressed in liver cancer (449). Squalene administration reduced its expression, a phenomenon that seems to be independent on the previous expression levels, as they are not connected in the gene network we proposed (Figure 4, manuscript 3). The phenotype may be a balance of the expression pattern of these genes that could be involved in the progression of NASH to cirrhosis and cancer. Collectively, the results indicate that squalene accumulates in the liver of male Large White x Landrace pigs and is able to modulate expression changes of a network of genes that may influence the fate of NASH via reduced TG content and

Discussion

LDs area, while cellular ballooning score, NASH activity and SAF score increased. Figure 14 provides a general overview of all the findings.

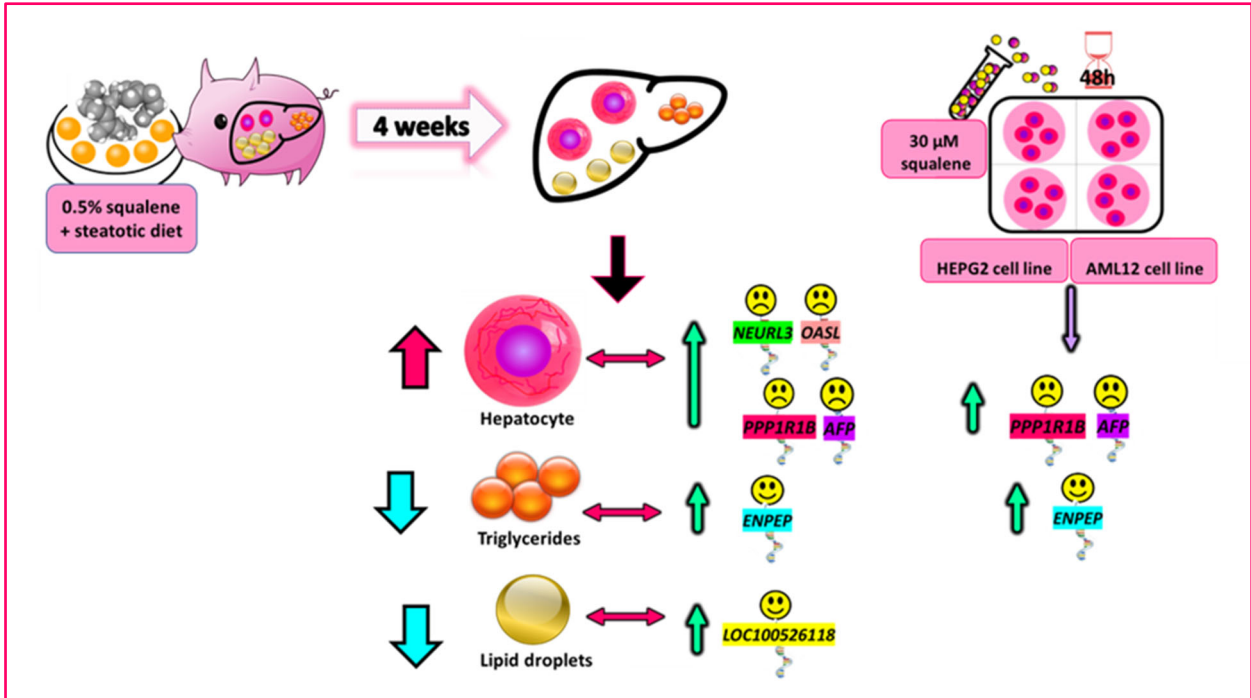


Figure 14. Summary of findings observed in this objective.

VII. CONCLUSIONS

1. The administration of 0.01% erythrodiol (10 mg/kg) in the Western diet to *Apoe*-deficient mice for 12 weeks significantly upregulated 68 and down-regulated 124 hepatic genes at the level of 2-fold change. These genes belonged to detoxification processes, protein metabolism and nucleic acid related metabolites. Gene expression changes of 21 selected transcripts were verified by RT-qPCR. *Ccl19*, *Ps2*, *Cyp2b10*, *Rbm14-Rbm4*, *Sec61g*, *Tmem81*, *Prtn3*, *Amy2a5*, *Cyp2b9* and *Mup1* showed significant changes by erythrodiol administration. When *Cyp2b10*, *Dmbt1*, *Cyp2b13*, *Prtn3* and *Cyp2b9* were analyzed in female *Apoe*-deficient mice, no change was observed. Likewise, no significant variation was observed in *Apoa1*- or in *Apoe*-deficient mice receiving doses ranging from 0.5 to 5 mg/kg erythrodiol. Our results give evidence that erythrodiol exerts a hepatic transcriptional role, but this is selective in terms of sex and requires a threshold dose.
2. The squalene administration downregulated 9 transcripts and upregulated 13 transcripts in the liver of male New Zealand rabbits fed either a diet enriched with 1% sunflower oil or the same diet with 0.5% squalene for 4 weeks. The gene ontology of transcripts fitted into the following main categories: transporter of proteins and sterols, lipid metabolism, lipogenesis, anti-inflammatory and anti-cancer properties. When the results were confirmed by RT-qPCR, rabbits receiving squalene displayed significant hepatic expression changes of *LOC100344884* (*PNPLA3*), *GCK*, *TFCP2L1*, *ASCL1*, *ACSS2*, *OST4*, *FAM91A1*, *MYH6*, *LRRC39*, *LOC108176846*, *GLT1D1* and *TREH*. A squalene-enriched diet increased hepatic levels of squalene, lanosterol, dihydrolanosterol, lathosterol, zymostenol and desmosterol. Strong correlations were found among specific sterols and some squalene-changed transcripts. Incubation of the murine AML12 hepatic cell line in the presence of lanosterol, dihydrolanosterol, zymostenol and desmosterol reproduced the observed changes in the expressions of *Acss2*,

Conclusions

Fam91a1 and *Pnpla3*. In conclusion, these findings indicate that the squalene and post-squalene metabolites play important roles in hepatic transcriptional changes required to protect the liver against malfunction.

3. The effect of squalene on the hepatic transcriptome, RNA-sequencing was carried out in two groups of male Large White x Landrace pigs developing nonalcoholic steatohepatitis by feeding them a high fat/cholesterol/fructose and methionine and choline-deficient steatotic diet or the same diet with 0.5% squalene for 1 month. Hepatic lipids, squalene content, steatosis, activity (ballooning + inflammation) and SAF (steatosis + activity + fibrosis) scores were analyzed. Pigs receiving the latter diet showed hepatic squalene accumulation and significant twelve differentially expressed hepatic genes correlating in a gene network. These pigs also had lower hepatic triglycerides and LD areas and higher cellular ballooning. Glutamyl aminopeptidase (*ENPEP*) was correlated with triglyceride content, while alpha-fetoprotein (*AFP*), neuralized E3 ubiquitin protein ligase 3 (*NEURL3*), 2'-5'-oligoadenylate synthase-like protein (*OASL*), and protein phosphatase 1 regulatory inhibitor subunit 1B (*PPP1R1B*) were correlated with activity reflecting inflammation and ballooning, and *NEURL3* with the SAF score. *AFP*, *ENPEP* and *PPP1R1B* exhibited a remarkable strong discriminant power compared to those pathological parameters between both experimental groups. Moreover, the expression of *PPP1R1B*, *TMEM45B*, *AFP* and *ENPEP* followed the same pattern *in vitro* using human hepatoma (HEPG2) and mouse liver 12 (AML12) cell lines incubated with squalene, indicating a direct effect of squalene on these expressions. These findings suggest that squalene accumulated in the liver is able to modulate gene expression changes that may influence the progression of non-alcoholic steatohepatitis.

VII. CONCLUSIONES

1. La administración de eritrodiol al 0,01% (10 mg/kg) en la dieta occidental a ratones deficientes en *ApoE* durante 12 semanas reguló significativamente al alza 68 y reguló a la baja 124 genes hepáticos a un nivel de cambio de 2 veces. Estos genes pertenecían a procesos de desintoxicación, metabolismo de proteínas y metabolitos relacionados con los ácidos nucleicos. Los cambios en la expresión génica de 21 transcritos seleccionados se verificaron mediante RT-qPCR. *Ccl19*, *Ps2*, *Cyp2b10*, *Rbm14-Rbm4*, *Sec61g*, *Tmem81*, *Prtn3*, *Amy2a5*, *Cyp2b9* y *Mup1* mostraron cambios significativos por la administración de eritrodiol. Cuando se analizaron *Cyp2b10*, *Dmbt1*, *Cyp2b13*, *Prtn3* y *Cyp2b9* en ratones hembra con deficiencia de *ApoE*, no se observó ningún cambio. Asimismo, no se observó variación significativa en ratones con deficiencia de *ApoA1* o *ApoE* que recibieron dosis que oscilaron entre 0,5 y 5 mg/kg de eritrodiol. Nuestros resultados evidencian que el eritrodiol ejerce una función transcripcional hepática, pero ésta es selectiva en función del sexo y requiere una dosis umbral.
2. La administración de escualeno reguló a la baja 9 transcritos y al alza 13 transcritos en el hígado de conejos machos de Nueva Zelanda alimentados con una dieta enriquecida con aceite de girasol al 1% o la misma dieta con un 0,5% de escualeno durante 4 semanas. La ontología génica de los transcritos se encuadró en las siguientes categorías principales: transportadores de proteínas y esteroides, metabolismo lipídico, lipogénesis, propiedades antiinflamatorias y anticancerígenas. Cuando los resultados fueron confirmados por RT-qPCR, los conejos que recibieron escualeno mostraron cambios significativos en la expresión hepática de *LOC100344884* (*PNPLA3*), *GCK*, *TFCP2L1*, *ASCL1*, *ACSS2*, *OST4*, *FAM91A1*, *MYH6*, *LRRC39*, *LOC108176846*, *GLT1D1* y *TREH*. Una dieta enriquecida con escualeno aumentó los niveles hepáticos de escualeno, lanosterol, dihidrolanosterol, lathosterol, zymostenol y desmosterol. Se encontraron fuertes correlaciones entre esteroides específicos y algunos transcritos modificados por escualeno. La incubación de la línea celular hepática murina

Conclusions

AML12 en presencia de lanosterol, dihidrolanosterol, zymostenol y desmosterol reprodujo los cambios observados en las expresiones de *Acss2*, *Fam91a1* y *Pnpla3*. En conclusión, estos hallazgos indican que el escualeno y los metabolitos post-escualeno juegan un papel importante en los cambios transcripcionales hepáticos necesarios para proteger el hígado contra el mal funcionamiento.

3. El efecto del escualeno sobre el transcriptoma hepático, la secuenciación del ARN se llevó a cabo en dos grupos de cerdos machos Large White x Landrace que desarrollaron esteatohepatitis no alcohólica alimentándolos con una dieta esteatótica alta en grasas/colesterol/fructosa y baja en metionina y colina o la misma dieta con 0,5% de escualeno durante 1 mes. Se analizaron los lípidos hepáticos, el contenido de escualeno, la esteatosis, la actividad (ballooning + inflamación) y las puntuaciones de SAF (esteatosis + actividad + fibrosis). Los cerdos que recibieron esta última dieta mostraron una acumulación hepática de escualeno y doce genes hepáticos expresados diferencialmente que se correlacionan en una red de genes. Estos cerdos también tenían niveles más bajos de triglicéridos hepáticos y áreas de gotas de lípidos y un mayor *ballooning* celular. La glutamil aminopeptidasa (*ENPEP*) se correlacionó con el contenido de triglicéridos, mientras que la alfa-fetoproteína (*AFP*), la proteína ligasa 3 de ubiquitina E3 neuralizada (*NEURL3*), la proteína similar a la 2'-5'-oligoadenilato sintasa (*OASL*) y la subunidad 1B (*PPP1R1B*) del inhibidor regulador de la proteína fosfatasa 1 se correlacionaron con la actividad que refleja la inflamación y el abombamiento, y *NEURL3* con la puntuación SAF. *AFP*, *ENPEP* y *PPP1R1B* mostraron un notable poder discriminante en comparación con esos parámetros patológicos entre ambos grupos experimentales. Además, la expresión de *PPP1R1B*, *TMEM45B*, *AFP* y *ENPEP* siguió el mismo patrón *in vitro* utilizando líneas celulares de hepatoma humano (HEPG2) e hígado de ratón (AML12) incubadas con escualeno, lo que indica un efecto directo del escualeno sobre estas expresiones. Estos hallazgos sugieren que el escualeno acumulado en el hígado es capaz de modular los cambios en la expresión génica que pueden influir en la progresión de la esteatohepatitis no alcohólica

VIII. REFERENCES

1. Adenote A, Dumic I, Madrid C, Barusya C, Nordstrom CW, Rueda Prada L. NAFLD and infection, a nuanced relationship. *Can J Gastroenterol Hepatol* 2021;5556354
2. Pu W, Zhou B. Hepatocyte generation in liver homeostasis, repair, and regeneration. *Cell Regeneration*. 2022;11(1):2.
3. Saxena R, Theise ND, Crawford JM. Microanatomy of the human liver—exploring the hidden interfaces. *Hepatology*. 1999;30(6):1339-46.
4. Mitra V, Metcalf J. Metabolic functions of the liver. *Anaesthesia & Intensive Care Medicine*. 2012;13(2):54-5.
5. Schulze RJ, Schott MB, Casey CA, Tuma PL, McNiven MA. The cell biology of the hepatocyte: a membrane trafficking machine. *Journal of Cell Biology*. 2019;218(7):2096-112.
6. Vollmar B, Menger MD. The hepatic microcirculation: mechanistic contributions and therapeutic targets in liver injury and repair. *Physiological Reviews*. 2009;89(4):1269-339.
7. Zhou Z, Xu M-J, Gao B. Hepatocytes: a key cell type for innate immunity. *Cellular & Molecular Immunology*. 2016;13(3):301-15.
8. Braet F, Taatjes DJ, Wisse E, editors. Probing the unseen structure and function of liver cells through atomic force microscopy. *Seminars in Cell & Developmental Biology*; 2018: Elsevier.
9. Van Son KC, Verschuren L, Hanemaaijer R, Reeves H, Takkenberg RB, Drenth JPH, et al. Non-parenchymal cells and the extracellular matrix in hepatocellular carcinoma in non-alcoholic fatty liver disease. *Cancers (Basel)*. 2023;15(4).
10. Ishibashi H, Nakamura M, Komori A, Migita K, Shimoda S, editors. Liver architecture, cell function, and disease. *Seminars in Immunopathology*; 2009: Springer.
11. Dufour J-F, Clavien P-A, Graf R, Trautwein C. *Signaling pathways in liver diseases*: Springer; 2010.
12. Smedsrød B, De Bleser P, Braet F, Lovisetti P, Vanderkerken K, Wisse E, et al. Cell biology of liver endothelial and kupffer cells. *Gut*. 1994;35(11):1509.
13. Senoo H, Mezaki Y, Fujiwara M. The stellate cell system (vitamin A-storing cell system). *Anatomical Science International*. 2017;92:387-455.
14. Liu Z, Li C, Kang N, Malhi H, Shah VH, Maiers JL. Transforming growth factor β (TGF β) cross-talk with the unfolded protein response is critical for hepatic stellate cell activation. *Journal of Biological Chemistry*. 2019;294(9):3137-51.
15. Harmon C, Robinson MW, Fahey R, Whelan S, Houlihan DD, Geoghegan J, et al. Tissue-resident Eomes(hi) T-bet(lo) CD56(bright) NK cells with reduced

References

- proinflammatory potential are enriched in the adult human liver. *Eur J Immunol*. 2016;46(9):2111-20.
16. Mikulak J, Bruni E, Oriolo F, Di Vito C, Mavilio D. Hepatic natural killer cells: organ-specific sentinels of liver immune homeostasis and physiopathology. *Front Immunol*. 2019;10:946.
 17. Rao R, Samak G. Bile duct epithelial tight junctions and barrier function. *Tissue Barriers*. 2013;1(4):e25718.
 18. Stanger BZ. Cellular homeostasis and repair in the mammalian liver. *Annu Rev Physiol*. 2015;77:179-200.
 19. Blovin A, Bolender R, Weibel E. Distribution of organelles and membranes between hepatocytes and nonhepatocytes in the rat liver parenchyma. *J Cell Biol*. 1977;72:441-55.
 20. Gille C, Bölling C, Hoppe A, Bulik S, Hoffmann S, Hübner K, et al. Hepatonet1: a comprehensive metabolic reconstruction of the human hepatocyte for the analysis of liver physiology. *Molecular Systems Biology*. 2010;6(1):411.
 21. Megías M, Molist P, Pombal M. Atlas of plant and animal histology. Retrieved (June 2023) from: <https://mmegiaswebsuvigoes/02-english/indexhtml>.
 22. Seviour DK, Pelkonen O, Ahokas JT. Hepatocytes: the powerhouse of biotransformation. *The International Journal of Biochemistry & Cell Biology*. 2012;44(2):257-61.
 23. Jaeschke H, Gores GJ, Cederbaum AI, Hinson JA, Pessayre D, Lemasters JJ. Mechanisms of hepatotoxicity. *Toxicological Sciences*. 2002;65(2):166-76.
 24. Zanger UM, Schwab M. Cytochrome P450 enzymes in drug metabolism: regulation of gene expression, enzyme activities, and impact of genetic variation. *Pharmacology & Therapeutics*. 2013;138(1):103-41.
 25. Rui L. Energy metabolism in the liver. *Comprehensive Physiology*. 2014;4(1):177.
 26. Agius L. Glucokinase and molecular aspects of liver glycogen metabolism. *Biochemical Journal*. 2008;414(1):1-18.
 27. Han H-S, Kang G, Kim JS, Choi BH, Koo S-H. Regulation of glucose metabolism from a liver-centric perspective. *Experimental & Molecular Medicine*. 2016;48(3):e218-e.
 28. Engelking L. Textbook of veterinary physiological chemistry. Third ed: Academic Press; 2010.
 29. Exton JH, Friedmann N, Wong EH-A, Brineaux JP, Corbin JD, Park CR. Interaction of glucocorticoids with glucagon and epinephrine in the control of gluconeogenesis and glycogenolysis in liver and of lipolysis in adipose tissue. *Journal of Biological Chemistry*. 1972;247(11):3579-88.
 30. Edwards M, Mohiuddin SS. Biochemistry, lipolysis. StatPearls. Treasure Island (FL): StatPearls Publishing LLC; 2023.

References

31. Laffel L. Ketone bodies: a review of physiology, pathophysiology and application of monitoring to diabetes. *Diabetes/Metabolism Research and Reviews*. 1999;15(6):412-26.
32. Adeva-Andany MM, Funcasta-Calderón R, Fernández-Fernández C, Castro-Quintela E, Carneiro-Freire N. Metabolic effects of glucagon in humans. *Journal of Clinical & Translational Endocrinology*. 2019;15:45-53.
33. Seebacher F, Zeigerer A, Kory N, Kraemer N, editors. *Hepatic lipid droplet homeostasis and fatty liver disease*. Seminars in Cell & Developmental Biology; 2020: Elsevier.
34. Nelson DL, Lehninger AL, Cox MM. *Lehninger principles of biochemistry*: Macmillan; 2018.
35. Kapourchali FR, Surendiran G, Goulet A, Moghadasian MH. The role of dietary cholesterol in lipoprotein metabolism and related metabolic abnormalities: a mini-review. *Critical Reviews in Food Science and Nutrition*. 2016;56(14):2408-15.
36. Luo J, Yang H, Song B-L. Mechanisms and regulation of cholesterol homeostasis. *Nature Reviews Molecular Cell Biology*. 2020;21(4):225-45.
37. Craig M, Yarrarapu SNS, Dimri M. *Biochemistry, cholesterol*: StatPearls Publishing, Treasure Island (FL); 2022.
38. Vance DE, Van den Bosch H. Cholesterol in the year 2000. *Biochimica et Biophysica Acta (BBA)-Molecular and Cell Biology of Lipids*. 2000;1529(1-3):1-8.
39. Schade DS, Shey L, Eaton RP. Cholesterol review: a metabolically important molecule. *Endocrine Practice*. 2020;26(12):1514-23.
40. Errico TL, Chen X, JM MC, Julve J, Escolà-Gil JC, Blanco-Vaca F. Basic mechanisms: structure, function and metabolism of plasma lipoproteins. *Clinica e Investigacion en Arteriosclerosis*. 2013;25(2):98-103.
41. Eisenberg S, Levy RI. Lipoprotein metabolism. *Advances in Lipid Research*. 1975;13:1-89.
42. Gluchowski NL, Becuwe M, Walther TC, Farese Jr RV. Lipid droplets and liver disease: from basic biology to clinical implications. *Nature Reviews Gastroenterology & Hepatology*. 2017;14(6):343-55.
43. Martin S, Parton RG. Lipid droplets: a unified view of a dynamic organelle. *Nat Rev Mol Cell Biol*. 2006;7(5):373-8.
44. Olzmann JA, Carvalho P. Dynamics and functions of lipid droplets. *Nature Reviews Molecular Cell Biology*. 2019;20(3):137-55.
45. Schulze RJ, McNiven MA, editors. *Lipid droplet formation and lipophagy in fatty liver disease*. Seminars in Liver Disease; 2019: Thieme Medical Publishers.
46. Scorletti E, Carr RM. A new perspective on NAFLD: focusing on lipid droplets. *J Hepatol*. 2022;76(4):934-45.
47. Thiam AR, Farese Jr RV, Walther TC. The biophysics and cell biology of lipid droplets. *Nature Reviews Molecular Cell Biology*. 2013;14(12):775-86.

References

48. Jacquier N, Choudhary V, Mari M, Toulmay A, Reggiori F, Schneiter R. Lipid droplets are functionally connected to the endoplasmic reticulum in *Saccharomyces cerevisiae*. *J Cell Sci.* 2011;124(Pt 14):2424-37.
49. Jacquier N, Mishra S, Choudhary V, Schneiter R. Expression of oleosin and perilipins in yeast promotes formation of lipid droplets from the endoplasmic reticulum. *J Cell Sci.* 2013;126(Pt 22):5198-209.
50. Henne WM, Reese ML, Goodman JM. The assembly of lipid droplets and their roles in challenged cells. *The EMBO Journal.* 2018;37(12):e98947.
51. Wilfling F, Haas JT, Walther TC, Farese Jr RV. Lipid droplet biogenesis. *Current Opinion in Cell Biology.* 2014;29:39-45.
52. Choudhary V, Ojha N, Golden A, Prinz WA. A conserved family of proteins facilitates nascent lipid droplet budding from the ER. *Journal of Cell Biology.* 2015;211(2):261-71.
53. Walther TC, Farese Jr RV. Lipid droplets and cellular lipid metabolism. *Annual Review of Biochemistry.* 2012;81:687-714.
54. Wilfling F, Wang H, Haas JT, Krahmer N, Gould TJ, Uchida A, et al. Triacylglycerol synthesis enzymes mediate lipid droplet growth by relocalizing from the ER to lipid droplets. *Developmental Cell.* 2013;24(4):384-99.
55. Dupont N, Chauhan S, Arko-Mensah J, Castillo EF, Masedunskas A, Weigert R, et al. Neutral lipid stores and lipase PNPLA5 contribute to autophagosome biogenesis. *Current Biology.* 2014;24(6):609-20.
56. Murphy S, Martin S, Parton RG. Quantitative analysis of lipid droplet fusion: inefficient steady state fusion but rapid stimulation by chemical fusogens. *PloS One.* 2010;5(12):e15030.
57. Krahmer N, Guo Y, Wilfling F, Hilger M, Lingrell S, Heger K, et al. Phosphatidylcholine synthesis for lipid droplet expansion is mediated by localized activation of CTP: phosphocholine cytidylyltransferase. *Cell Metabolism.* 2011;14(4):504-15.
58. Grabner GF, Xie H, Schweiger M, Zechner R. Lipolysis: cellular mechanisms for lipid mobilization from fat stores. *Nat Metab.* 2021;3(11):1445-65.
59. Fader Kaiser CM, Romano PS, Vanrell MC, Pocognoni CA, Jacob J, Caruso B, et al. Biogenesis and breakdown of lipid droplets in pathological conditions. *Front Cell Dev Biol.* 2021;9:826248.
60. Onal G, Kutlu O, Gozuacik D, Dokmeci Emre S. Lipid droplets in health and disease. *Lipids Health Dis.* 2017;16(1):128.
61. Gatica D, Lahiri V, Klionsky DJ. Cargo recognition and degradation by selective autophagy. *Nature Cell Biology.* 2018;20(3):233-42.
62. Okamoto K. Organellophagy: eliminating cellular building blocks via selective autophagy. *Journal of Cell Biology.* 2014;205(4):435-45.

References

63. Schulze RJ, Krueger EW, Weller SG, Johnson KM, Casey CA, Schott MB, et al. Direct lysosome-based autophagy of lipid droplets in hepatocytes. *Proc Natl Acad Sci U S A*. 2020;117(51):32443-52.
64. Schott MB, Weller SG, Schulze RJ, Krueger EW, Drizyte-Miller K, Casey CA, et al. Lipid droplet size directs lipolysis and lipophagy catabolism in hepatocytes. *J Cell Biol*. 2019;218(10):3320-35.
65. Welte MA, Gould AP. Lipid droplet functions beyond energy storage. *Biochimica et Biophysica Acta (BBA)-Molecular and Cell Biology of Lipids*. 2017;1862(10):1260-72.
66. DeVries-Seimon T, Li Y, Yao PM, Stone E, Wang Y, Davis RJ, et al. Cholesterol-induced macrophage apoptosis requires ER stress pathways and engagement of the type A scavenger receptor. *The Journal of Cell Biology*. 2005;171(1):61-73.
67. Koliwad SK, Streeper RS, Monetti M, Cornelissen I, Chan L, Terayama K, et al. DGAT1-dependent triacylglycerol storage by macrophages protects mice from diet-induced insulin resistance and inflammation. *The Journal of Clinical Investigation*. 2010;120(3):756-67.
68. Rambold AS, Cohen S, Lippincott-Schwartz J. Fatty acid trafficking in starved cells: regulation by lipid droplet lipolysis, autophagy, and mitochondrial fusion dynamics. *Developmental Cell*. 2015;32(6):678-92.
69. Nassir F. NAFLD: mechanisms, treatments, and biomarkers. *Biomolecules*. 2022;12(6).
70. Jin Y, Tan Y, Zhao P, Ren Z. SEIPIN: a key factor for nuclear lipid droplet generation and lipid homeostasis. *International Journal of Molecular Sciences*. 2020;21(21):8208.
71. Tchernof A, Després J-P. Pathophysiology of human visceral obesity: an update. *Physiological Reviews*. 2013;93(1):359-404.
72. Francque SM, Marchesini G, Kautz A, Walmsley M, Dorner R, Lazarus JV, et al. Non-alcoholic fatty liver disease: A patient guideline. *JHEP Rep*. 2021;3(5):100322.
73. Heyens LJM, Busschots D, Koek GH, Robaey G, Francque S. Liver fibrosis in non-alcoholic fatty liver disease: from liver biopsy to non-invasive biomarkers in diagnosis and treatment. *Front Med (Lausanne)*. 2021;8:615978.
74. Mashek DG. Hepatic lipid droplets: a balancing act between energy storage and metabolic dysfunction in NAFLD. *Molecular Metabolism*. 2021;50:101115.
75. Ramos VM, Kowaltowski AJ, Kakimoto PA. Autophagy in hepatic steatosis: a structured review. *Front Cell Dev Biol*. 2021;9:657389.
76. Wei Y, Rector RS, Thyfault JP, Ibdah JA. Nonalcoholic fatty liver disease and mitochondrial dysfunction. *World J Gastroenterol*. 2008;14(2):193-9.
77. Overi D, Carpino G, Franchitto A, Onori P, Gaudio E. Hepatocyte injury and hepatic stem cell niche in the progression of non-alcoholic steatohepatitis. *Cells*. 2020;9(3):590.
78. Paschos P, Paletas K. Non alcoholic fatty liver disease and metabolic syndrome. *Hippokratia*. 2009;13(1):9-19.

References

79. Loomba R, Sanyal AJ. The global NAFLD epidemic. *Nat Rev Gastroenterol Hepatol*. 2013;10(11):686-90.
80. Kaya E, Yilmaz Y. Non-alcoholic fatty liver disease: a global public health issue. *Obesity and Diabetes: Scientific Advances and Best Practice*. 2020:321-33.
81. Kaya E, Yilmaz Y. Metabolic-associated fatty liver disease (MAFLD): a multi-systemic disease beyond the liver. *J Clin Transl Hepatol*. 2022;10(2):329-38.
82. Kotronen A, Westerbacka J, Bergholm R, Pietiläinen KH, Yki-Järvinen H. Liver fat in the metabolic syndrome. *The Journal of Clinical Endocrinology & Metabolism*. 2007;92(9):3490-7.
83. Kotronen A, Yki-Järvinen H. Fatty liver: a novel component of the metabolic syndrome. *Arteriosclerosis, Thrombosis, and Vascular Biology*. 2008;28(1):27-38.
84. Najjar SM, Perdomo G. Hepatic insulin clearance: mechanism and physiology. *Physiology*. 2019;34(3):198-215.
85. Fabbrini E, Sullivan S, Klein S. Obesity and nonalcoholic fatty liver disease: biochemical, metabolic, and clinical implications. *Hepatology*. 2010;51(2):679-89.
86. Ruderman N, Prentki M. AMP kinase and malonyl-CoA: targets for therapy of the metabolic syndrome. *Nature Reviews Drug Discovery*. 2004;3(4):340-51.
87. Eslam M, Newsome PN, Sarin SK, Anstee QM, Targher G, Romero-Gomez M, et al. A new definition for metabolic dysfunction-associated fatty liver disease: an international expert consensus statement. *J Hepatol*. 2020;73(1):202-9.
88. Geisler CE, Renquist BJ. Hepatic lipid accumulation: cause and consequence of dysregulated glucoregulatory hormones. *J Endocrinol*. 2017;234(1):R1-r21.
89. Rossi AP, Fantin F, Zamboni GA, Mazzali G, Rinaldi CA, Del Giglio M, et al. Predictors of ectopic fat accumulation in liver and pancreas in obese men and women. *Obesity (Silver Spring)*. 2011;19(9):1747-54.
90. Haemmerle G, Lass A. Genetically modified mouse models to study hepatic neutral lipid mobilization. *Biochim Biophys Acta Mol Basis Dis*. 2019;1865(5):879-94.
91. Zhang S, Peng X, Yang S, Li X, Huang M, Wei S, et al. The regulation, function, and role of lipophagy, a form of selective autophagy, in metabolic disorders. *Cell Death Dis*. 2022;13(2):132.
92. Park HW, Park H, Semple IA, Jang I, Ro SH, Kim M, et al. Pharmacological correction of obesity-induced autophagy arrest using calcium channel blockers. *Nat Commun*. 2014;5:4834.
93. Arruda AP, Hotamisligil GS. Calcium homeostasis and organelle function in the pathogenesis of obesity and diabetes. *Cell Metab*. 2015;22(3):381-97.
94. Degli Esposti D, Hamelin J, Bosselut N, Saffroy R, Sebah M, Pommier A, et al. Mitochondrial roles and cytoprotection in chronic liver injury. *Biochem Res Int*. 2012;2012:387626.
95. Weinberg SE, Chandel NS. Targeting mitochondria metabolism for cancer therapy. *Nat Chem Biol*. 2015;11(1):9-15.

References

96. Kastaniotis AJ, Autio KJ, Kerätär JM, Monteuuis G, Mäkelä AM, Nair RR, et al. Mitochondrial fatty acid synthesis, fatty acids and mitochondrial physiology. *Biochim Biophys Acta Mol Cell Biol Lipids*. 2017;1862(1):39-48.
97. Léveillé M, Estall JL. Mitochondrial dysfunction in the transition from NASH to HCC. *Metabolites*. 2019;9(10):233.
98. Masarone M, Rosato V, Dallio M, Gravina AG, Aglitti A, Loguercio C, et al. Role of oxidative stress in pathophysiology of nonalcoholic fatty liver disease. *Oxidative Medicine and Cellular Longevity*. 2018;2018:9547613.
99. Gurung P, Lukens JR, Kanneganti TD. Mitochondria: diversity in the regulation of the NLRP3 inflammasome. *Trends Mol Med*. 2015;21(3):193-201.
100. Delli Bovi AP, Marciano F, Mandato C, Siano MA, Savoia M, Vajro P. Oxidative stress in non-alcoholic fatty liver disease. An updated mini review. *Frontiers in Medicine*. 2021;8:595371.
101. Arroyave-Ospina JC, Wu Z, Geng Y, Moshage H. Role of oxidative stress in the pathogenesis of non-alcoholic fatty liver disease: implications for prevention and therapy. *Antioxidants (Basel)*. 2021;10(2):174.
102. Ore A, Akinloye OA. Oxidative stress and antioxidant biomarkers in clinical and experimental models of non-alcoholic fatty liver disease. *Medicina*. 2019;55(2):26.
103. Rolo AP, Teodoro JS, Palmeira CM. Role of oxidative stress in the pathogenesis of nonalcoholic steatohepatitis. *Free Radical Biology and Medicine*. 2012;52(1):59-69.
104. Serviddio G, Bellanti F, Vendemiale G. Free radical biology for medicine: learning from nonalcoholic fatty liver disease. *Free Radical Biology and Medicine*. 2013;65:952-68.
105. Chen Z, Tian R, She Z, Cai J, Li H. Role of oxidative stress in the pathogenesis of nonalcoholic fatty liver disease. *Free Radical Biology and Medicine*. 2020;152:116-41.
106. Watanabe S, Yaginuma R, Ikejima K, Miyazaki A. Liver diseases and metabolic syndrome. *Journal of Gastroenterology*. 2008;43:509-18.
107. Kneeman JM, Misdraji J, Corey KE. Secondary causes of nonalcoholic fatty liver disease. *Therapeutic Advances in Gastroenterology*. 2012;5(3):199-207.
108. Duvnjak M, Lerotić I, Barsić N, Tomasić V, Virović Jukić L, Velagić V. Pathogenesis and management issues for non-alcoholic fatty liver disease. *World J Gastroenterol*. 2007;13(34):4539-50.
109. Hashimoto E, Taniai M, Tokushige K. Characteristics and diagnosis of NAFLD/NASH. *J Gastroenterol Hepatol*. 2013;28 Suppl 4:64-70.
110. Lonardo A, Mantovani A, Lugari S, Targher G. NAFLD in some common endocrine diseases: prevalence, pathophysiology, and principles of diagnosis and management. *International Journal of Molecular Sciences*. 2019;20(11):2841.
111. Chander PN, Gealekman O, Brodsky SV, Elitok S, Tojo A, Crabtree M, et al. Nephropathy in zucker diabetic fat rat is associated with oxidative and nitrosative

References

- stress: prevention by chronic therapy with a peroxynitrite scavenger ebselen. *Journal of the American Society of Nephrology*. 2004;15(9):2391-403.
112. Almeda-Valdés P, Cuevas-Ramos D, Aguilar-Salinas CA. Metabolic syndrome and non-alcoholic fatty liver disease. *Annals of Hepatology*. 2009;8(S1):18-24.
113. Bedossa P. Pathology of non-alcoholic fatty liver disease. *Liver International*. 2017;37(S1):85-9.
114. Feldstein AE, Canbay A, Angulo P, Taniguchi M, Burgart LJ, Lindor KD, et al. Hepatocyte apoptosis and fas expression are prominent features of human nonalcoholic steatohepatitis. *Gastroenterology*. 2003;125(2):437-43.
115. Cohen JC, Horton JD, Hobbs HH. Human fatty liver disease: old questions and new insights. *Science*. 2011;332(6037):1519-23.
116. Tilg H, Moschen AR. Evolution of inflammation in nonalcoholic fatty liver disease: the multiple parallel hits hypothesis. *Hepatology*. 2010;52(5):1836-46.
117. Gordaliza-Alaguero I, Cantó C, Zorzano A. Metabolic implications of organelle-mitochondria communication. *EMBO Rep*. 2019;20(9):e47928.
118. Cai Q, Wang Z, Zhang R, Zhang L, Cui S, Lin H, et al. Huangjia ruangan granule inhibits inflammation in a rat model with liver fibrosis by regulating TNF/MAPK and NF- κ B signaling pathways. *Evid Based Complement Alternat Med*. 2022;2022:8105306.
119. Kisseleva T, Brenner D. Molecular and cellular mechanisms of liver fibrosis and its regression. *Nat Rev Gastroenterol Hepatol*. 2021;18(3):151-66.
120. Vilar-Gomez E, Calzadilla-Bertot L, Wai-Sun Wong V, Castellanos M, Aller-de la Fuente R, Metwally M, et al. Fibrosis severity as a determinant of cause-specific mortality in patients With advanced nonalcoholic fatty liver disease: a multinational cohort study. *Gastroenterology*. 2018;155(2):443-57.e17.
121. Loomba R, Huang DQ, Sanyal AJ, Anstee QM, Trauner M, Lawitz EJ, et al. Liver stiffness thresholds to predict disease progression and clinical outcomes in bridging fibrosis and cirrhosis. *Gut*. 2023;72(3):581-9.
122. Kumar R, Priyadarshi RN, Anand U. Non-alcoholic fatty liver disease: growing burden, adverse outcomes and associations. *J Clin Transl Hepatol*. 2020;8(1):76-86.
123. Gomaa AI, Khan SA, Toledano MB, Waked I, Taylor-Robinson SD. Hepatocellular carcinoma: epidemiology, risk factors and pathogenesis. *World J Gastroenterol*. 2008;14(27):4300-8.
124. El-Serag HB, Rudolph KL. Hepatocellular carcinoma: epidemiology and molecular carcinogenesis. *Gastroenterology*. 2007;132(7):2557-76.
125. Marrero JA, Fontana RJ, Su GL, Conjeevaram HS, Emick DM, Lok AS. NAFLD may be a common underlying liver disease in patients with hepatocellular carcinoma in the United States. *Hepatology*. 2002;36(6):1349-54.
126. Balogh J, Victor III D, Asham EH, Burroughs SG, Boktour M, Saharia A, et al. Hepatocellular carcinoma: a review. *Journal of Hepatocellular Carcinoma*. 2016:41-53.

References

127. Suresh D, Srinivas AN, Kumar DP. Etiology of hepatocellular carcinoma: special focus on fatty liver disease. *Front Oncol.* 2020;10:601710.
128. Brunt EM, Wong VWS, Nobili V, Day CP, Sookoian S, Maher JJ, et al. Nonalcoholic fatty liver disease. *Nature Reviews Disease Primers.* 2015;1(1):15080.
129. Farrell GC, Larter CZ. Nonalcoholic fatty liver disease: from steatosis to cirrhosis. *Hepatology.* 2006;43(2 Suppl 1):S99-s112.
130. Hynes RO. The extracellular matrix: not just pretty fibrils. *Science.* 2009;326(5957):1216-9.
131. Rahman S, Patel Y, Murray J, Patel KV, Sumathipala R, Sobel M, et al. Novel hepatocyte growth factor (HGF) binding domains on fibronectin and vitronectin coordinate a distinct and amplified Met-integrin induced signalling pathway in endothelial cells. *BMC Cell Biol.* 2005;6(1):8.
132. Chitturi S, Farrell G, Frost L, Kriketos A, Lin R, Fung C, et al. Serum leptin in NASH correlates with hepatic steatosis but not fibrosis: a manifestation of lipotoxicity? *Hepatology.* 2002;36(2):403-9.
133. Siegel AB, Zhu AX. Metabolic syndrome and hepatocellular carcinoma: two growing epidemics with a potential link. *Cancer.* 2009;115(24):5651-61.
134. Bessone F, Razori MV, Roma MG. Molecular pathways of nonalcoholic fatty liver disease development and progression. *Cell Mol Life Sci.* 2019;76(1):99-128.
135. Bellentani S. The epidemiology of non-alcoholic fatty liver disease. *Liver Int.* 2017;37 Suppl 1:81-4.
136. Xu L, Nagata N, Ota T. Impact of glucoraphanin-mediated activation of Nrf2 on non-alcoholic fatty liver disease with a focus on mitochondrial dysfunction. *Int J Mol Sci.* 2019;20(23).
137. Plaz Torres MC, Aghemo A, Lleo A, Bodini G, Furnari M, Marabotto E, et al. Mediterranean diet and NAFLD: what we know and questions that still need to be answered. *Nutrients.* 2019;11(12).
138. Bach-Faig A, Berry EM, Lairon D, Reguant J, Trichopoulou A, Dernini S, et al. Mediterranean diet pyramid today. Science and cultural updates. *Public Health Nutr.* 2011;14(12a):2274-84.
139. Guasch-Ferré M, Willett WC. The Mediterranean diet and health: a comprehensive overview. *J Intern Med.* 2021;290(3):549-66.
140. Anania C, Perla FM, Olivero F, Pacifico L, Chiesa C. Mediterranean diet and nonalcoholic fatty liver disease. *World J Gastroenterol.* 2018;24(19):2083-94.
141. Lou-Bonafonte JM, Arnal C, Navarro MA, Osada J. Efficacy of bioactive compounds from extra virgin olive oil to modulate atherosclerosis development. *Molecular Nutrition & Food Research.* 2012;56(7):1043-57.
142. Keys A. Coronary heart disease in seven countries. *Circulation.* 1970;41(1):186-95.

References

143. Keys A, Mienotti A, Karvonen MJ, Aravanis C, Blackburn H, Buzina R, et al. The diet and 15-year death rate in the seven countries study. *American Journal of Epidemiology*. 1986;124(6):903-15.
144. Jimenez-Lopez C, Carpena M, Lourenço-Lopes C, Gallardo-Gomez M, Lorenzo JM, Barba FJ, et al. Bioactive compounds and quality of extra virgin olive oil. *Foods*. 2020;9(8).
145. Schröder H. Protective mechanisms of the Mediterranean diet in obesity and type 2 diabetes. *J Nutr Biochem*. 2007;18(3):149-60.
146. Esposito K, Maiorino MI, Bellastella G, Chiodini P, Panagiotakos D, Giugliano D. A journey into a Mediterranean diet and type 2 diabetes: a systematic review with meta-analyses. *BMJ Open*. 2015;5(8):e008222.
147. Esposito K, Giugliano D. Mediterranean diet and type 2 diabetes. *Diabetes/Metabolism Research and Reviews*. 2014;30(S1):34-40.
148. De Pergola G, D'Alessandro A. Influence of Mediterranean diet on blood pressure. *Nutrients*. 2018;10(11).
149. Gelli C, Tarocchi M, Abenavoli L, Di Renzo L, Galli A, De Lorenzo A. Effect of a counseling-supported treatment with the Mediterranean diet and physical activity on the severity of the non-alcoholic fatty liver disease. *World J Gastroenterol*. 2017;23(17):3150-62.
150. Trichopoulou A, Costacou T, Bamia C, Trichopoulos D. Adherence to a Mediterranean diet and survival in a Greek population. *New England Journal of Medicine*. 2003;348(26):2599-608.
151. Mitrou PN, Kipnis V, Thiébaud AC, Reedy J, Subar AF, Wirfält E, et al. Mediterranean dietary pattern and prediction of all-cause mortality in a US population: results from the NIH-AARP diet and health study. *Arch Intern Med*. 2007;167(22):2461-8.
152. Gaforio JJ, Visioli F, Alarcón-de-la-Lastra C, Castañer O, Delgado-Rodríguez M, Fitó M, et al. Virgin olive oil and health: summary of the III International conference on virgin olive oil and health consensus report, JAEN (spain) 2018. *Nutrients*. 2019;11(9):2039.
153. Estruch R, Ros E, Salas-Salvado J, Covas MI, Corella D, Aros F, et al. Primary prevention of cardiovascular disease with a Mediterranean diet supplemented with extra-virgin olive oil or nuts. *N Engl J Med*. 2018;378(25):e34.
154. Delgado-Lista J, Alcalá-Díaz JF, Torres-Peña JD, Quintana-Navarro GM, Fuentes F, García-Ríos A, et al. Long-term secondary prevention of cardiovascular disease with a Mediterranean diet and a low-fat diet (CORDIOPREV): a randomised controlled trial. *Lancet*. 2022;399(10338):1876-85.
155. Romagnolo DF, Selmin OI. Mediterranean diet and prevention of chronic diseases. *Nutr Today*. 2017;52(5):208-22.
156. Berná G, Romero-Gomez M. The role of nutrition in non-alcoholic fatty liver disease: Pathophysiology and management. *Liver Int*. 2020;40 Suppl 1:102-8.

References

157. Rodriguez-Rodriguez R, Perona JS, Herrera MD, Ruiz-Gutierrez V. Triterpenic compounds from “orujo” olive oil elicit vasorelaxation in aorta from spontaneously hypertensive rats. *Journal of Agricultural and Food Chemistry*. 2006;54(6):2096-102.
158. Marquez-Martin A, De La Puerta R, Fernandez-Arche A, Ruiz-Gutierrez V, Yaqoob P. Modulation of cytokine secretion by pentacyclic triterpenes from olive pomace oil in human mononuclear cells. *Cytokine*. 2006;36(5-6):211-7.
159. González-Rámila S, Sarriá B, Seguido MA, García-Cordero J, Mateos R, Bravo L. Olive pomace oil can improve blood lipid profile: a randomized, blind, crossover, controlled clinical trial in healthy and at-risk volunteers. *Eur J Nutr*. 2023;62(2):589-603.
160. Piroddi M, Albin A, Fabiani R, Giovannelli L, Luceri C, Natella F, et al. Nutrigenomics of extra-virgin olive oil: A review. *Biofactors*. 2017;43(1):17-41.
161. Pérez-Camino MC, Cert A. Quantitative determination of hydroxy pentacyclic triterpene acids in vegetable oils. *J Agric Food Chem*. 1999;47(4):1558-62.
162. Ghanbari R, Anwar F, Alkharfy KM, Gilani AH, Saari N. Valuable nutrients and functional bioactives in different parts of olive (*Olea europaea* L.)-a review. *Int J Mol Sci*. 2012;13(3):3291-340.
163. Tsimidou MZ. Virgin olive oil (VOO) and other olive tree products as sources of α -tocopherol. updating and perspective. Nova Science Publisher: New York, NY, USA; 2012. p. 1-21.
164. Mateos R, Domínguez MM, Espartero JL, Cert A. Antioxidant effect of phenolic compounds, alpha-tocopherol, and other minor components in virgin olive oil. *J Agric Food Chem*. 2003;51(24):7170-5.
165. Spanova M, Daum G. Squalene—biochemistry, molecular biology, process biotechnology, and applications. *European Journal of Lipid Science and Technology*. 2011;113(11):1299-320.
166. Martinez-Beamonte R, Sanclemente T, Surra JC, Osada J. Could squalene be an added value to use olive by-products? *J Sci Food Agric*. 2020;100(3):915-25.
167. Simon SA, Lis LJ, MacDonald RC, Kauffman JW. The noneffect of a large linear hydrocarbon, squalene, on the phosphatidylcholine packing structure. *Biophys J*. 1977;19(1):83-90.
168. Lou-Bonafonte JM, Martinez-Beamonte R, Sanclemente T, Surra JC, Herrera-Marcos LV, Sanchez-Marco J, et al. Current insights into the biological action of squalene. *Mol Nutr Food Res*. 2018;8:e1800136.
169. Fahy E, Subramaniam S, Murphy RC, Nishijima M, Raetz CR, Shimizu T, et al. Update of the lipid maps comprehensive classification system for lipids. *J Lipid Res*. 2009;50 Suppl(Suppl):S9-14.
170. Ernst J, Sheldrick WS, Fuhrhop JH. The crystal structure of squalene. *Angew Chem Int Ed Engl*. 1976;15(12):778.
171. Shahidi F, Varatharajan V, Peng H, Senadheera R. Utilization of marine by-products for the recovery of value-added products. *Journal of Food Bioactives*. 2019;6:10-61.

References

172. Popa O, Băbeanu NE, Popa I, Niță S, Dinu-Pârvu CE. Methods for obtaining and determination of squalene from natural sources. *Biomed Res Int.* 2015;2015:367202.
173. Pham DM, Boussouira B, Moyal D, Nguyen QL. Oxidization of squalene, a human skin lipid: a new and reliable marker of environmental pollution studies. *Int J Cosmet Sci.* 2015;37(4):357-65.
174. Patel A, Bettiga M, Rova U, Christakopoulos P, Matsakas L. Microbial genetic engineering approach to replace shark livering for squalene. *Trends Biotechnol.* 2022;40(10):1261-73.
175. Turchini GM, Ng W-K, Tocher DR. Fish oil replacement and alternative lipid sources in aquaculture feeds: CRC Press; 2010.
176. Schnetzler KA. Food uses and amaranth product research: a comprehensive review. *Amaranth Biology, Chemistry, and Technology.* 2018:155-84.
177. Lozano-Grande MA, Gorinstein S, Espitia-Rangel E, Dávila-Ortiz G, Martínez-Ayala AL. Plant sources, extraction methods, and uses of squalene. *International Journal of Agronomy.* 2018;2018.
178. Smith TJ. Squalene: potential chemopreventive agent. *Expert Opinion on Investigational Drugs.* 2000;9(8):1841-8.
179. Kostyuk V, Potapovich A, Stancato A, De Luca C, Lulli D, Pastore S, et al. Photo-oxidation products of skin surface squalene mediate metabolic and inflammatory responses to solar UV in human keratinocytes. *PLoS One.* 2012;7(8):e44472.
180. Rajaratnam RA, Gylling H, Miettinen TA. Serum squalene in postmenopausal women without and with coronary artery disease. *Atherosclerosis.* 1999;146(1):61-4.
181. Strandberg TE, Tilvis RS, Miettinen TA. Metabolic variables of cholesterol during squalene feeding in humans: comparison with cholestyramine treatment. *J Lipid Res.* 1990;31(9):1637-43.
182. Tilvis RS, Miettinen TA. Absorption and metabolic fate of dietary 3H-squalene in the rat. *Lipids.* 1983;18(3):233-8.
183. Gylling H, Miettinen TA. Postabsorptive metabolism of dietary squalene. *Atherosclerosis.* 1994;106(2):169-78.
184. Goldstein JL, DeBose-Boyd RA, Brown MS. Protein sensors for membrane sterols. *Cell.* 2006;124(1):35-46.
185. Veillard NR, Mach F. Statins: the new aspirin? *Cell Mol Life Sci.* 2002;59(11):1771-86.
186. Goldstein JL, Brown MS. Regulation of the mevalonate pathway. *Nature.* 1990;343(6257):425-30.
187. Edwards PA, Ericsson J. Sterols and isoprenoids: signaling molecules derived from the cholesterol biosynthetic pathway. *Annu Rev Biochem.* 1999;68:157-85.
188. Brown MS, Goldstein JL. Multivalent feedback regulation of HMG CoA reductase, a control mechanism coordinating isoprenoid synthesis and cell growth. *J Lipid Res.* 1980;21(5):505-17.

References

189. Brown MS, Goldstein JL, Siperstein MD. Regulation of cholesterol synthesis in normal and malignant tissue. *Fed Proc.* 1973;32(12):2168-73.
190. Tansey TR, Shechter I. Structure and regulation of mammalian squalene synthase. *Biochim Biophys Acta.* 2000;1529(1-3):49-62.
191. Mitsche MA, McDonald JG, Hobbs HH, Cohen JC. Flux analysis of cholesterol biosynthesis in vivo reveals multiple tissue and cell-type specific pathways. *Elife.* 2015;4:e07999.
192. Bloch K. The biological synthesis of cholesterol. *Science.* 1965;150(3692):19-28.
193. Kandutsch AA, Russell AE. Preputial gland tumor sterols. 2. The identification of 4 alpha-methyl-Delta 8-cholesten-3 beta-ol. *J Biol Chem.* 1960;235:2253-5.
194. Kelly GS. Squalene and its potential clinical uses. *Altern Med Rev.* 1999;4(1):29-36.
195. Huang ZR, Lin YK, Fang JY. Biological and pharmacological activities of squalene and related compounds: potential uses in cosmetic dermatology. *Molecules.* 2009;14(1):540-54.
196. Hancock JF, Magee AI, Childs JE, Marshall CJ. All ras proteins are polyisoprenylated but only some are palmitoylated. *Cell.* 1989;57(7):1167-77.
197. Sheares BT, White SS, Molowa DT, Chan K, Ding VD, Kroon PA, et al. Cloning, analysis, and bacterial expression of human farnesyl pyrophosphate synthetase and its regulation in Hep G2 cells. *Biochemistry.* 1989;28(20):8129-35.
198. Wolda SL, Glomset JA. Evidence for modification of lamin B by a product of mevalonic acid. *J Biol Chem.* 1988;263(13):5997-6000.
199. Rao CV, Newmark HL, Reddy BS. Chemopreventive effect of squalene on colon cancer. *Carcinogenesis.* 1998;19(2):287-90.
200. Herrera-Marcos LV, Martínez-Beamonte R, Arnal C, Barranquero C, Puente-Lanzarote JJ, Herrero-Continente T, et al. Dietary squalene supplementation decreases triglyceride species and modifies phospholipid lipidomic profile in the liver of a porcine model of non-alcoholic steatohepatitis. *J Nutr Biochem.* 2023;112:109207.
201. Llovet JM, Willoughby CE, Singal AG, Greten TF, Heikenwälder M, El-Serag HB, et al. Nonalcoholic steatohepatitis-related hepatocellular carcinoma: pathogenesis and treatment. *Nat Rev Gastroenterol Hepatol.* 2023;20(8):487-503.
202. Ronco AL, De Stéfani E. Squalene: a multi-task link in the crossroads of cancer and aging. *Functional Foods in Health and Disease.* 2013;3(12):462-76.
203. Mariani C. On the complexity of sterol fraction in olive oil. *Rivista Italiana Delle Sostanze Grasse* 2016;93(3):147-55.
204. Blanch GP, Villén J, Herraiz M. Rapid analysis of free erythrodiol and uvaol in olive oils by coupled reversed phase liquid chromatography- gas chromatography. *Journal of Agricultural and Food Chemistry.* 1998;46(3):1027-30.

References

205. Allouche Y, Jiménez A, Uceda M, Aguilera MP, Gaforio JJ, Beltrán G. Triterpenic content and chemometric analysis of virgin olive oils from forty olive cultivars. *J Agric Food Chem.* 2009;57(9):3604-10.
206. Acin S, Navarro MA, Perona JS, Surra JC, Guillen N, Arnal C, et al. Microarray analysis of hepatic genes differentially expressed in the presence of the unsaponifiable fraction of olive oil in apolipoprotein E-deficient mice. *Br J Nutr.* 2007;97(4):628-38.
207. Abboud R, Charcosset C, Greige-Gerges H. Tetra- and penta-cyclic triterpenes interaction with lipid bilayer membrane: a structural comparative study. *J Membr Biol.* 2016;249(3):327-38.
208. Guinda A, Rada M, Delgado T, Gutiérrez-Adán P, Castellano JM. Pentacyclic triterpenoids from olive fruit and leaf. *J Agric Food Chem.* 2010;58(17):9685-91.
209. Peragón J. Time course of pentacyclic triterpenoids from fruits and leaves of olive tree (*Olea europaea* L.) cv. Picual and cv. Cornezuelo during ripening. *J Agric Food Chem.* 2013;61(27):6671-8.
210. Abbass HS, Ragab EA, Mohammed A, El-Hela A. Phytochemical and biological investigation of *Ficus mysorensis* cultivated in Egypt. *J Pharm Chem Biol Sci.* 2015;3:396-407.
211. Chen HL, Lin KW, Huang AM, Tu HY, Wei BL, Hour TC, et al. Terpenoids induce cell cycle arrest and apoptosis from the stems of *Celastrus kusanoi* associated with reactive oxygen species. *J Agric Food Chem.* 2010;58(6):3808-12.
212. Nkengfack AE, Azebaze AG, Waffo AK, Fomum ZT, Meyer M, van Heerden FR. Cytotoxic isoflavones from *Erythrina indica*. *Phytochemistry.* 2001;58(7):1113-20.
213. Ebeling S, Naumann K, Pollok S, Wardecki T, Vidal YSS, Nascimento JM, et al. From a traditional medicinal plant to a rational drug: understanding the clinically proven wound healing efficacy of birch bark extract. *PLoS One.* 2014;9(1):e86147.
214. Xiaoli L, Naili W, Sau WM, Chen AS, Xinsheng Y. Four new isoflavonoids from the stem bark of *Erythrina variegata*. *Chem Pharm Bull (Tokyo).* 2006;54(4):570-3.
215. Peñas-Fuentes JL, Siles E, Rufino-Palomares EE, Pérez-Jiménez A, Reyes-Zurita FJ, Lupiáñez JA, et al. Effects of erythrodiol on the antioxidant response and proteome of HepG2 Cells. *Antioxidants (Basel).* 2021;11(1):73.
216. Juan ME, Wenzel U, Daniel H, Planas JM. Erythrodiol, a natural triterpenoid from olives, has antiproliferative and apoptotic activity in HT-29 human adenocarcinoma cells. *Mol Nutr Food Res.* 2008;52(5):595-9.
217. Perona JS, Arcemis C, Ruiz-Gutierrez V, Catalá A. Effect of dietary high-oleic-acid oils that are rich in antioxidants on microsomal lipid peroxidation in rats. *J Agric Food Chem.* 2005;53(3):730-5.
218. Sánchez-Quesada C, López-Biedma A, Warleta F, Campos M, Beltrán G, Gaforio JJ. Bioactive properties of the main triterpenes found in olives, virgin olive oil, and leaves of *Olea europaea*. *J Agric Food Chem.* 2013;61(50):12173-82.

References

219. Allouche Y, Warleta F, Campos M, Sánchez-Quesada C, Uceda M, Beltrán G, et al. Antioxidant, antiproliferative, and pro-apoptotic capacities of pentacyclic triterpenes found in the skin of olives on MCF-7 human breast cancer cells and their effects on DNA damage. *J Agric Food Chem.* 2011;59(1):121-30.
220. Martín R, Ibeas E, Carvalho-Tavares J, Hernández M, Ruiz-Gutierrez V, Nieto ML. Natural triterpenic diols promote apoptosis in astrocytoma cells through ROS-mediated mitochondrial depolarization and JNK activation. *PLoS One.* 2009;4(6):e5975.
221. Rodríguez-Rodríguez R, Herrera MD, Perona JS, Ruiz-Gutiérrez V. Potential vasorelaxant effects of oleanolic acid and erythrodiol, two triterpenoids contained in 'orujo' olive oil, on rat aorta. *British Journal of Nutrition.* 2004;92(4):635-42.
222. Martín R, Miana M, Jurado-López R, Martínez-Martínez E, Gómez-Hurtado N, Delgado C, et al. DIOL triterpenes block profibrotic effects of angiotensin II and protect from cardiac hypertrophy. *PLoS One.* 2012;7(7):e41545.
223. Allouche Y, Beltrán G, Gaforio JJ, Uceda M, Mesa MD. Antioxidant and antiatherogenic activities of pentacyclic triterpenic diols and acids. *Food and Chemical Toxicology.* 2010;48(10):2885-90.
224. Rodríguez-Rodríguez R, Herrera MD, De Sotomayor MA, Ruiz-Gutierrez V. Pomace olive oil improves endothelial function in spontaneously hypertensive rats by increasing endothelial nitric oxide synthase expression. *American Journal of Hypertension.* 2007;20(7):728-34.
225. Rodríguez-Rodríguez R, Herrera MD, De Sotomayor MA, Ruiz-Gutierrez V. Effects of pomace olive oil-enriched diets on endothelial function of small mesenteric arteries from spontaneously hypertensive rats. *British Journal of Nutrition.* 2009;102(10):1435-44.
226. Kontogianni VG, Tsoumani ME, Kellici TF, Mavromoustakos T, Gerothanassis IP, Tselepis AD, et al. Deconvoluting the dual antiplatelet activity of a plant extract. *J Agric Food Chem.* 2016;64(22):4511-21.
227. Waterston RH, Lindblad-Toh K, Birney E, Rogers J, Abril JF, Agarwal P, et al. Initial sequencing and comparative analysis of the mouse genome. *Nature.* 2002;420(6915):520-62.
228. Rydell-Törmänen K, Johnson JR. The applicability of mouse models to the study of human disease. *Methods Mol Biol.* 2019;1940:3-22.
229. Guilbault C, Saeed Z, Downey GP, Radzioch D. Cystic fibrosis mouse models. *Am J Respir Cell Mol Biol.* 2007;36(1):1-7.
230. Nagy A. Manipulating the mouse embryo. A laboratory manual. Cold Spring Harbor Laboratory Press. 2003.
231. Ajayi AF, Akhigbe RE. Staging of the estrous cycle and induction of estrus in experimental rodents: an update. *Fertil Res Pract.* 2020;6:5.
232. Ihara T. Comparative study of developmental progress in the mouse, rat and rabbit in their stages of organogenesis. *Congenital Anomalies.* 1970;10(2):67-81.

References

233. Mapara M, Thomas BS, Bhat KM. Rabbit as an animal model for experimental research. *Dent Res J (Isfahan)*. 2012;9(1):111-8.
234. Zhang X, Lerman LO. Investigating the metabolic syndrome: contributions of swine models. *Toxicol Pathol*. 2016;44(3):358-66.
235. Jiang C, Li P, Ruan X, Ma Y, Kawai K, Suemizu H, et al. Comparative transcriptomics analyses in livers of mice, humans, and humanized mice define human-specific gene networks. *Cells*. 2020;9(12).
236. Pendse AA, Arbones-Mainar JM, Johnson LA, Altenburg MK, Maeda N. Apolipoprotein E knock-out and knock-in mice: atherosclerosis, metabolic syndrome, and beyond. *J Lipid Res*. 2009;50 Suppl(Suppl):S178-82.
237. Arias-Mutis Ó J, Genovés P, Calvo CJ, Díaz A, Parra G, Such-Miquel L, et al. An experimental model of diet-induced metabolic syndrome in rabbit: methodological considerations, development, and assessment. *J Vis Exp*. 2018(134).
238. Marais AD. Apolipoprotein E in lipoprotein metabolism, health and cardiovascular disease. *Pathology*. 2019;51(2):165-76.
239. Yao X, Gordon EM, Figueroa DM, Barochia AV, Levine SJ. Emerging roles of apolipoprotein E and apolipoprotein A-I in the pathogenesis and treatment of lung disease. *Am J Respir Cell Mol Biol*. 2016;55(2):159-69.
240. Valanti EK, Dalakoura-Karagkouni K, Sanoudou D. Current and emerging reconstituted HDL-apoA-I and HDL-apoE approaches to treat atherosclerosis. *J Pers Med*. 2018;8(4):34.
241. Osada J, Joven J, Maeda N. The value of apolipoprotein E knockout mice for studying the effects of dietary fat and cholesterol on atherogenesis. *Current Opinion in Lipidology*. 2000;11(1):25-9.
242. Mahley RW, Weisgraber KH, Huang Y. Apolipoprotein E: structure determines function, from atherosclerosis to Alzheimer's disease to AIDS. *J Lipid Res*. 2009;50 Suppl(Suppl):S183-8.
243. Saito H, Lund-Katz S, Phillips MC. Contributions of domain structure and lipid interaction to the functionality of exchangeable human apolipoproteins. *Prog Lipid Res*. 2004;43(4):350-80.
244. Niemeier A, Gåfvels M, Heeren J, Meyer N, Angelin B, Beisiegel U. VLDL receptor mediates the uptake of human chylomicron remnants in vitro. *J Lipid Res*. 1996;37(8):1733-42.
245. Sarria AJ, Surra JC, Acin S, Carnicer R, Navarro MA, Arbones-Mainar JM, et al. Understanding the role of dietary components on atherosclerosis using genetic engineered mouse models. *Front Biosci*. 2006;11:955-67.
246. Zheng F, Cai Y. Concurrent exercise improves insulin resistance and nonalcoholic fatty liver disease by upregulating PPAR- γ and genes involved in the beta-oxidation of fatty acids in ApoE-KO mice fed a high-fat diet. *Lipids Health Dis*. 2019;18(1):6.
247. Kampschulte M, Stöckl C, Langheinrich AC, Althöhn U, Bohle RM, Krombach GA, et al. Western diet in ApoE-LDLR double-deficient mouse model of atherosclerosis

References

- leads to hepatic steatosis, fibrosis, and tumorigenesis. *Lab Invest.* 2014;94(11):1273-82.
248. Padró T, Cubedo J, Camino S, Béjar MT, Ben-Aicha S, Mendieta G, et al. Detrimental effect of hypercholesterolemia on high-density lipoprotein particle remodeling in pigs. *J Am Coll Cardiol.* 2017;70(2):165-78.
249. Rader DJ. Molecular regulation of HDL metabolism and function: implications for novel therapies. *J Clin Invest.* 2006;116(12):3090-100.
250. Wang N, Silver DL, Costet P, Tall AR. Specific binding of apoA-I, enhanced cholesterol efflux, and altered plasma membrane morphology in cells expressing ABC1. *J Biol Chem.* 2000;275(42):33053-8.
251. Rigotti A, Trigatti B, Babitt J, Penman M, Xu S, Krieger M. Scavenger receptor BI--a cell surface receptor for high density lipoprotein. *Curr Opin Lipidol.* 1997;8(3):181-8.
252. Castro GR, Fielding CJ. Early incorporation of cell-derived cholesterol into pre-beta-migrating high-density lipoprotein. *Biochemistry.* 1988;27(1):25-9.
253. Frank PG, Marcel YL. Apolipoprotein AI: structure-function relationships. *Journal of Lipid Research.* 2000;41(6):853-72.
254. Zannis VI, Chroni A, Krieger M. Role of apoA-I, ABCA1, LCAT, and SR-BI in the biogenesis of HDL. *J Mol Med (Berl).* 2006;84(4):276-94.
255. Gordon SM, Hofmann S, Askew DS, Davidson WS. High density lipoprotein: it's not just about lipid transport anymore. *Trends Endocrinol Metab.* 2011;22(1):9-15.
256. Barker WC, Dayhoff MO. Evolution of lipoproteins deduced from protein sequence data. *Comp Biochem Physiol B.* 1977;57(4):309-15.
257. Fitch WM. Phylogenies constrained by the crossover process as illustrated by human hemoglobins and a thirteen-cycle, eleven-amino-acid repeat in human apolipoprotein A-I. *Genetics.* 1977;86(3):623-44.
258. Li WH, Tanimura M, Luo CC, Datta S, Chan L. The apolipoprotein multigene family: biosynthesis, structure, structure-function relationships, and evolution. *J Lipid Res.* 1988;29(3):245-71.
259. McLachlan AD. Repeated helical pattern in apolipoprotein-A-I. *Nature.* 1977;267(5610):465-6.
260. Williamson R, Lee D, Hagaman J, Maeda N. Marked reduction of high density lipoprotein cholesterol in mice genetically modified to lack apolipoprotein A-I. *Proc Natl Acad Sci U S A.* 1992;89(15):7134-8.
261. Osada J, Maeda N. Preparation of knockout mice. In: Ordovas JM, editor. *Lipoprotein Protocols.* Totowa, NJ: Humana Press; 1998. p. 79-92.
262. Hovingh GK, de Groot E, van der Steeg W, Boekholdt SM, Hutten BA, Kuivenhoven JA, et al. Inherited disorders of HDL metabolism and atherosclerosis. *Curr Opin Lipidol.* 2005;16(2):139-45.

References

263. Karavia EA, Papachristou DJ, Liopeta K, Triantaphyllidou IE, Dimitrakopoulos O, Kypreos KE. Apolipoprotein A-I modulates processes associated with diet-induced nonalcoholic fatty liver disease in mice. *Mol Med*. 2012;18(1):901-12.
264. Mo ZC, Ren K, Liu X, Tang ZL, Yi GH. A high-density lipoprotein-mediated drug delivery system. *Adv Drug Deliv Rev*. 2016;106(Pt A):132-47.
265. Weber J, Peng H, Rader C. From rabbit antibody repertoires to rabbit monoclonal antibodies. *Exp Mol Med*. 2017;49(3):e305.
266. Graur D, Duret L, Gouy M. Phylogenetic position of the order Lagomorpha (rabbits, hares and allies). *Nature*. 1996;379(6563):333-5.
267. James J, Martin L, Krenz M, Quatman C, Jones F, Klevitsky R, et al. Forced expression of alpha-myosin heavy chain in the rabbit ventricle results in cardioprotection under cardiomyopathic conditions. *Circulation*. 2005;111(18):2339-46.
268. Zschaler J, Schlorke D, Arnhold J. Differences in innate immune response between man and mouse. *Crit Rev Immunol*. 2014;34(5):433-54.
269. Yanni AE. The laboratory rabbit: an animal model of atherosclerosis research. *Lab Anim*. 2004;38(3):246-56.
270. Esteves PJ, Abrantes J, Baldauf HM, BenMohamed L, Chen Y, Christensen N, et al. The wide utility of rabbits as models of human diseases. *Exp Mol Med*. 2018;50(5):1-10.
271. Fan J, Watanabe T. Cholesterol-fed and transgenic rabbit models for the study of atherosclerosis. *J Atheroscler Thromb*. 2000;7(1):26-32.
272. Fan J, Kitajima S, Watanabe T, Xu J, Zhang J, Liu E, et al. Rabbit models for the study of human atherosclerosis: from pathophysiological mechanisms to translational medicine. *Pharmacol Ther*. 2015;146:104-19.
273. Yang BC, Phillips MI, Mohuczy D, Meng H, Shen L, Mehta P, et al. Increased angiotensin II type 1 receptor expression in hypercholesterolemic atherosclerosis in rabbits. *Arterioscler Thromb Vasc Biol*. 1998;18(9):1433-9.
274. Bassols A, Costa C, Eckersall PD, Osada J, Sabria J, Tibau J. The pig as an animal model for human pathologies: A proteomics perspective. *Proteomics Clin Appl*. 2014;8(9-10):715-31.
275. Wernersson R, Schierup MH, Jørgensen FG, Gorodkin J, Panitz F, Staerfeldt HH, et al. Pigs in sequence space: a 0.66X coverage pig genome survey based on shotgun sequencing. *BMC Genomics*. 2005;6:70.
276. Walters EM, Prather RS. Advancing swine models for human health and diseases. *Mo Med*. 2013;110(3):212-5.
277. Hou N, Du X, Wu S. Advances in pig models of human diseases. *Animal Model Exp Med*. 2022;5(2):141-52.
278. Spurlock ME, Gabler NK. The development of porcine models of obesity and the metabolic syndrome. *J Nutr*. 2008;138(2):397-402.

References

279. Herrera-Marcos LV, Martinez-Beamonte R, Macias-Herranz M, Arnal C, Barranquero C, Puente-Lanzarote JJ, et al. Hepatic galectin-3 is associated with lipid droplet area in non-alcoholic steatohepatitis in a new swine model. *Sci Rep.* 2022;12(1):1024.
280. Reyer H, Varley PF, Murani E, Ponsuksili S, Wimmers K. Genetics of body fat mass and related traits in a pig population selected for leanness. *Sci Rep.* 2017;7(1):9118.
281. Getz GS, Reardon CA. Pig and mouse models of hyperlipidemia and atherosclerosis. *Methods Mol Biol.* 2022;2419:379-411.
282. Xi S, Yin W, Wang Z, Kusunoki M, Lian X, Koike T, et al. A minipig model of high-fat/high-sucrose diet-induced diabetes and atherosclerosis. *Int J Exp Pathol.* 2004;85(4):223-31.
283. McKenney ML, Schultz KA, Boyd JH, Byrd JP, Alloosh M, Teague SD, et al. Epicardial adipose excision slows the progression of porcine coronary atherosclerosis. *J Cardiothorac Surg.* 2014;9:2.
284. Borbouse L, Dick GM, Asano S, Bender SB, Dincer UD, Payne GA, et al. Impaired function of coronary BK(Ca) channels in metabolic syndrome. *Am J Physiol Heart Circ Physiol.* 2009;297(5):H1629-37.
285. Schleimer A, Richart L, Drygala F, Casabianca F, Maestrini O, Weigand H, et al. Introgressive hybridisation between domestic pigs (*Sus scrofa domesticus*) and endemic Corsican wild boars (*S. s. meridionalis*): effects of human-mediated interventions. *Heredity (Edinb).* 2022;128(4):279-90.
286. Falconer DS. Introduction to quantitative genetics: Pearson Education India; 1996.
287. Cheng J, Newcom DW, Schutz MM, Muir WM, Cui Q, Li B, et al. Selection for feed efficiency in duroc pigs with the addition of daily feed intake data in a 2-stage selection procedure. *Applied Animal Science.* 2019;35(1):20-9.
288. Martínez Soriano B, Güemes A, Pola G, Gonzalo A, Palacios Gasós P, Navarro AC, et al. Effect of melatonin as an antioxidant drug to reverse hepatic steatosis: experimental model. *Can J Gastroenterol Hepatol.* 2020;2020:7315253.
289. Segeritz C-P, Vallier L. Cell culture: growing cells as model systems in vitro. *Basic Science Methods For Clinical Researchers: Elsevier;* 2017. p. 151-72.
290. Hudu SA, Alshrari AS, Syahida A, Sekawi Z. Cell culture, technology: enhancing the culture of diagnosing human diseases. *Journal of Clinical and Diagnostic Research.* 2016;10(3):DE01–DE5.
291. Li F, Vijayasankaran N, Shen AY, Kiss R, Amanullah A. Cell culture processes for monoclonal antibody production. *MAbs.* 2010;2(5):466-79.
292. Nagarajan SR, Paul-Heng M, Krycer JR, Fazakerley DJ, Sharland AF, Hoy AJ. Lipid and glucose metabolism in hepatocyte cell lines and primary mouse hepatocytes: a comprehensive resource for in vitro studies of hepatic metabolism. *Am J Physiol Endocrinol Metab.* 2019;316(4):E578-e89.

References

293. Sefried S, Häring HU, Weigert C, Eckstein SS. Suitability of hepatocyte cell lines HepG2, AML12 and THLE-2 for investigation of insulin signalling and hepatokine gene expression. *Open Biol.* 2018;8(10).
294. Ramboer E, Vanhaecke T, Rogiers V, Vinken M. Immortalized human hepatic cell lines for in vitro testing and research purposes. *Methods Mol Biol.* 2015;1250:53-76.
295. Kaur G, Dufour JM. Cell lines: valuable tools or useless artifacts. *Spermatogenesis.* 2012;2(1):1-5.
296. Arzumanyan VA, Kiseleva OI, Poverennaya EV. The Curious case of the HepG2 cell line: 40 years of expertise. *Int J Mol Sci.* 2021;22(23):13135.
297. Alturkistani HA, Tashkandi FM, Mohammedsaleh ZM. Histological stains: a literature review and case study. *Glob J Health Sci.* 2015;8(3):72-9.
298. Gurina TS, Simms L. *Histology, staining.* StatPearls. Treasure Island (FL): StatPearls Publishing LLC; 2023.
299. Hollywood K, Brison DR, Goodacre R. Metabolomics: current technologies and future trends. *Proteomics.* 2006;6(17):4716-23.
300. Dong Z, Chen Y. Transcriptomics: advances and approaches. *Sci China Life Sci.* 2013;56(10):960-7.
301. Lowe R, Shirley N, Bleackley M, Dolan S, Shafee T. Transcriptomics technologies. *PLoS Computational Biology.* 2017;13(5):e1005457.
302. Wang Z, Gerstein M, Snyder M. RNA-Seq: a revolutionary tool for transcriptomics. *Nat Rev Genet.* 2009;10(1):57-63.
303. Huang H, Hu Y, Huang G, Ma S, Feng J, Wang D, et al. Tag-seq: a convenient and scalable method for genome-wide specificity assessment of CRISPR/Cas nucleases. *Commun Biol.* 2021;4(1):830.
304. Li BT, Lim JX, Ling MHT. Analyzing transcriptome-phenotype correlations. In: Ranganathan S, Gribskov M, Nakai K, Schönbach C, editors. *Encyclopedia of Bioinformatics and Computational Biology.* Oxford: Academic Press; 2019. p. 819-24.
305. Finotello F, Di Camillo B. Measuring differential gene expression with RNA-seq: challenges and strategies for data analysis. *Brief Funct Genomics.* 2015;14(2):130-42.
306. O'Donnell M, Axilbund J, Euhus DM. Breast cancer genetics: syndromes, genes, pathology, counseling, testing, and treatment. *The Breast: Elsevier;* 2018. p. 237-49. e5.
307. Kukurba KR, Montgomery SB. RNA sequencing and analysis. *Cold Spring Harb Protoc.* 2015;2015(11):951-69.
308. Bakhtiarizadeh MR, Alamouti AA. RNA-Seq based genetic variant discovery provides new insights into controlling fat deposition in the tail of sheep. *Sci Rep.* 2020;10(1):13525.
309. Mackenzie RJ. RNA-seq: basics, applications and protocol. Retrieved from Technology Networks:

References

- <https://www.technologynetworks.com/genomics/articles/rna-seq-basics-applications-and-protocol-29946>. 2018.
310. Hu Y, Wang K, He X, Chiang DY, Prins JF, Liu J. A probabilistic framework for aligning paired-end RNA-seq data. *Bioinformatics*. 2010;26(16):1950-7.
311. Li H, Homer N. A survey of sequence alignment algorithms for next-generation sequencing. *Brief Bioinform*. 2010;11(5):473-83.
312. Ching T, Huang S, Garmire LX. Power analysis and sample size estimation for RNA-Seq differential expression. *RNA*. 2014;20(11):1684-96.
313. Ji F, Sadreyev RI. RNA-seq: basic bioinformatics analysis. *Curr Protoc Mol Biol*. 2018;124(1):e68.
314. Koch CM, Chiu SF, Akbarpour M, Bharat A, Ridge KM, Bartom ET, et al. A Beginner's guide to analysis of RNA sequencing data. *Am J Respir Cell Mol Biol*. 2018;59(2):145-57.
315. Valasek MA, Repa JJ. The power of real-time PCR. *Adv Physiol Educ*. 2005;29(3):151-9.
316. Coenye T. Do results obtained with RNA-sequencing require independent verification? *Biofilm*. 2021;3:100043.
317. Derveaux S, Vandesompele J, Hellemans J. How to do successful gene expression analysis using real-time PCR. *Methods*. 2010;50(4):227-30.
318. Supplitt S, Karpinski P, Sasiadek M, Laczmanska I. Current achievements and applications of transcriptomics in personalized cancer medicine. *Int J Mol Sci*. 2021;22(3).
319. Brankatschk R, Bodenhausen N, Zeyer J, Bürgmann H. Simple absolute quantification method correcting for quantitative PCR efficiency variations for microbial community samples. *Appl Environ Microbiol*. 2012;78(12):4481-9.
320. VanGuilder HD, Vrana KE, Freeman WM. Twenty-five years of quantitative PCR for gene expression analysis. *Biotechniques*. 2008;44(5):619-26.
321. Pfaffl MW. A new mathematical model for relative quantification in real-time RT-PCR. *Nucleic Acids Res*. 2001;29(9):e45.
322. Kühne BS, Oschmann P. Quantitative real-time RT-PCR using hybridization probes and imported standard curves for cytokine gene expression analysis. *Biotechniques*. 2002;33(5):1078-89.
323. Guo J, Ju J, Turro NJ. Fluorescent hybridization probes for nucleic acid detection. *Anal Bioanal Chem*. 2012;402(10):3115-25.
324. Teunissen C, Verheul C, Willemse E. The use of cerebrospinal fluid in biomarker studies. *Handbook of Clinical Neurology*. 2018;146:3-20.
325. Dhanjai, Sinha A, Lu X, Wu L, Tan D, Li Y, et al. Voltammetric sensing of biomolecules at carbon based electrode interfaces: A review. *TrAC Trends in Analytical Chemistry*. 2018;98:174-89.

References

326. Yang Q, Zhang AH, Miao JH, Sun H, Han Y, Yan GL, et al. Metabolomics biotechnology, applications, and future trends: a systematic review. *RSC Adv.* 2019;9(64):37245-57.
327. Zhang A, Sun H, Wang P, Han Y, Wang X. Modern analytical techniques in metabolomics analysis. *Analyst.* 2012;137(2):293-300.
328. Dadi M, Yasir M. Spectroscopy and spectrophotometry: principles and applications for colorimetric and related other analysis. *Colorimetry.* 2022:81.
329. Marczenko Z, Balcerzak M. Principles of spectrophotometry. Elsevier; 2000. p. 26-38.
330. Nilapwar SM, Nardelli M, Westerhoff HV, Verma M. Chapter four - absorption spectroscopy. In: Jameson D, Verma M, Westerhoff HV, editors. *Methods in Enzymology.* 500: Academic Press; 2011. p. 59-75.
331. Câmara JS, Martins C, Pereira JAM, Perestrelo R, Rocha SM. Chromatographic-based platforms as new avenues for scientific progress and sustainability. *Molecules.* 2022;27(16):5267.
332. Urban PL. Quantitative mass spectrometry: an overview. *Philosophical Transactions of the Royal Society A: Mathematical, Physical and Engineering Sciences.* 2016;374(2079):20150382.
333. Chauhan A, Goyal MK, Chauhan P. GC-MS technique and its analytical applications in science and technology. *J Anal Bioanal Tech.* 2014;5(6):222.
334. Siegel JA, Saukko PJ. *Encyclopedia of forensic sciences:* Academic Press; 2012.
335. Beale DJ, Pinu FR, Kouremenos KA, Poojary MM, Narayana VK, Boughton BA, et al. Review of recent developments in GC-MS approaches to metabolomics-based research. *Metabolomics.* 2018;14(11):152.
336. Putri SP, Ikram MMM, Sato A, Dahlan HA, Rahmawati D, Ohto Y, et al. Application of gas chromatography-mass spectrometry-based metabolomics in food science and technology. *J Biosci Bioeng.* 2022;133(5):425-35.
337. Surra JC, Guillén N, Arbonés-Mainar JM, Barranquero C, Navarro MA, Arnal C, et al. Sex as a profound modifier of atherosclerotic lesion development in apolipoprotein E-deficient mice with different genetic backgrounds. *J Atheroscler Thromb.* 2010;17(7):712-21.
338. Gabas-Rivera C, Barranquero C, Martinez-Beamonte R, Navarro MA, Surra JC, Osada J. Dietary squalene increases high density lipoprotein-cholesterol and paraoxonase 1 and decreases oxidative stress in mice. *PLoS One.* 2015;9(8):e104224.
339. Carnicer R, Navarro MA, Arbonés-Mainar JM, Arnal C, Surra JC, Acín S, et al. Genetically based hypertension generated through interaction of mild hypoalphalipoproteinemia and mild hyperhomocysteinemia. *J Hypertens.* 2007;25(8):1597-607.
340. Gabas-Rivera C, Martinez-Beamonte R, Rios JL, Navarro MA, Surra JC, Arnal C, et al. Dietary oleanolic acid mediates circadian clock gene expression in liver

References

- independently of diet and animal model but requires apolipoprotein A1. *J Nutr Biochem*. 2013;24(12):2100-9.
341. Martinez-Beamonte R, Alda O, Sanclemente T, Felices MJ, Escusol S, Arnal C, et al. Hepatic subcellular distribution of squalene changes according to the experimental setting. *J Physiol Biochem*. 2018;74:531-8.
342. Cock PJ, Fields CJ, Goto N, Heuer ML, Rice PM. The Sanger FASTQ file format for sequences with quality scores, and the solexa/illumina FASTQ variants. *Nucleic Acids Res*. 2010;38(6):1767-71.
343. Kim D, Langmead B, Salzberg SL. HISAT: a fast spliced aligner with low memory requirements. *Nat Methods*. 2015;12(4):357-60.
344. Pertea M, Pertea GM, Antonescu CM, Chang T-C, Mendell JT, Salzberg SL. StringTie enables improved reconstruction of a transcriptome from RNA-seq reads. *Nature Biotechnology*. 2015;33(3):290-5.
345. Trapnell C, Roberts A, Goff L, Pertea G, Kim D, Kelley DR, et al. Differential gene and transcript expression analysis of RNA-seq experiments with TopHat and Cufflinks. *Nature Protocols*. 2012;7(3):562-78.
346. McKenna A, Hanna M, Banks E, Sivachenko A, Cibulskis K, Kernytsky A, et al. The genome analysis toolkit: a mapreduce framework for analyzing next-generation DNA sequencing data. *Genome Res*. 2010;20(9):1297-303.
347. Shen S, Park JW, Lu Z-x, Lin L, Henry MD, Wu YN, et al. rMATS: robust and flexible detection of differential alternative splicing from replicate RNA-Seq data. *Proceedings of the National Academy of Sciences*. 2014;111(51):E5593-E601.
348. Langmead B, Salzberg SL. Fast gapped-read alignment with Bowtie 2. *Nature Methods*. 2012;9(4):357-9.
349. Li B, Dewey CN. RSEM: accurate transcript quantification from RNA-Seq data with or without a reference genome. *BMC Bioinformatics*. 2011;12(1):323.
350. Bustin SA, Benes V, Garson JA, Hellems J, Huggett J, Kubista M, et al. The MIQE guidelines: minimum information for publication of quantitative real-time PCR experiments. *Clin Chem*. 2009;55(4):611-22.
351. Folch J, Less M, Sloan-Stanley GH. A simple method for the isolation and purification of total lipids from the animal tissues. *J Biol Chem*. 1957;33:497-509.
352. Marcelino G, Hiane PA, Freitas KC, Santana LF, Pott A, Donadon JR, et al. Effects of olive oil and its minor components on cardiovascular diseases, inflammation, and gut microbiota. *Nutrients*. 2019;11(8):1826.
353. Moreno JJ. Effect of olive oil minor components on oxidative stress and arachidonic acid mobilization and metabolism by macrophages raw 264.7. *Free Radic Biol Med*. 2003;35(9):1073-81.
354. Guillen N, Acín S, Surra JC, Arnal C, Godino J, García-Granados A, et al. Apolipoprotein E determines the hepatic transcriptional profile of dietary maslinic acid in mice. *J Nutr Biochem*. 2009;20(11):882-93.

References

355. Rajkumar AP, Qvist P, Lazarus R, Lescai F, Ju J, Nyegaard M, et al. Experimental validation of methods for differential gene expression analysis and sample pooling in RNA-seq. *BMC Genomics*. 2015;16(1):1-8.
356. Peng X, Wood CL, Blalock EM, Chen KC, Landfield PW, Stromberg AJ. Statistical implications of pooling RNA samples for microarray experiments. *BMC Bioinformatics*. 2003;4(1):1-9.
357. Renaud HJ, Cui JY, Khan M, Klaassen CD. Tissue distribution and gender-divergent expression of 78 cytochrome P450 mRNAs in mice. *Toxicol Sci*. 2011;124(2):261-77.
358. Waskell L, Kim J-JP. Electron transfer partners of cytochrome P450. In: Ortiz de Montellano PR, editor. *Cytochrome P450: Structure, Mechanism, and Biochemistry*. Cham: Springer International Publishing; 2015. p. 33-68.
359. Koga T, Yao PL, Goudarzi M, Murray IA, Balandaram G, Gonzalez FJ, et al. Regulation of cytochrome P450 2B10 (CYP2B10) expression in liver by peroxisome proliferator-activated receptor- β/δ modulation of SP1 promoter occupancy. *J Biol Chem*. 2016;291(48):25255-63.
360. Gabas-Rivera C, Jurado-Ruiz E, Sanchez-Ortiz A, Romanos E, Martinez-Beamonte R, Navarro MA, et al. Dietary squalene induces cytochromes Cyp2b10 and Cyp2c55 independently of sex, dose, and diet in several mouse models. *Mol Nutr Food Res*. 2020;64(20):e2000354.
361. Heintz MM, Kumar R, Rutledge MM, Baldwin WS. Cyp2b-null male mice are susceptible to diet-induced obesity and perturbations in lipid homeostasis. *J Nutr Biochem*. 2019;70:125-37.
362. Zhao J, Wang Y, Wu X, Tong P, Yue Y, Gao S, et al. Inhibition of CCL19 benefits non-alcoholic fatty liver disease by inhibiting TLR4/NF- κ B-p65 signaling. *Mol Med Rep*. 2018;18(5):4635-42.
363. Zhou Y, Jiang L, Rui L. Identification of MUP1 as a regulator for glucose and lipid metabolism in mice. *J Biol Chem*. 2009;284(17):11152-9.
364. Fan Y, Fang X, Tajima A, Geng X, Ranganathan S, Dong H, et al. Evolution of hepatic steatosis to fibrosis and adenoma formation in liver-specific growth hormone receptor knockout mice. *Front Endocrinol (Lausanne)*. 2014;5:218.
365. Mirea AM, Stienstra R, Kanneganti TD, Tack CJ, Chavakis T, Toonen EJM, et al. Mice deficient in the IL-1 β activation genes Prtn3, Elane, and Casp1 are protected against the development of obesity-induced NAFLD. *Inflammation*. 2020;43(3):1054-64.
366. Chen J, Qian Z, Li F, Li J, Lu Y. Integrative analysis of microarray data to reveal regulation patterns in the pathogenesis of hepatocellular carcinoma. *Gut Liver*. 2017;11(1):112-20.
367. Sultana N, Rahman M, Myti S, Islam J, Mustafa MG, Nag K. A novel knowledge-derived data potentizing method revealed unique liver cancer-associated genetic variants. *Hum Genomics*. 2019;13(1):30.

References

368. Reichold A, Brenner SA, Förster-Fromme K, Bergheim I, Mollenhauer J, Bischoff SC. Dmbt1 does not affect a Western style diet-induced liver damage in mice. *J Clin Biochem Nutr.* 2013;53(3):145-9.
369. Deng H, Gao YB, Wang HF, Jin XL, Xiao JC. Expression of deleted in malignant brain tumours 1 (DMBT1) relates to the proliferation and malignant transformation of hepatic progenitor cells in hepatitis B virus-related liver diseases. *Histopathology.* 2012;60(2):249-60.
370. Kwekel JC, Desai VG, Moland CL, Branham WS, Fuscoe JC. Age and sex dependent changes in liver gene expression during the life cycle of the rat. *BMC Genomics.* 2010;11:675.
371. Herrera-Marcos LV, Sancho-Knapik S, Gabas-Rivera C, Barranquero C, Gascon S, Romanos E, et al. Pgc1a is responsible for the sex differences in hepatic Cidec/Fsp27beta mRNA expression in hepatic steatosis of mice fed a Western diet. *Am J Physiol Endocrinol Metab.* 2020;318(2):E249-E61.
372. Xie X, Miao L, Yao J, Feng C, Li C, Gao M, et al. Role of multiple microRNAs in the sexually dimorphic expression of Cyp2b9 in mouse liver. *Drug Metab Dispos.* 2013;41(10):1732-7.
373. Kumar R, Mota LC, Litoff EJ, Rooney JP, Boswell WT, Courter E, et al. Compensatory changes in CYP expression in three different toxicology mouse models: CAR-null, Cyp3a-null, and Cyp2b9/10/13-null mice. *PLoS One.* 2017;12(3):e0174355.
374. Jarukamjorn K, Sakuma T, Nemoto N. Discriminating activation of CYP2B9 expression in male C57BL/6 mouse liver by beta-estradiol. *Biochem Biophys Res Commun.* 2000;279(1):288-92.
375. Sato Y, Kaneko Y, Cho T, Goto K, Otsuka T, Yamamoto S, et al. Prolactin upregulates female-predominant P450 gene expressions and downregulates male-predominant gene expressions in mouse liver. *Drug Metab Dispos.* 2017;45(6):586-92.
376. Martín R, Hernández M, Córdova C, Nieto ML. Natural triterpenes modulate immune-inflammatory markers of experimental autoimmune encephalomyelitis: therapeutic implications for multiple sclerosis. *Br J Pharmacol.* 2012;166(5):1708-23.
377. Giménez E, Juan ME, Calvo-Melià S, Planas JM. A sensitive liquid chromatography-mass spectrometry method for the simultaneous determination in plasma of pentacyclic triterpenes of *Olea europaea* L. *Food Chem.* 2017;229:534-41.
378. Acín S, Navarro MA, Perona JS, Arbonés-Mainar JM, Surra JC, Guzmán MA, et al. Olive oil preparation determines the atherosclerotic protection in apolipoprotein E knockout mice. *J Nutr Biochem.* 2007;18(6):418-24.
379. Hall DW, Marshall SN, Gordon KC, Killeen DP. Rapid quantitative determination of squalene in shark liver oils by Raman and IR spectroscopy. *Lipids.* 2016;51(1):139-47.
380. Ramírez-Torres A. Squalene: current knowledge and potential therapeutical uses: Nova Science Publishers, Incorporated; 2011.

References

381. Martinez-Beamonte R, Sanchez-Marco J, Felices MJ, Barranquero C, Gascon S, Arnal C, et al. Dietary squalene modifies plasma lipoproteins and hepatic cholesterol metabolism in rabbits. *Food Funct.* 2021;12(17):8141-53.
382. Fromme JC, Munson M. Capturing endosomal vesicles at the golgi. *Nat Cell Biol.* 2017;19(12):1384-6.
383. Barr FA, Short B. Golgins in the structure and dynamics of the golgi apparatus. *Curr Opin Cell Biol.* 2003;15(4):405-13.
384. Guo T, Mao Y, Li H, Wang X, Xu W, Song R, et al. Characterization of the gene expression profile of heterozygous liver-specific glucokinase knockout mice at a young age. *Biomed Pharmacother.* 2012;66(8):587-96.
385. Huang Z, Zhang M, Plec AA, Estill SJ, Cai L, Repa JJ, et al. ACS2 promotes systemic fat storage and utilization through selective regulation of genes involved in lipid metabolism. *Proc Natl Acad Sci U S A.* 2018;115(40):E9499-e506.
386. Xu H, Luo J, Ma G, Zhang X, Yao D, Li M, et al. Acyl-coA synthetase short-chain family member 2 (ACS2) is regulated by SREBP-1 and plays a role in fatty acid synthesis in caprine mammary epithelial cells. *J Cell Physiol.* 2018;233(2):1005-16.
387. Trépo E, Romeo S, Zucman-Rossi J, Nahon P. PNPLA3 gene in liver diseases. *J Hepatol.* 2016;65(2):399-412.
388. Kawaguchi T, Sumida Y, Umemura A, Matsuo K, Takahashi M, Takamura T, et al. Genetic polymorphisms of the human PNPLA3 gene are strongly associated with severity of non-alcoholic fatty liver disease in Japanese. *PLoS One.* 2012;7(6):e38322.
389. Oesterreicher TJ, Markesich DC, Henning SJ. Cloning, characterization and mapping of the mouse trehalase (Treh) gene. *Gene.* 2001;270(1-2):211-20.
390. Packard CJ, Boren J, Taskinen MR. Causes and consequences of hypertriglyceridemia. *Front Endocrinol (Lausanne).* 2020;11:252.
391. Mardones P, Rubinsztein DC, Hetz C. Mystery solved: trehalose kickstarts autophagy by blocking glucose transport. *Sci Signal.* 2016;9(416):fs2.
392. Dumax-Vorzet A, Roboti P, High S. OST4 is a subunit of the mammalian oligosaccharyltransferase required for efficient N-glycosylation. *J Cell Sci.* 2013;126(Pt 12):2595-606.
393. Clarke JD, Novak P, Lake AD, Hardwick RN, Cherrington NJ. Impaired N-linked glycosylation of uptake and efflux transporters in human non-alcoholic fatty liver disease. *Liver Int.* 2017;37(7):1074-81.
394. Mohanty S, Chaudhary BP, Zoetewey D. Structural insight into the mechanism of N-linked glycosylation by oligosaccharyltransferase. *Biomolecules.* 2020;10(4).
395. van den Boogert MAW, Larsen LE, Ali L, Kuil SD, Chong PLW, Loregger A, et al. N-Glycosylation defects in humans lower low-density lipoprotein cholesterol through increased low-density lipoprotein receptor expression. *Circulation.* 2019;140(4):280-92.
396. Schiaffino S. Muscle fiber type diversity revealed by anti-myosin heavy chain antibodies. *Febs J.* 2018;285(20):3688-94.

References

397. Will RD, Eden M, Just S, Hansen A, Eder A, Frank D, et al. Myomasp/LRRC39, a heart- and muscle-specific protein, is a novel component of the sarcomeric M-band and is involved in stretch sensing. *Circ Res.* 2010;107(10):1253-64.
398. Huang X, Yan L, Kou S, Meng J, Lu Z, Lin CP, et al. Generation and characterization of a Myh6-driven Cre knockin mouse line. *Transgenic Res.* 2021;30(6):821-35.
399. Ehrlich KC, Lacey M, Ehrlich M. Epigenetics of skeletal muscle-associated genes in the ASB, LRRC, TMEM, and OSBPL gene families. *Epigenomes.* 2020;4(1).
400. Gortan Cappellari G, Zanetti M, Semolic A, Vinci P, Ruozi G, Falcione A, et al. Unacylated ghrelin reduces skeletal muscle reactive oxygen species generation and inflammation and prevents high-fat diet-induced hyperglycemia and whole-body insulin resistance in rodents. *Diabetes.* 2016;65(4):874-86.
401. Garcia-Bermudez J, Baudrier L, Bayraktar EC, Shen Y, La K, Guarecuco R, et al. Squalene accumulation in cholesterol auxotrophic lymphomas prevents oxidative cell death. *Nature.* 2019;567(7746):118-22.
402. Kargbo RB. Inhibition of ACS2 for treatment of cancer and neuropsychiatric diseases. *ACS Med Chem Lett.* 2019;10(8):1100-1.
403. Wei J, Ran G, Wang X, Jiang N, Liang J, Lin X, et al. Gene manipulation in liver ductal organoids by optimized recombinant adeno-associated virus vectors. *J Biol Chem.* 2019;294(38):14096-104.
404. Kotarba G, Krzywinska E, Grabowska AI, Taracha A, Wilanowski T. TFCP2/TFCP2L1/UBP1 transcription factors in cancer. *Cancer Lett.* 2018;420:72-9.
405. Shastri B. Functional characterisation of glycosyltransferase 1 domain containing 1 gene in mammary carcinoma cells: ResearchSpace@ Auckland; 2013.
406. Guillen N, Acin S, Navarro MA, Perona JS, Arbones-Mainar JM, Arnal C, et al. Squalene in a sex-dependent manner modulates atherosclerotic lesion which correlates with hepatic fat content in apoE-knockout male mice. *Atherosclerosis.* 2008;197(1):72-83.
407. Takahashi Y, Fukusato T. Animal models of liver diseases. *Animal Models for The Study of Human Disease: Elsevier;* 2017. p. 313-39.
408. Muriel P, Ramos-Tovar E, Montes-Páez G, Buendía-Montaño L. Experimental models of liver damage mediated by oxidative stress. *Liver Pathophysiology: Elsevier;* 2017. p. 529-46.
409. Abuobeid R, Sánchez-Marco J, Felices MJ, Arnal C, Burillo JC, Lasheras R, et al. Squalene through its post-squalene metabolites is a modulator of hepatic transcriptome in rabbits. *International Journal of Molecular Sciences.* 2022;23(8):4172.
410. Prather RS, Lorson M, Ross JW, Whyte JJ, Walters E. Genetically engineered pig models for human diseases. *Annual Review of Animal Biosciences.* 2013;1:203.
411. Karlsson M, Sjöstedt E, Oksvold P, Sivertsson Å, Huang J, Álvez MB, et al. Genome-wide annotation of protein-coding genes in pig. *BMC Biology.* 2022;20(1):1-18.

References

412. Hoang TMH, Nguyen CH, Le TT, Hoang THQ, Ngo THT, Hoang TLA, et al. Squalene isolated from *Schizochytrium mangrovei* is a peroxisome proliferator-activated receptor- α agonist that regulates lipid metabolism in HepG2 cells. *Biotechnology Letters*. 2016;38:1065-71.
413. Raza-Iqbal S, Tanaka T, Anai M, Inagaki T, Matsumura Y, Ikeda K, et al. Transcriptome analysis of K-877 (a novel selective PPAR α modulator (SPPARM α))-regulated genes in primary human hepatocytes and the mouse liver. *Journal of Atherosclerosis and Thrombosis*. 2015:28720.
414. Fruchart J-C. Pemafibrate (K-877), a novel selective peroxisome proliferator-activated receptor alpha modulator for management of atherogenic dyslipidaemia. *Cardiovascular Diabetology*. 2017;16(1):1-12.
415. Florentin M, Kostapanos MS, Anagnostis P, Liamis G. Recent developments in pharmacotherapy for hypertriglyceridemia: what's the current state of the art? *Expert Opinion on Pharmacotherapy*. 2020;21(1):107-20.
416. Niu L, Geyer PE, Wewer Albrechtsen NJ, Gluud LL, Santos A, Doll S, et al. Plasma proteome profiling discovers novel proteins associated with non-alcoholic fatty liver disease. *Mol Syst Biol*. 2019;15(3):e8793.
417. Rosenblat M, Volkova N, Aviram M. Pomegranate juice (PJ) consumption antioxidative properties on mouse macrophages, but not PJ beneficial effects on macrophage cholesterol and triglyceride metabolism, are mediated via PJ-induced stimulation of macrophage PON2. *Atherosclerosis*. 2010;212(1):86-92.
418. Cichoż-Lach H, Michalak A. Oxidative stress as a crucial factor in liver diseases. *World Journal of Gastroenterology: WJG*. 2014;20(25):8082.
419. Lee J, Homma T, Kurahashi T, Kang ES, Fujii J. Oxidative stress triggers lipid droplet accumulation in primary cultured hepatocytes by activating fatty acid synthesis. *Biochemical and Biophysical Research Communications*. 2015;464(1):229-35.
420. Malott KF, Reshel S, Ortiz L, Luderer U. Glutathione deficiency decreases lipid droplet stores and increases reactive oxygen species in mouse oocytes. *Biology of Reproduction*. 2022;106(6):1218-31.
421. Guzmán TJ, Vargas-Guerrero B, García-López PM, Gurrola-Díaz CM. Analysis of hepatic transcriptome modulation exerted by γ -conglutin from lupins in a streptozotocin-induced diabetes model. *Gene*. 2020;761:145036.
422. Parhofer KG. Interaction between glucose and lipid metabolism: more than diabetic dyslipidemia. *Diabetes & Metabolism Journal*. 2015;39(5):353-62.
423. Jiang H, Liu Y, Qian Y, Shen Z, He Y, Gao R, et al. CHL1 promotes insulin secretion and negatively regulates the proliferation of pancreatic β cells. *Biochemical and Biophysical Research Communications*. 2020;525(4):1095-102.
424. Taneera J, Dhaiban S, Hachim M, Mohammed AK, Mukhopadhyay D, Bajbouj K, et al. Reduced expression of Ch11 gene impairs insulin secretion by down-regulating the expression of key molecules of β -cell function. *Experimental and Clinical Endocrinology & Diabetes*. 2019;129(12):864-72.

References

425. Chirieac DV, Chirieac LR, Corsetti JP, Cianci J, Sparks CE, Sparks JD. Glucose-stimulated insulin secretion suppresses hepatic triglyceride-rich lipoprotein and apoB production. *American Journal of Physiology-Endocrinology and Metabolism*. 2000;279(5):E1003-E11.
426. Adiels M, Taskinen M-R, Borén J. Fatty liver, insulin resistance, and dyslipidemia. *Current Diabetes Reports*. 2008;8(1):60-4.
427. Tricò D, Natali A, Mari A, Ferrannini E, Santoro N, Caprio S. Triglyceride-rich very low-density lipoproteins (VLDL) are independently associated with insulin secretion in a multiethnic cohort of adolescents. *Diabetes Obes Metab*. 2018;20(12):2905-10.
428. Khan A, Molitor A, Mayeur S, Zhang G, Rinaldi B, Lannes B, et al. A Homozygous missense variant in PPP1R1B/DARPP-32 Is associated with generalized complex dystonia. *Mov Disord*. 2022;37(2):365-74.
429. Brady MJ, Saltiel AR. The role of protein phosphatase-1 in insulin action. *Recent Progress in Hormone Research*. 2001;56(1):157-74.
430. Allende DS, Gawrieh S, Cummings OW, Belt P, Wilson L, Van Natta M, et al. Glycogenesis is common in nonalcoholic fatty liver disease and is independently associated with ballooning, but lower steatosis and lower fibrosis. *Liver International*. 2021;41(5):996-1011.
431. Nishihira J, Koyama Y, Sakai M, Nishi S. The fatty acid binding site of human alpha-fetoprotein. *Biochem Biophys Res Commun*. 1993;196(3):1049-57.
432. Yamada K, Mizukoshi E, Sunagozaka H, Arai K, Yamashita T, Takeshita Y, et al. Characteristics of hepatic fatty acid compositions in patients with nonalcoholic steatohepatitis. *Liver International*. 2015;35(2):582-90.
433. Yoo W, Gjuka D, Stevenson HL, Song X, Shen H, Yoo SY, et al. Fatty acids in non-alcoholic steatohepatitis: Focus on pentadecanoic acid. *PloS One*. 2017;12(12):e0189965.
434. Xu F, Liu C, Zhou D, Zhang L. TGF- β /SMAD pathway and its regulation in hepatic fibrosis. *Journal of Histochemistry & Cytochemistry*. 2016;64(3):157-67.
435. Zhou G, Lin W, Fang P, Lin X, Zhuge L, Hu Z, et al. MiR-10a improves hepatic fibrosis by regulating the TGF β 1/Smads signal transduction pathway. *Exp Ther Med*. 2016;12(3):1719-22.
436. Arimoto KI, Miyauchi S, Stoner SA, Fan JB, Zhang DE. Negative regulation of type I IFN signaling. *Journal of Leukocyte Biology*. 2018;103(6):1099-116.
437. Zhang C, Liu S, Yang M. The Role of interferon regulatory factors in non-alcoholic fatty liver disease and non-alcoholic steatohepatitis. *Gastroenterology Insights*. 2022;13(2):148-61.
438. Kersten S, Stienstra R. The role and regulation of the peroxisome proliferator activated receptor alpha in human liver. *Biochimie*. 2017;136:75-84.

References

439. Xu M, Tan J, Dong W, Zou B, Teng X, Zhu L, et al. The E3 ubiquitin-protein ligase Trim31 alleviates non-alcoholic fatty liver disease by targeting Rhbdf2 in mouse hepatocytes. *Nature Communications*. 2022;13(1):1052.
440. Gawrieh S, Baye TM, Carless M, Wallace J, Komorowski R, Kleiner DE, et al. Hepatic gene networks in morbidly obese patients with nonalcoholic fatty liver disease. *Obesity Surgery*. 2010;20(12):1698-709.
441. van Huizen NA, van den Braak RRC, Doukas M, Dekker LJ, IJzermans JN, Luijckx TM. Up-regulation of collagen proteins in colorectal liver metastasis compared with normal liver tissue. *Journal of Biological Chemistry*. 2019;294(1):281-9.
442. Sirivatanauksorn Y, Sirivatanauksorn V, Srisawat C, Khongmanee A, Tongkham C. Differential expression of sprouty genes in hepatocellular carcinoma. *Journal of Surgical Oncology*. 2012;105(3):273-6.
443. Ghosheh N, Küppers-Munther B, Asplund A, Edsbacke J, Ulfenborg B, Andersson TB, et al. Comparative transcriptomics of hepatic differentiation of human pluripotent stem cells and adult human liver tissue. *Physiological Genomics*. 2017;49(8):430-46.
444. Chan K-M, Wu T-H, Wu T-J, Chou H-S, Yu M-C, Lee W-C. Bioinformatics microarray analysis and identification of gene expression profiles associated with cirrhotic liver. *The Kaohsiung Journal of Medical Sciences*. 2016;32(4):165-76.
445. Hu R, Hu F, Xie X, Wang L, Li G, Qiao T, et al. TMEM45B, up-regulated in human lung cancer, enhances tumorigenicity of lung cancer cells. *Tumor Biology*. 2016;37(9):12181-91.
446. Zhao LC, Shen BY, Deng XX, Chen H, Zhu ZG, Peng CH. TMEM45B promotes proliferation, invasion and migration and inhibits apoptosis in pancreatic cancer cells. *Mol Biosyst*. 2016;12(6):1860-70.
447. Shen K, Yu W, Yu Y, Liu X, Cui X. Knockdown of TMEM45B inhibits cell proliferation and invasion in gastric cancer. *Biomedicine & Pharmacotherapy*. 2018;104:576-81.
448. Wang G, Guo S, Zhang W, Li D, Wang Y, Zhan Q. Co-expression network analysis identifies key modules and hub genes implicated in esophageal squamous cell cancer progression. *Medicine in Omics*. 2021;1:100003.
449. Senchenko VN, Krasnov GS, Dmitriev AA, Kudryavtseva AV, Anedchenko EA, Braga EA, et al. Differential expression of CHL1 gene during development of major human cancers. *PloS One*. 2011;6(3):e15612.